

**Rapid microscale evaluation of the impact of
fermentation conditions on inclusion body formation,
solubilisation and protein refolding yields**

A thesis submitted to University College London for the degree of

Doctor of Philosophy

Gemma Claire Ordidge

Department of Biochemical Engineering

University College London

2012

I, Gemma Claire Ordidge, confirm that the work presented in this thesis is my own. Where information has been derived from other sources, I confirm that this has been indicated in the thesis.

Signature: _____ Date: _____.

Acknowledgements

I would like to thank my supervisors Martina Micheletti, John Liddell and Paul Dalby for their support and guidance throughout the project. Without all their expertise and help the project would have been considerably harder.

For the collaborative work with Fujifilm, I would like to thank all those who helped me in Microbial Fermentation and Process and Analytical Sciences. A special thanks goes to Mark Carlile, Jonathon Gunnell, Simon Dewar, Phil and Megan Miedzak.

For funding the project, I would like to acknowledge both the BBSRC and Fujifilm Diosynth Biotechnologies.

Thanks also to the team at Tecan and Veronica Tewson for her program for the automated liquid handling to achieve a random plate layout for refolding.

I would also like to thank Gareth Mannall for all his help in the early stages and time spent in the pilot plant with me, and Alexandre Vaury for his hard work and enthusiasm during his MSc project.

I would like to acknowledge my colleagues at the Department of Biochemical Engineering for their support, training and feedback. In particular I'd like to thank my good friends Shahina Ahmad, Jasmin Baboo and Lourdes Velez-Suberbie for their encouragement, advice and all the tea and lunch breaks!

Outside of work, I owe a huge debt to Andy McCarthy for his support, patience and never failing to make me smile even after the toughest of days! I only hope I can return the favour and be as much help to you during your PhD as you have been during mine. Finally I'd like to thank my parents, friends and family for always supporting me and encouraging my interest in science from a young age.

Abstract

Heterologous protein expression in *E. coli* can lead to the formation of dense insoluble aggregates named inclusion bodies (IB). The refolding of protein derived from IB is often characterised by low yields of active product. Process optimisation is often achieved empirically and requires significant resource and time efforts. Microscale experimentation may provide a valuable alternative by enabling representative process studies to be conducted early on in process development, using minimal quantities of product, parallel experimentation and automated liquid handling procedures.

An automated robotic platform has been used to develop a dilution refold microscale process-screening tool with a set of hierarchical assays to rapidly determine optimal refolding conditions. The hierarchical orthogonal assays enable the simplest, cheapest and most generic high-throughput assays to first screen for a smaller subset of potentially high-yielding conditions. Absorbance can be used as an initial filter to measure particulate formation and fluorescence boundaries can then be used to select the conditions with the most native-like tertiary structure. The subset can then be analysed for native protein yield by slower, more expensive or protein specific assays, thus saving resources whilst maximising information output, alleviating the analytical bottleneck. This approach has been demonstrated in this work using lysozyme, with fluorescence boundaries to select 30% of highest yielding samples, and also with DHFR.

An automated whole bioprocess sequence comprising fermentation, cell harvest and lysis, inclusion body harvest, denaturation and refolding has been developed at the microscale to study the effect of fermentation conditions on inclusion body yield and quality. The approach has been applied to dihydrofolate reductase (DHFR) and insulin, allowing a more thorough understanding of the effect of fermentation feeding, media and induction strategies on protein refolding yield and purity. This approach allowed yields of active insulin of increased from 10% to 68%. The results obtained from this approach have been compared to larger scales of operation, illustrating the challenges of scale-up. The process sequence, integrated with rapid analytical assays, provides a

powerful tool for understanding the interaction between fermentation conditions and downstream processing yields, allowing a whole process approach to optimisation.

Table of contents

ACKNOWLEDGEMENTS	3
ABSTRACT	4
TABLE OF CONTENTS	6
ABBREVIATIONS	10
UNITS	12
LIST OF FIGURES	13
LIST OF TABLES	23
1 INTRODUCTION	25
1.1 THE CONTEXT OF THE RESEARCH.....	25
1.1.2 <i>Escherichia coli</i> as an expression system.....	27
1.1.3 <i>Protein structure and folding</i>	27
1.1.4 <i>Inclusion Bodies</i>	31
1.1.5 <i>Misfolding and Aggregation</i>	33
1.1.6 <i>Inclusion bodies in industry</i>	39
1.1.7 <i>Microscale Bioprocessing Techniques</i>	46
1.1.8 <i>Analytical methods</i>	50
1.1.9 <i>Proteins studied</i>	51
1.2 MAIN CONCLUSIONS OF THE LITERATURE SURVEY	58
1.3 THESIS AIMS AND OUTLINE	58
2 MATERIALS AND METHODS	61
2.1 LYSOZYME	61
2.1.1 <i>Materials and Equipment</i>	61
2.1.2 <i>Denaturation and Refolding</i>	61
2.1.3 <i>Automated Hierarchy and oxidation experiments</i>	64
2.2 DHFR.....	66
2.2.1 <i>Materials and Equipment</i>	66
2.2.2 <i>Large scale process</i>	69
2.2.3 <i>IB washing</i>	69
2.2.4 <i>Purification for standards</i>	70
2.2.5 <i>Microscale Bioprocess Sequence</i>	71
2.2.6 <i>Denaturation and Refolding</i>	74
2.3 INSULIN	75
2.3.1 <i>Materials and equipment</i>	75
2.3.2 <i>Large scale process</i>	76
2.3.3 <i>IB washing</i>	79

2.3.4	<i>Denaturation and Refolding</i>	79
2.3.5	<i>Microscale Bioprocess Sequence</i>	79
2.3.6	<i>Denaturation and Refolding</i>	81
2.4	DETERMINATION OF K_{1A} USING STATIC GASSING OUT METHOD	81
2.4.1	<i>Large scale fermenter</i>	81
2.4.2	<i>Microscale DSW plate</i>	82
2.5	ANALYTICAL TECHNIQUES	83
2.5.1	<i>Sodium dodecyl sulfate polyacrylamide gel electrophoresis (SDS-PAGE)</i>	83
2.5.2	<i>Total protein concentration</i>	84
2.5.3	<i>Flow cytometry</i>	85
2.5.4	<i>Particle sizing</i>	85
2.5.5	<i>Cell concentration (biomass)</i>	85
2.5.6	<i>Acetic acid quantification</i>	86
2.5.7	<i>Lysozyme assays</i>	86
2.5.8	<i>DHFR Assays</i>	87
2.5.9	<i>Insulin Assays</i>	88
3	ASSAY DEVELOPMENT	90
3.1	INTRODUCTION	90
3.2	MATERIALS AND METHODS	92
3.3	RESULTS AND DISCUSSION	95
3.3.1	<i>High-throughput assay selection</i>	95
3.3.2	<i>Translation from manual to automated set-up</i>	107
3.3.3	<i>Developing a set of hierarchical generic assays</i>	112
3.3.4	<i>Hierarchical assays using lysozyme</i>	121
3.3.5	<i>Hierarchical assays using DHFR IBs</i>	125
3.4	CONCLUSIONS	129
4	DEVELOPMENT OF LINKED AUTOMATED MICROSCALE UNIT OPERATIONS	130
4.1	INTRODUCTION	130
4.2	MATERIALS AND METHODS.....	131
4.3	RESULTS AND DISCUSSION	131
4.3.1	<i>Introduction to Automated Microscale Bioprocess Sequence</i>	131
4.3.2	<i>Fermentation</i>	135
4.3.3	<i>Centrifugation for cell harvest</i>	145
4.3.4	<i>Resuspension</i>	147
4.3.5	<i>Cell lysis using sonication and AFA</i>	148
4.3.6	<i>Centrifugation for IB harvest</i>	165
4.4	CONCLUSIONS	168

5	APPLICATION OF THE MICROSCALE SEQUENCE TO STUDY THE EFFECT OF FERMENTATION VARIABLES ON INCLUSION BODY REFOLDING YIELD	169
5.1	INTRODUCTION	169
	MATERIALS AND METHODS	171
5.1.1	<i>DHFR</i>	171
5.1.2	<i>Insulin</i>	172
5.2	RESULTS AND DISCUSSIONS	173
5.2.1	<i>DHFR</i>	173
5.2.2	<i>Insulin</i>	188
5.3	CONCLUSIONS	210
6	TRANSLATION OF FERMENTATION AND REFOLDING PROCESSES.....	212
6.1	INTRODUCTION	212
6.2	MATERIALS AND METHODS.....	214
6.3	RESULTS AND DISCUSSION	216
6.3.1	<i>Volumetric mass transfer (k_La) determination</i>	216
6.3.2	<i>Fed batch 100L fermentation</i>	220
6.3.3	<i>Fed batch 70 L low k_La fermentation</i>	222
6.3.4	<i>Batch 70 L high k_La fermentation</i>	225
6.3.5	<i>Experimental k_La determination at the microscale</i>	228
6.3.6	<i>Batch microwell fermentation</i>	231
6.3.7	<i>Scalability of refolding</i>	232
6.3.8	<i>Effect of oxygen limitation on IB refolding yield</i>	235
6.3.9	<i>Microscale fermentation and refold system for large scale yield predictions</i>	237
6.3.10	<i>The effect of refold buffer on purity of refold</i>	239
6.3.11	<i>Effect of different refold conditions on insulin</i>	241
6.4	CONCLUSIONS	242
7	CONCLUSIVE REMARKS AND FUTURE RECOMMENDATIONS.....	245
7.1	AUTOMATED, HIGH THROUGHPUT ASSAYS FOR IB YIELD DETERMINATION	245
7.2	DEVELOPING AN AUTOMATED, WHOLE BIOPROCESS FOR IB PRODUCTION AT THE MICROSCALE.	246
7.3	THE EFFECT OF FERMENTATION CONDITIONS ON REFOLDING.....	246
7.4	SCALE UP OF FERMENTATION AND REFOLDING PROCESSES.....	247
7.5	FUTURE RECOMMENDATIONS	248
7.6	OVERALL CONCLUSIONS	250
8	REFERENCES	252
9	APPENDIX	270
9.1	APPENDIX FOR CHAPTER 3	270
9.2	APPENDIX FOR CHAPTER 4	272
9.2.1	<i>Plasmid Information</i>	275

9.3	APPENDIX FOR CHAPTER 5	276
9.4	APPENDIX FOR CHAPTER 6	278
9.4.1	<i>Estimating k_{La}</i>	278
9.4.2	<i>Acetic acid determination</i>	278
9.4.3	<i>Fermentation data</i>	279

Abbreviations

ρ	Density of the liquid phase (kg.m^{-3})
μ	Viscosity ($\text{kg.s}^{-1}\text{m}^{-1}$)
ν	Kinematic viscosity of the liquid phase (m^2s^{-1})
a_i	Initial specific surface area (m)
Bo	Bond number
BSA	Bovine serum albumin
c_1	Geometrical constant
CD	Circular dichroism
D	Gas diffusivity in the liquid (m^2s^{-1})
DHFR	Dihydrofolate reductase
DO_2	Oxygen diffusion coefficient (m^2s^{-1})
DOT	Dissolved oxygen tension (%)
DTT	Dithiothreitol
d_w	Well diameter (m)
e	Total specific power dissipated in the liquid volume (W.m^{-3})
<i>E. coli</i>	<i>Escherichia coli</i>
EDTA	Ethylenediaminetetraacetic acid
Fr	Froude number
GdnHCl	Guanidine hydrochloride
HCl	Hydrochloric acid
HEWL	Hen egg white lysozyme
HPLC	High performance liquid chromatography
IB	Inclusion bodies
IPTG	Isopropyl β -D-1-thiogalactopyranoside
k_{La}	Mass transfer coefficient for oxygen (h^{-1})
LB	Luria broth
MRE	Mean residue ellipticity ($\text{degrees.cm}^2.\text{dmol}^{-1}.\text{residue}^{-1}$)
MW	Molecular weight (Da)
N	Impeller speed (rps)
OD	Optical density (A.U.)
PBS	Phosphate buffered saline

Re	Reynolds number
RP-HPLC	Reverse phase high performance liquid chromatography
Sc	Schmidt number
SDS-PAGE	Sodium dodecyl sulphate polyacrylamide gel electrophoresis
TB	Terrific broth
TFA	Trifluoroacetic acid
Tris	Tris(hydroxymethyl)aminomethane
Triton X	Octyl phenol ethoxylate

Units

°C	degrees Celsius
g	gram
h	hour
L	litre
M	mole
mg	milligram
min	minute
ml	millilitre
mM	millimole
nm	nanometre
rpm	revolutions per minute
v/v	volume per volume
w/v	weight per volume
Δ OD	change in OD
μ l	micro litre

List of Figures

Figure 1.1 Formation of a disulphide bond, taken from Berg et al. (2002).	28
Figure 1.2 Scanning electron micrograph of purified VP1LAC inclusion bodies, taken from Carrió et al., (2000).	32
Figure 1.3 A schematic showing the accessible states for a polypeptide chain following its synthesis. The population of these states and the interconversions are determined by the thermodynamic and kinetic stabilities. This is highly regulated by controlling the environment in the cell, and through the action of molecular chaperones, proteolytic enzymes and other factors.....	34
Figure 1.4 Chaperones involved in protein folding and disaggregation in <i>E.coli</i> . The DnaK system (DnaK, DnaJ, GrpE) and the chaperonins (GroESL) may assist the protein intermediates to reach their native structure. The small heat-shock proteins IbpAB bind misfolded proteins during aggregation and ClpB triggers the disaggregation process, in combination with there DnaK system, allowing refolding. Taken from Baneyx and Mujacic, (2004).....	36
Figure 1.5 The sequence of operations involved in an inclusion body process.....	41
Figure 1.6 Methods for solubilization and renaturation, taken from Clark, (2001).....	42
Figure 1.7 Operating frequency of the adaptive focused acoustics of the Covaris device compared to a sonicator.	48
Figure 1.8 The adaptive focusing acoustic (AFA) process. Bursts of ultrasonic acoustic energy are focused on a discrete area in the sample vial, allowing lysis without contact and less sample heating. The process is controlled by a computer which allows the duty cycle, intensity and duration of these bursts to be programmed and the automated treatment of multiple samples sequentially.	49
Figure 1.9 Schematic view of hen egg white lysozyme. The α -domain is shown in red and the β -domain in blue). Taken from (Radford et al., 1992b).....	52
Figure 1.10 Schematic of an averaged effective energy surface based on experimental results for lysozyme refolding. P is related to the configurational entropy of the system (the extent of accessible space available to the molecule), E is the averaged effective energy and Q is a progress variable corresponding to the number of native contacts. Three different possible trajectories are illustrated with coloured arrows. Yellow- the fast folding pathway, green- a slow folding pathway that must overcome a high energy barrier, and red- a slow folding pathway that must return	

to a less folded state before proceeding along the valley corresponding to the fast folding pathway. Taken from Dobson et al., (1998).....	53
Figure 1.11 The structure of human proinsulin, taken from Heath et al., (1992)	56
Figure 1.12 The structure of insulin lispro, taken from prescribing information for Humalog® available online (http://pi.lilly.com/us/humalog-pen-pi.pdf)	56
Figure 1.13 A schematic showing the early refolding stages of porcine insulin precursor (PIP), taken from (Yan et al., 2009).....	57
Figure 2.1 Photographs showing the external (A), internal view (B) and the software user interface (C) of the Tecan platform, demonstrating the containment of the whole bioprocess on one platform (with the exception of the AFA device).	68
Figure 2.2 Automated program structure, showing the main scripts on the left and sub-programs represented on the right.....	72
Figure 2.3 Diagram of microwell oxygen probe for k_{La} determination.....	83
Figure 3.1 The effect of different wavelengths on the absorbance profile of refolds in different buffers a) 280 nm, b) 340 nm and c) 600 nm.	97
Figure 3.2 The concentration of soluble protein during the course of a refold experiment at two different DTT concentrations (25 mM and 0.625 mM).	99
Figure 3.3 Absorbance at 600 nm over time during a refold with different redox couples, (○) DTT cystamine, (●) cysteine, cystine.....	101
Figure 3.4 Fluorescence over time for refolds at different redox potentials.....	103
Figure 3.5 Absorbance at 280 nm for refolds at different final protein concentrations. Standards of the same protein concentration as refold shown with best fit line. Standard deviations are shown for each point, which is an average of three experimental repeats.....	104
Figure 3.6 Fluorescence for refolds at different final protein concentrations.....	105
Figure 3.7 Activity for refolds at different final protein concentrations. Error bars represent averages of duplicate or triplicate refolds.	106
Figure 3.8 Schematic of automated refolding process and assays	108
Figure 3.9 Absorbance at 280 nm of refolds prepared manually compared with refolds prepared using an automated platform.	109
Figure 3.10 Fluorescence of refolds prepared manually compared with refolds prepared using an automated platform.	110
Figure 3.11 Activity of refolds prepared manually compared with refolds prepared using an automated platform.....	111

Figure 3.12 Schematic of proposed structure for hierarchical assays.....	113
Figure 3.13 Absorbance at 600 nm at three different redox potentials (oxidising, balanced and reducing) after refolding lysozyme for 24 h in static and shaking 96-deep square microwells.....	115
Figure 3.14 Relative fluorescence at three different redox potentials (oxidising, balanced and reducing) after refolding lysozyme for 24 h in static and shaking 96-deep square microwells.....	116
Figure 3.15 Activity at three different redox potentials (oxidising, balanced and reducing) after refolding lysozyme for 24 h in static and shaking 96-deep square microwells. Activity is expressed as a percentage of the activity of a native standard.....	117
Figure 3.16 Circular dichroism spectra of a high activity refold (–) and native active lysozyme (- -).....	119
Figure 3.17 Circular dichroism spectra of a low activity refold (–) and native active lysozyme (- -).....	120
Figure 3.18 Absorbance (600 nm) as a function of activity for lysozyme refolds. Aggregating samples (○), soluble samples (●) and cut-off line at 0.25 A.U. (- -).....	122
Figure 3.19 An activity measurement as a function of relative fluorescence for lysozyme refolds. Each point represents a triplicate or average of 9 data points. Aggregating samples (○), soluble samples (●) and cut-off lines at 0.83 and 1.02 A.U. (-).....	124
Figure 3.20 Absorbance (600 nm) as a function of activity for DHFR refolds. Each point represents a triplicate. Soluble refold samples, purified (●), unwashed (◆), washed (▲), and aggregated refold samples, purified (○), unwashed (◇), washed (Δ), and cut-off at 0.25 A.U. (- -).....	126
Figure 3.21 Activity measurements as a function of relative fluorescence for DHFR refolds. Each point represents a triplicate. Soluble refold samples, purified (●), unwashed (◆), washed (▲), and aggregated refold samples, purified (○), unwashed (◇), washed (Δ), and cut-off lines shown at fluorescence of 5110 and 7610 (–) and 2446 and 9962 (- -) A.U.....	128
Figure 4.1 Microscale Automated Bioprocess Sequence.....	133
Figure 4.2 Common Inclusion Body Bioprocess Sequence.....	134

Figure 4.3 20 L DHFR fermentations at different post induction temperatures. Induction time denoted by the line labelled I.....	136
Figure 4.4 20L Fermentation profile with early exponential induction, grown at 37°C. Figure a) shows the dissolved oxygen tension (DOT), dry cell weight (DCW) and impeller speed. Figure b) illustrates the oxygen uptake rate (OUR) and carbon dioxide evolution rate (CER).	138
Figure 4.5 SDS PAGE of 20 L Fermentation at 37 °C at different time points. Lanes:	139
Figure 4.6 Soluble and insoluble protein fractions during 20L fermentation at 37 °C measured by Bradford Assay	140
Figure 4.7 20L Fermentation profile with early exponential induction and a temperature drop to 25 °C.....	141
Figure 4.8 SDS PAGE of insoluble cell fraction from 20 L Fermentation with post induction temperature drop to 25 °C. Lanes contain the insoluble cell fractions for the following:	142
Figure 4.9 Comparison of growth at 37°C with no induction in microwell (fill volume 1 ml, shaking 1000 rpm) and 1L shake flasks (fill volume 100 ml, shaking 200 rpm)	144
Figure 4.10 Automated microwell fermentation at 37 °C, with induction at 4 hours using 0.125 mM IPTG, fill volume of 1 ml and shaking at 1000 rpm.....	145
Figure 4.11 Clarification of supernatant after removal of different volumes from the pellet.....	147
Figure 4.12 Cell losses during the microwell process for induced and non-induced cells, showing the cell concentration at fermentation harvest, in the broth removed after centrifugation, at the resuspension stage and the total cell loss from fermentation through to resuspension.	148
Figure 4.13 Protein release under different conditions, showing unlysed cells, cells treated with AFA in microwells for different lengths of time, sonicated cells and chemically lysed cells. The concentration of protein in soluble and insoluble cell fractions is determined by Bradford assay.....	150
Figure 4.14 SDS PAGE analysis of soluble and insoluble cell fractions of cell suspension exposed to sonication and different AFA (Covaris) treatment times in microwells. Lanes:	151

Figure 4.15 SDS PAGE analysis of soluble and insoluble fractions of cell suspension exposed to sonication, AFA (Covaris) and chemical lysis. Lanes:.....	152
Figure 4.16 SDS PAGE analysis of cell suspension exposed to sonication, AFA (Covaris) in vials and in microwells using different volumes. Lanes:.....	154
Figure 4.17 Protein release using AFA with different formats (microwell and vial) compared with sonication. The concentration of protein in soluble and insoluble cell fractions is determined by Bradford assay.	155
Figure 4.18 SDS PAGE analysis of cell suspension exposed to sonication and AFA in vials using different volumes. Lanes:	156
Figure 4.19 Protein release using AFA in vials with different volumes, compared with a control of no lysis. The concentration of protein in soluble and insoluble cell fractions is determined by Bradford assay.	157
Figure 4.20 Particle size distribution for material from a 20 L fermentation, determined using laser diffraction for intact cells. Whole cells and harvested IBs were compared with cells which had undergone different numbers of homogenisation passes at 500 bar in a Manton-Gaulin Lab 60 high pressure homogeniser.....	158
Figure 4.21 Fluorescence (525 nm emission) histograms (a) and light scatter plots (b) for intact (unruptured) cells from microwell DHFR fermentation, stained with SYTOX Green and measured for their fluorescence, particle size and granularity using a flow cytometer (see Section Error! Reference source not found. for method).	161
Figure 4.22 Fluorescence (525 nm emission) histograms (a) and light scatter plots (b) for isolated unwashed DHFR inclusion bodies produced by 20L fermentation, stained with SYTOX Green and measured for their fluorescence, particle size and granularity using a flow cytometer (see Section Error! Reference source not found. for method).....	162
Figure 4.23 Fluorescence (525 nm emission) histograms (a) and light scatter plots (b) for sonicated cells (see Section 2.2.5.3 for conditions) from a microwell DHFR fermentation, stained with SYTOX Green and measured for their fluorescence, particle size and granularity using a flow cytometer (see Section Error! Reference source not found. for method).....	163
Figure 4.24 Fluorescence (525 nm emission) histograms (a) and light scatter plots (b) for AFA treated (see Section 2.2.5.4) cells from microwell DHFR fermentation,	

stained with SYTOX Green and measured for their fluorescence, particle size and granularity using a flow cytometer (see Section 2.5.3 for method).	164
Figure 4.25 Protein concentration of insoluble and soluble fractions of centrifugation solids and supernatant, as using determined by Bradford assay.	165
Figure 4.26 SDS PAGE showing soluble and insoluble fractions of supernatant and solids discharge of the first centrifugation step (cell harvest) and second centrifugation step after homogenisation (IB harvest).....	166
Figure 4.27 SDS-PAGE showing the purification achieved for IBs harvested after different cell lysis methods. Lanes:.....	167
Figure 5.1 The activity of refolded DHFR under two different buffer conditions for washed and unwashed inclusion bodies, where buffer 1 (B1) is 0.288 mM cystamine, 10% v/v hexylene glycol, 20 mM ethanolamine, pH 10.5 and buffer 3 (B3) is 1M acetic acid pH 3.8.	174
Figure 5.2 The growth profile of <i>E. coli</i> during fermentation in microwells and induction by different concentrations of IPTG.	176
Figure 5.3 The production of DHFR under different induction regimes. DHFR concentration was determined by densitometry and purity from its relation to the total amount of protein determined by Bradford assay.	177
Figure 5.4 Refolding yield of unwashed IBs produced as a result of induction using 0.125, 0.25 and 0.5 mM IPTG. A) Refolded using buffer 1 or 3 and a diluting either 15 or 20 fold. B) Refolded using buffer 1 and 15 fold dilution. Measurements are an average of 3.	179
Figure 5.5 Refolding yield of washed IBs produced as a result of induction using 0.125, 0.25 and 0.5 mM IPTG and renatured using buffer 1 or 3. Measurements are an average of 3, with error bars too small to be discernible for the condition of 0.5 mM IPTG, buffer 3 and 20 fold dilution.....	181
Figure 5.6 Growth curves for <i>E. coli</i> induced at different times.....	183
Figure 5.7 DHFR concentration and purity under different induction regimes.....	183
Figure 5.8 Refolding yield of washed IBs produced as a result of induction at 3, 3.5, 4, 4.5 and 5 hours during fermentation and renatured using buffer 1 to achieve a 20 fold dilution. The averages of triplicate refolds are shown.....	184
Figure 5.9 Refolding yield of washed IBs produced as a result of induction at 3, 3.5, 4, 4.5 and 5 hours during fermentation and renatured using buffer 3 to achieve a 20 fold dilution. The averages of triplicate refolds are shown.....	185

Figure 5.10 Refolding yield of washed IBs produced by large scale fermentation, stored at -20 or -80 °C and renatured using 3 different buffers. The averages of triplicate refolds are shown.	186
Figure 5.11 Refolding yield of washed IBs produced by microscale fermentation, stored at -20 or -80 °C and renatured using 2 different buffers to give a final protein concentration of 0.02 mg.ml ⁻¹ . The averages of triplicate refolds are shown.	187
Figure 5.12 Growth profile for <i>E. coli</i> containing the insulin plasmid grown in shake flasks with no induction using two different media.	189
Figure 5.13 Growth profile for <i>E. coli</i> expressing insulin grown in microwells and induced at 10 h.	190
Figure 5.14 SDS PAGE of induced cells during fermentation. Lane 1 contains molecular weight ladder. Lane 2 and 3 are the soluble and insoluble fraction respectively of pre-induction cells. Lane 4 and 5 are the soluble and insoluble fraction respectively of cells 3 hours after induction. Lane 6 and 7 are the soluble and insoluble fraction respectively of cells 7.5 hours after induction. Lane 8 and 9 are the soluble and insoluble fraction respectively of cells harvested after 11 hours. Lane 10 and 11 are the soluble and insoluble fraction respectively of non-induced cells harvested after 11 hours. Lane 12 contains a Humalog insulin standard. ...	191
Figure 5.15 Growth profile for insulin expressing <i>E. coli</i> grown in microwells and induced at 3.5, 4, 4.5 and 5 hours. Feeding commences at 5 h hours.	192
Figure 5.16 Acetate concentration at harvest under different induction conditions (induction at 3.5, 4, 4.5 and 5 hours)	193
Figure 5.17 Inclusion bodies from fermentations induced at different time points and refolded in buffer 1. A) Absorbance at different wavelengths. B) Intrinsic fluorescence and yield.	195
Figure 5.18 Inclusion bodies from fermentations induced at different time points refolded in buffer 2. A) Absorbance at different wavelengths. B) Intrinsic fluorescence and yield.	197
Figure 5.19 Growth profile for <i>E. coli</i> expressing insulin grown in microwells and induced at 6 h. Feeding commences at 5 h for fed-batch fermentation.	199
Figure 5.20 Acetate concentration at harvest for batch and fed-batch fermentations..	199

Figure 5.21	Inclusion bodies from batch and fed-batch fermentations refolded in acetic acid buffer 3. A) Absorbance at different wavelengths. B) Intrinsic fluorescence and yield.....	201
Figure 5.22	Inclusion bodies from batch and fed-batch fermentations refolded in buffer 2. A) Absorbance at different wavelengths. B) Intrinsic fluorescence and yield.	204
Figure 5.23	Growth profile for <i>E. coli</i> expressing insulin grown in microwells and induced at 3.5 h. Cells are grown in 4 different medias: Luria Bertani (LB), Terrific Broth (TB), glycerol based complex media and glucose based complex media.....	206
Figure 5.24	Acetate concentration and final pH at harvest for cells fermented in different medias, grown in microwells.....	207
Figure 5.25	Inclusion bodies from fermentations in 4 different medias refolded in buffer 2. A) Absorbance at different wavelengths. B) Intrinsic fluorescence and yield.....	208
Figure 5.26	Yield as a function of relative fluorescence for insulin refolds. Each point represents a duplicate (yield measurements) or triplicate (fluorescence measurements). Cut-off lines at 10500 and 35000 Fl.U. (– –).....	209
Figure 6.1	$K_L a$ determined in large scale fermenter with 70L of media and at varying impeller speeds. Points were fitted to an exponential growth curve with the equation $y = (0.6542(e^{(0.0018x)} - 1)/0.0018) - 47.6714$	218
Figure 6.2	Growth profiles showing the optical density, wet and dry cell weight for 100 L fermentation with cascade control and enriched oxygen.....	221
Figure 6.3	Fermentation trace of the dissolved oxygen (pO_2), pH, respiratory quotient (RQ), and volume of acid, base and antifoam added.	221
Figure 6.4	Growth profiles showing the optical density, wet and dry cell weight for 70 L fermentation with a Reynolds number of 132,000.	223
Figure 6.5	Fermentation traces of 1) dissolved oxygen (pO_2), pH, inlet oxygen concentration, stirrer speed and airflow rate. 2) Volume of acid, base and antifoam added. 3) respiratory quotient (RQ), carbon dioxide evolution rate (CER) and oxygen uptake rate (OUR).	225
Figure 6.6	Growth profiles showing the optical density, wet and dry cell weight for 70 L fermentation with a Reynolds number of 215,000.	226

Figure 6.7	Fermentation traces of A) inlet oxygen concentration, stirrer speed, dissolved oxygen (pO_2), pH and airflow rate. B) respiratory quotient (RQ), carbon dioxide evolution rate (CER) and oxygen uptake rate (OUR).....	227
Figure 6.8	Measured k_{La} values in a 96 DSW plate as a function of shaking speed with a shaking diameter of 3 mm and fermentation media, plus additions and no antifoam. Error bars are shown for an average of 3 measurements per data point	229
Figure 6.9	Measured k_{La} values in a 96 DSW plate as a function of fill volume for fermentation batch media and 0.02% antifoam (PPG). Error bars are shown for an average of 3 measurements per data point.	229
Figure 6.10	Growth profile showing the optical density of the microscale batch fermentation with a fill volume of 1 ml and a shaking speed of 1000 rpm.	231
Figure 6.11	Refolding washed and unwashed inclusion bodies from the first fermentation in buffer 1 and 2 at different scales.	234
Figure 6.12	Refolding washed and unwashed inclusion bodies from the first fermentation in buffer 1 and 2 at different scales, with yield determined from concentration of fully solubilised protein as tested by HPLC method	234
Figure 6.13	The effect of fermentation conditions on yield after refolding at the microscale washed inclusion bodies in two different buffers. F1: Fermentation with cascade control and enriched oxygen and a maximum impeller speed of 700 rpm. F3: Fermentation at the high k_{La} matched condition, with a constant impeller speed of 450 rpm. Buffer 1 0.288 mM cystamine, 10% v/v hexylene glycol, 20 mM ethanolamine, pH 10.5. Buffer 2 10 mM Tris, 10 mM glycine, 1 mM EDTA, 0.5 mM cysteine, 4.5 mM cystine, pH 10.5.	236
Figure 6.14	Maximum yields obtained from refolding at the microscale IB material from the fermentations. Maximum conditions for each of the fermentation conditions are as follows, F1: washed IB, buffer 1, 0.1 $g.L^{-1}$. F3: washed IB, buffer 1, 0.15 $g.L^{-1}$. Microscale fermentation: unwashed IB in buffer 2.	238
Figure 6.15	Purity of active protein in 200 ml refolds for the different large scale fermentations, with different IB washing regimes and refold buffers. Refolds used material solubilised at a concentration of 1.5 $g.L^{-1}$ and an 18 fold dilution factor. F1: Fermentation with cascade control and enriched oxygen and a maximum impeller speed of 700 rpm. F3: Fermentation at the high k_{La} matched condition, with a constant impeller speed of 450 rpm.	240

Figure 6.16 Yield as a function of purity for refolds at the 200 ml scale with varying refold conditions (IB washing, buffer, dilution factor, final protein concentration).	241
Figure 6.17 The refolding yield of IB material from the first fermentation (cascade control and enriched oxygen) and the high k_{La} fermentation. For details of each refolding condition see Table 6.2.....	242
Figure 9.1 Absorbance of denatured and native protein in different buffers and at different concentrations.....	270
Figure 9.2 Fluorescence intensity fluctuations with temperature	271
Figure 9.3 Calibration Curve for conversion between dry cell weight and OD. Best fit line: $y=0.394x+0.32$	272
Figure 9.4 Calibration curve for conversion between wet cell weight and OD. Best fit line: $y=2.620x +10.566$	272
Figure 9.5 Relative fluorescence of unstained inclusion bodies determined using flow cytometry.....	273
Figure 9.6 Relative fluorescence of stained inclusion bodies determined using flow cytometry.....	273
Figure 9.7 Relative fluorescence of unstained whole cells determined using flow cytometry.....	274
Figure 9.8 Relative fluorescence of stained whole cells determined using flow cytometry.....	274
Figure 9.9 Dry cell weight calibration curve	276
Figure 9.10 Inclusion bodies from fermentations in 4 different medias refolded in buffer 3. A) Absorbance at different wavelengths. B) Intrinsic fluorescence and yield.....	277
Figure 6.9.11 Fermentation trace of the stirrer speed, dissolved oxygen (pO_2), oxygen uptake rate (OUR), carbon evolution rate (CER), oxygen saturation in air inlet (Inlet_ O_2) and airflow rate (AIRFL)	279
Figure 6.9.12 A summary of the yield and purity results of the 200 ml refold conditions detailed in Table X.....	280
Figure 6.9.13 A summary of the yield of the microscale refolds of the large scale fermentation material	280
Figure 6.9.14 DOT profiles for different shaking speeds of 800, 700, 600 and 500 rpm	281

Figure 6.9.15 The acid, base and antifoam additions of the higher $k_L a$ fermentation .282

List of Tables

Table 2.1 Lysozyme refold buffers	62
Table 2.2 Denatured protein and refold buffer conditions	63
Table 2.3 Refold buffers and DTT concentration in denatured protein to give different redox potentials	64
Table 2.4 Refold buffers used for lysozyme	65
Table 2.5 Refold buffers used for DHFR.....	75
Table 2.6 vLB Basal Media	76
Table 2.7 Trace metals composition	77
Table 2.8 Media composition for all three fermentations. Concentrations shown are per litre of media.	77
Table 2.9 Media composition for Terrific Broth (TB) pH 7.2	80
Table 2.10 Feed solution	80
Table 2.11 Medium composition for batch versus fed batch comparison experiment pH 7.0.....	80
Table 2.12 Fermentation conditions.....	81
Table 2.13 Insulin refold buffers.....	81
Table 3.1 Lysozyme refold buffers for 3.3.1.1 Selection of wavelengths for aggregation detection and solubility, 3.3.1.2 Absorbance changes during refolding and buffer 2 and 3.3.1.4 Example of end point analysis	92
Table 3.2 Denatured protein and refold buffer conditions for 3.3.1.2 Absorbance changes during refolding.....	93
Table 3.3 Refold buffers and DTT concentration in denatured protein to give different redox potentials, as used in 3.3.1.3 Fluorescence changes during refolding and 3.3.3.1 Oxidation.....	93
Table 3.4 Refold buffers used for 3.3.4 Hierarchical assays using lysozyme	94
Table 3.5 Refold buffers used for DHFR.....	94
Table 4.1 Cell growth at harvest (8 hours of fermentation).....	135
Table 4.2 Clarification achieved for supernatant fraction after centrifuging microplate at 4000 rpm	146
Table 5.1 Conditions used during microscale DHFR fermentations	171

Table 5.2 DHFR refold buffers	171
Table 5.3 Fermentation conditions.....	172
Table 5.4 Conditions used during microscale insulin fermentations	172
Table 5.5 Summarised optimal conditions for a high yield of active DHFR.....	188
Table 5.6 Fermentation titre as determined by HPLC and dry cell weight.....	202
Table 5.7 Summarised optimal conditions for a high yield of active insulin	210
Table 6.1 Fermentation conditions.....	214
Table 6.2 Refold conditions for 200 ml dilution refolding. Fermentation material 1: 100 L fed batch fermentation with cascade control with enriched oxygen, 3: 70 L batch fermentation at 475 rpm. Refold buffer 1: 0.288 mM cystamine, 10% v/v hexylene glycol and 20 mM ethanolamine, 2: 10 mM Tris, 10 mM glycine, 1 mM EDTA, 0.5 mM cysteine, 4.5 mM cystine.	215
Table 6.3 K_{La} values determined with a fill volume of 1 ml and shaking speed of 1000 rpm using Equation 1.	216
Table 6.4 K_{La} values determined with different fill volumes of a 146.5 L fermenter at different impeller speeds using Equation 2.....	217
Table 6.5 Experimentally predicted k_{La} based on regression shown in Figure 6.1	218
Table 6.6 Comparison of growth characteristics and titre for the fermentation conditions studied.	232

1 Introduction

1.1 *The context of the research*

Biopharmaceuticals are products consisting of (glyco)proteins, which include recombinant therapeutic proteins, monoclonal antibodies and nucleic acid based medicinal products (Crommelin et al., 2003). They now represent one in four of new molecular entities reaching the market, generating €30 billion in sales annually. Approximately 160 biopharmaceuticals have been approved for clinical use (Walsh, 2005) and some of these have revolutionized the traditional treatment of many diseases (Schellekens, 2002). These biological products introduce new challenges due to their complex conformational structure that is easily disrupted in comparison to traditional low molecular weight chemicals (Crommelin et al., 2003). Consequently, their performance relies on strict production protocols in both upstream and downstream processing, as a number of factors are thought to influence biopharmaceuticals immunogenicity (Schellekens, 2002). The manufacturing process has to be designed to consistently deliver a product with the necessary quality attributes. This requires extensive process characterisation during process development, which usually involves evaluating a wide range of process parameters (Rathore et al. 2007).

Microscale processing techniques involve the study of unit operations at the microlitre scale (20-2000 μ l) using microwell or microfluidic formats (Micheletti and Lye, 2006) to predict the performance of individual bioprocess unit operations at larger scale. It offers the potential to speed up process development, reduce development costs and deliver new drugs to the market quicker. In particular the study of bioprocess unit operations in microwell plate formats and the use of automation can significantly enhance experimental throughput and facilitate the parallel evaluation of a large number of process conditions (Jackson et al., 2006; Nealon et al., 2006). The majority of microscale studies have focused on microbial fermentation, whilst comparatively little work has addressed downstream processing operations. This potential bottleneck requires considerable attention if significant step-wise process enhancements are to be gained. In particular the impact of fermentation conditions on whole process performance must be understood in order to prevent downstream processing from becoming rate limiting (Micheletti and Lye, 2006). The refolding of recombinant

protein from inclusion bodies (IB) represents a specific example that could greatly benefit from this approach. During heterologous expression in a host organism, inclusion bodies can form which contain a high concentration of very pure therapeutic protein. The inclusion bodies represent a high yielding system with an easily isolated high purity product (albeit in an aggregated form that requires refolding). However protein refolding yields at industrially relevant concentrations are restricted by aggregation of protein upon the initiation of dilution refolding. A number of studies have investigated chemical (Buswell and Middelberg, 2002; Mannall et al., 2007) as well as physical (Mannall et al., 2006) factors affecting the dilution refolding in small (20-200ml) bioreactors. However, for the majority of proteins a large number of refold conditions usually need to be tested in order to optimize this processing step. The use of microwell plates as a format in which to perform protein refold experiments has been preliminary investigated and initial scalability between microwell and bench scale operation has been demonstrated (Mannall et al., 2009). Microwell refolding allowed a significant amount of information to be gained in a short period of time using a small amount of the valuable IB-derived protein. In this project the automated microwell approach will be developed for the rapid optimization of the protein refolding step by: 1) adopting a whole process approach to optimization which investigates the effect of fermentation conditions on subsequent refolding yields and product quality 2) establishing the automation of the refolding step, both in terms of liquid handling operations and associated analytical methods, to speed up the investigation of multiple variables under different mixing conditions.

1.1.1.1 Literature survey

The following review is concerned with the current understanding of inclusion bodies as a result of over expression in *Escherichia coli* (*E. coli*). Protein folding is discussed in general terms for the refolding step and also in the *in vivo* context, describing the factors involved with IB formation. Particular attention is paid to the key factors and fermentation conditions leading to IB formation over soluble protein. The role of inclusion bodies in industry is also discussed, along with the use of microscale bioprocessing methods and how these could be used to speed up development. Lastly, some background information is provided on the protein systems studied.

1.1.2 *Escherichia coli* as an expression system

Advances in molecular biology and directed evolution techniques, coupled with the human genome project, have led to an increasing interest in the efficient production of genetically engineered proteins. The most widely used prokaryote for genetic manipulations and industrial production is the enteric bacterium *Escherichia coli* (*E. coli*) (Ferrer-Miralles et al., 2009). *E. coli* is a highly versatile host organism and it has been extensively used to achieve protein expression rapidly and economically. Its long history as a model system means that extensive knowledge of its genetics is currently available. There is a diverse range of tools for chromosome engineering, gene cloning and expression vectors, allowing the creation of mutant strains (Baneyx and Mujacic, 2004). Additionally *E. coli* metabolism is well studied, which has allowed studies on the optimisation of media and culture conditions due to its relatively simple nutritional requirements (Kolaj et al., 2009). *E. coli* grows on inexpensive carbon sources and its ability to rapidly accumulate biomass make it amenable for high cell density fermentation and scale-up (Ferrer-Miralles et al., 2009). *E. coli* is typically selected for expression if the heterologous protein does not require post-translational modifications and is produced in soluble form. However over expression of the protein can occur, resulting in a protein with an incorrect conformation. The misfolded protein can then form insoluble aggregates called inclusion bodies (Ferrer-Miralles et al., 2009). Additionally product loss due to membrane leakiness and cell lysis have been reported, leading to further yield reductions (Kolaj et al., 2009). However *E. coli* continues to be an important host system with new strains being developed that allow post translational modifications (Wacker et al., 2002), improved strategies for soluble expression using folding chaperones (Marco, 2007), and progress towards disulphide bond formation and extracellular excretion (Makrides, 1996).

1.1.3 Protein structure and folding

1.1.3.1 General overview

Proteins are constructed from a repertoire of 20 amino acids, linked by peptide bonds. The folding of a chain of amino acids to form the native conformation is a complex process with four levels of structure involved. The sequence of amino acids forms the primary structure of the protein and confers the three dimensional structure of a protein, as demonstrated by Anfinsen (1973) with the spontaneous refolding of denatured

ribonuclease. The polypeptide chain folds to give a secondary structure as a result of the formation of hydrogen bonds that give regular structures such as an alpha helix, a beta sheet, turns and loops. These secondary structure domains come together, giving the overall conformation of the polypeptide protein its tertiary structure. The polypeptide folds so that the hydrophobic side chains are buried in the centre and the polar charged chains are on the surface of the protein. The compact globular structure is stabilized by non-specific hydrophobic interactions between non-polar side chains, specific hydrogen bonds between polar side chains and salt bridges (Dill et al., 2008). The tertiary structure also includes the formation of disulphide bonds, which involves the oxidation of a pair of cysteine residues to give a pair of cystines (Figure 1.1). As these interactions are weak the polypeptide maintains some flexibility, which is important for the function and regulation of the protein. For multimeric proteins a further stage requiring the formation of quaternary structure is required, where subunits interact to form the final structure (Berg et al., 2002).

Figure 1.1 Formation of a disulphide bond, taken from Berg et al. (2002).

1.1.3.2 Folding- a search for a low energy conformation

Folding is known as an “all or nothing” process as half-folded protein is thermodynamically unstable and only exists transiently (Berg et al., 2002). The folding of proteins is highly co-operative due to their thermodynamic properties. In order for proteins to find their native confirmation they utilise cumulative selection, rather than a random search method. This is because partly folded intermediates are retained and interactions with other local regions result in them adopting their preferred structure,

progressively stabilising the structure. A partially folded polypeptide chain is flexible and fluctuations in the conformation allow amino acids far apart in sequence to come into contact. Native-like interactions are more on average more stable, and consequently are favoured over less stable non-native interactions, and therefore retained. This search mechanism drives the search in the direction of the lowest energy structure, the native state, and ensures that only a very small fraction of the possible conformations needs to be sampled (Dobson, 2004b).

1.1.3.3 Mechanisms of folding

Studies using site-directed mutagenesis to map the free energy of a polypeptide chain as a function of its conformational properties suggest that the fundamental method of folding for small molecules involves “nucleation-condensation”. This is the formation of a folding nucleus consisting of a few key residues around which the rest of the structure condenses (Fersht, 2000). It has been observed that a key feature of the transition state in some proteins is that it has the same overall topology of the native fold. Despite having a highly disordered structure, the interactions of the key core residues force the polypeptide chain to adopt a native-like architecture. The creation of the correct topology in the transition state invariably leads to the creation of the native structure during the final stages of folding.

Larger proteins (greater than 100 residues) on the other hand fold by a slightly different mechanism. This generally involves passing through one or more partially folded intermediates before the native state is reached. Studies of these intermediates using near-UV CD, far-UV CD and NMR suggest that larger proteins fold in modules. This means that they largely fold independently to form segments or domains (Panchenko et al., 1996; Ellis and Minton, 2003; Khan et al., 2003). As with smaller proteins, the native-like fold within these local regions forms from the interaction of key residues. Once this structured domain is created, other key residues interact with independent regions of structure to assemble into the correct overall fold.

1.1.3.4 Timescale of folding

The secondary structure affects the rate of protein folding. It has been observed that individual α -helices can fold in 100 ns and β -turns in circa 1 μ s (Eaton et al.; Snow et al., 2002). Small helical bundles have been observed to fold in less than 50 μ s, and the

“speed limit” for simpler proteins has been estimated a tenth of this time (Mayor et al., 2003; Yang and Gruebele, 2003). However proteins that contain an extensive β – structure take several orders of magnitude longer to fold. The stability also influences the folding rate of small proteins due to the contact order, the average space in terms of sequence between residues in contact in the native structure. The process of a stochastic search is more efficient if the nucleus forming residues are close together in sequence, and hence folding occurs faster. However, the most important factor affecting the folding is thought to be the sequence of amino acids and the pattern of hydrophilic and hydrophobic residues.

1.1.3.5 Folding *in vivo*

The interior of a cell is a crowded environment where the concentration of macromolecules is approximately 300-400 mg.ml⁻¹ (Ellis and Minton, 2003). One protein chain is released from the ribosome every 35 seconds (Lorimer, 1996). This represents two main challenges for *in vivo* folding. Firstly undesirable interactions with other cell components in the crowded interior must be avoided as it will prevent the formation of a folded structure. Chaperones and enzymes are used to prevent aggregation or misfolding. Chaperones favour the formation of on-pathway folding species by shielding interactive surfaces of partially folded protein (Baneyx and Mujacic, 2004). The second challenge is the slow steps involved in protein folding. These rate limiting steps are overcome by folding catalysts such as peptidyl proline isomerase and protein disulphide isomerase, which accelerate peptide and disulphide bond formation respectively.

In conclusion, proteins are not searching randomly for the correct native conformation, but are driven by a decrease in free energy. Fluctuations in the polypeptide allow amino acids distant in sequence to interact, and when these interactions are native-like, they are more likely to be retained. Once the key residues of the folding nucleus have formed the correct interactions, the polypeptide chain is forced to form a native-like overall fold and the transition state is formed. This state then leads to the creation of the native state, as the highly disordered structure folds and condenses around the folding nucleus.

1.1.4 Inclusion Bodies

1.1.4.1 Structure

Inclusion bodies (IBs) are commonly found in the cytoplasm of bacteria, but they have also been reported to form in the periplasmic space (Georgiou et al., 1986; Bowden and Georgiou, 1990). They consist of refractile, dense aggregates of insoluble misfolded protein that are less than 2 μ m long (Carrió et al., 2006). Despite their dense nature, analysis has shown that they have a porous structures with a high level of hydration (Taylor et al., 1986a). Proteolytic digestion studies have shown inclusion bodies are non-homogeneous structures where more than one protein species may coexist with different protease susceptibility (Carrió et al., 2000). Scanning electron microscopy and kinetic analysis studies of tryptic digests have revealed the formation of clustered sub-unit structures (Carrió et al., 2000), possibly resulting from the IB construction process. A high level of secondary structure and native-like structure can also exist in inclusion bodies (Oberge et al., 1994). . Inclusion bodies share some of the properties of amyloid fibrils, such as the presence of additional β -structure not observed in the native state (Villaverde and Carrió, 2003). A decrease in alpha-helix content of the protein, and an increase in beta-sheet conformation, has also been reported in IB when compared to the native protein structure (Przybycien et al., 1994). These elements of native-like structure, in conjunction with the high porosity of inclusion bodies could help explain the enzyme activity observed in some cases of IB forming enzymes, although contamination with active native during purification cannot be completely ruled out (Carrió and Villaverde, 2002). Different morphologies have also been reported, with some inclusion bodies forming rod shaped particles (Carrió et al., 2000), whilst others having an ovoid shape (Bowden and Georgiou, 1990). In addition, the topology may vary from rough to smooth (Bowden and Georgiou, 1990); however this may result from the different recombinant protein studied.

1.1.4.2 Composition

The major component of inclusion bodies in recombinant *E. coli* cells is the target protein. The amount of protein varies, but it is thought to be in the range of 50 to 95% of the total protein (Valax and Georgiou, 1993). Additionally other contaminants are also present such as protein and phospholipids. Some of these contaminants are derived from an incomplete purification process and the unspecific co-precipitation of unrelated

polypeptides (Carrió and Villaverde, 2002). Other contaminants can be incorporated *in vivo* during the growth of the inclusion body, such as folding chaperones. The small heat shock proteins IbpA and IbpB are involved in protein folding and cell survival under thermal stress and are common components of IBs. Other chaperones, DnaK and GroEL have also been reported to be present in inclusion bodies (Allen et al., 1992) as well as ribosomal components and translation factors (Kane and Hartley, 1988). However it is not yet understood if these chaperones are trapped during the growth of the inclusion body or if they play a role in the construction and deconstruction process.

Figure 1.2 Scanning electron micrograph of purified VP1LAC inclusion bodies, taken from Carrió et al., (2000).

1.1.4.3 Factors causing IB formation

Inclusion bodies are thought to form from the aggregation of partially folded intermediates as a result of the competition between folding and aggregation. A relatively high concentration of unfolded protein in the cell during the production of recombinant protein results in a “crowding effect” where intrachain interactions compete with intermolecular interactions. However not all non-secreted proteins form inclusion bodies. Some factors contributing to their formation (Fahnert et al., 2004b) are:

- **Post-translational folding:** When a eukaryotic protein is produced in a prokaryotic host instead of folding happening co-translationally, as in eukaryotes, it occurs post-translationally.
- **Glycosylation:** In a prokaryotic host, glycosylation is absent. Glycosylation often improves solubility and it is necessary for the folding of some proteins.
- **Disulphide bond formation:** The cytoplasm of prokaryotes, where disulphide bonds form in the host, is reducing. In eukaryotes disulphide bonds form in the oxidising environment of the endoplasmic reticulum (ER) which is a more favourable environment.
- **Number of cysteine residues:** Mammalian proteins that are cysteine rich are reported to be more difficult to express in *E. coli* in their soluble form.

The formation of inclusion bodies appears to be structure and therefore sequence dependent. Sequence modifications have been used to increase solubility during production or improve in vitro refolding yields (Rinas et al., 1992). In order to reduce aggregation of over expressed recombinant protein and combat inclusion body formation many parameters have been explored such as gene dosage, promoter strength, mRNA stability, codon usage, culture temperature, protein and genetic engineering and over expression of folding modulators to obtain soluble expression protein in *E. coli* (Martínez-Alonso et al., 2009).

1.1.5 Misfolding and Aggregation

A polypeptide chain can adopt a range of different states, as illustrated in Figure 1.3. The state adopted depends on the relative thermodynamic stabilities of these different states and the kinetics that govern their conversion between states (Dobson, 2004b). For example, concentration is a critical parameter in the formation of aggregates or oligomers. The conformations accessible are also regulated by the action of molecular chaperones and degradation mechanisms (Dobson, 2004a). Biological systems exploit the many states available in order to generate specificity and control the cellular environment. The outcome of *in vivo* folding is determined by the rate of protein synthesis, growth conditions, interactions with cellular components, and the folding pathway for that particular protein (Valax and Georgiou, 1993).

Misfolding has been described as “processes that result in a protein acquiring a sufficient number of persistent non-native interactions to affect its overall architecture and/or its properties in a biologically significant manner” (Dobson, 2004b), for example an intermediate with non-native topology. Misfolding may result from the newly synthesized chain failing to fold to the native conformation, premature termination of translation or loss of structure due to environmental stress (Baneyx and Mujacic, 2004). Heterologous protein expression can lead to misfolding as, in addition to these factors, the use of strong promoters and high inducer concentrations results a in high protein concentration *in vivo*. The inability of *E. coli* to provide the post translational modifications required for the folding of some proteins, such as the formation of disulphide bonds, introduces further challenges.

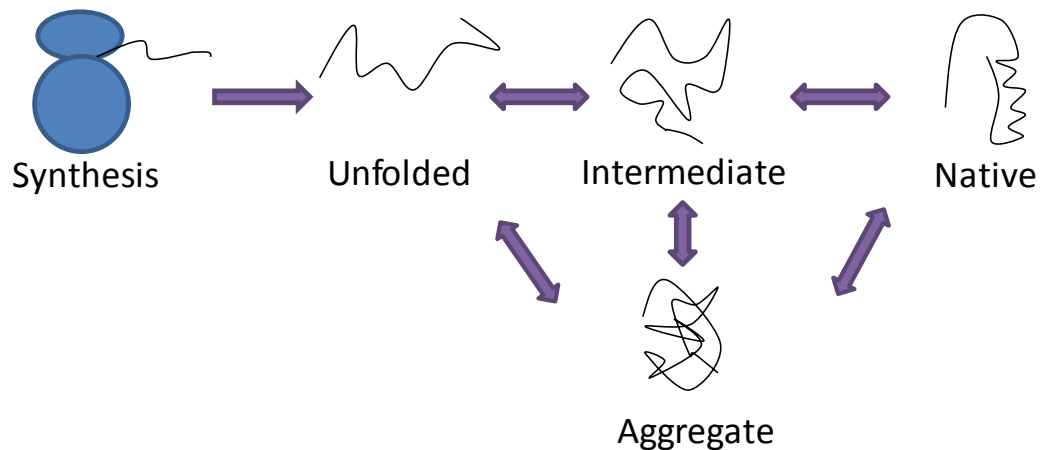


Figure 1.3 A schematic showing the accessible states for a polypeptide chain following its synthesis. The population of these states and the interconversions are determined by the thermodynamic and kinetic stabilities. This is highly regulated by controlling the environment in the cell, and through the action of molecular chaperones, proteolytic enzymes and other factors.

Misfolding is not uncommon for host cell proteins, and consequently cells have evolved mechanisms that favour *de novo* protein synthesis, refold partially folded protein, dissolve aggregates and dispose of irretrievably damaged protein (Baneyx and Mujacic, 2004). Protein folding *in vivo* is aided by molecular chaperones and foldases. Chaperones help the protein to escape metastable and misfolded states that occur during the folding process (Vendruscolo and Dobson, 2005). They interact transiently with unfolded and partially folded intermediates, and shelter the exposed hydrophobic patches to prevent them interacting inappropriately (Kopito, 2000). Folding chaperones

can be divided into three functional classes. Firstly there are folding chaperones which use conformational changes driven by ATP to refold or unfold the protein; in this category are DnaK-DnaJ-GrpE (Hsp70-Hsp40) and GroEL-GroES (Hsp60- Hsp10) systems. Secondly there are holding proteins, small heat shock protein (IpbAB), which act as a holding system passively stabilizing partially folded protein until folding chaperones become available. The third class are disaggregating chaperones, such as ClpB in *E. coli*, which undergo ATP fuelled conformational changes to solubilise aggregates and transfer partially folded protein to folding chaperones for refolding (Baneyx, 2004). Foldases on the other hand are enzymes which catalyse rate limiting reactions in the folding pathway, such as the *cis trans* isomerisation of peptidyl-prolyl bonds by peptidyl-prolyl isomerases and the formation and isomerisation of disulphide bonds by oxidoreductases (Baneyx, 1999; Miot and Betton, 2004). The final components of these systems are proteases, which degrade irreparably damaged proteins. Aggregation *in vivo* is controlled by the chaperones DnaK and GroEL. Studies also indicate that ClpB may play a large or moderate role as it binds preferentially to the hydrophobic surface of aggregated proteins (Ventura, 2005).

Figure 1.4 Chaperones involved in protein folding and disaggregation in *E.coli*. The DnaK system (DnaK, DnaJ, GrpE) and the chaperonins (GroESL) may assist the protein intermediates to reach their native structure. The small heat-shock proteins IbpAB bind misfolded proteins during aggregation and ClpB triggers the disaggregation process, in combination with there DnaK system, allowing refolding. Taken from Baneyx and Mujacic, (2004).

1.1.5.1 The role of inclusion bodies

Protein aggregates do not usually accumulate in an unstressed cell due to the quality control mechanisms present. However when a cell is being used for the recombinant expression of protein, the over expression of the plasmid encoding genes acts as a form of artificial stress and redirects the metabolism of the cell towards the production of the specific target protein. This triggers a variety of stress responses (stringent, SOS, heat shock) and the transcription of other sets of stress genes (Villaverde and Carrió, 2003), leading to protein accumulating as inactive and insoluble aggregates (IBs), instead of remaining as soluble active protein. This mechanism may have evolved to reduce the potential toxicity of polypeptides with partially exposed hydrophobic patches which could interact with cellular machinery, thereby playing a cellular protective role (Ventura, 2005). Inclusion bodies could also act as a transient store of incorrectly folded polypeptides during stress conditions, which can later be further processed by refolding or proteolysis (Villaverde and Carrió, 2003). Carrió and Villaverde (2001) showed that inclusion bodies are not inert protein aggregates but transient deposits, resulting from an imbalance between *in vivo* protein aggregation and solubilisation. When protein synthesis is arrested, the equilibrium is displaced back towards protein refolding.

1.1.5.2 The mechanism

A range of proteins are incorporated into inclusion bodies; small, large, multimeric or monomeric. The amount of secondary structure and disordered structure varies between proteins. Studies using attenuated total reflectance FTIR have shown an increase in β -structure in inclusion bodies, relative to the native conformation (Ventura, 2005). Other FTIR studies have also suggested that β -sheet like interactions are involved in aggregation and inclusion bodies contain newly formed β -sheet which are tightly packed by hydrogen bonds providing stability (Carrió et al., 2005).

Inclusion body formation was initially considered a non-specific process resulting from non-native interactions between hydrophobic patches on the surface of unfolded or partially unfolded conformations such as folding intermediates. However recent work suggests aggregation in bacterial inclusion bodies is a specific event (Ventura, 2005). There are usually only one or two inclusion bodies per cell. This low number suggest

inclusion bodies grow in a nucleation-like mechanism from a reduced number of “founder” aggregates (Ventura, 2005). The specificity of protein aggregation during refolding has been investigated by refolding mixtures of P22 tail spike and coat polypeptide chains. When the partially folded intermediates of the two are mixed together *in vitro*, they independently self-associate and no co-aggregation occurs, despite them both forming inclusion bodies when expressed individually with bacteria (Speed et al., 1996).

1.1.5.3 Fermentation conditions influencing IB formation

A number of process parameters influence inclusion body formation. They include media composition, growth temperature, the production rate (which results from a multitude of factors such as gene dosage, codon usage, promoter strength, mRNA stability) and the availability of heat shock chaperones in the cell (Strandberg and Enfors, 1991; Carrió and Villaverde, 2002; Ventura and Villaverde, 2006). During fermentation several conditions can be manipulated in order to promote solubility, but the operational range of these process variables are limited as a means to provide a completely soluble product. The following cultivation conditions increase the likelihood of inclusion body formation (Schein and Noteborn, 1988; Wang et al., 1999; Choi et al., 2000; Fahnert et al., 2004b):

- High temperatures
- High cell density
- High concentration of inducer
- Short induction time (2-5hrs)
- Complex media

The above conditions influence the aggregation kinetics by varying the protein concentration in the cell, synthesis rate or, in the case of high temperatures, by crossing the thermodynamic threshold needed for intermolecular interactions. In addition to the cultivation conditions, other factors such as a strong promoter or large plasmid copy number result in an increased protein synthesis rate which overwhelms cellular folding machinery resulting in aggregation (Fahnert et al., 2004a). Some methods are available to reduce aggregation in order to optimise the production of a soluble active protein

Such methods include cultivation at low temperatures, limited induction times, fusion to solubilising partners, co-expression of chaperones and foldases.

1.1.6 Inclusion bodies in industry

Protein synthesis in a recombinant host allows the production of high concentrations of target protein in a short space of time. However proteins can fail to reach the native conformation due to the corresponding increase in aggregation, the availability of chaperones and the necessity for post translational modifications. This leads to the protein either being deposited into inclusion bodies or degraded (Baneyx and Mujacic, 2004).

1.1.6.1 The advantages of inclusion body production

The numerous factors involved with *in vivo* folding means the optimisation of soluble protein expression is usually a time consuming and unpredictable process, and consequently soluble expression may be difficult to achieve. Additionally there are considerable advantages to expressing protein as insoluble inclusion bodies that make their formation desirable for some products.

1. The expression levels are often high, resulting in a large amount of protein present. Yields of around 30% of the total cellular protein content and approximately 8.5 g.L⁻¹ have been reported in an *E. coli* with transient over expression and a high cell density (Li et al., 2004).
2. Inclusion bodies are a highly enriched source of protein product, with 40-50% of the target protein present (Buswell et al., 2002).
3. Proteins are protected from proteolytic degradation as they are trapped in insoluble aggregates. This increased protein stability results in less product loss via degradation by host cell enzymes.
4. Inclusion bodies can be easily separated from soluble and insoluble contaminants using centrifugation due to their density difference (Buswell et al., 2002). This reduces the number of purification steps required, increasing the overall yield. Additionally, inclusion bodies can also be easily separated from soluble contaminants using filtration or size exclusion chromatography.

5. If the expressed protein is toxic or lethal to the cell, the formation of inactive inclusion bodies protects the cells from this affect, increasing viability and the yield of the target protein.
6. The optimisation of a refolding step (to convert the insoluble inactive inclusion to soluble native protein) involves a limited number of parameters, whereas optimisation *in vivo* to achieve soluble product can be far more complicated (Fahnert et al., 2004b).

Production in inclusion bodies does have some disadvantages however, the major one being the efficiency of the refolding step. A low yield in this unit operation due to aggregation problems impacts heavily on the overall achievable yield. Consequently it is often the efficiency of refolding step that determines overall economic viability (Buswell et al., 2002).

1.1.6.2 Inclusion Body Process

After expression of the target protein product as inclusion bodies in *E. coli*, the cells are harvested from the fermentation broth using centrifugation and resuspended in buffer. The cells are then mechanically lysed using high pressure homogenisation to release the inclusion bodies and generate micronized cell debris. The inclusion bodies then require isolation from the cell components using centrifugation or filtration. One of the advantages of inclusion bodies over soluble expression is the simple primary recovery step to separate the dense inclusion bodies from the lighter cell membrane components and soluble contaminants. A washing step is typically performed to remove impurities associated with the surface of the inclusion bodies. The inclusion bodies are then solubilised in high concentrations of chaotropes such as urea or guanidine to unfold the protein. A reducing agent is also added to break any disulphide bonds to allow denaturation. A refolding step follows to obtain active folded product, which is then further purified before formulation.

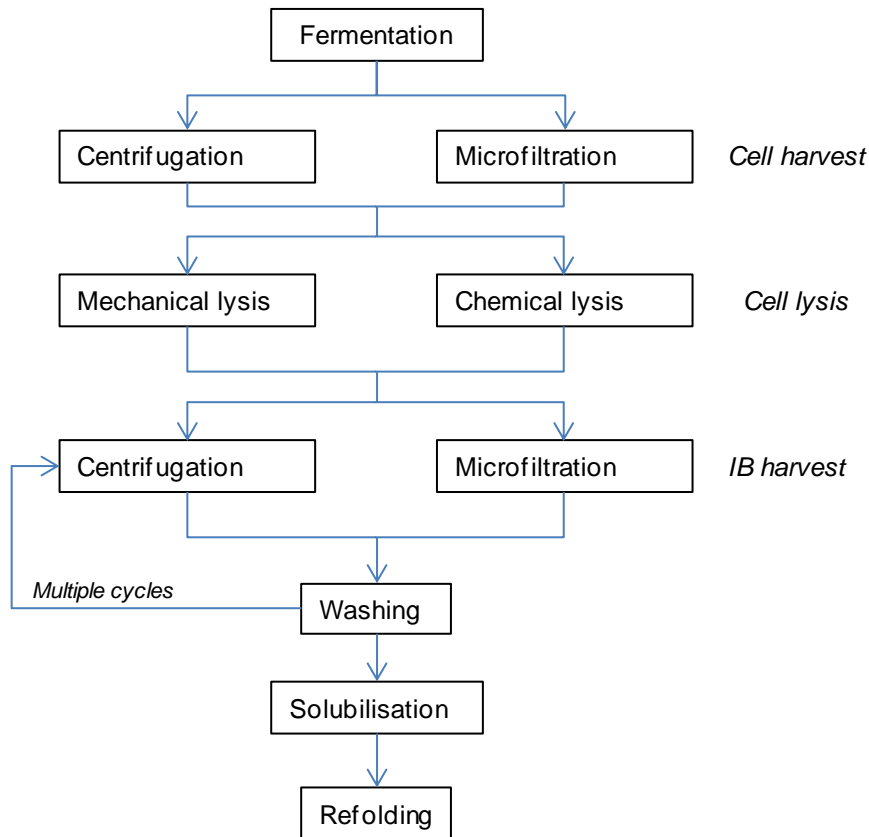


Figure 1.5 The sequence of operations involved in an inclusion body process

1.1.6.3 Washing

A washing step can reduce the number of steps in purification and increase refolding yields. It has been reported that a purity of up to 90% can be achieved by using an optimal washing procedure (Panda, 2003). Contaminants present in the refolding step can significantly reduce the refolding yield. Inclusion bodies can contain other proteins such as RNA polymerase subunits, outer membrane proteins, 16S and 23S RNA, plasmid DNA and other enzymes (Fischer et al., 1993). Plasmid DNA, lipopolysaccharide and protein have been shown to increase aggregation during the renaturation of hen egg-white lysozyme and hence decrease yield (Middelberg, 2002). The most common method for washing involves using EDTA and low concentrations of denaturant (1-4M urea), sucrose or detergents such as Triton X-100, deoxycholate and octylglucoside to reduce the level of contaminants (Clark, 2001). However, this step increases the cost and complexity of the process (Middelberg, 2002). Centrifugation or microfiltration can then be used after addition, although centrifugation results in a higher protein purity (Clark, 2001).

1.1.6.4 Solubilisation and denaturation

Inclusion bodies are generally soluble in high concentrations of chaotropic solvents at a concentration of 6-8 M to give a protein concentration of 1-10 mg.ml⁻¹ (Clark, 2001). This can sometimes be difficult at a larger scale if the moisture content of the inclusion body paste is high, leading to a lower effective concentration of your chaotroph (Buswell et al., 2002). Another component of the solubilisation buffer is a reducing agent such as DTT or β -mercaptoethanol, which maintains the cysteine residues in a reduced state thus preventing non-native disulphide bond formation. It has also been shown to improve the solubilisation yield. Chelating agents such as EDTA are often used to prevent metal-catalysed air oxidation of cysteine residues (Panda, 2003). In order to make this step efficient and economically viable, the minimum concentration of denaturant required to solubilise the protein, allowing it to recover its full activity in the following step, must be determined. Alternative methods to solubilise inclusion bodies such as extremes of pH and detergents are also available. However, the use of extreme pH may not be applicable for most pharmaceutical protein as prolonged exposure can lead to irreversible chemical modifications. Detergents such as sodium dodecyl sulphate (SDS) can be used, but the main drawback is that the detergent may interfere with downstream chromatographic steps (Clark, 2001).

Figure 1.6 Methods for solubilization and renaturation, taken from Clark, (2001)

1.1.6.5 Refolding

The refolding step involves renaturation of the solubilised recombinant proteins. This is achieved by the removal or dilution of the denaturing agent, producing a chemical environment that favours folding (Buswell et al., 2002). The buffer must also contain reducing and oxidising agents to aid disulphide bond shuffling. The oxidising agent is required for the formation of disulphide bonds and can be achieved by air oxidation, or the addition of a mixture of reduced and oxidised thiol species. The most commonly used thiol reagents are reduced/oxidised glutathione (GSH/GSSH), DTT/GSSH, cysteine/cystine and cysteamine/cystamine to give a total concentration of between 5 and 15mM and a ratio of reduced to oxidised species of 1:1 to 5:1 (Panda, 2003). The use of these reagents improves the solubility of the protein during refolding and reduces the formation of incorrect disulphides bonds as the protein can undergo disulphide bond shuffling. Low molecular weight additives can also be added to reduce aggregation and improve yields such as acetone, urea, detergents, sugars, short-chain alcohols and PEG. The most commonly used additives are L-arginine, low concentrations of urea or guanidine hydrochloride and detergents. The mechanism of how arginine reduces aggregation is not precisely understood, but it is thought that its guanidino structure aids the solubilisation of the folding intermediates without destabilizing them.

1.1.6.5.1 Refolding techniques

The refolding of denatured inclusion bodies to form soluble bioactive product is a major hurdle in the production of inclusion body derived therapeutic proteins (De Bernardez Clark et al., 1998; Buswell and Middelberg, 2003). The yields from dilution refolding are often low due to protein misfolding and aggregation of partially folded intermediates (Goldberg et al., 1991; Buswell and Middelberg, 2002). Refolding follows first order kinetics, whereas aggregation follows second or higher order kinetics. This results in competing kinetic reactions and, consequently, at high initial protein concentrations the rate of aggregation is higher than the rate of folding. Therefore protein refolding is favoured at a lower denatured protein concentration (Kiefhaber et al., 1991). Low protein concentrations of 10-100 $\mu\text{g}\cdot\text{ml}^{-1}$ are typically used to minimise aggregation ((Rudolph and Lilie, 1996; Buswell and Middelberg, 2002). However they require large mixing vessels, high volumes of refolding buffer and a subsequent ultrafiltration step to concentrate the final protein solution for downstream processing (Panda, 2003; Vallejo and Rinas, 2004). Disulphide bond

formation is the rate-limiting step in refolding as non-native disulphide bonds must be continuously broken by re-oxidation to allow the correct pairings to form. This disulphide bond shuffling can be achieved by controlled air oxidation, or using redox shuffling systems such as mixed disulphides (Fischer et al., 1993). Air oxidation is simple and inexpensive, but is typically characterised by low refolding rates and yields (Rudolph and Lilie, 1996). It is less favoured in industry as it does not allow precise control of the process (Fischer et al., 1993). Air oxidation is usually achieved by aeration or static exposure of the vessel to air or oxygen. The dissolved oxygen can then oxidise the reduced thiol compound forming a disulphide bond, leading to the creation of a redox pair that causes disulphide-bond shuffling. This system is limited by the slow mass transfer rate of oxygen and increasing agitation rates to overcome this can result in increased shear and interfacial stress which may lead to aggregation (Clark, 2001). Redox shuffling systems, while more expensive, often result in higher rates and yields by accelerating the rate of shuffling (De Bernardez Clark 1998, Hevehan De Bernardez Clark 1997). Typically they consist of low molecular weight thiols in both reduced and oxidised forms, with reduced thiol at around 1-3 mM and a reduced to oxidised thiol ratio between 5:1 and 10:1 (Rudolph and Lilie, 1996).

There are three main methods for refolding:

1. Dilution

This involves diluting the solubilised protein directly into a renaturation buffer. Dilution refolding is extensively used in industry due to its simplicity. The disadvantage of this method is that it is time consuming and requires large buffer volumes. Therefore it is less than optimal at a large scale as an added concentration step will be needed afterwards and, in comparison to other methods, the yield of native protein is lower (Li et al., 2004). Since the overall cost of the process usually increases with the use of more sophisticated equipment, simple dilution refolding can be economic as it only requires a stirred tank vessel (Buswell et al., 2002). In order for the dilution refolding to be successful, the rate of denatured protein to the renaturation buffer must be controlled and good mixing provided to maintain a low protein concentration and prevent aggregation (Clark, 2001). A variation of this method is represented by “pulse renaturation”, where aliquots of denatured protein are added to buffer in a step-wise fashion, or semi continuously in fed-batch mode. This can result in yields 10% higher (Katoh and Katoh, 2000). This method was chosen for further

study in this thesis as it is the preferred method in industry, the most common method in literature (Buckle et al., 2005) and the method can be achieved at the microscale (see Section 1.1.7.3).

2. Solvent exchange by dialysis, diafiltration or size exclusion chromatography.

Dialysis and diafiltration can be performed using an ultrafiltration membrane to reduce the denaturant concentration of the solubilised inclusion bodies to a low concentration, causing the protein to spontaneously fold. However, renaturation yields can be affected by protein binding to the membrane (fouling), which also reduces the lifetime of the membrane (Li et al., 2004). This effect can be minimized by using highly hydrophilic membranes that reduce binding, such as cellulose acetate. Unfolded protein can also be lost in significant amounts through transmission across the membrane. This can be overcome by dialysing against a lower concentration of denaturing buffer, so that the protein forms a molten-globule state or native configuration (Clark, 2001). Size-exclusion chromatography (SEC) is another buffer-exchanging method that aims to inhibit aggregation by restricting diffusion of partially folded intermediates. A method comparison study conducted by Fahey et al., (2000) showed SEC results in higher yields when the dilution factor is below 40. Conversely, a study by Werner et al., (1994) using lysozyme showed that SEC offered no advantage over traditional dilution in terms of yield. SEC method does, however, offer advantages in terms of purification because the material leaving the column is fractionated by size and hence the protein is free from contaminants and aggregates. The disadvantages of SEC are that the yield of folded protein decreases with higher protein concentrations, higher sample volumes and lower flow rates. Problems can occur with sample application, as the sudden change in conditions leads to a rapid structural collapse which can cause aggregation. However this can be overcome by adding the protein under denaturing conditions and flowing renaturation buffer through the column (Clark, 2001). The application of these buffer exchanging methods in the microscale format are more complex than simple dilution refolding, however some work has already addressed the use of microfiltration for inclusion body refolding (Davies, R., 2009).

3. Reversible adsorption onto a solid support.

This method involves binding the denatured protein transiently to a solid support. This minimizes intermolecular interactions that lead to aggregation by isolating the

molecules spatially and preventing the partially folded intermediates from diffusing and aggregating (Li et al., 2004). In order to allow the structure further freedom for folding, a fusion partner can be added such as a His-tag or cellulose binding domain, which is able to bind at denaturing conditions. The protein can then be purified by washing the bound protein before eluting (Clark, 2001). However a commercially viable refolding step involves minimising the number of steps and reducing the cost (and amounts) of chemicals required (Li et al., 2004) and consequently dilution refolding fulfils these criteria better. Further work is required to fine tune the on-column refolding process for industrial applications (Jungbauer et al., 2004).

1.1.7 Microscale Bioprocessing Techniques

The cost of bringing a drug to the market is currently estimated to be between \$500 and \$2000 million (depending on the therapy and developing firm), with an average cost of \$868 million (Adams and Brantner, 2006). The time needed to develop a drug from the discovery stage to its release on the market is on average 10 years (Dickson and Gagnon, 2004). Before clinical trials, the final manufacturing process has to be determined due to regulatory requirements. Therefore techniques aiming to increase the speed at which drugs are delivered to the market are really desirable at bioprocess development stage. Decreasing the time and cost required to develop a robust manufacturing process would have clear advantages. For a blockbuster drug, every day lost on the market represents a loss of sales of \$4-5 million (Frantz, 2004).

The microscale approach involves the study of unit operations at the microlitre scale (20-2000 μ l) using microwell or microfluidic formats (Micheletti and Lye, 2006). This methodology can be used to predict the performance of individual bioprocess unit operations at larger scale. It offers a potential solution to lengthy development timelines, providing the means to investigate operating variables with small quantities of material early on in process development. The process conditions can then be optimised to develop a robust manufacturing process with a lower cost of goods. Miniaturization has already been successful for increasing productivity during early drug discovery, increasing throughput and allowing parallel experimentation, whilst decreasing processing time, reagent volumes and waste (Kapur et al., 1999; Sundberg, 2000). Miniaturization is being increasingly applied to bioprocess development activities such as microbial fermentation (Duetz et al., 2000; Elmahdi et al., 2003;

Duetz, 2007), mammalian cell culture (Micheletti et al., 2006), biocatalysis (Lye et al., 2003; Ferreira-Torres et al., 2005; Baboo et al., 2012), ultra scale down (USD) centrifugation (Tustian et al., 2007), microfiltration (Jackson et al., 2006; Rayat, 2011), cell lysis (Wenger et al., 2008), protein refolding (Vincentelli et al., 2004; Dechavanne et al., 2011) and chromatography (Wenger et al., 2007). Ultimately, linking different microscale unit operation could lead to the creation of a whole bioprocess to study the complex interactions between process variables and operating conditions.

The microwell format is readily compatible with automation, improving efficiency and throughput further (Major, 1998). This allows automated mixing, addition and removal of liquids (liquid handling), as well as robotic arm movements, which transport each plate between different devices and analytical equipment such as plate readers and HPLC systems. Automation offers the advantages of liquid handling precision and accuracy, enhancing reproducibility between experiments due to improved consistency. It also allows walk away and 24 hour operation, resulting in higher workloads, thus boosting productivity. However these higher workloads result in a large number of samples requiring analysis by techniques such as HPLC, and consequently fast analytics need to be developed in tandem to enable the high throughput study of conditions.

1.1.7.1 Scale-up

It is important that studies performed at the microscale translate to the larger scales of operation at which industrial manufacture occurs for the majority of biotherapeutics. Therefore results gained at the microscale need to be scaled up, and offer either insight into scaling issues or act as direct mimics of the large scale. The characterisation of microwell systems in terms of oxygen transfer (Hermann et al., 2003; Doig et al., 2005a; Puskeiler et al., 2005), mixing times (Nealon et al., 2006; Tissot et al., 2010) and engineering environment (Zhang et al., 2008) aids this objective by providing fundamental characteristics that can be matched at the large scale, allowing direct scale-up of results. This is particularly important for microwell fermentation studies, where sufficient dissolved oxygen is required to meeting the oxygen demands of aerobically growing microbial cells and oxygen limited conditions would give suboptimal results. For this reason, the volumetric mass transfer coefficient is often chosen as an appropriate scaling parameter for aerobic fermentations (Ferreira-Torres et al., 2005; Micheletti et al., 2006; Islam et al., 2008).

1.1.7.2 Cell lysis at microscale using Adaptive focused acoustics (AFA)

At the industrial scale, high pressure homogenisation is used to lyse *E. coli* cells with multiple passes at a high pressure (Balasundaram et al., 2009). Bench-top equivalents exist for laboratory scale experiments with volume requirements of 10-100 ml. When the volumes involved are less than 10 ml, sonication or chemical lysis are used, but they are not representative of the large scale due to the different contamination profiles resulting from the reduced efficiency of cell rupture (Wenger et al., 2008). A new technology has been developed for small volumes of 50 μ l to several 100 μ ls using adaptive focused acoustics (AFA), which allows the automated treatment of multiple samples. It operates at a higher frequency range than a conventional sonicator (Figure 1.7), resulting in shorter wavelengths than can be more easily scaled down to small volumes (Wenger et al., 2008). The high frequency of the burst of ultrasonic acoustic energy results in a wavelength of a few millimetres that can be focused on a discrete zone in a sample vial immersed in a water bath.

Figure 1.7 Operating frequency of the adaptive focused acoustics of the Covaris device compared to a sonicator.

It also has an isothermal advantage when compared to sonication as the operating wavelength is similar to the path length of the treatment vessel. This results in less scattering of the acoustic energy field, so samples are not heated to the same high temperatures as in sonication and there is a better efficiency of cell breakage. The acoustic energy field can be transmitted across the liquid contained in the chilled water bath, and the plastic or glass of the vessel being treated (Figure 1.8). The mechanism of lysis is thought to be similar to the ultrasonic cavitations seen in sonication, where

expanding and collapsing bubbles result in a shock wave which cause viscous dissipative eddies resulting in shear stress (Davies, 1959; Clarke, 1970; Doulah, 1977). The release of product and other soluble proteins has been shown to be the same as high-pressure homogenisation for *Saccharomyces cerevisiae* cells expressing recombinant human papillomavirus (HPV) virus-like particles (VLPs) (Wenger et al. 2008). Additionally the process is controlled by a computer and capable of processing multiple samples in parallel, making it highly compatible with high throughput automation and integration within a microscale process sequence.

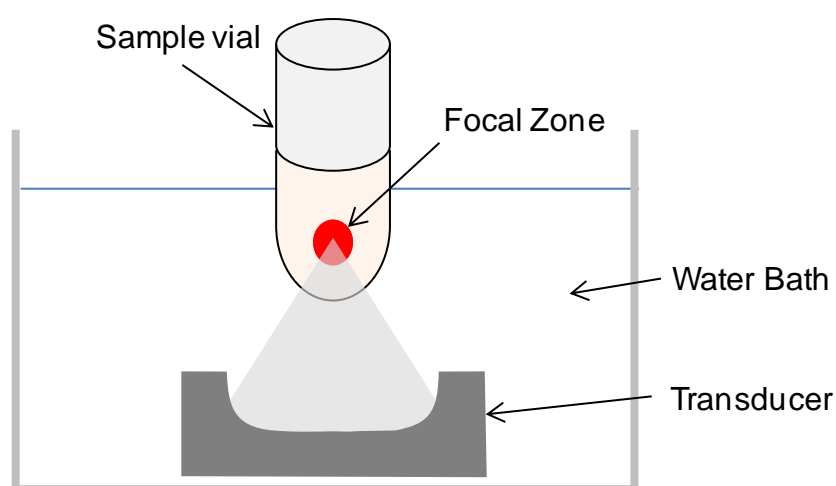


Figure 1.8 The adaptive focusing acoustic (AFA) process. Bursts of ultrasonic acoustic energy are focused on a discrete area in the sample vial, allowing lysis without contact and less sample heating. The process is controlled by a computer which allows the duty cycle, intensity and duration of these bursts to be programmed and the automated treatment of multiple samples sequentially.

1.1.7.3 Microscale Refolding

The optimal conditions for refolding have to be determined for every new inclusion body product due to the absence of a universal refolding buffer. This requires the empirical investigation of multiple parameters, which is both time consuming and resource intensive. Protein refolding is largely scale-invariant, therefore the microwell plate format can be used for the rapid and meaningful screening of many process conditions (Middelberg, 2002). A microscale approach enables rapid optimization early on in process development by using low quantities of often expensive material and allows multiple conditions to be tested in parallel. In addition, the integration of microscale approaches with robotic platforms allows high throughput studies. The microwell format has been successfully utilised for the high-throughput screening of protein refolding reagents in the microwell format by several authors (Vincentelli et al.,

2004; Willis et al., 2005; Mannall et al., 2009; Dechavanne et al., 2011). This approach has been combined with fractional factorial and other Design of Experiment (DoE) approaches, and has been reported to efficiently screen many combinations of additives to optimise refolding yields (Williams et al., 1982; Mannall et al., 2009; Dechavanne et al., 2011).

1.1.8 Analytical methods

In order to study different stages of the inclusion body process, techniques are required that can assess the effectiveness of different methods of cell lysis and the release of inclusion bodies. Additionally a generic method is required able to analyse refolds in a way compatible with high throughput microscale methodology.

1.1.8.1 Laser diffraction

Laser diffraction particle size analysers can be used to measure particle size distribution. They benefit from high speeds, good reliability, high reproducibility, they cover a wide particle size range and require small sample volumes (Ma et al., 2000; Storti and Balsamo, 2010). They provide an indirect measurement of spherically equivalent particles. The technique is based on the principle that particles diffract light at an angle which relates to their size, and as particle size decreases this angle of diffraction increases logarithmically (smaller particles diffract light at high angles) (Beuselinck et al., 1998).

1.1.8.2 Intrinsic Fluorescence

Proteins have intrinsic fluorophores resulting from aromatic amino acid side chains, generally tryptophan and tyrosine residues. The polarity of the environment the tryptophan residue is experiencing affects the emission wavelength, providing information on the conformational changes of the protein (Renard et al., 1998). Hence fluorescence is often used to monitor protein folding (Pace and Laurents, 1989; Vidugiris et al., 1995; Chiti et al., 1999).

1.1.8.3 Flow cytometry

During cell lysis, inclusion bodies must be completely released so they can be harvested using centrifugation to exploit the density difference between the inclusion bodies and cell debris. In order to improve downstream recovery productivity, a technique is required that can be used to distinguish inclusion bodies from intact cells to monitor the

efficiency of release. The number of techniques available to measure cell rupture is scarce. Phase contract microscopy is used as standard, but it is time consuming and subject to large errors. Flow cytometry methods have been developed for monitoring bacterial cell viability using a variety of dyes. These methods rely on a dye which targets DNA to distinguish between live and ruptured cells, but all dyes have varying degrees of membrane permeability. Recently a newer dye, SYTOX Green, has been developed which is impermeable to cells and consequently only binds nucleic acid with a high affinity when cells have been ruptured (Millard et al., 1995; Roth et al., 1997; Lebaron et al., 1998). It has recently been explored as a technique for studying inclusion body release as well as bacterial lysis, and allows resolution of the IB granules from cell debris and whole cells (Medwid et al., 2007). This enables cell rupture to be followed, in this example during different passes of homogenisation, and potentially allows the quantification of IBs during fermentation. Wållberg et al. (2005) used multi-parameter flow cytometry to quantify the production of promegapointin (PMP) IBs during fermentation, which were labelled with primary and secondary fluorescent antibodies. This allowed them to follow the accumulation of protein during the fermentation and the heterogeneity in the population of cells producing inclusion bodies.

1.1.8.4 Summary

In conclusion, devices on the market exist which could be integrated with the sequence to determine particle size and hence gain process information. The intrinsic fluorescence techniques described in literature could also be applied on top of an automated platform to determine the folding environment at high throughput. These techniques will be studied and further developed in this work.

1.1.9 Proteins studied

1.1.9.1 Lysozyme

Hen egg white lysozyme (HEWL) is one of the best characterized and most studied biological macromolecule (Matagne et al., 1997) and therefore is an ideal model system for refolding studies.

1.1.9.1.1 Structure

HEWL is a small protein of 129 amino acids, with a molecular weight (M_r) of 14305. It consists of two main structural domains:

1. Four α -helices and a C-terminal 3_{10} helix (α -domain)
2. A triple-stranded antiparallel β -sheet, a 3_{10} helix and a long loop (β -domain)

These are linked by a short double-stranded antiparallel β -sheet and four disulphide bonds, as illustrated in Figure 1.9.

Figure 1.9 Schematic view of hen egg white lysozyme. The α -domain is shown in red and the β -domain in blue). Taken from (Radford et al., 1992b)

1.1.9.1.2 Folding

The earliest detectable event in lysozyme folding, less than 1 ms, is the formation of an extensive fluctuating secondary structure and a substantial degree of hydrophobic collapse, where the hydrophobic residues are buried in the centre of the structure (Wildegger and Kiefhaber, 1997). Far UV experiments show that a substantial area of native secondary structure is formed within a few milliseconds (Matagne and Dobson, 1998). “Dead-time” labelling reveals the presence of embryonic native-like structure in α -domain forms at a very early stage in folding. Different kinetic pathways (fast or slow) can be taken after the initial events of secondary structure formation and hydrophobic collapse, as the collapsed states are highly heterogeneous (Matagne and Dobson, 1998). Secondary structure develops independently in the two distinct structural domains to form intermediates. The slow and fast pathways of folding are illustrated in the schematic of the energy surface for lysozyme folding shown in Figure

1.10. This is based on simulations performed using a simple lattice model to describe folding and is consistent with experimental data currently available (Dobson et al., 1998).

Figure 1.10 Schematic of an averaged effective energy surface based on experimental results for lysozyme refolding. P is related to the configurational entropy of the system (the extent of accessible space available to the molecule), E is the averaged effective energy and Q is a progress variable corresponding to the number of native contacts. Three different possible trajectories are illustrated with coloured arrows. Yellow- the fast folding pathway, green- a slow folding pathway that must overcome a high energy barrier, and red- a slow folding pathway that must return to a less folded state before proceeding along the valley corresponding to the fast folding pathway. Taken from Dobson et al., (1998).

1.1.9.1.2.1 Fast track of lysozyme folding

Approximately 25% of molecules fold along the fast track. The polypeptide has been observed to form native-like structure in a time constant of approximately 10 ms, normally seen for the folding rate of small, single-domain protein, which has a 2 state folding process and has no detectable intermediates (Kiefhaber, 1995; Radford and Dobson, 1995; Matagne et al., 1997). The pathway has been proposed to occur via an intermediate with extensive native-like structure in both α and β -domains, as hydrogen-

exchange protection occurs fast for both domains (shown as the minimum on the left-hand side of Figure 1.10) (Matagne and Dobson, 1998). However this intermediate is not entirely native as it lacks the ability to bind a competitive inhibitor of the enzyme and hence the active site cleft has not yet formed. Following the formation of the intermediate is the rate-limiting step. The two partly folded structural domains then need to coalesce, overcoming an energy barrier, in order for the native state to be formed (Matagne and Dobson, 1998).

1.1.9.1.2.2 Slow track of lysozyme refolding

The remaining 75% of molecules fold via the slow track, of which 15% fold very slowly with time constant in the range of 20 s. This could be due to limitations caused by the *cis-trans* isomerisation of one or both proline containing peptides bonds. Hydrogen exchange labelling studies (Miranker et al., 1991; Radford et al., 1992b) show that the majority of the remaining molecules gain extensive hydrogen-exchange protection in the α -domain. This indicates an intermediate is formed with a structured alpha domain, but an unstable β -domain where the amides present become protected at a slower rate in a rate-limiting reaction (time constant \approx 350 ms) (Matagne and Dobson, 1998). This partially folded state then has two pathways available. The structure can either overcome a high energy barrier (the rate-limiting step) to achieve the native state by a process of rearrangement, or alternatively, it can unfold and fold via the fast pathway (Matagne and Dobson, 1998).

1.1.9.2 Dihydrofolate reductase

Dihydrofolate reductase (DHFR) is a small, monomeric protein which catalyses the reduction of dihydrofolate to tetrahydrofolate by NADPH (Buchwalder et al., 1992). The kinetics of this reaction have been well described previously (Thillet et al., 1990). Tetrahydrofolate is an essential cofactor for the synthesis of several amino acids, purines and thymidylate. DHFR also binds several synthetic antifolate drugs very strongly and is therefore the target for drugs such as methotrexate (a cancer drug used to kill tumour cells) and trimethoprim (an antibacterial drug) (Thillet et al., 1990).

1.1.9.2.1 Structure

DHFR has a highly conserved structure between vertebrates with a sequence homology of 89 % between mouse and human (Stammers et al., 1987). The murine DHFR (mDHFR) used in this work has a molecular weight of 21,446 (Clark et al., 1996) and is

186 residues in length (Uversky et al., 1996). A high resolution crystal structure for mDHFR has been reported by Stammers et al., (1987). The active site occupies a large surface area of the structure due to the large nature of aromatic moieties of its ligands. The binding of one ligand greatly increases the affinity for the other by several thousand fold, due to ligand induced conformation changes in loops distant from the active site (Buchwalder et al., 1992). The binding of ligands to a mutated DHFR has been shown to convert the structure from a molten globule state to a native-like state with functional activity (Uversky et al., 1996).

1.1.9.2.2 Folding

The folding of *E. coli* derived DHFR is thought to proceed through a two state transition and kinetic studies have shown the presence of several transient intermediates during folding (Clark et al., 1996). Although the sequence homology is lower between eukaryotes and prokaryotes, crystal structures *E. coli* and human DHFR have shown the native conformation has been evolutionary conserved (Bolin et al., 1982; Davies et al., 1990) and hence folding mechanisms may also be similar for mDHFR.

1.1.9.3 Insulin lispro

Insulin (Humulin[®]) was the first recombinant product to gain market approval in 1982. The hunt for an insulin analogue with improved therapeutic properties led to the release of Insulin Lispro (Humalog[®]) (Walsh and Murphy, 1999).

1.1.9.3.1 Structure

Insulin is a small globular protein composed of an A-chain (21 residues) and B-chain (30 residues), with three disulphide bonds (two interchain, A7-B7, A20-B19 and one intrachain A6-A11). The structure of Insulin Lispro is very similar to the native form of insulin, but the Pro-Lys amino acid residues are reversed at position B28 and B29. This modification results in a faster acting insulin, with a shorter duration of action and an equal ability to lower glucose levels compared to normal insulin. It also shows improvements in terms of better postprandial glucose control.

Figure 1.11 The structure of human proinsulin, taken from Heath et al., (1992)

Figure 1.12 The structure of insulin lispro, taken from prescribing information for Humalog® available online (<http://pi.lilly.com/us/humalog-pen-pi.pdf>)

1.1.9.3.2 Folding

The A-chain and B-chain contain all the information needed to form the native structure. The 3D structure of insulin shows it is mostly composed of three α -helical segments stabilised by the disulphide bonds. Deletion of any these disulphide bonds leads to unfolding, however the A20-B19 disulphide bond appears to be the most important (Yan et al., 2009). *In vitro* refolding of porcine insulin precursor (PIP) showed that the A6-A11 and A20-B19 disulphides form quickly. The formation of A6-A11 does not result in a more ordered structure (Qiao et al., 2001) and consequently

probably develops as a result from the proximity of these two cysteine residues in the polypeptide sequence (Hua et al., 2001). The A20 and B19 residues are distant in sequence and hence must result from the structure becoming more ordered. Yan et al., (2009) proposed that long range interactions of some side chains result in the polypeptide chain forming a transient unstable partially folded conformation where A20 and B19 are in close proximity, as shown in Figure 1.13. This results in the formation of a disulphide bond which stabilises the partially folded structure and is the critical step in order to allow further refolding.

Figure 1.13 A schematic showing the early refolding stages of porcine insulin precursor (PIP), taken from (Yan et al., 2009)

1.1.9.3.3 Manufacture

Insulin lispro is produced from fermentation in *E. coli* of a precursor molecule with a short amino acid sequence. This sequence is removed enzymatically to give proinsulin ($M_r = 9390$ Da (Heath et al., 1992)), which is then hydrolysed with trypsin and carboxypeptidase B to yield insulin lispro. This then undergoes purification by chromatography and is crystallised with zinc and phenol. The final product is typically formulated with M-cresol, zinc oxide, glycerol and a phosphate based buffer (Walsh, 2004).

1.1.9.4 Summary

Lysozyme was selected for study as it is well characterised and often used as a model protein for the study of folding. Therefore it could act as a model system for refold

assay development. DHFR was chosen as previous work has been performed on its large scale production and refolding at the microscale, but there is a lack of published work regarding the impact of fermentation conditions on IB quality and refold yield. Therefore it provides an ideal protein for challenging the developed assays with IB material. Insulin was studied as a more industrially relevant therapeutic protein and because of a lack of work investigating its refolding at the microscale and the effect of fermentation conditions on the IBs produced.

1.2 Main conclusions of the literature survey

Inclusion bodies are commonly formed in *E. coli* as a result of the high synthesis rates, overwhelming cellular folding machinery and altering the equilibrium between folding and aggregation. Other contributing factors include the cellular stress brought on by heterologous protein expression and the differences in the folding environment from a eukaryotic cell. Fermentation conditions influence whether the protein product is expressed solubly or as an inactive aggregated inclusion body. However, little work has investigated the link between fermentation conditions and IB quality or refolding yield. The high concentration and purity of the protein formed in IBs can be advantageous for the production of therapeutic proteins, and their physical properties can be exploited in industrial processes. However, for an economic process the efficiency of the refold step must be improved to maximise yield of soluble active product. Dilution refolding is the most commonly used step for renaturation of protein in industry, where dilution of the denaturant in refold buffer causes spontaneous refolding of the protein. Previous work has shown the yield is dependent on a range of factors such as protein concentration, final denaturant concentration, redox ratios and additives. Optimising the refolding condition requires considerable effort during process development and is therefore a prime target for microscale processing to investigate important parameters.

1.3 Thesis aims and outline

The overall aim of this thesis was to establish a whole bioprocess to investigate the effect of upstream fermentation conditions on the final yield of active product from refolding. This is based on the hypothesis that protein refolding can be performed and optimised at a microlitre scale and once established, can rapidly evaluate the impact of earlier bioreactor stages on whole bioprocess performance. The equipment, materials

and methods used are detailed in Chapter 2. The overall thesis aim required the following objectives to be achieved:

- 1) Develop an automated microwell dilution refolding system and demonstrate its suitability for investigating multiple refold variables. In order to analyse the yield obtained in a 96-well microtitre plate, high throughput automated assays are required that can be generically applied to model systems as well as material from an industrially relevant strain. This is demonstrated in Chapter 3.
- 2) Extend the automated microscale refold operation with analytics to form an automated whole bioprocess at the microscale, encompassing fermentation, cell harvest by centrifugation, cell resuspension, lysis using AFA, IB harvest by centrifugation, IB solubilisation. This allows the generation of *E. coli* fermentation broths under different fermentation conditions, which can then undergo processing in parallel to investigate the effect of process parameters on inclusion bodies. This is detailed in Chapter 4.
- 3) Adopt a whole bioprocess approach to optimisation and utilise the whole bioprocess sequence to investigate the effect of upstream fermentation conditions on downstream refolding yields and product quality. This will allow optimisation of the fermentation process to maximise inclusion body refolding yield, rather than the typical approach to maximise fermentation product titre. The whole bioprocess was then applied to an industrially relevant strain provided by Fujifilm Diosynth Biotechnologies. The results obtained are presented in Chapter 5.
- 4) The final objective of the thesis was to validate the dilution refolding system by comparing refold yields to larger scales of operation for the industrially relevant strain. The fermentation results and those obtained using the sequence as a whole were compared to pilot scale results for an industrially relevant protein to demonstrate the suitability for the microscale process as a tool for optimising yield during process development. Chapter 6 presents the scale-up studies carried out with insulin.

- 5) The final chapter, Chapter 7, summarises the main findings and recommendations for future work.

2 Materials and Methods

2.1 Lysozyme

2.1.1 Materials and Equipment

Hen egg white lysozyme lyophilized powder (HEWL) was obtained from Sigma-Aldrich Ltd (Poole, Dorset, UK), at 50,000 units/mg protein and dialysed (10,000 MCW Snakeskin, Perbio Science UK Ltd, Cramlington, Northumberland, UK), DTT (Fermentas, York, UK). All other chemicals used in this experimental section were purchased from Sigma-Aldrich Company Limited (Poole, Dorset, UK). Refolds were conducted in UV-transparent 96 standard round well (SRW) microplates (“UV-star”, Grenier Bio-One, Gloucestershire, UK) unless stated otherwise.

2.1.1.1 Equipment for manual refolds

For manual experiments, some pipetting operations were performed using the plate reader (FLUOstar, BMG LABTECH, Ortenberg, Germany) to add liquid by direct injection into the microplate. Absorbance and fluorescence measurements for these experiments were also performed using the same plate reader.

2.1.1.2 Robotic platform equipment for automated refolds

For the automated experiments, all refold plate preparations were fully automated using a robotic platform (TECAN Freedom EVO[®], Reading, UK). Shaking was achieved on a thermomixer orbital shaker platform (Eppendorf UK Limited, Cambridge, UK). For the manual and automated comparison, oxidation and hierarchical experiments the absorbance and fluorescence measurements were carried out in a plate reader on the platform (TECAN Infinite 2000, Reading, UK).

2.1.2 Denaturation and Refolding

Refolds were conducted in triplicate, with standards and controls present in duplicate or triplicate. Standards were prepared by dissolving lyophilised HEWL into aliquots of refold buffer to give the correct final protein concentration, whereas controls were buffer only. Refolding was initiated by the addition of refold buffer to denatured protein, with the exception of experiments performed in the FLUOstar microplate reader where denatured protein was added to buffer containing wells. Refolds were mixed after additions by pipette aspiration for at least 3 cycles.

2.1.2.1 Selection of wavelengths for aggregation detection and solubility

HEWL was dissolved in a denaturing solution of 6M guanidine hydrochloride (GdnHCl) and 25mM dithiothreitol (DTT) to give a concentration of 10 mg.ml⁻¹. The solution was then vortexed for 1 minute and incubated for two hours at room temperature. Buffers were prepared with different excipients as shown in Table 2.1 and were incubated for 1 hour to equilibrate before use. Standards were prepared by dissolving lyophilised HEWL into aliquots of the buffers in Table 2.1. A volume of 300 µl of standard and control (buffer only) solutions were added to different wells in a microwell plate format. A volume of 280 µl of buffer was added to different wells for the refold, and the microwell plate was placed in the microplate reader. A volume of 20 µl of denatured protein solution was then added to the wells containing 280 µl in order for refolding to take place.

Table 2.1 Lysozyme refold buffers

Buffer components	
1	25 mM cysteine, 1 mM EDTA and 0.1 M Tris-HCl pH 8.2.
2	L-arginine 0.14 M, 25 mM cysteine, 1 mM EDTA and 0.1 M Tris-HCl pH 8.2.
3	Sucrose 0.20 M, 25 mM cysteine, 1 mM EDTA and 0.1 M Tris-HCl pH 8.2.

2.1.2.2 Absorbance changes during refolding

2.1.2.2.1 *Quantifying aggregation*

Sample preparation was as in Section 2.1.2.1. Two plates were prepared identically with 15 µl of denatured protein and 285 µl of Buffer 1 (Table 2.1). Two refold conditions were tested, half of the refolds (18 repeats per plate) and standards (6 repeats per plate) with a high DTT (25 mM) concentration during denaturation, whereas the other half had low DTT (0.625 mM) concentration. One plate was placed in the plate reader and the other plate was left on the bench at room temperature. At the time points (0, 50 and 100 min), the contents of three of the wells on the corresponding bench microplate were pipetted into eppendorfs and centrifuged (13000 rpm, 5 min). This was repeated for both DTT concentrations.

2.1.2.2.2 Inducing aggregation to monitor formation over time

Denatured HEWL was prepared as described in 2.1.2.3 but at two different protein concentrations and 4 different DTT concentrations in order to give the refold conditions shown in Table 2.2. Plates were prepared as in Section 2.1.2.3.

Table 2.2 Denatured protein and refold buffer conditions

[Protein] (mg.ml ⁻¹)	[DTT] (mM)	Redox pair	Redox potential	Buffer components	[Final Protein] (mg.ml ⁻¹)
7.5	25	Cysteine:cystine	Balanced	5 mM cystine, 10 mM cysteine, 50 mM Tris	0.5
7.5	25	Cysteine:cystine	Oxidising	10 mM cystine, 50 mM Tris	0.5
15	32	DTT:cystamine	Balanced	4 mM cystamine, 50 mM Tris	1
15	6	DTT:cystamine	Oxidising	4 mM cystamine, 50 mM Tris	1
15	62	DTT:cystamine	Reducing	4 mM cystamine, 50 mM Tris	1

2.1.2.3 Fluorescence changes during refolding (fluorescence over time at different redox ratios)

HEWL was solubilised in a denaturing buffer of 8M GdnHCl, 50mM Tris.HCl, 6mM DTT to give a final concentration of 15 g.l⁻¹ and left at room temperature for 2 hours to equilibrate. The excess DTT in the solubilised denatured protein was used to establish varying redox ratios in the refold buffer by reducing different portions of the oxidised form. Refolding buffers were prepared as shown in Table 2.3 and equilibrated for 1 hour. Standards were prepared by adding HEWL to the refold buffers to give a concentration of 1 mg.ml⁻¹. Refold buffer was then added to microwells to give a volume of 280 µl in each well. The denatured protein and denaturing buffer (for the control wells) were then added via injection in the plate reader of 20 µl to give a 15 fold dilution and a final concentration of 1 mg.ml⁻¹ in the refold.

Table 2.3 Refold buffers and DTT concentration in denatured protein to give different redox potentials

Buffer (redox pair)	[DTT] (mM)	Redox potential	Components
DTT:cystamine	32	Balanced	4 mM Cystamine 50 mM Tris
DTT:cystamine	6	Oxidising	4 mM Cystamine 50 mM Tris
DTT:cystamine	62	Reducing	4 mM Cystamine 50 mM Tris

2.1.2.4 Example of end point analysis (effect of final lysozyme concentration)

Denatured HEWL was prepared as in Section 2.1.2.1 and a serial dilution was performed using denaturing buffer (6M GdnHCl, 25mM DTT) to give a range of concentrations. These were then refolded by adding 15 μ l denatured protein to 285 μ l of refold buffer 2 (Table 2.1) using injection in the BMG plate reader (1:20 dilution). Control buffer (0.3M GdnHCl, 25 mM DTT, L-arginine 0.14 M, 25 mM cysteine, 1 mM EDTA and 0.1 M Tris-HCl pH 8.2) and standard (1 mg.ml⁻¹ in control buffer) were prepared as in Section 2.1.2.1, but the standard was then serially diluted in control buffer.

2.1.3 Automated Hierarchy and oxidation experiments

HEWL was denatured in 8 M guanidine hydrochloride (GdnHCl), 50 mM Tris.HCl, pH 7.2, and 6, 26 or 56 mM dithiothreitol (DTT) to a final lysozyme concentration of 15 mg.ml⁻¹, vortexed for 1 minute and incubated for two hours at room temperature. For the oxidation experiments a different set of redox potentials were used, 6 mM DTT was used to create a very oxidising condition (ratio of 0.1:1), 32 mM DTT to give a balanced condition (redox ratio of 2:1) and 62 mM DTT to give an almost entirely reducing condition (redox ratio 1:0.009). The total concentrations of guanidine and of reduced and oxidised cystamine were kept constant. The final concentration of guanidine after a 1:20 dilution was 1.2 M. In all other experiments, refold buffers were prepared with various redox potentials and concentrations of Tris.HCl, pH 7.2, EDTA and GdnHCl (Table 2.4). All buffers were equilibrated for one hour prior to use. Standards contained lysozyme prepared in the appropriate final refold conditions, equilibrated for two hours before use. 300 μ l of native protein standards, denaturing buffer and refold buffer controls were each added in triplicates to random wells of a microplate, denatured protein was then added (20 or 15 μ l) to remaining wells.

Refolding was initiated by the addition of 280 μ l or 285 μ l refold buffer to the denatured protein giving a dilution factor of 15 or 20, respectively.

Experiments to investigate the effect of oxidation were also carried out in SPE 96-Deep Square Well (DSW) plates (Sigma-Aldrich, Dorset, UK). DSW plate format has been reported to improve surface aeration and increase air-liquid mass transfer due to the baffling action of the square edges (**Duetz and Witholt, 2004; Doig et al., 2005b**). Final volumes of 1 ml were used while maintaining a 20-fold dilution factor. Two identical plates were prepared and tested under shaken and static conditions, respectively. One DSW plate was shaken at 1000 rpm and a 3 mm shaking diameter, corresponding to an estimated gas-liquid mass transfer coefficient (k_{La}) of 0.072 s^{-1} (**Micheletti et al., 2006**).

Table 2.4 Refold buffers used for lysozyme

Buffer components	
1	25 mM cysteine, 1 mM EDTA, 0.1 M Tris.HCl
2	25 mM cysteine, 1 mM EDTA, 0.1 M Tris.HCl, 0.14M arginine
3	25 mM cysteine, 1 mM EDTA, 0.1 M Tris.HCl, 0.3M GdnHCl
4	25 mM cysteine, 1 mM EDTA, 0.1 M Tris.HCl, 0.3M GdnHCl, 0.14M arginine
5	25mM cystamine, 50mM Tris.HCl and 0.717M GdnHCl, 1mM EDTA
6	4mM cystamine, 50mM Tris.HCl and 0.715M GdnHCl (used in oxidation experiment with different [DTT] to create different redox potentials)
7	4mM cystamine, 50mM Tris.HCl and 0.678M GdnHCl
8	5mM cystine, 10mM cysteine, 50mM Tris.HCl, 0.717M GdnHCl (balanced)
9	2.86mM cystine, 14.29mM cysteine, 50mM Tris.HCl, 0.717M GdnHCl (reducing)
10	10mM cystine, 50mM Tris.HCl, 0.717M GdnHCl (oxidising)

2.2 DHFR

2.2.1 Materials and Equipment

Dihydrofolate reductase (DHFR) was expressed as inclusion bodies in *E. coli* XL10-Gold Kan^r pQE40. All chemicals used in this experimental section were purchased from Sigma-Aldrich Company Limited (Poole, Dorset, UK), with the exception of the following; NADPH tetrasodium salt from VWR International (Lutterworth, Leicester, UK), DTT from Fermentas (Sheriff Hutton, York, UK), Ni-NTA His Bind resin (Novagen, Merck), orthophosphoric acid and glycerol from Alfa Aesar (Heysham, Lancaster, UK). Shake flasks were prepared in a laminar flow hood (Herasafe, Heraeus, Thermo Scientific) incubated in an incubator shaker (ISF-1-W, Kühner AG, Basel, Switzerland).

2.2.1.1 Large scale Equipment

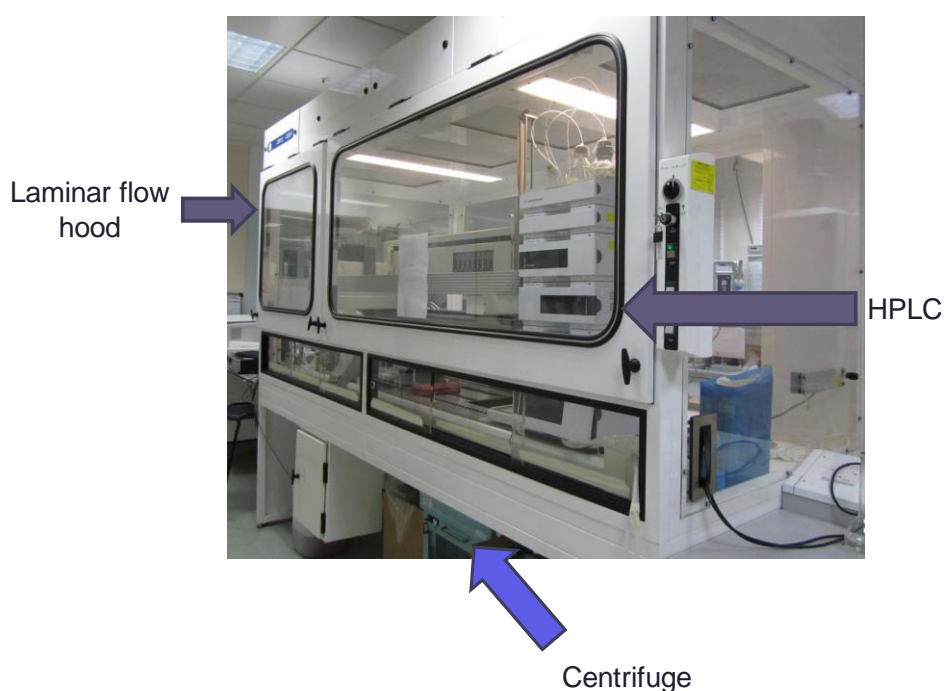
Fermentations were conducted in a stainless steel 20 L bioreactor (Applikon Biotechnology, Schiedam, Holland) with a top driven impeller. The impeller has three 6-bladed Rushton turbine type impellers of diameter 0.75 m. The bioreactor had 4 equally spaced baffles, and a working volume of 15 L and an aspect ratio of 3. Temperature control was achieved via a vessel jacket, through which either steam or cooling water was passed. The dissolved oxygen tension (DOT) was measured using DOT probe (Broadley Technologies Ltd., Bedford, UK) that was calibrated with nitrogen and air for 0% and 100% respectively. pH was measured by pH probe (Broadley Technologies Ltd., Bedford, UK), which was calibrated using standards. The DOT and pH probes were sterilised *in situ* along with the media. Cell and inclusion body harvest was achieved by centrifugation at the pilot scale using the CSA-1 disk stack centrifuge (GEA Westfalia Separator Inc, NJ, USA). Cells were lysed using the Manton-Gaulin Lab 60 high pressure homogeniser (APV Baker, Crawley, UK). Inclusion body pellets were centrifuged in the Avanti J-E lab-scale centrifuge (Beckman Coulter, High Wycombe, UK).

2.2.1.2 Microscale Equipment

For the refold experiments in Chapter 3, refold plate preparations were fully automated using a robotic platform (TECAN Freedom EVO[®], Reading, UK). Shaking was achieved on a thermomixer orbital shaker platform (Eppendorf UK Limited, Cambridge, UK) and the absorbance and fluorescence measurements were carried out in a plate reader on the platform (TECAN Infinite 2000, Reading, UK).

For the microscale bioprocess sequence experiments in Chapter 4, experiments were performed using an alternative robotic platform (Gemini, Tecan Reading, UK) and a different plate reader (GENios, Tecan, Reading, UK), all contained in a laminar flow hood (Bigneat Cabinet, Waterlooville, UK). Incubation during fermentation and thermochemical cell lysis was achieved by incubating a 96-DSW on a thermomixer (Thermomixer Comfort, Eppendorf AG, Hamburg, Germany). Disposable polypropylene troughs (Tecan Reading, UK) Deep square well polypropylene plates were used for the microwell fermentations (SPE 96-Deep Square Well collection (DSW) plate, Sigma-Aldrich, Dorset, UK). After fermentation, plates were covered with plastic covers (AxyMat Silicone sealing mat, Axygen, CA, USA) and centrifuged (Rotanta 46 RSC, Hettish Zentrifugen, Germany). Cell lysis was achieved with adaptive focused acoustics AFA in the Covaris E210 (Woburn, MA, US) in either 96-well round bottom well microplates (96 Well MasterBlock, 1ml, Polypropylene, Greiner Bio-one, Gloucestershire, UK) or capped glass vials (13 x 65 mm tube, KBiosciences, Hertfordshire, UK). Thermochemical cell lysis was performed in 96-well, round bottom, polypropylene microplate (96 Well MasterBlock, 1ml, Polypropylene, Greiner Bio-one, Gloucestershire, UK) incubated on the thermomixer (Thermomixer Comfort, Eppendorf AG, Hamburg, Germany).

A)



B)



C)

Image is the copyright of Tecan, taken from the Gemini User Manual

Figure 2.1 Photographs showing the external (A), internal view (B) and the software user interface (C) of the Tecan platform, demonstrating the containment of the whole bioprocess on one platform (with the exception of the AFA device).

2.2.2 Large scale process

2.2.2.1 Inoculum preparation

The inoculum was prepared in two seed stages, 250 ml shake flask was inoculated with 1 ml of frozen cell stock, containing Terrific Broth (TB), pH 7.2, ampicillin 100 $\mu\text{g}\cdot\text{ml}^{-1}$, kanamycin 30 $\mu\text{g}\cdot\text{ml}^{-1}$ and cultured for 8 hours. This was then used to inoculate a 2 L shake flask with Terrific Broth (TB), pH 7.2, ampicillin 100 $\mu\text{g}\cdot\text{ml}^{-1}$, kanamycin 30 $\mu\text{g}\cdot\text{ml}^{-1}$ and cultured for 12 hours.

2.2.2.2 Large scale fermentation and processing

A 10% inoculum was used to inoculate TB media in a 20 L fermenter. Operating conditions were set at 37 °C, pH 7.2, with an airflow rate of 1 vvm and an initial stirrer speed of 400 rpm. The impeller was set on cascade control with a DOT threshold of 30%. Cells were induced during the early exponential phase (approx. at 3.5 hours) with a final concentration of 0.125 mM IPTG.

After 8 hours of fermentation, cells were harvested using a CSA-1 disk stack centrifuge run at 9860 rpm, at a flow rate of 100 $\text{L}\cdot\text{h}^{-1}$. Cells were resuspended in 50 mM Tris.HCl, pH 7.2 to approximately 50 $\text{g}\cdot\text{L}^{-1}$, then lysed using a high pressure homogeniser at 500 bar for 5 passes. Inclusion bodies were harvested using a flow rate of 100 $\text{L}\cdot\text{h}^{-1}$ in the CSA-1 centrifuge. The inclusion body paste was aliquoted and sedimented further in a lab-scale centrifuge for 5300 rpm for 30 minutes at 7 °C and the pellets stored at -80 °C or -20 °C. Pellets were then washed, denatured and used in refolds, or otherwise purified further by Ni-NTA affinity and refolded under the same conditions to be used as standards.

2.2.3 IB washing

A frozen IB pellet was first resuspended to give approximately 100 $\text{g}\cdot\text{L}^{-1}$ in 50 mM Tris pH 7.2 using sonication on ice and divided into two aliquots (washed and unwashed) before being centrifuged for 10 minutes at 13,300 rpm at 5 °C. The inclusion body aliquot for washing then had multiple cycles of resuspension on ice using sonication and centrifugation 10 minutes at 13,300 rpm at 5 °C. The first step in Triton buffer (0.5% v/v Triton X-100, 50 mM Tris, 50mM NaCl pH 7.2), then guanidine hydrochloride buffer (0.6 M GdnHCl, 50 mM Tris, 50 mM NaCl pH 7.2). The pellet undergoes 3

washes in Tris buffer (50 mM Tris, 50mM NaCl pH 7.2) to remove any traces of guanidine or Triton before refolding.

2.2.4 Purification for standards

DHFR IB pellets were denatured in 8 M urea, 0.01 M Tris.HCl, pH 8.0 and equilibrated onto Ni-NTA His Bind resin. The denatured protein was eluted with a gradient to 0.01 M Tris.HCl, 8 M urea pH 4.5, then dialysed against 0.01 M Tris.HCl, 8 M urea, pH 7.2. Protein concentrations were measured by absorbance at 280 nm, assuming a molar extinction coefficient of $25092 \text{ M}^{-1}\text{cm}^{-1}$ (Pace et al., 1995) and molecular weight of 21446 Da (Clark et al., 1996). SDS-PAGE showed the presence of a single protein. These samples were used as standards using the same dilution refolding procedure used for the denatured inclusion bodies.

2.2.5 Microscale Bioprocess Sequence

A fully automated bioprocess sequence was created, with all operations performed using a robotic arm and automated liquid handling. All process steps were performed on the Tecan robot, with the exception of cell lysis which was performed on the Covaris device (AFA). The Covaris was not located on the Tecan platform, but its operation was controlled by a computer that allows high throughput treatment of up to 24 glass vials at preselected conditions. The programs written (known as scripts) for the tecan robotic platform required extensive work as multiple iterations were required to ensure a script that allowed walk away operation. Otherwise unexpected errors might lead to the termination of the script (such as a failure to detect the liquid level during aspiration). This required a substantial research effort to ensure all eventualities had been planned for and included in the script to provide work arounds to errors (for example on detection failure move to maximum depth).

The bioprocess sequence was run as a series of programs, some of which contained sub programs. This made operation easier (run errors were problematic with the older Gemini software when re-initiating scripts part of the way through) and provided flexibility for adapting scripts. Figure 2.2 shows the structure and order of programs, with sub programs shown on the right hand side. Once created and tested extensively to ensure these programs ran reliably, they were saved for future use and modification for different experiments.

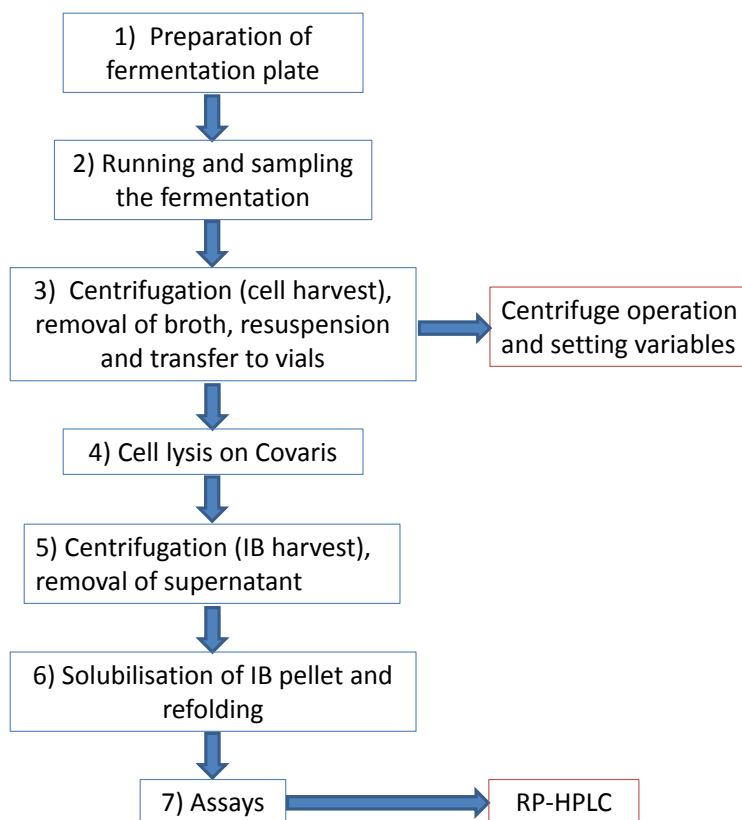


Figure 2.2 Automated program structure, showing the main scripts on the left and sub-programs represented on the right

2.2.5.1 Microwell fermentation

2.2.5.1.1 Inoculum preparation

Shake flasks (500 ml) containing 100 ml of Luria broth and $30 \mu\text{g.mL}^{-1}$ kanamycin and ampicillin $100 \mu\text{g.mL}^{-1}$ were inoculated by adding 0.9 ml of frozen cell stock of *Escherichia Coli* (*E. Coli*) XL10-Gold Kan^r pQE40, a construct that forms DHFR inclusion bodies during expression. The shake flasks were then left overnight (13-14 h) shaking at 200 rpm and 37°C.

2.2.5.1.2 Platform sterilisation

The platform located inside a laminar flow hood was sterilised prior to use with 70% ethanol and UV irradiation for 15 minutes. Disposable polypropylene troughs were used and pre-sterilised using UV irradiation for 15 minutes in a laminar flow hood. Deep square well polypropylene plates were used for the microwell fermentations and sterilised on the robotic platform.

2.2.5.1.3 Automated fermentation program

A program was initiated for the automated preparation of the fermentation plate. This involved the liquid handling arm of the robot filling each well with 950 μl of Terrific Broth containing 30 $\mu\text{g.mL}^{-1}$ kanamycin and ampicillin 100 $\mu\text{g.mL}^{-1}$. The media containing plate was then pre-warmed to 37°C on a thermomixer for 15 minutes. The plate was then inoculated using 50 μl of overnight culture and agitated at 1000 rpm and 37°C. Another program was then immediately initiated for automated fermentation sampling during the fermentation, which employed the liquid handling arm for sacrificial well sampling and the robotic arm to transfer the microplate to a platereader for measurement of the optical density (absorbance at 600 nm). This program enabled the sampling to be repeated every hour until the end of the fermentation by aspirating a minimum volume of 10 μl from duplicate wells and transferring to a SRW 96 well plate and diluting with water to give a final volume of 250 μl . The absorbance at 600 nm was then measured using a plate reader located on the platform. Expression was induced by the addition of 10 μl of isopropylthiogalactosidase (IPTG) to give a final concentration of 0.125 mM.

2.2.5.2 Cell harvest and Resuspension

The 96-DSW plates were covered with plastic covers, and are the only step that requires manual intervention other than offline cell lysis. The microwell plate is then transferred via robotic handling arm (RoMa) to the centrifuge and spun down at 5°C, 4000 rpm for 15 minutes. The fermentation broth was then removed using the liquid handling arm and 300 μl transferred to a 96 well plate. The robotic arm then transferred the plate to a microplate reader to measure absorbance at 600 nm. Following centrifugation, the cells must be resuspended in 50 mM Tris buffer pH 7.2 to give a solids concentration of approximately 50 g.L^{-1} wet cell weight in order to match large scale processing conditions. The fermentations reached an OD of 12 A.U., which using the calibration curve corresponds to a dry cell weight of 5 g.L^{-1} and hence a wet cell weight of approximately 20 g.L^{-1} . Therefore in order to achieve a concentration of 50 g.L^{-1} the cells need to be resuspended in 400 μl of buffer using 3 pipette aspiration cycles and 30 minutes of shaking using a thermomixer.

2.2.5.3 Lysis by Sonication

Resuspended cells were lysed on ice in 2.2 ml eppendorf tubes by sonication (10 cycles 10 s on, 10 s off). Most experiments were instead carried out using an alternative

method with longer treatment times (8 cycles 20 s on, 20 s off) as it was noted this led to smaller errors.

2.2.5.4 Lysis by Adaptive Focusing Acoustic (AFA)

Resuspended cells were either transferred to 96-well round bottom well microplates or to capped glass vials in a 4 by 6 rack, using an automated script on the Tecan platform. Cells were then lysed using AFA in the Covaris E210 after part submersion of the plate or vials in the degassed water bath of the instrument, at an incubation temperature of 8 ± 4 °C, above the acoustic transducer. Wenger et al (2008) reported complete release of virus-like particles from recombinant human papillomavirus at a duty cycle of 20%, 500 cycles per burst and an acoustic radiation intensity of 85W, and found these comparable to using a high pressure homogenisation. Therefore these conditions were initially chosen with a 4 minute treatment time. Due to product release problems, this was later increased to 4 minutes of duty cycle 20%, 1000 cycles per burst and an intensity of 10. This lysis step in the Covaris was controlled by software that enabled the automated treatment of up to 24 sample vials by moving the rack in relation to the transducer at the bottom of the water bath.

2.2.5.5 Thermo-chemical lysis

Cell pellets were incubated in a solution of 50 mM Tris, 0.1% v/v Triton X-100, 5 mM EDTA, 50 $\mu\text{g}\cdot\text{ml}^{-1}$ lysozyme, pH 7.2, with a total volume of 1 ml and an approximate cell concentration of 50 $\text{g}\cdot\text{l}^{-1}$ wet cell weight. The pH was adjusted to pH 9 with 8M sodium hydroxide (NaOH). Cells were then incubated in a 96-well, round bottom, polypropylene microplate at 37°C and 200 rpm using a thermomixer.

2.2.5.6 IB harvest

The lysed cells were centrifuged in tubes for 10 min at 13300 rpm and 5°C. The supernatant was then discarded to leave the inclusion body. For the experiments on the effect of fermentation conditions on DHFR IBs, the lysed cells were transferred to a 96-DSW well plate using automated liquid handling, covered and centrifuged at 5°C, 4000 rpm for 15 minutes to pellet the inclusion bodies. The supernatant was removed using automated liquid handling again.

2.2.6 Denaturation and Refolding

IB pellets were resuspended in solubilisation buffer (50mM Tris.HCl, 6M GdnHCl, 2mM DTT pH 7.2) and subjected to 3 cycles of sonication (10 s on, 10 s off).

Denatured inclusion body and purified DHFR samples were refolded by 1:20 or 1:15 dilution in each of the refold buffers (Table 2.5). Tris buffer was chosen as a benchmark and the other two buffers were chosen based from previously established work to optimise a buffer for this protein (Davies 2009). The automated protocol described previously for lysozyme was adapted for use with DHFR. Refold dilutions were carried out with either 20 μ l denatured protein and 280 μ l refold buffer (1:15), or 15 μ l denatured protein and 285 μ l refold buffer (1:20). Plates were covered and incubated for 24 hours before assaying.

For the study of the effect of fermentation conditions on DHFR refolding, inclusion body pellets were solubilised to 0.5-0.64 mg.ml⁻¹ in 50 mM Tris.HCl, 6 M GdnHCl, 2 mM DTT, pH 7.2 by shaking at 22 °C for 4 hours, centrifuged for 10 minutes at 13000 rpm and 4 °C to remove any remaining solids, and the supernatant of denatured protein used for refolding.

Table 2.5 Refold buffers used for DHFR

Buffer	Components
1 Tris	50mM Tris.HCl, pH 7.2
2 Optimised	50mM Tris.HCl, 0.25M arginine, 2mM cystine.2HCl, 2mM cysteine, pH 7.2
3 Reducing	0.25 M Potassium phosphate, 0.1 M potassium chloride, 1 mM DTT

2.3 Insulin

2.3.1 Materials and equipment

2.3.1.1 Materials

The expression host used was *E. coli* BL21 (DE3) with the expression vector pET-29a containing the gene for Humalog insulin and kanamycin resistance. All chemicals used in this experimental section were purchased from Sigma-Aldrich Company Limited (Poole, Dorset, UK), with the exception of the following; ethanolamine from Fischer Scientific (Loughborough, Leicestershire, UK), glycerol from Alfa Aesar (Heysham, Lancaster, UK), magnesium sulphate heptahydrate from VWR International (Lutterworth, Leicester, UK) and DTT from Fermentas (Sheriff Hutton, York, UK).

2.3.1.2 Large scale Equipment

A jacketed 146.5 L fermenter was used for the large scale fermentations (Biostat[®] D100, B. Braun Biotech International, Melsungen, Germany), with a working volume of 100 L and a top driven impeller of 3 Rushton turbines ($D_i = 0.16$ m). It was equipped with a digital control tower (DCU 3, Braun Biotech International). The fermenter has 4 equally spaced baffles and an aspect ratio of 3. Inoculation occurred by pumping inoculums from a shake flask (101U/R Sci-Q, Watson-Marlow, Falmouth, Cornwall, UK). Feed was also pumped into the fermenter from a sealed, sterile carboy (323S/D Sci-Q, Watson-Marlow). Cells were harvested by aliquoting into 1 L bottles and centrifuging (Avanti J-20 XP, Beckman Coulter, High Wycombe, UK). high performance disperser (T 25 digital Ultra-Turrax, IKA[®]-Werke, Staufen, Germany) homogenisation (Niro-Soavi high pressure homogeniser “Panda 2K”, GEA Process Engineering, Columbia, MD, US)

2.3.1.3 Microscale Equipment

The equipment used is identical to that in Section 2.2.1.2 for the microscale bioprocess sequence.

2.3.2 Large scale process

2.3.2.1 Inoculum Preparation

Media was prepared as detailed in Table 2.6 and adjusted to a pH of 7.2 with 1M sodium hydroxide. Two 2L baffled shake flasks containing 450 ml of media were autoclaved at 121°C for 30 minutes, along with a solution of 50% w/v glucose monohydrate solution. A 50 mg.ml⁻¹ kanamycin solution was prepared and sterilised using a 0.22 µm sterile syringe disc filter (Acrodisc, Pall, NY, US). Kanamycin and glucose monohydrate were then added aseptically to the cooled shake flask to give a final concentration of 0.05 mg.ml⁻¹ and 1% w/v, respectively. The flasks were pre-warmed in an incubator at 200 rpm and 37°C for 1 hour and then 200 µl of thawed cells were aseptically transferred to both flasks. The flasks were then incubated for 10 hours.

Table 2.6 vLB Basal Media

Component	Concentration (g.L ⁻¹)
Bacto Yeast Extract	5
Select soytone	10
NaCl	10

2.3.2.2 Large scale fermentation

Trace metal solution was prepared as detailed in Table 2.7, along with 1M magnesium sulphate solution, 1M Calcium chloride solution, 10% v/v orthophosphoric acid, 25% w/w ammonia solution and 50 mg.ml⁻¹ kanamycin. The feed solution was prepared as detailed in

Table 2.10 and autoclaved at 121°C for 30 minutes. Valves for phosphoric acid, ammonia, feed, inoculum and were prepared along with a valve for post sterilisation media supplements with a filter (0.2 µm Sartopore 2 150 capsule filter, Sartorius Stedim) and autoclaved at 121°C for 30 minutes.

Table 2.7 Trace metals composition

Components	Trace elements (per L)
Ortho-phosphoric acid	48.00 ml
FeSO ₄ .7H ₂ O	3.36 g
ZnSO ₄ .7H ₂ O	0.84 g
MnSO ₄ .H ₂ O	0.51 g
Na ₂ MoO ₄ .2H ₂ O	0.25 g
CuSO ₄ .5H ₂ O	0.12 g
H ₃ BO ₃	0.36 g

Table 2.8 Media composition for all three fermentations. Concentrations shown are per litre of media.

	1	2	3
NH ₄ SO ₄	14.0 g	14.0 g	14.0 g
Glycerol	35.0 g	15.0 g	40.0 g
Yeast Extract	20.0 g	20.0 g	40.0 g
KH ₂ PO ₄	2.0 g	2.0 g	2.0 g
K ₂ HPO ₄	16.5 g	16.5 g	16.5 g
NaCl	0.5 g	0.5 g	0.5 g
Citric Acid Anhydrous	7.5 g	7.5 g	7.5 g
Ortho-phosphoric acid	1.5 ml	1.5 ml	1.5 ml
Mazu Antifoam	0.2 ml	0.2 ml	0.2 ml

After preparation of the fermenter and calibration of pH and O₂ probes, the fermenter was filled with media, prepared as described in Table 2.8, and the fermenter and base

media were sterilised in situ at 121°C for 30 minutes. After cooling, lines were primed and the base media was supplemented with 1M magnesium sulphate solution (10 ml per L), 1M Calcium chloride solution (140 ml per L) and trace metals solution (34 ml per L). The fermentation operating parameters were set as temperature 37°C, stirrer speed $N = 250$ rpm (unless stated otherwise), airflow rate 1 vvm and pH 7.0. The pO_2 was calibrated and a sample removed to confirm pH values using an off-line system. The pO_2 controller was set using a minimum set point of 30% using a cascade method and then gas mix using oxygen enrichment. The kanamycin (1 ml per L) was then added immediately prior to inoculation. The fermenter was inoculated with shake flask culture (5 ml per L) using a pump. Samples were removed aseptically via the sample valve at frequent intervals to measure OD. Feeding was initiated after a DOT spike via a pump. Induction occurred 1 hour after feeding commenced by aseptically adding sterile filtered 0.5 M IPTG stock solution to give a final concentration of 0.5 mM. Samples were taken approximately every 3 hours for OD, wet and dry cell weight measurements. The fermentation was complete approximately 12 hours after induction (unless stated otherwise).

The media used in each of the three different fermentations in Chapter 6 are shown in Table 2.8. The first and second fermentations were fed batch, whereas the third fermentation was batch and hence no feeding took place. The second and third fermentations (low and high k_La matched conditions) were run with no cascade control and consequently no enriched oxygen gas blending and a constant impeller speed. Control of the pH was utilised (unlike in the microwell k_La run where this is not an option) due to the precipitation problems of the media at high pH.

2.3.2.3 Downstream processing

The harvested cells were centrifuged in 1 L bottles for 15 minutes at 8000 rpm and 4°C. The cell pellets were stored in the freezer at -20°C. Cells were defrosted and resuspended using a high performance disperser in phosphate buffered saline (PBS), 137 mM NaCl, 10 mM phosphate, 2.7 mM KCl, pH 7.4 to give a volume which is double the original fermentation volume. Cells were lysed using homogenisation and 3 passes at 800 ±100 bar at 15°C. The inclusion bodies were then harvested by centrifugation for 20 minutes at 8000 rpm and 4°C.

2.3.3 IB washing

The inclusion bodies were then washed by resuspension in purified water to the equivalent volume as the original fermentation volume and re-centrifuging twice. The washed and unwashed inclusion bodies were then resuspended to give a 5% or 10% slurry in purified water and stored in the freezer at 20°C.

2.3.4 Denaturation and Refolding

For the large scale refolds, washed and unwashed inclusion bodies were solubilised in 4.5 M urea, 365 mM ethanolamine, 10 mM DTT to give a concentration of 10 g.L⁻¹ or 1.5 g.L⁻¹ for 1 hour. The protein was then refolded by rapid dilution in buffer at varying dilution factors by the addition of protein to a 250 ml bottle with magnetic stirrer to give a final volume of 200 ml. For condition 13, the refold was conducted with a final volume of 4.5 L in a 5 L plastic container with liner and mixing was achieved using a top driven motorised impeller. The refold buffers used were buffer 1 (0.288 mM cystamine, 10% v/v hexylene glycol, 20 mM ethanolamine, pH 10.5) and buffer 2 (10 mM Tris, 10 mM glycine, 1 mM EDTA, 0.5 mM cysteine, 4.5 mM cystine pH 10.5).

2.3.5 Microscale Bioprocess Sequence

2.3.5.1 Microwell fermentation

2.3.5.1.1 *Inoculum preparation*

A baffled shake flask containing 100 ml of Luria Bertani (LB) media, 5 g.L⁻¹ yeast extract, 10 g.L⁻¹ tryptone and 10 g.L⁻¹ NaCl pH 7.2, was inoculated with 1 ml of defrosted *E. coli* cell stock and 50 µg.ml⁻¹ kanamycin and grown overnight at 37°C and 250 rpm. The inoculums typically reached an OD of 2.5-3 A.U.

2.3.5.1.2 *Fermentation preparation*

Media was prepared with the compositions detailed in Table 2.9, Table 2.9 and Table 2.11, the pH adjusted with NaOH or hydrochloric acid, and sterilised for 30 minutes at 121°C. Stock solutions of 1 M MgSO₄·7H₂O and 1 M CaCl₂·2H₂O were prepared and sterilised for 30 minutes at 121°C. The feed was prepared by combining MgSO₄·7H₂O (30 ml.L⁻¹ 1 M stock solution) and glycerol (714 g.L⁻¹) and sterilised for 30 minutes at 121°C. For the glucose batch media, glucose was also sterilised separately as a high concentration stock solution. The trace metal stock solution and antibiotics were sterilised by filtration (Minisart NML Syringe Filters, Sartorius Stedim, Surrey, UK). After cooling and aliquoting the media into sterilised troughs, trace metals (34 ml per

L), supplements of 1 M MgSO₄·7H₂O (10 ml per L) and 1 M CaCl₂·2H₂O (2 ml per L) and kanamycin were added and mixed to give the final media. This was then added to the sterilised platform along with the inoculums and sterile water for dilutions.

An IPTG stock solution of 50 mM was prepared and filtered sterilised into a sterilised trough and place on the platform. Cells were induced by the addition of 10 µl at the programmed time point to give a final concentration of 0.5 mM.

Table 2.9 Media composition for Terrific Broth (TB) pH 7.2

Components	Terrific Broth (per L)
Yeast Extract	24.00 g
Tryptone	12.00 g
Glycerol	4.00 ml
KH ₂ PO ₄	2.31 g
K ₂ HPO ₄	12.54 g

Table 2.10 Feed solution

Component	Concentration (per L)
1M MgSO ₄ ·7H ₂ O	30 ml
Glycerol	714 g

Table 2.11 Medium composition for batch versus fed batch comparison experiment pH 7.0

Components	Batch medium (per L)	Fed batch medium (per L)
NH ₄ SO ₄	14.0 g	14.0 g
Glycerol	40.0 g	35.0 g
Yeast Extract	40.0 g	20.0 g
KH ₂ PO ₄	2.0 g	2.0 g
K ₂ HPO ₄	16.5 g	16.5 g
NaCl	0.5 g	0.5 g
Citric Acid Anhydrous	7.5 g	7.5 g
Ortho-phosphoric acid	1.5 ml	1.5 ml

2.3.5.1.3 Automated fermentation program

The fermentation was performed as described for DHFR with automated plate preparation, inoculation, induction and hourly sampling with OD measurements. A

feeding strategy was added into the existing loop to give a feeding rate of approximately $11 \text{ g.L}^{-1}.\text{h}^{-1}$. When comparing batch and fed batch, sterilised distilled water was added to the batch wells instead of feed to ensure volumes were constant between the two conditions. A summary of the fermentation conditions used in this chapter are shown in Table 2.12.

Table 2.12 Fermentation conditions

Variable	Induction time (h)	Media	Feeding started (h)	Fermentation length (h)
Induction time	3.5, 4, 4.5, 5	Glycerol fed batch	5	18
Batch and Fed-batch	6	Glycerol batch, glycerol fed batch	5	18
Carbon source	3.5	LB, TB, Glucose batch, Glycerol batch	n/a	22

2.3.6 Denaturation and Refolding

Inclusion body pellets were defrosted and solubilised in a denaturing buffer of 4.5 M urea, 365 mM ethanolamine, 10 mM DTT pH 10.6 at a concentration of 0.4 mg.ml^{-1} and left to shake at 800 rpm for 4 hours. Refolding was achieved by automated microscale dilution refolding, with a dilution factor of 18 fold and a final refold volume of $300 \mu\text{l}$. The buffers used for refolding are shown in Table 2.13.

Table 2.13 Insulin refold buffers

Refold Buffer	Components
1	0.288 mM cystamine, 10% v/v hexylene glycol, 20 mM ethanolamine, pH 10.5
2	10 mM Tris, 10 mM glycine, 1 mM EDTA, 0.5 mM cysteine, 4.5 mM cystine pH 10.5
3	1M acetic acid pH 3.8

2.4 Determination of k_{La} using static gassing out method

2.4.1 Large scale fermenter

The static gassing out technique (Suhaili et al., 2010) was used to calculate the k_{La} in a baffled 146.5 L fermenter, with 3 Rushton impellers, filled with the media detailed in

Table 2.8. The probe (InPro 600, Mettler Toledo, Leicester, UK) was calibrated by zeroing during sterilisation and set to 100% using air and the maximum impeller speed. The media was purged of oxygen using nitrogen to achieve a DOT below 20%. The increase in DOT over time was then recorded at various impeller speeds, with a constant gas flow rate of 1 vvm and a temperature of 37°C. The probe response time was also measured as a 63.2% stepwise change (Tribe et al., 1995) and the response time with no mixing (impeller speed= 0 rpm) was $0.011 \text{ h} \pm 0.007$. At the lowest impeller speed the delay was found to be negligible and therefore neglected in the calculation of k_{La} .

$$1/k_{La} = 0.053 \text{ h}$$

$$\tau = 0.011 \text{ h} \ll 1/k_{La}$$

2.4.2 Microscale DSW plate

The static gassing out technique (Doig et al., 2005a; Islam et al., 2008) was used to calculate k_{La} in microwell plate format using batch media (Table 2.11) and a temperature of 37°C. The probe was calibrated to 0% using a superficial nitrogen gas stream. The probe response time was calculated by purging the oxygen saturated system (DOT= 100%) by gassing in nitrogen until a DOT below 37%. The probe response time was defined as the time needed to achieve a 63% stepwise change. It was calculated as $4.96 \pm 0.013 \text{ h}^{-1}$. As the probe response time is very small in comparison to the k_{La} 's expected, it was considered to be negligible and not taken into account in the calculation of k_{La} .

The dissolved oxygen tension (DOT) was measured using an oxygen sensitive fluorescence patch connected by a fibre optic cable to an oxygen measuring instrument (Oxy4 Oxygen Metre, PreSens, Regensburg, Germany). A DSW plate was adapted to include a well with a 3 mm diameter Perspex window at the bottom. The oxygen patch can then be placed inside the well at the Perspex window and the detection probe to be attached to the outside of the window using a connector (Figure 2.3). This allows the measurement of the fluorescent signal and consequently the dissolved oxygen concentration the patch is exposed to (using PreSens software to convert the signal to DOT). Details of the design can be found in Islam, (2007); Ferreira-Torres, (2008).

The gas-liquid mass transfer k_{La} was measured at different shaking speeds and fill volumes using the set-up described. The well was filled with batch media (and in some

experiments 0.02% PPG) and pre-warmed for 30 minutes, the shaking speed set and a nitrogen stream was introduced until the DOT had decreased to below 20%. Once the nitrogen had been removed, air was allowed to transfer to the media via superficial gas transfer. The instrument recorded the DOT values every 2 seconds.

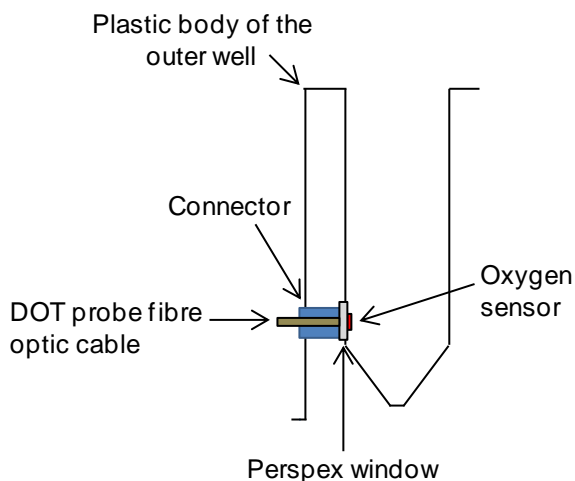


Figure 2.3 Diagram of microwell oxygen probe for k_La determination.

2.5 Analytical Techniques

2.5.1 Sodium dodecyl sulfate polyacrylamide gel electrophoresis (SDS-PAGE)

Fermentation samples were prepared by pipetting 1 ml of cell broth into 2.2ml eppendorf tubes. The cells were then cooled to 4°C in ice and centrifuged at 13000 rpm and 4°C for 10 minutes to harvest the cells. The supernatant was then discarded and the pellet resuspended in 50mM Tris.HCl pH 7.2. This was then sonicated on ice (10 cycles, 10 s on, 10 s off) to lyse the cells and release the inclusion bodies. The disrupted cells were then centrifuged again at 13000 rpm, 4°C, for 10 minutes. The supernatant was decanted and collected as the soluble fraction for analysis. The pellet was then re-suspended in 50mM Tris.HCl pH 7.2 and vortexed to mix or denatured in 50mM Tris.HCl, 6 M Urea, pH 7.2.

SDS-PAGE was performed using NuPAGE[®] Tris Glycine 12% pre-cast gels (Invitrogen, USA) and 1x Tris-glycine running buffer. Samples were denatured and reduced by adding 2x concentrated Laemmli sample buffer (% (w/v) SDS, 20% glycerol (v/v), 10% (v/v) 2-mercaptoethanol, 0.004% (w/v) bromophenol blue and 0.125 M Tris HCl, pH 6.8) in a ratio of 1:1 and heated to 90°C for 8 minutes in a thermomixer. The

samples were then mixed and 10 or 20 μl loaded onto the wells of the gel, along with 5 μl of ladder. Electrophoresis was then conducted at 80V for approximately 90 minutes (Invitrogen Novex Mini Cell, Life Technologies, NY, USA). The bands were then visualised by staining with Coomassie stain for 1 hour (0.5g/l coomassie blue, 50% methanol, 10% acetic acid) and then destaining with purified water overnight. The gel was then captured using Gel Doc-It Imaging system (UVP, CA, USA) and protein bands were quantified using Labworks software (UVP, CA, USA).

2.5.2 Total protein concentration

The total protein concentration was determined using a Bradford assay. A standard curve was prepared from a solution of $2\text{mg}\cdot\text{ml}^{-1}$ bovine serum albumin (BSA) serially diluted in Tris buffer to give concentrations ranging from 0.1 to $1.4\text{ mg}\cdot\text{ml}^{-1}$. Bradford Reagent was gently mixed and allowed to come to room temperature. 5 μl of the protein standards, buffer for controls, and samples of unknown concentration (diluted to give an approximate protein concentration of below $1.4\text{ mg}\cdot\text{ml}^{-1}$) were added to a 96 well plate in triplicate. 250 μl of Bradford Reagent was then added to each well and mixed by 3 cycles of pipette aspiration. The samples were left to incubate at room temperature for 5 to 15 minutes and then absorbance measured at 595 nm in a microplate reader (Safire, TECAN, Reading, UK). The net absorbance of each standard was then plotted against the protein concentration and used to determine the protein concentration of the unknown samples. For the large scale fermentation experiments this was performed manually, but in all other experiments this was automated on the Genesis platform and absorbance measured on a different microplate reader (Infinite 2000, TECAN, Reading, UK).

Samples were prepared from cell suspensions were spun down at 13000 rpm and 4°C for 10 minutes. The supernatant (soluble fraction) was removed via pipetting and reserved. The pellet (insoluble protein fraction) was resuspended in 50 mM Tris, 6 M GdnHCl using sonication (3 cycles of 10 s on, 10 s off). A standard curve was prepared with BSA dissolved and serially diluted in 50 mM Tris, 6 M GdnHCl.

2.5.3 Flow cytometry

2.5.3.1 Fluorescence staining

Samples were diluted using 0.2 μm filtered 0.5 M Tris pH 8.5 to give a cell concentration of approximately 1×10^6 cells. ml^{-1} before staining (to result in 10,000 events in 300 s time frame). The cell count was established using the CASY cell counter and analyser (Roche Diagnostics, West Sussex, UK). SYTOX Green Nucleic Acid Stain (Molecular Probes, Invitrogen) was used as provided in a 5 mM solution in DMSO. Cells were stained by the addition of 4 μl to 1 ml of diluted cells, gently mixed and left for a minimum of 40 minutes prior to analysis.

2.5.3.2 Measurement

Samples were analysed using a Beckman Coulter XL MCL flow cytometer (Beckman Coulter, Fullertone, CA, USA), which detected light scattering and fluorescence emissions. Samples were illuminated by an air cooled argon ion laser (488 nm, 15 mW) and fluorescence detection occurred using a standard filter configuration. Each experiment was set to collect 10,000 events or to timeout after 300s. Voltages and gains were set as follows: 50 V and 2.0 for forward scatter (FS), 131 V and 5.0 for side scatter (SS), 286 V and 1.0 for fluorescence filter with bandwidth 525 nm (FL1). Data was analysed using EXPO32 ADC Analysis.

2.5.4 Particle sizing

The Malvern Mastersizer 2000 laser sizer (Malvern, Worcestershire, U.K.) enabled the measurement of particle size between 0.02 to 2000 μm by laser diffraction. Drops of the homogenised sample were added to the small volume sample dispersion unit until the level of obscuration reached 15%.

2.5.5 Cell concentration (biomass)

2.5.5.1 Insulin fermentation

For wet and dry cell weight measurements, 10 ml of sample was added to pre weighed glass test tubes and centrifuged in a bench top centrifuge for 15 minutes at 5000 rpm. The supernatant was then discarded and mass of the tube with wet pellet was measured and the wet cell weight calculated. The test tube was then placed in an oven at 80°C and left overnight to dry, before it was then re-weighed to determine the dry cell weight. OD measurements were performed by blanking the spectrophotometer with water,

diluting the sample to within the appropriate linear range (<1 A.U.) and measuring the absorbance at 600 nm.

2.5.5.2 DHFR and microscale fermentation

Wet cell weight and dry cell weight were determined by adding 2 ml of cell suspension to a pre-weighed 2.2 ml tube (Eppendorf). This was then centrifuged at 13000 rpm and 4°C for 10 minutes. The supernatant was then removed using a pipette and discarded. The tube was then weighed and the wet cell weight calculated. The tube was then placed in an oven at 80°C and dried for 24 hours prior to re-weighing to give the dry cell weight.

2.5.6 Acetic acid quantification

A Megazyme (Co. Wicklow, Ireland) acetic acid kit was used to determine the concentration in fermentation broth samples. Samples were heated to approximately 80°C for 20 minutes to denature enzymes that might interfere with the assay. Undiluted samples were mixed in a plastic cuvette with distilled water, a buffer containing nicotinamide adenine dinucleotide hydride (NADH), adenosine triphosphate (ATP), phosphoenolpyruvate (PEP), polyvinylpyrrolidone (PVP) and coenzyme A (CoA) solution and a solution containing D-lactate dehydrogenase (D-LDH), phosphotransacetylase (PTA) and pyruvate kinase (PK). The spectrophotometer was blanked against water at 340 nm, and after 2 minutes the absorbance of the samples was read. The reaction was then started by adding acetate kinase suspension, mixing by gentle inversion whilst covered in parafilm and reading the absorbance again after 4 minutes. The absorbance change was then used to calculate the concentration of acetic acid (See Appendix 9.4.2).

2.5.7 Lysozyme assays

2.5.7.1 Absorbance

Absorbance was measured at 280, 340 and 600 nm. The buffer control was subtracted from all standards and refolds.

2.5.7.2 Intrinsic Fluorescence

Intrinsic fluorescence was measured by excitation at 280 nm and emission at 340 nm, as described previously (Aucamp et al., 2005, 2008). The buffer control was subtracted from all standards and refolds. Intrinsic fluorescence was determined relative to that of a standard in the same buffer condition to account for effects of the buffer on

fluorescence intensity, and experimental variations in the voltage gain applied to the instrument photomultiplier tube, to give relative fluorescence (where a relative fluorescence of 1 is a refold with the same intrinsic fluorescence as the standard).

2.5.7.3 Lysozyme activity

Samples of 10 μl were taken after 24 hours, transferred to a 96-SRW plates (96- well micro test plates PS, Sarstedt, Leicester, UK), and diluted 1:10 with 0.1 M potassium phosphate, pH 6.6 for the activity assay. Diluted samples were assayed by transferring 10 μl into a new plate and adding 290 μl of *Micrococcus lysodeikticus* cell suspension (0.3 g/L in 0.1M potassium phosphate pH 7). The decrease in absorbance at 450 nm and at room temperature was measured for 3 minutes and activities determined as the gradient of the initial linear region of the curves. Rates calculated from buffer only samples were subtracted and the final rates compared with those obtained for standards of native lysozyme (assigned an activity value of 100%).

2.5.7.4 Circular dichroism

Prior to circular dichroism (CD), samples were dialysed for at least 24 hours using a buffer of 1.2M guanidine hydrochloride, 50mM Tris.HCl and 4mM cystamine to decrease the concentration of DTT present. The protein concentration was determined using a spectrophotometer and then adjusted to 0.1 $\text{mg}\cdot\text{ml}^{-1}$ by diluting with dialysis buffer. Samples were then filtered through a 0.2 μm filter. Refold samples and standards were measured in 300 μl cuvettes with 0.1 cm pathlength. The mean ellipticity (ΔMRE , $\text{deg cm}^2 \text{dmol}^{-1}$) was used to monitor the secondary structure of lysozyme. Data was smoothed for repeats by taking the average for two points either side of each data point. Circular dichroism spectra (190-300 nm) were measured on a 202 SF spectrometer (AVIV Associates, Lakewood, NJ) at 25°C using a quartz precision cell cuvette with a pathlength of 1 mm.

2.5.8 DHFR Assays

2.5.8.1 Absorbance

Absorbance at 280, 340 and 600 nm was measured in a plate reader. The buffer control was subtracted from all standards and refolds.

2.5.8.2 Intrinsic fluorescence

Intrinsic fluorescence of refolded samples was measured in the plate reader (TECAN Infinite 2000, Reading, UK), using 280 nm excitation and 340 nm emission.

Fluorescence intensities were simultaneously measured for the standard native proteins at the same buffer conditions for direct comparability, however due to their poor refolding they were not used as standards as for lysozyme.

2.5.8.3 DHFR activity

The activity was determined in 96-well plates from the rate of decrease in absorbance at 340 nm (A₃₄₀) for NADPH consumption as DHFR reduced dihydrofolate (DHF) to tetrahydrofolate (THF). 40 µl of assay buffer (50mM Tris.HCl, 50µM EDTA, pH 7.2) was added to each well,, followed by 50 µl of 1 mM NADPH in assay buffer. 60 µl of undiluted sample was then added and incubated for 5 minutes. Reactions were initiated by the addition of 50 µl 1 mM DHF in assay buffer and mixed by aspiration-dispense. The A₃₄₀ was measured every minute for 25 minutes in the plate reader. The rate of decrease in absorbance was then normalised by the final protein concentration.

2.5.9 Insulin Assays

Absorbance and fluorescence assays were performed as previously detailed in Section 2.5.8.1 and 2.5.8.2.

2.5.9.1.1 Preparation of fermentation samples for HPLC

Fermentation samples were pelleted by centrifugation at 13300 rpm for 5 minutes at 5°C, then resuspended in phosphate buffered saline (PBS) by vortexing. Cells were then lysed using sonication (20 cycles, 8 s on, 8 s off). The lysed cells were then centrifuged 13300 rpm for 10 minutes at 5°C to harvest the IBs. The IBs were then solubilised in 7.6 M urea, 24 mM DTT, 343 mM ethanolamine, mixed by vortexing and left to mix on a shaker for 30 minutes. Aliquots were then transferred to microcentrifuge tube and centrifuged 13300 rpm for 5 minutes at 5°C and filtered using an 0.22 µm syringe filter into HPLC vials. Refold samples were either transferred straight to HPLC vials with inserts or if aggregates were present they were filtered first before transferring to vials.

2.5.9.1.2 Reverse phase HPLC for titre and refolding yield determination

A reverse phase HPLC assay was used to quantify the titre of insulin in crude fermentation samples and the yield of bioactive insulin in refold samples. A C18 Nucleosil[®] 100-5 reverse phase column (Agilent Technologies, CA, US), was used on an Agilent 1200 series High Pressure Liquid Chromatography System using ChemStation software and a detection wavelength of 210 nm. A linear

acetonitrile/water gradient of 0.1% (v/v) TFA (18-90 % over 39 minutes) at a flow rate of 1 ml.min⁻¹ was used, with a sample injection volume of 100 µl. A standard curve was created using recombinant human insulin solution (Sigma-Aldrich, Gillingham, UK) of varying concentrations (0.05-0.75 mg.ml⁻¹) in order to calculate the insulin concentration. The yield for the large scale fermentations was determined using a lower injection volume of 50 µl using a different column (Poros R2/10, Applied Biosystems) and HPLC system (Walters Alliance HPLC system with Empower software). The yield for the large scale refolds were determined by RP-HPLC using the same method and system but a different column (XBRIDGE, Waters, Elstree, Hertfordshire). Refold samples were taken after 16 hours after the initiation of refolding, centrifuged (Multifuge 1 S-R, Heraeus DJB Labcare, Newport Pagnell, Buckinghamshire, UK) for 10 minutes at 13,200 rpm and filtered through a 0.2 µm syringe filter (Acrodisc Syringe filter or Fluorodyne II Membrane, Pall, Portsmouth, UK).

3 Assay Development¹

3.1 Introduction

The optimisation of the refolding step is crucial during process development and must be determined on a case by case basis for every new inclusion body product. Despite knowledge of the main factors involved in refolding, no universal refolding buffer has been reported to date, and so multiple parameters must be investigated empirically to optimise the refolding yield of each new protein. Such protein screening studies can be time consuming given the large number of potential parameters that may affect yield. A high-throughput microscale screening approach is a possible solution. It would enable rapid optimization early on in process development using low quantities of often expensive material and allow multiple conditions to be tested in parallel. Protein refolding is largely scale-invariant, therefore the microwell plate format can be used for the rapid and meaningful screening of many process conditions (Middelberg, 2002). In addition, the integration of microscale approaches with robotic platforms allows higher throughput studies and greater precision and accuracy of liquid handling operations. Numerous studies have used a microwell format for the high-throughput screening of protein refolding reagents (Vincentelli et al., 2004; Willis et al., 2005; Mannall et al., 2009; Dechavanne et al., 2011). The combination of high-throughput microwell screening methods with fractional factorial and other Design of Experiment (DoE) approaches have been reported to efficiently screen and allow the optimisation of many combinations of additives to improve refolding yields (Williams et al., 1982; Mannall et al., 2009; Dechavanne et al., 2011). Therefore the microwell approach was used to analyse multiple refolding parameters at a high throughput.

A common challenge experienced in microplate-based refolding is the analytical bottleneck caused by the parallel study of a large number of conditions and the absence of suitably high-throughput and generic assays of biological function to identify the correct folding of most proteins. Absorbance measurements can be used as a rapid

¹ Results from Section 3.3.2 onwards have been published Ordidge, G.C., Mannall, G., Liddell, J., Dalby, P.A., and Micheletti, M. (2012). A generic hierarchical screening method for the analysis of microscale refolds using an automated robotic platform. *Biotechnology Progress* 28, 435–444.

method to differentiate aggregates from soluble protein. Several wavelengths have been previously used to indirectly measure the concentration of insoluble aggregates by scattering light (Vincentelli et al., 2004; Mannall et al., 2009). However single measurements with surrogate assays such as turbidity or absorbance cannot readily distinguish between soluble native and misfolded proteins. Intrinsic tryptophan fluorescence can be a suitable probe for studying refolding as it can distinguish the folding environment of the protein and has already been used to follow lysozyme refolding (Dobson et al., 1994; Raman et al., 1996; Terashima et al., 1996; Katoh et al., 1999). The gold standard for establishing yield however remains an activity assay or HPLC assay. Reversed-phase HPLC assays can be used to resolve native and misfolded species, but the technique is relatively slow and time consuming. Therefore, it is important to minimise the number of samples that require analysis by more costly and time intensive techniques such as HPLC or biological function assays. The absorbance and fluorescence assays were employed with a view to reducing the analytical bottleneck caused by high throughput microwell studies.

The microscale approach was demonstrated using two different proteins. Lysozyme was selected as a model protein for initial studies due to its readily available supply, well characterised folding pathway and the large number of previous refolding studies (Buswell and Middelberg 2002; Buswell and Middelberg 2003; Lee et al. 2002; T. Kiefhaber 1995; Wildegger and Thomas Kiefhaber 1997; Radford et al. 1992; Roux et al. 1997). Yields for lysozyme refolds appear to be optimal at a ratio of 1:1-3:1 and a total thiol concentration of 5-15 mM (Hevehan and De Bernardez Clark 1997). Several studies have reported high yields of lysozyme when refolding at high protein concentrations (up to 5 mg/ml) whilst maintaining a concentration of 1-2M of denaturant (Hevehan and De Bernardez Clark 1997; Mannall et al. 2007). Additionally a number of low molecular weight additives are known to reduce lysozyme aggregation, therefore there is plenty of scope for studying yield improvements. DHFR was chosen as it could be produced in inclusion bodies by fermentation in *E. coli* and the assays could be tested using a more challenging feed stream to give more industrially relevant results. Inclusion bodies are contaminated by varying levels of impurities such as host proteins, nucleic acids and cell membrane components, which can affect renaturation yields (Maachupalli-Reddy et al. 1997). It is also possible that their presence may interfere with some of the assays to be tested. Therefore the assays were developed

using readily available lysozyme and then challenged with inclusion body material to test their effectiveness.

The aim of this chapter is to develop a generic, automated and high-throughput microscale process sequence with suitable assays for protein refolding. This will enable rapid process development and a deeper understanding of their contribution to yield using a one factor at a time approach. The microwell format was used to investigate the factors affecting refolding as it gives rapid, meaningful information and allows automated high throughput experimentation. The assays for protein refolding must be reproducible, accurate, and allow rapid ranking of refold conditions in order to optimise the protein refolding process based on factors such as pH, buffer, excipients, protein concentration and dilution ratios. They also must be capable of handling a large number of samples in order to avoid an analytical bottleneck. Absorbance, fluorescence and activity assays were considered for information richness, generic application and capacity for high throughput analysis.

3.2 Materials and Methods

Experiments with lysozyme were conducted as described in 2.1.1 (Materials and Equipment) and 2.1.2 (Denaturation and Refolding). Refold buffers are summarised again here to aid referral. Assays were carried out as described in 2.5.7 Lysozyme assays.

Table 3.1 Lysozyme refold buffers for 3.3.1.1 Selection of wavelengths for aggregation detection and solubility, 3.3.1.2 Absorbance changes during refolding and buffer 2 and 3.3.1.4 Example of end point analysis

	Buffer components
1	25 mM cysteine, 1 mM EDTA and 0.1 M Tris-HCl pH 8.2.
2	L-arginine 0.14 M, 25 mM cysteine, 1 mM EDTA and 0.1 M Tris-HCl pH 8.2.
3	Sucrose 0.20 M, 25 mM cysteine, 1 mM EDTA and 0.1 M Tris-HCl pH 8.2.

Table 3.2 Denatured protein and refold buffer conditions for 3.3.1.2 Absorbance changes during refolding

[Protein] (mg.ml ⁻¹)	[DTT] (mM)	Redox pair	Redox potential	Buffer components	[Final Protein] (mg.ml ⁻¹)
7.5	25	Cysteine:cystine	Balanced	5 mM cystine, 10 mM cysteine, 50 mM Tris	0.5
7.5	25	Cysteine:cystine	Oxidising	10 mM cystine, 50 mM Tris	0.5
15	32	DTT:cystamine	Balanced	4 mM cystamine, 50 mM Tris	1
15	6	DTT:cystamine	Oxidising	4 mM cystamine, 50 mM Tris	1
15	62	DTT:cystamine	Reducing	4 mM cystamine, 50 mM Tris	1

Table 3.3 Refold buffers and DTT concentration in denatured protein to give different redox potentials, as used in 3.3.1.3 Fluorescence changes during refolding and 3.3.3.1 Oxidation

Buffer (redox pair)	[DTT] (mM)	Redox potential	Components
DTT:cystamine	32	Balanced	4 mM Cystamine 50 mM Tris
DTT:cystamine	6	Oxidising	4 mM Cystamine 50 mM Tris
DTT:cystamine	62	Reducing	4 mM Cystamine 50 mM Tris

Table 3.4 Refold buffers used for 3.3.4 Hierarchical assays using lysozyme

Buffer components	
1	25 mM cysteine, 1 mM EDTA, 0.1 M Tris.HCl
2	25 mM cysteine, 1 mM EDTA, 0.1 M Tris.HCl, 0.14M arginine
3	25 mM cysteine, 1 mM EDTA, 0.1 M Tris.HCl, 0.3M GdnHCl
4	25 mM cysteine, 1 mM EDTA, 0.1 M Tris.HCl, 0.3M GdnHCl, 0.14M arginine
5	25mM cystamine, 50mM Tris.HCl and 0.717M GdnHCl, 1mM EDTA
6	4mM cystamine, 50mM Tris.HCl and 0.715M GdnHCl (used in oxidation experiment with different [DTT] to create different redox potentials)
7	4mM cystamine, 50mM Tris.HCl and 0.678M GdnHCl
8	5mM cystine, 10mM cysteine, 50mM Tris.HCl, 0.717M GdnHCl (balanced)
9	2.86mM cystine, 14.29mM cysteine, 50mM Tris.HCl, 0.717M GdnHCl (reducing)
10	10mM cystine, 50mM Tris.HCl, 0.717M GdnHCl (oxidising)

Experiments with DHFR were conducted as described in 2.2.1 (Materials and Equipment) and 2.2.6 (Denaturation and Refolding). Refold buffers are summarised again here to aid referral. Assays were carried out as described in 2.5.8 DHFR Assays.

Table 3.5 Refold buffers used for DHFR

Buffer	Components
1 Tris	50mM Tris.HCl, pH 7.2
2 Optimised	50mM Tris.HCl, 0.25M arginine, 2mM cystine.2HCl, 2mM cysteine, pH 7.2
3 Reducing	0.25 M Potassium phosphate, 0.1 M potassium chloride, 1 mM DTT

3.3 Results and Discussion

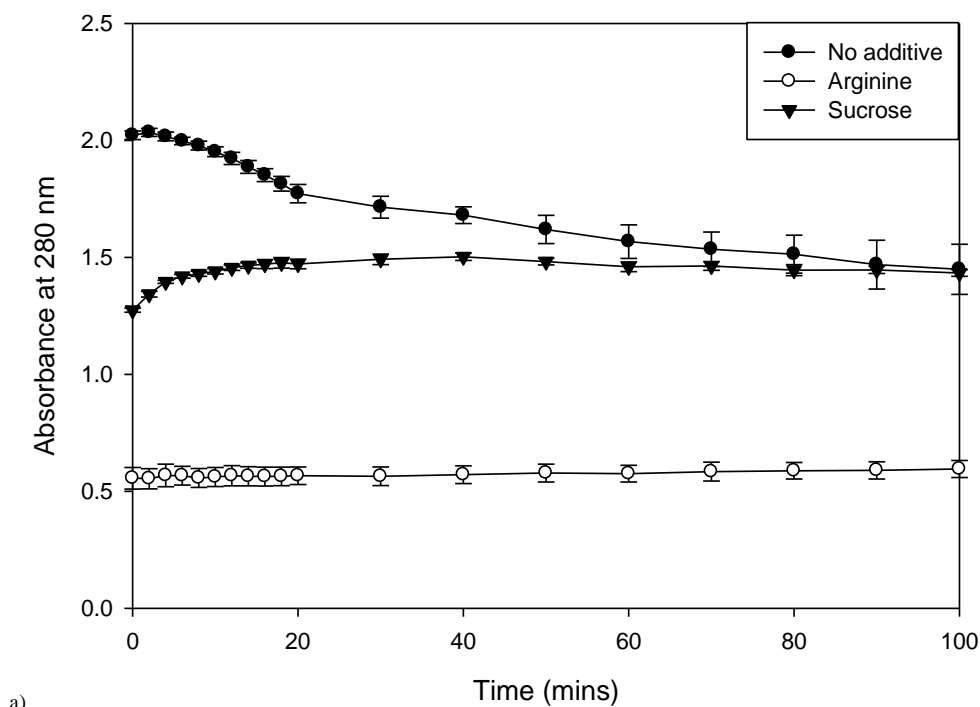
3.3.1 High-throughput assay selection

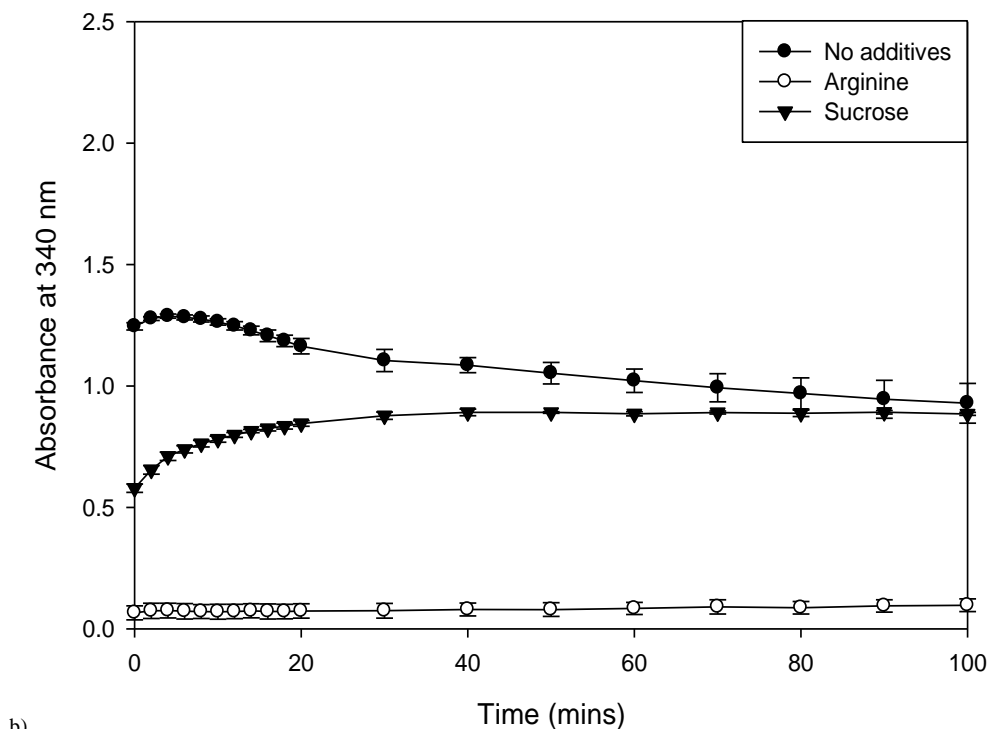
3.3.1.1 Selection of wavelengths for aggregation detection and solubility

A number of different wavelengths have been reported in the literature for detecting aggregate particles, such as 450 nm (Raman et al., 1996), 340 nm, 390 nm (Vincentelli et al., 2004) and 600 nm. Conventionally 280 nm is used for determining protein concentration. In order to select the appropriate wavelengths, experiments were conducted with buffers containing different excipients. Figure 3.1 (a, b, c) shows the absorbance profile during refolding for three widely used wavelengths, 280 nm, 340 nm and 600 nm, under three different buffer conditions. Despite all the refold conditions having the same protein concentration in the refold (and buffer effects removed by subtracting a control), the refolds have vastly different absorbencies ranging in starting absorbance from 0.5 to 2.0 A.U. At 280 nm the absorbance of each of the three conditions is separated by approximately 0.75 arbitrary units (A.U.). Compared with higher wavelengths the degree of separation between the refolds in different conditions is much better at 280 nm, at 600 nm the separation is much smaller ranging only from 0.1 to 0.6. This highlights that 280 nm can separate distinct refold conditions to a greater degree and might be expected to reflect a combination of differences in the concentration of soluble protein, the degree of light scattering by particles, or in the relative populations of natively folded, misfolded, and unfolded proteins.

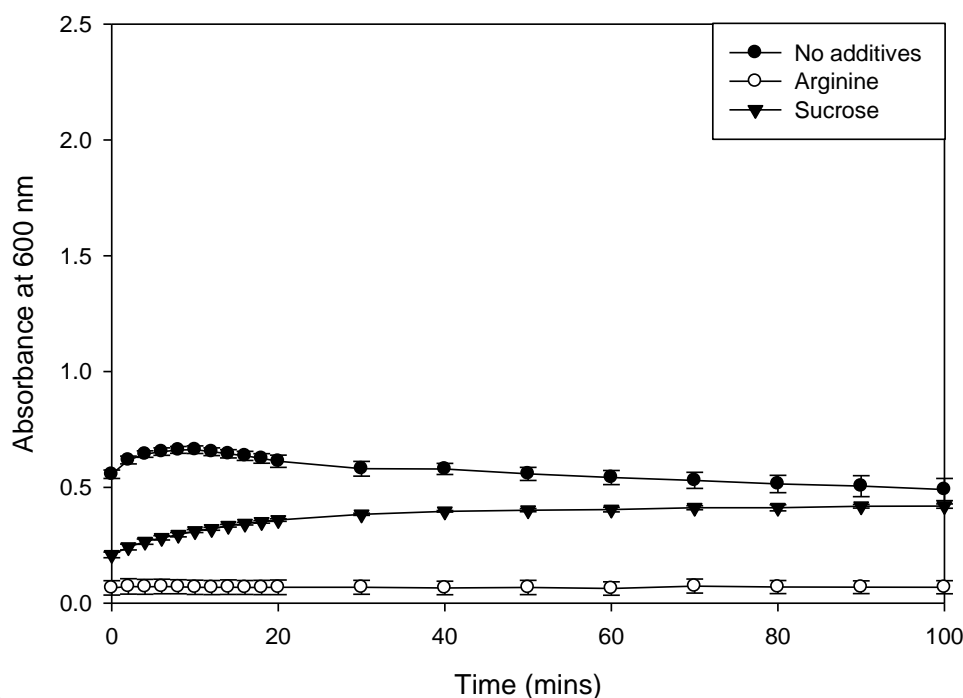
The ranking remains the same for all three wavelengths, the refolds in a buffer with no excipients have the highest absorbance, followed by sucrose buffer. Overall, the high absorbance values correlated with the visible appearance of aggregation. The refolds in arginine buffer have the lowest absorbance, with the absorbance remaining constant over time, indicating a soluble refold. Arginine is known to act like a mild denaturant, maintaining conformational flexibility and preventing intramolecular interaction and aggregation during refolding. It is often used as an excipient to aid refolding and suppresses aggregation of partially unfolded proteins and intermediates (Marston 1986). In the other conditions the absorbance changes over time and reaching a steady state appears to be slower in these conditions. For 280 and 340 nm the absorbance decreases over the first 20 minutes for a buffer with no additives from a very high absorbance,

which indicates the fast formation of aggregates followed by some dissolution. On the other hand in the sucrose buffer a small increase is observed from a lower starting absorbance, which shows the rate of aggregation formation is different between these conditions. The changing absorbance at 280 nm does not result from different proportions of folded and unfolded protein during refolding as the absorbance remains fairly constant for folded and unfolded protein (see Figure 9.1 in Appendix for absorbance of denatured and native protein in different buffers at different concentrations). Unfolded protein results in more subtle variations in absorbance at 280 nm, and denaturing the protein with guanidine hydrochloride results in a shift of the maximum absorbance to a shorter wavelength (Pace 1995). Therefore the four times greater absorbance for additive free refolds compared to the refold in arginine results from light scattering by the presence of aggregates. In conclusion, absorbance changes over time for some of the refold conditions, which reflects a transition from unfolded protein to both soluble native, and insoluble aggregated protein.





b)



c)

Figure 3.1 The effect of different wavelengths on the absorbance profile of refolds in different buffers a) 280 nm, b) 340 nm and c) 600 nm.

3.3.1.2 Absorbance changes during refolding

Absorbance changes that occur as a function of time during refolding can be explained in part by the formation of insoluble protein. This is illustrated during experiments to

investigate the impact of DTT and redox couples on the formation of insoluble protein. Figure 3.2 shows the effect of DTT concentration on the amount of soluble protein present during the course of refolding. It demonstrates that the concentration of soluble protein increases with time during a refold at high DTT concentration, whereas at a lower DTT concentration the soluble protein concentration is stable at 0.17 mg.ml^{-1} . This indicates that at a low DTT concentration there are no significant changes in the partition between soluble protein and insoluble aggregates, and any aggregates formed early on are not deconstructed to soluble protein to be refolded. At a higher DTT concentration, the concentration of soluble protein immediately after the start of refolding is lower at 0.107 mg.ml^{-1} , but increases to 0.156 mg.ml^{-1} after 50 minutes reaching a similar level as for a lower DTT concentration. This shows that more soluble protein has become available for folding and the partition between soluble and insoluble protein is not constant for a high DTT concentration.

The final yield of soluble protein after 100 minutes of refolding for a high DTT concentration is greater than at a low DTT concentration. A lower concentration of DTT could result in a lack of reducing power, altering the redox potential and resulting in a lack of reducing species to break incorrectly formed disulphide bonds in misfolded protein, resulting in a lower final yield of 0.167 mg.ml^{-1} . At a higher DTT concentration, the yield is initially lower but increases over time to reach a higher yield of 0.205 mg.ml^{-1} . Gerami et al. (2011) have shown that the refolding of recombinant tissue plasminogen activator (rPA) is sensitive to residual DTT concentration and DTT inhibits refolding. Guise and Chaudhuri (2001) found that refolding yield of lysozyme is highest at low DTT concentrations and yield fell rapidly at concentrations above 0.6 mM with their redox system (3 mM reduced glutathione, 0.3 mM oxidised glutathione). A high DTT concentration could affect the rate of folding by breaking disulphide bonds in correctly folded protein or rapidly formed misfolds, resulting in a lower yield of native protein at the early stages. If misfolded protein with incorrect disulphide bond pairs formed either intra-molecularly or inter-molecularly, high DTT concentrations could provide the reducing power to allow these disulphide bonds to break. This provides the protein with another chance of folding to soluble native protein, allowing it to recycle through the refolding pathway again. This demonstrates that absorbance changes over time as a result of refolding and aggregation kinetics. Large changes in absorbance result from the scattering of aggregates. This effect is combined with small absorbance changes, which reflect native soluble protein folding.

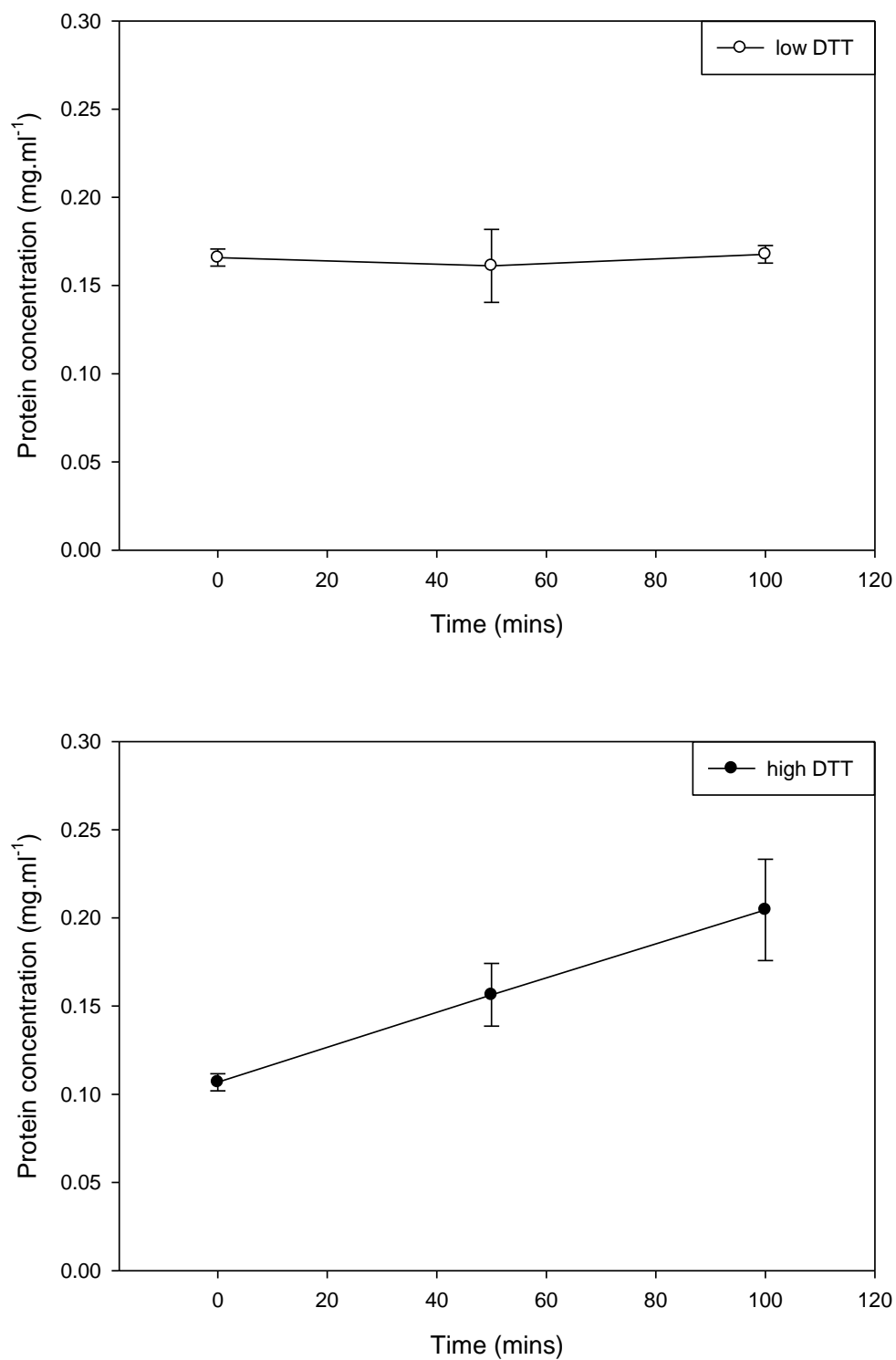


Figure 3.2 The concentration of soluble protein during the course of a refold experiment at two different DTT concentrations (25 mM and 0.625 mM).

In addition to monitoring fluctuations in soluble protein, absorbance can also be used to monitor aggregation over time. Aggregates can form at different rates and can be measured in real time using a wavelength of 600 nm. Figure 3.3 shows aggregates form much more slowly with a DTT: cystamine redox pair and a final protein concentration of 1 mg.ml^{-1} . Aggregate levels reach their maximum 2 hours after refolding has been initiated. In the presence of a different redox pair of cysteine: cystine aggregation occurs much faster with aggregate reaching a peak at 45 minutes after the start of the refold process even though the final protein concentration is half that of the DTT: cystamine redox pair (0.5 mg.ml^{-1}). At a lower protein concentration, refolding occurs at a faster rate giving higher yields (Raman 1996), therefore one would expect the lower protein concentration present in the cysteine: cystine condition to result in a higher yield and less protein aggregation. However Buswell and Middelberg (2002) show folded native protein could also become incorporated into aggregates either via an intermediate or directly through the surface, so the increased aggregation found at a low protein concentration may result from the incorporation of native protein. A decrease in absorbance is then observed between 1 and 4 hours for cysteine: cystine as aggregates become smaller in size and as a result scatter less light, suggesting deconstruction to form soluble protein as previously observed for high DTT concentrations.

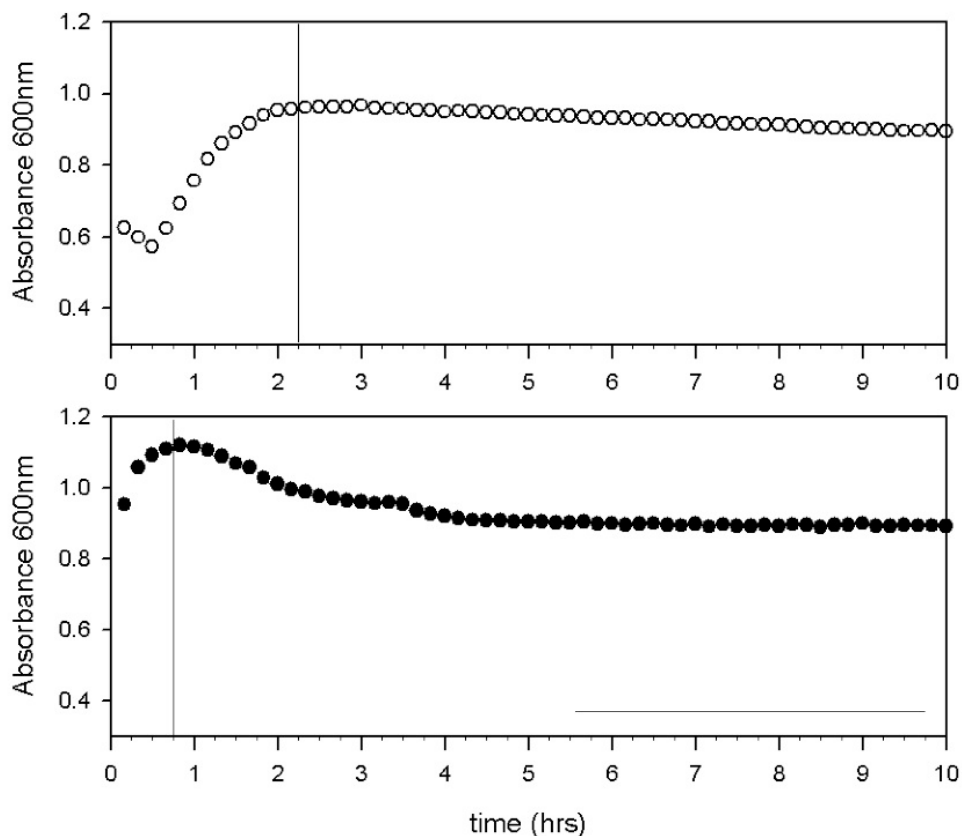


Figure 3.3 Absorbance at 600 nm over time during a refold with different redox couples, (○) DTT cystamine, (●) cysteine, cystine.

Figure 3.3 shows the formation of aggregates immediately after the addition of buffer to protein, demonstrating the short time scale involved in aggregation under certain conditions. Goldberg (1991) reported that the majority of aggregation occurs by 5 seconds, whereas the timescale of renaturation is minutes. The results are in good agreement with the findings of Raman (1996) who used 450 nm to monitor the formation of aggregates and found that aggregation in the first 5 minutes was negligible but increased sharply afterwards reaching an absorbance of 1 A.U. after 30 minutes. Once aggregates form they may not be stable, as shown by the decreasing absorbance for cysteine: cystine in Figure 3.3 b). Therefore it is important when assessing the highest yielding condition to choose an appropriate end point as early measurements may give misleading results. It also illustrates how a steady state of aggregate formation is reached at different times depending on the redox pair used. Therefore aggregation is not only dependent on the presence of excipients and the concentration of DTT, but also on the redox pair selected. A limitation of this assay is that even if soluble protein is present, it does not necessarily mean that it is natively folded active

protein. Therefore another assay is needed in order to evaluate the remaining soluble species and whether they have formed native protein.

3.3.1.3 Fluorescence changes during refolding

In order to rapidly assess the yield of soluble protein, fluorescence excitation at 280 nm and emission at 340 nm can be used to give information on the secondary structure of the protein. Figure 3.4 shows the relative fluorescence of refolds at three different redox potentials and demonstrates the effect of redox potential on refolding. Relative fluorescence was found to decrease during refolding. Katoh et al. (1999) also demonstrated that relative fluorescence intensity sharply decreased during refolding, becoming constant after 100 minutes. Raman et al. (1996) showed that denatured and reduced lysozyme has the highest fluorescence, followed by intermediate and native lysozyme. The observed decrease in fluorescence may indicate the transition from unfolded to folded native protein.

The ranking of the different redox potentials changes over time. Initially the reducing condition has the highest fluorescence, and oxidising the lowest fluorescence which is the most similar to native state. However the trend observed changes over time as the oxidising condition reaches the highest final fluorescence value similar to the native state with a fluorescence of 0.914 after 1200 minutes. The balanced redox condition has the lowest final relative fluorescence of 0.827, suggesting a lower yield was achieved. From the fluorescence data you would conclude that the oxidising redox is the highest yielding condition. It also highlights the different folding behaviour found for different redox potentials as they all display different fluorescence profiles and demonstrates again that an appropriate end point must be chosen for comparison.

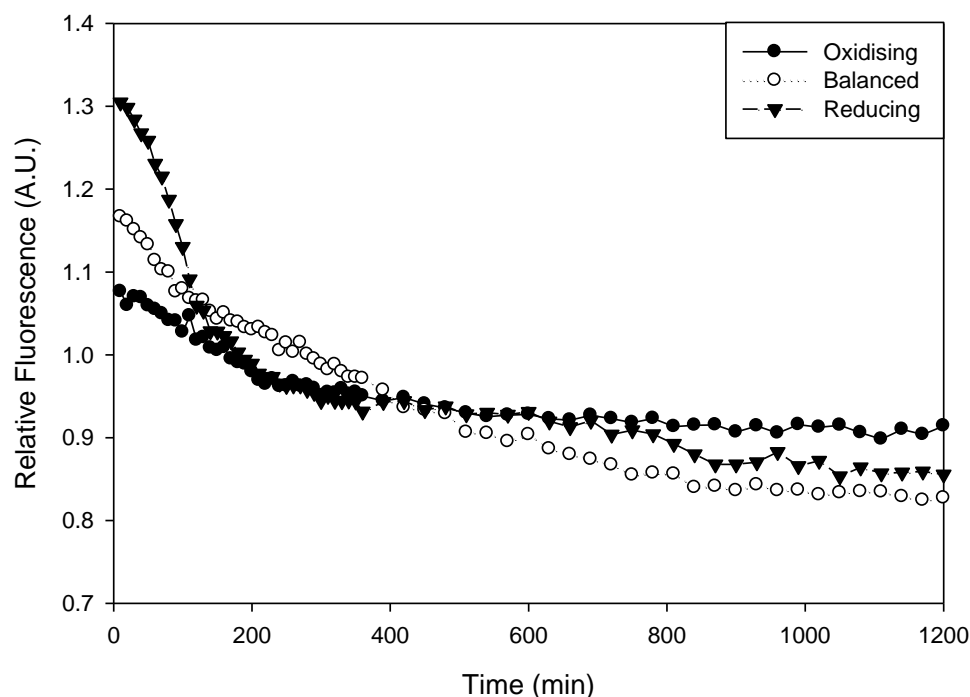


Figure 3.4 Fluorescence over time for refolds at different redox potentials

In conclusion kinetic measurements of fluorescence can increase the complexity of data analysis when multiple conditions are tested. Additionally, it is time consuming in a microwell plate format, and the repeated measurement of fluorescence at short intervals can result in temperature changes in the plate which may affect evaporation and edge effects (Grant et al., 2009). A constant temperature is hard to maintain in the microplate reader and the degree to which the temperature rises is subject to environmental conditions, an example of the temperature profile in the microplate is shown in Figure .9.2 of the Appendix. The amount of information obtained by following the refold throughout time may not be necessary for a screening study of large numbers of refolding conditions as the final yield is the criteria for assessment. Therefore the decision was made to focus on end-point analysis. In fact the buffer that allows the fastest rate of refolding might not be beneficial as longer process times allow an overnight step, which does not rely on user interaction and can act as a break in the process. This is often done as standard in process development buffer screens in industry.

3.3.1.4 Example of end point analysis

End point analysis allows ranking of refold conditions by their overall performance in terms of final yield. It was used to investigate the effect of protein concentration on refolding. The final concentration of protein in the refold is known to affect the refolding yield (Goldberg et al., 1991; Raman et al., 1996). Figure 3.5 shows the absorbance at 280 nm of refolds performed at different final lysozyme concentration. For most of the protein concentrations tested the absorbance of the refold is the same as the standard, indicating that all of the protein present in the refold solution is soluble. At higher lysozyme concentrations, however, the standards and refold values differ slightly. This could be due to aggregation resulting in less soluble protein concentration as observed at 0.7 and 0.8 mg.ml⁻¹ (Figure 3.5). It could also results from the increased measurement error at absorbance values above 1 A.U or the error associated with the preparation of the samples.

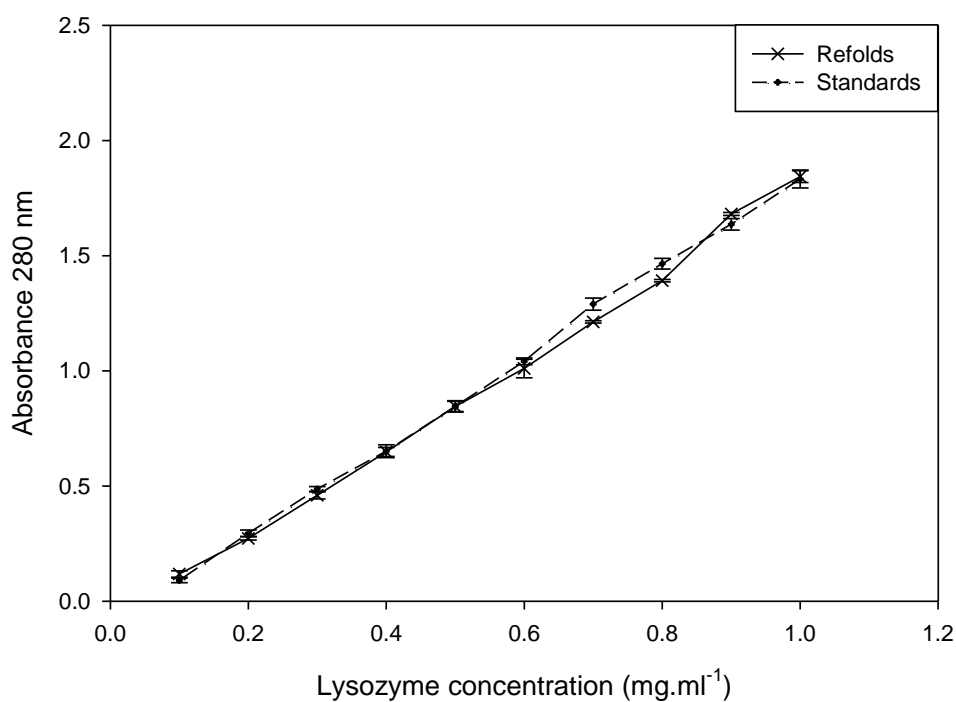


Figure 3.5 Absorbance at 280 nm for refolds at different final protein concentrations. Standards of the same protein concentration as refold shown with best fit line. Standard deviations are shown for each point, which is an average of three experimental repeats.

Figure 3.6 shows the relationship between relative fluorescence (relative to a native standard) and refolds at different final protein concentrations. Initially the fluorescence decreases rapidly between a protein concentration of 0.1 and 0.2 mg.ml⁻¹, and then it

decreases relatively less as the protein concentration increases to 0.6 mg.ml^{-1} , before increasing slightly to 1.0 mg.ml^{-1} . Refolds with similar relative fluorescence have protein folded similarly as their tryptophan residues are reporting the same environment. This indicates that the refolds at protein concentrations of $0.2\text{-}1 \text{ mg.ml}^{-1}$ may have similar yields.

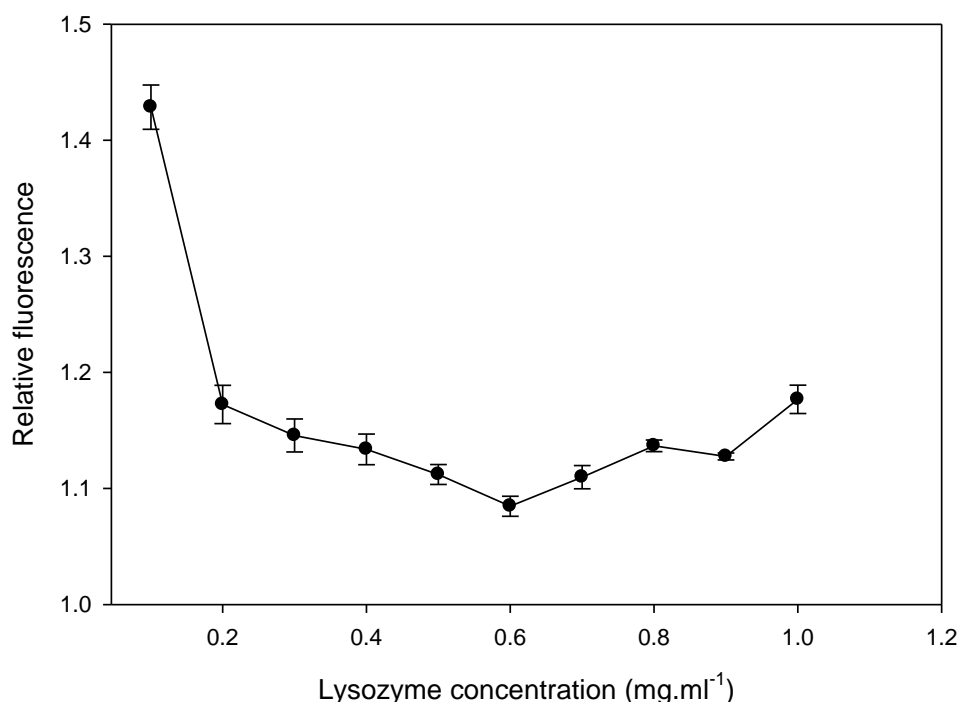


Figure 3.6 Fluorescence for refolds at different final protein concentrations

In order to confirm the yield predicted using intrinsic fluorescence, an activity assay was used. Figure 3.7 shows the relationship between activity and the final lysozyme concentration of the refold. The lowest concentration of 0.1 mg.ml^{-1} gives the highest refold yield of $0.0173 \Delta\text{OD.min}^{-1}.\text{mg}^{-1}$. The refold yield decreases rapidly to only $0.010 \Delta\text{OD.min}^{-1}.\text{mg}^{-1}$ for a protein concentration of 0.2 mg.ml^{-1} . The renaturation yield remains fairly constant for further increases in protein concentration until a concentration of 0.9 mg.ml^{-1} is reached where yield decreases again. The highest final protein concentration of 1.0 mg.ml^{-1} has the lowest yield with an activity of only $0.04 \Delta\text{OD.min}^{-1}.\text{mg}^{-1}$. The relative fluorescence for the most active protein is 1.4 Fl.U. , which appears to indicate a native or near native state. The decreasing fluorescence up to a concentration of 0.6 mg.ml^{-1} correlates to a decrease in activity, which could result from folding to a less active but native form or due to the formation of misfolded soluble protein. The increase in fluorescence for a concentration above 0.6 mg.ml^{-1}

correlates with the decrease in activity and is probably due to the formation of insoluble aggregates, which scatter the fluorescence signal. Therefore fluorescence provides information regarding the folding environment, which can potentially be combined with an absorbance assay to filter out aggregating samples.

The relationship between protein concentration and yield agrees with the results obtained by Goldberg et al. (1991) which showed activity decreasing when the protein concentration increases from 0.05 to 1 mg.ml⁻¹. Raman et al. (1996) also showed activity decreases when protein concentration increases from 0.05 to 0.25 mg.ml⁻¹, and found the activity decreases rapidly between 0.1 and 0.2 mg.ml⁻¹ with yields of approximately 70 and 30% respectively. The protein concentration for refolding, based on the results obtained in this work, is 0.1 mg.ml⁻¹ as this concentration gives the highest yield. Lower concentrations are known to be the best for refolding but not always economical (Rudolph and Lilie 1996). For an industrial process the yield is not the only factor to consider. In fact, a high final protein concentration is also desirable to avoid costly concentration steps after refolding. Based on the results obtained in this work it is advisable to conduct the refold with a final concentration of 0.8 mg.ml⁻¹ to maximise both yield and concentration.

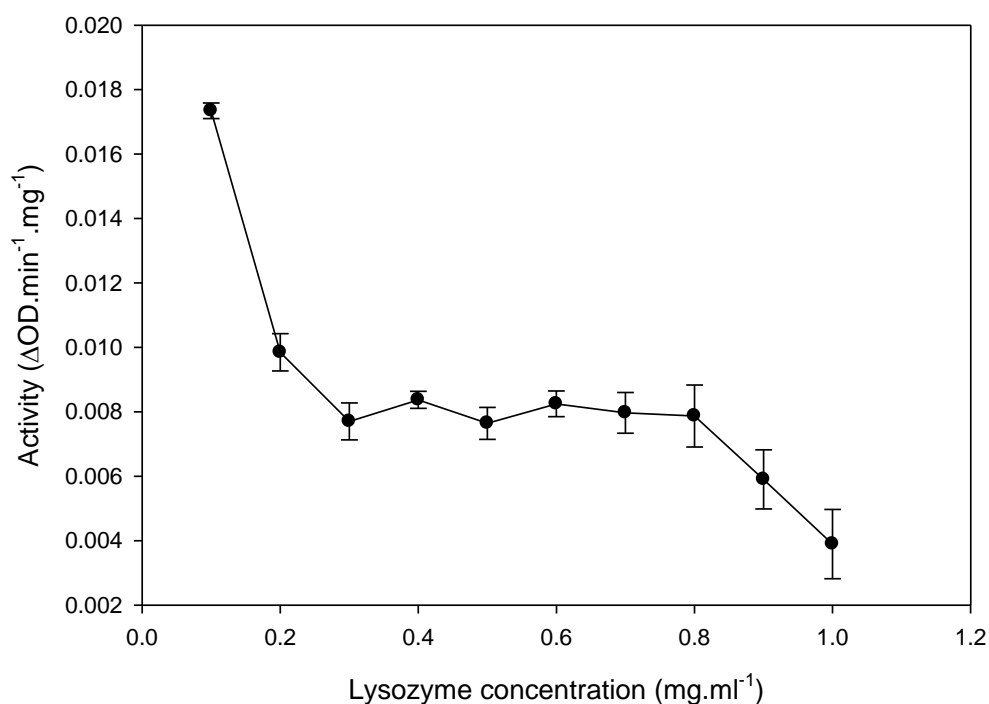


Figure 3.7 Activity for refolds at different final protein concentrations. Error bars represent averages of duplicate or triplicate refolds.

3.3.2 Translation from manual to automated set-up

Refolding protein from inclusion bodies is the rate-limiting step in process development as a large number of conditions needed to be screened on a trial and error basis. Therefore using a 96-well format allows the parallel screening of many different conditions, for example different buffers, redox reagents and additives, using minimal quantities of product. Combining this approach with the use of an automated robotic platform to perform the refolding process step and related assays offers distinct advantages over manual pipetting operations, including improved precision, accuracy, speed and process efficiency. Automated liquid handling should also improve reproducibility between experiments, giving more comparable results between experiments. In order to demonstrate that our automated process could reliably reproduce manually obtained results, experiments were performed with the same material and microplate reader for comparison. An illustration of the automated process is shown in Figure 3.8.

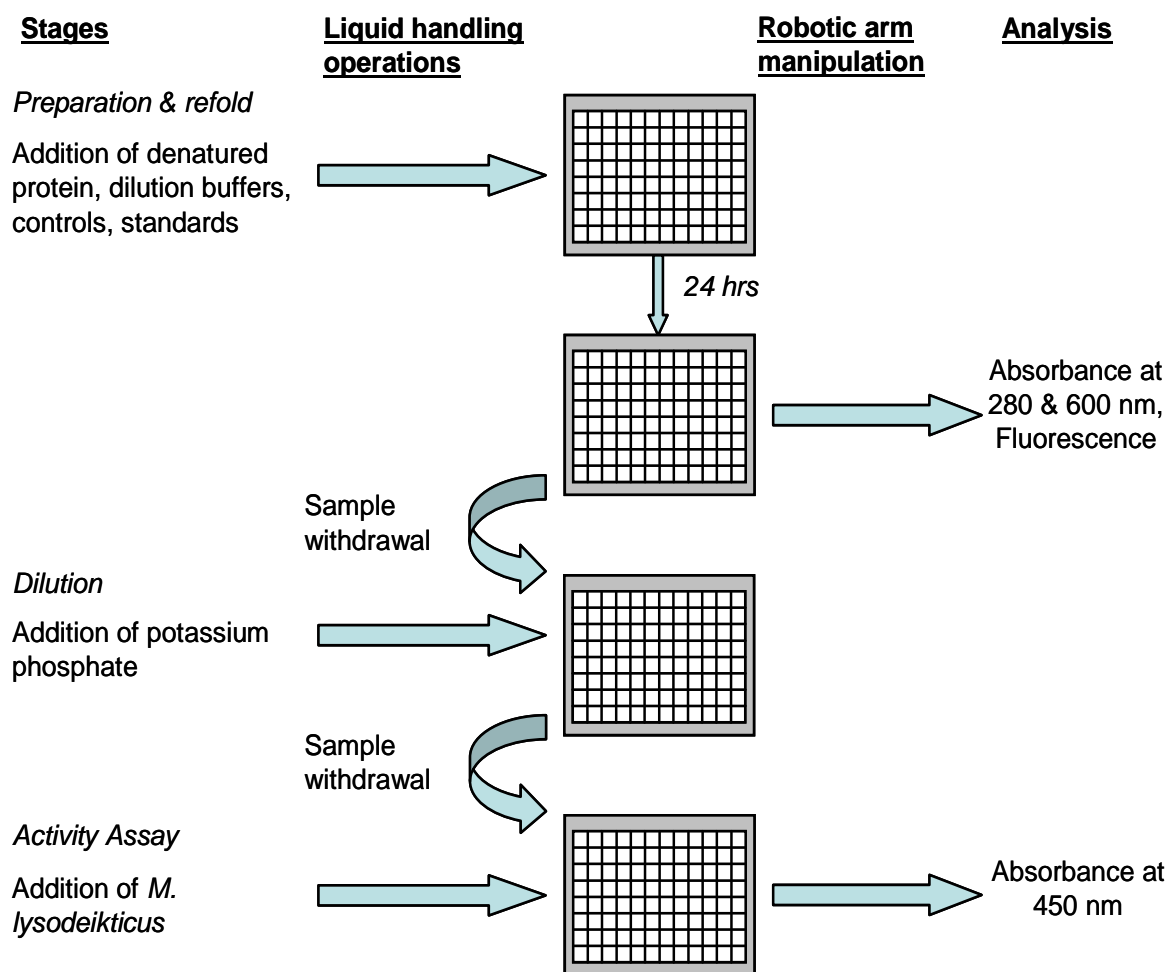


Figure 3.8 Schematic of automated refolding process and assays

A good correlation between manual and automated assays was obtained with only minor deviations from the parity line, which may be due to a small systematic error in the methods. Figure 3.9 shows a parity plot of the manual and automated absorbance data. Each datum represents an average of 3 values obtained in different wells, for a wide range of different refolding conditions, or experiments performed on separate days. The errors for manual and automated refolding measured using the absorbance assay are comparable, with an average error of ± 0.017 A.U. for manual and ± 0.020 A.U. for automated. The best fit line shows a slight offset from the line of parity, illustrating that manual refolds give slightly higher results at an absorbance above 1.8 A.U. and may be related to the difficulty to obtain accurate readings in microplate readers.

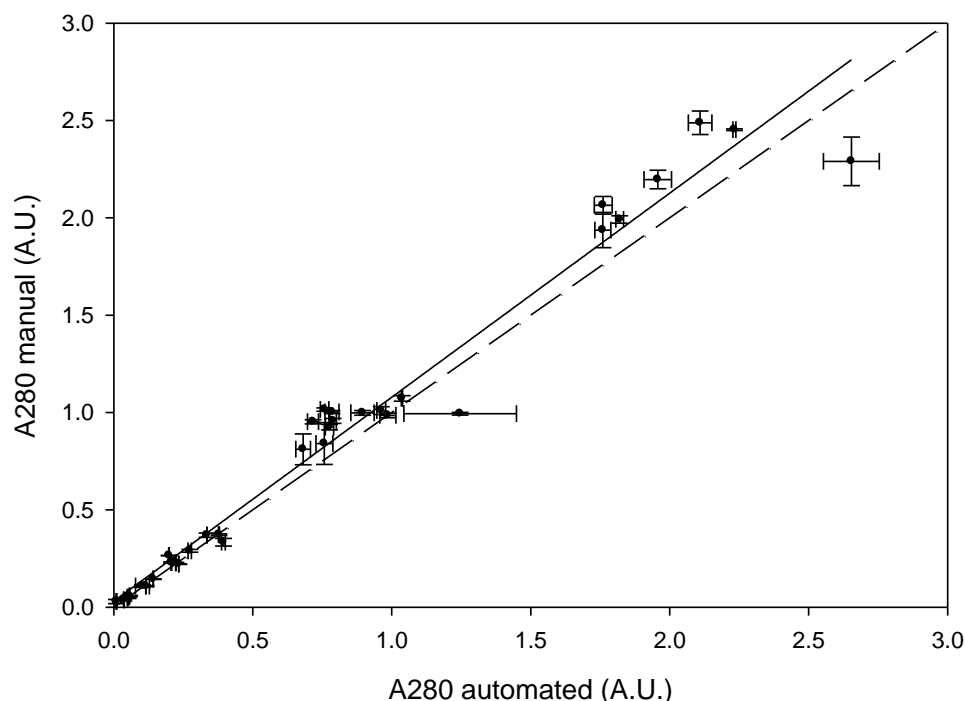


Figure 3.9 Absorbance at 280 nm of refolds prepared manually compared with refolds prepared using an automated platform.

Figure 3.10 shows a comparison between automated and manually obtained for fluorescence data. A very good agreement was obtained in this case. The average error for manual was ± 540 Fl.U compared with ± 503 Fl.U for automated data, showing greater accuracy for automated techniques. The average error for the activity assay also gave a smaller error for automated techniques, with ± 0.0019 and ± 0.0015 $\Delta\text{OD}\cdot\text{min}^{-1}\cdot\text{mg}^{-1}$ for manual and automated respectively. Once again a deviation from the line of

parity was observed for the activity measurements (Figure 3.11), which could result from the experimental methods. For the manual experiment, the plates experience different lag times after addition of the enzyme substrate to the first well and the first absorbance reading, leading to systematically decreased rate relative to the true initial rate. By contrast, automation allows the delay between the addition of the *M. lysodeikticus* and the first measurement in the plate reader to be shorter than when using the manual method and the delay can be kept constant between experiments.

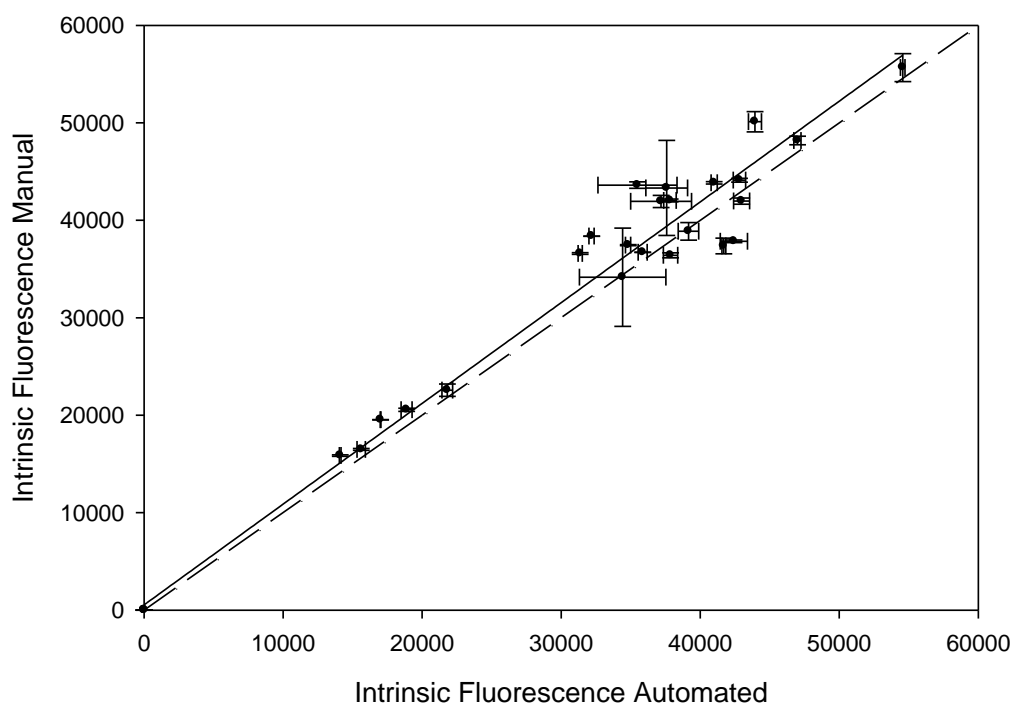


Figure 3.10 Fluorescence of refolds prepared manually compared with refolds prepared using an automated platform.

The best fit line for the activity data is skewed by a single datum point (-0.056, -0.072). This error could be a consequence of the small volumes involved in microscale techniques, which result in a greater source of random errors due to the pipetting accuracy of small volumes. The standard error for refolded samples is higher than that of standard and control solutions, perhaps due to the error involved in aliquoting small volumes of protein when preparing the refold. In addition, inherent with refolding is the stochastic nature of the formation of aggregates. Aggregates may be seeded by surface defects in the wells or by dust particles present in solution causing different results between wells of the same conditions. Standard errors were greater for the activity assay than absorbance or fluorescence measurements, indicating that errors with this

3.3.3 Developing a set of hierarchical generic assays

An activity assay is the gold standard for assessing protein refolding because of the relationship between structure and function, but is not generically available for all proteins due to its specificity. While no single generic assay provides all the information needed to determine the refolding yield, several generic orthogonal assays can be used in conjunction (as shown in the previous section) and potentially applied to optimise any protein refolding process. However such assays still require confirmation of yield. A common problem when assessing the refolding of novel therapeutic proteins with no available activity assay is the lack of suitable high throughput assays. A RP-HPLC or UPLC assay could be developed but still require sample processing times of at least 15 minutes per sample to obtain quantitative yield information. This can be time consuming for a microwell plate where 96 different refold conditions can be evaluated. Therefore by combining the generic orthogonal assays described into a hierarchy, it enables the most rapid and lower cost assays to be performed as an initial screen to eliminate low-yielding refold conditions, saving the most resource intensive assays for the most promising conditions.

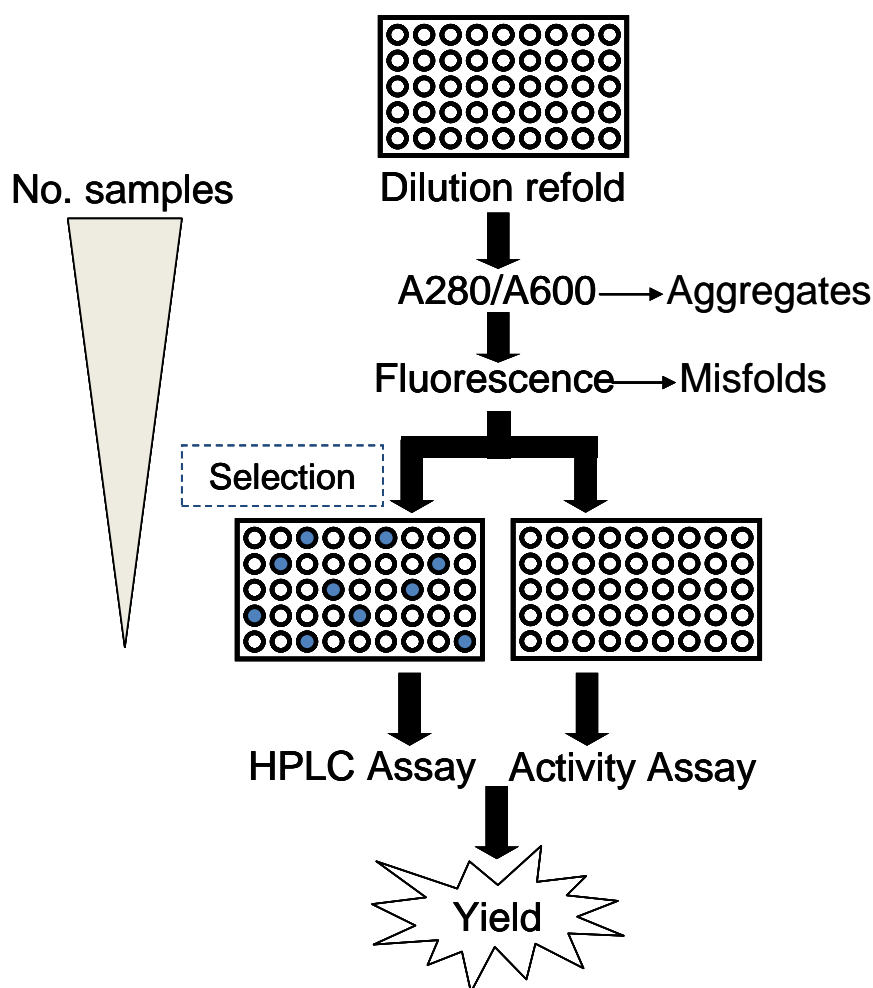


Figure 3.12 Schematic of proposed structure for hierarchical assays

The first stage of our hierarchy, absorbance at 600 and 280 nm (A600, A280), was chosen to detect aggregates that indicate poor refolding and to measure soluble protein (Figure 3.12). However, absorbance alone is not capable of distinguishing between native or misfolded soluble protein. Therefore a second screening step, measuring intrinsic protein fluorescence, was chosen to provide information on the degree of native-like tertiary structure formed relative to a native standard. The absorbance screen could potentially act as a filter to eliminate the frequently misleading influence of aggregate formation on the fluorescence assay. If a purified and natively folded protein standard is unavailable, a target fluorescence value can often be obtained from the protein folding literature, which indicates the direction that the fluorescence needs to change to increase the yield. The conditions with a high native-like structure can then be confirmed using the final stage in the hierarchy, an activity or HPLC assay to quantify yield in terms of functional protein present.

3.3.3.1 Oxidation

The automated microscale refolding process with integrated absorbance, fluorescence and activity assays was used to investigate the effect of two different mixing methods on the lysozyme refolding yield, pipette aspiration alone in a static system and pipette aspiration used in conjunction with shaking. It is not known if redox potential is constant throughout refolding or if it is altered by exposure to air and pipetting. Shaking allows the introduction of air bubbles which could potentially perturb the redox potential. If even vigorous shaking is not able to perturb redox ratio, then exposure to air in a static microwell system cannot alter redox potential.

It was hypothesized that shaking could affect the yield through two different mechanisms. In the first mechanism, shaking could increase the oxygen transfer rate and hence the dissolved oxygen in solution altering the redox potential. Air oxidation is used as a method for shuffling disulphide bonds during refolding through aeration or static exposure of the vessel to air. The dissolved oxygen can then oxidise the reduced thiol compound forming a disulphide bond, leading to the creation of a redox pair that causes disulphide-bond shuffling. Both shaking at high speeds and pipette mixing during plate preparation increases the amount of oxygen dissolved into the refolding solution and could potentially alter the redox ratio of the buffer on a timescale that is faster than the refolding process.

The second mechanism through which shaking could affect yield is by increasing the presence of air bubbles in the liquid phase which could act as seeding sites for aggregation. Vigorous shaking causes the formation of bubble and vortices, which increase the area of the air-liquid interface. Proteins commonly adsorb at the air-liquid interface, and due to the surfaces hydrophobicity it acts as a seeding site for aggregation (Treuheit et al., 2002). An increase in free energy occurs when the protein conformation changes and polar residues are orientated towards the aqueous phase and non-polar (hydrophobic) residues towards the air phase, thus leading to the denaturation of native protein at its surface (Wierenga et al., 2006). Enzymes have been reported to lose activity during adsorption. Furthermore, denatured and partially folded intermediates are prone to aggregation as hydrophobic regions normally buried in native protein are free to interact inter-molecularly to form aggregates (Fink, 1998).

A high refolding yield of lysozyme was previously obtained using a refolding buffer of 1.2 M GdnHCl, 4 mM cystamine and 50 mM Tris by Mannall et al. (2007). Therefore this refolding buffer and denatured lysozyme containing 6, 32 or 62 mM DTT (as described in Table 2.3) were selected to evaluate the impact of different redox and shaking conditions upon the refolding yield.

3.3.3.1.1 Generic assays

The generic absorbance and fluorescence assays were used as the first level of the hierarchy. Figure 3.13 shows the absorbance at 600 nm for shaking and static refolds using refold buffers with three different redox potentials. Aggregation was not observed under shaking or static conditions. Figure 3.14 shows only a marginal loss of fluorescence was observed for oxidising and balanced redox conditions when the refolds were shaken compared to static. In contrast, for the reducing condition the fluorescence of the shaken refold sample was approximately half that obtained for static conditions. This difference indicates the protein in the shaken refold is reporting a different average environment around the tryptophan and tyrosine fluorophores, due to either partial refolding or non-native tertiary structure, such as that in misfolded protein.

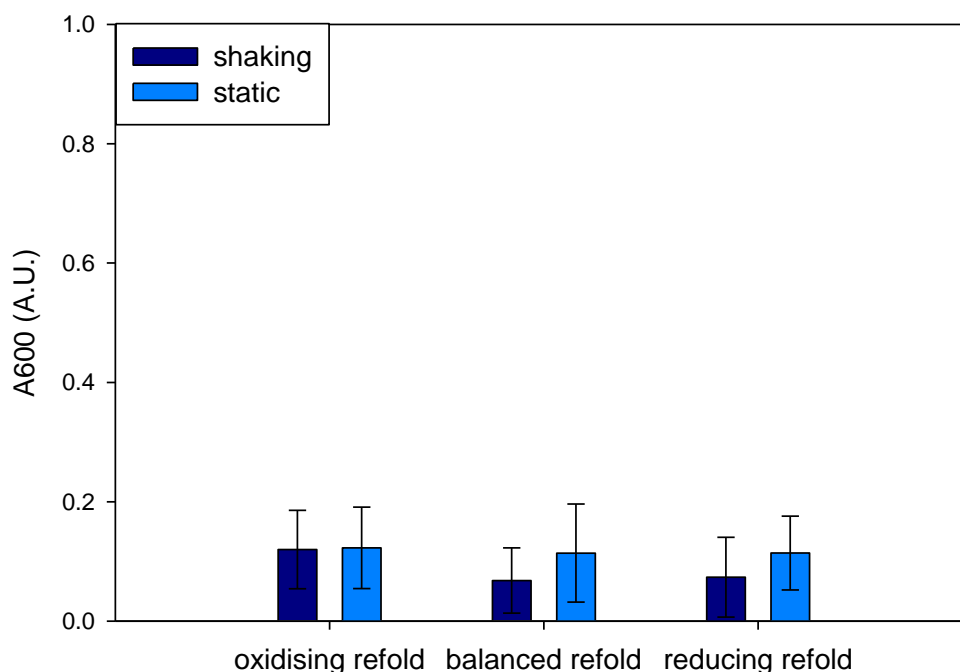


Figure 3.13 Absorbance at 600 nm at three different redox potentials (oxidising, balanced and reducing) after refolding lysozyme for 24 h in static and shaking 96-deep square microwells.

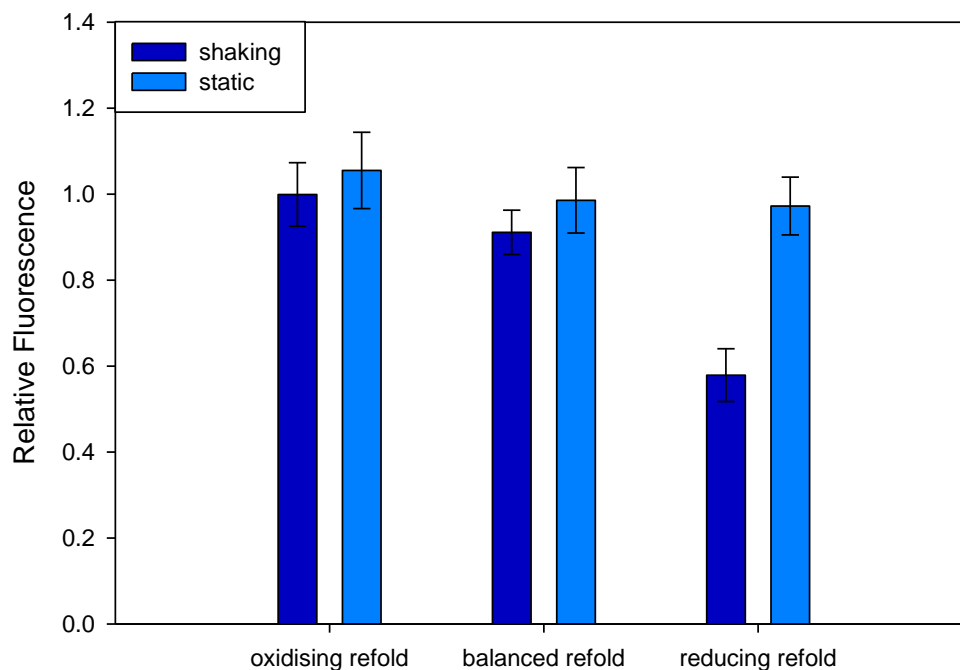


Figure 3.14 Relative fluorescence at three different redox potentials (oxidising, balanced and reducing) after refolding lysozyme for 24 h in static and shaking 96-deep square microwells.

3.3.3.1.2 Specific assays (2nd level of hierarchy)

The activity assays performed confirm the finding that agitation decreases the final refolding yield for the reducing condition, as can be shown in Figure 3.15. Initially, it was expected that shaking would enhance the oxidation of cysteamine in the reducing condition to establish a redox pair for disulphide bond shuffling, thus resulting in a higher refolding yield compared to the equivalent static condition. However the yield was lower when shaking, suggesting that shaking is unable to alter the redox potential to a more optimal redox potential for disulphide shuffling. The decrease in yield could be attributed to the physical effects of shaking. Shaking could increase the occurrence of misfolded protein and trap it at solid-liquid or air-liquid interfaces where hydrophobic residues preferentially interact with the interface or other proteins with exposed hydrophobic surface. The inability of shaking to increase yield through changing redox potential is supported by the findings under an oxidising and balancing redox potential. For a balanced redox condition, only a minor decrease in activity was observed from 84% to 75% upon shaking. Additionally, the low activity obtained for the static oxidising condition (37%) was not further diminished by shaking (42%), indicating that shaking potentially has no effect when further oxidation of the redox pair cannot take

place. This indicates that the redox potential is not perturbed significantly by shaking for different redox ratios.

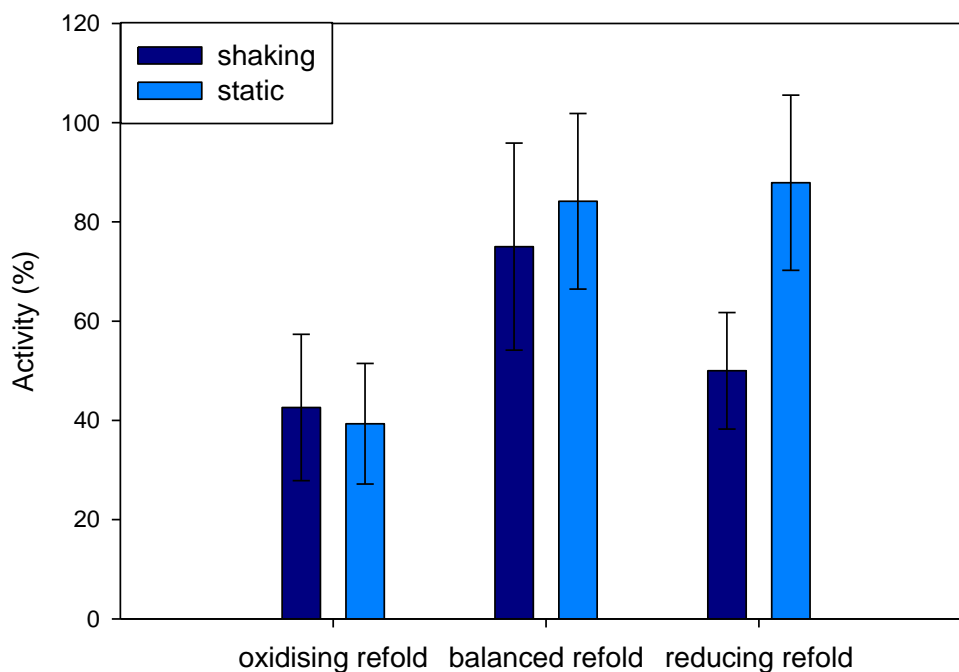


Figure 3.15 Activity at three different redox potentials (oxidising, balanced and reducing) after refolding lysozyme for 24 h in static and shaking 96-deep square microwells. Activity is expressed as a percentage of the activity of a native standard.

Figure 3.15 also shows that both the oxidising conditions gave a lower yield despite having the same fluorescence and absorbance as the balanced refold conditions (Figure 3.14 and Figure 3.13 respectively). This highlights that the fluorescence assay would in certain cases be misleading if used independently. The high intrinsic fluorescence observed for the low yielding oxidising condition does not represent fully active protein, but an inactive state with native-like fluorescence but only 50% of the maximum activity obtained. An oxidising redox potential has been reported to result in soluble inactive lysozyme as it can prevent the formation of correct disulphide pairings (De Bernardez Clark et al., 1998) and can lead to misfolded but stable states where the disulphide bonds are trapped in non-native pairs (Mannall et al. 2007). Therefore the high fluorescence and low yield could result from species trapped with non-native disulphide bonds due to the lack of reducing species available to break them. The tryptophan residues in these species report the same overall natively folded environment but are not within any slightly misfolded regions of the protein which lead to

inactivation, as shown by the high relative fluorescence. If this misfolding occurs rapidly, it is unlikely to be affected by the increase in air-liquid or solid-liquid interfaces under shaking, particularly if the protein forms stable near-native misfolds that do not expose hydrophobic surface. Similarly, if refolding to form stable native protein is rapid under a balanced redox, the refold yield would not be significantly affected by the physical effects of shaking, such as increased rate of interaction with air-liquid or solid-liquid interfaces. However, under the reducing condition the stability of the refolded protein would be low even if it is in a near-native state, due to the potential of the reducing redox to break native disulphide bonds. Consequently, the presence of air-liquid or solid-liquid interfaces upon shaking presents a surface upon which the unstable protein can readily unfold, leading to inactivation.

Shaking could also have a stronger impact on refolding under reducing conditions because the rate of folding is slower due to a lack of oxidising species in solution. Previous work has shown that the rate of active protein formation is slowed under strongly oxidising conditions because of the increased time taken to shuffle the disulphides into the native pairings (Mannall et al., 2007). Conversely the same could be said for a lack of oxidising species under a reducing condition, which would make disulphide bond formation difficult (much like the reducing conditions in the cytoplasm that lead to inclusion body formation initially). Three out of four disulphide bonds are required to form for lysozyme to be active (Eyles et al., 1994). Without the formation of disulphide bonds, the conformation would not be stabilised to the native state. Goldberg and Guillou (1994) found that substantial secondary structure was formed within 4 ms when refolding lysozyme, whereas when refolding under reducing conditions no such secondary structure was formed in this timescale. De Bernardez Clark et al. (1998) showed there was an optimum redox potential (GSH/GSSG ratio= 1.5-2.5) and outside this range refolding was slower for both more reducing and more oxidising redox potentials. Refolding outside of this range appears to affect the stability of the refold as they are more susceptible to the effects of shaking.

3.3.3.1.3 Verification of assay results using circular dichroism

In order to confirm that the assay was able to correctly identify active protein, further analysis of the secondary structure of the refolded lysozyme was carried out using circular dichroism (CD). Lysozyme is a globular protein with two domains, an α -

domain with 3 α -helices and 1 C-terminal 3_{10} helix, and a β -domain, consisting of a 3 stranded anti-parallel β -sheet and 1 loop and therefore possesses diverse structural elements. CD spectra of lysozyme are typically characterised by a peak around 210 nm followed by a shoulder which extends to 240 nm (Johnson 1990). Figure 3.16 shows the CD spectra of refolded lysozyme having an activity of 35%. It has a similar shape to the standard, as expected, and other reported spectra for lysozyme (Johnson, 1990; Gu et al., 2004). Lysozyme mostly consists of alpha helix, however the β -sheet normally overshadows the effect of the second α -helix peak, and in this work the noise caused by the presence of DTT eclipses this effect. Therefore the refolded protein shares the same structural features as the native lysozyme and some of the protein present has refolded to a native-like state. This supports the activity data and confirms that a folded state has been reached. However the signal for the refolded protein is lower than the standard, despite normalising by protein concentration, perhaps due to a mixed population of protein. It could result from the presence of intermediate, which Raman et al. (1996) showed to have a lower signal.

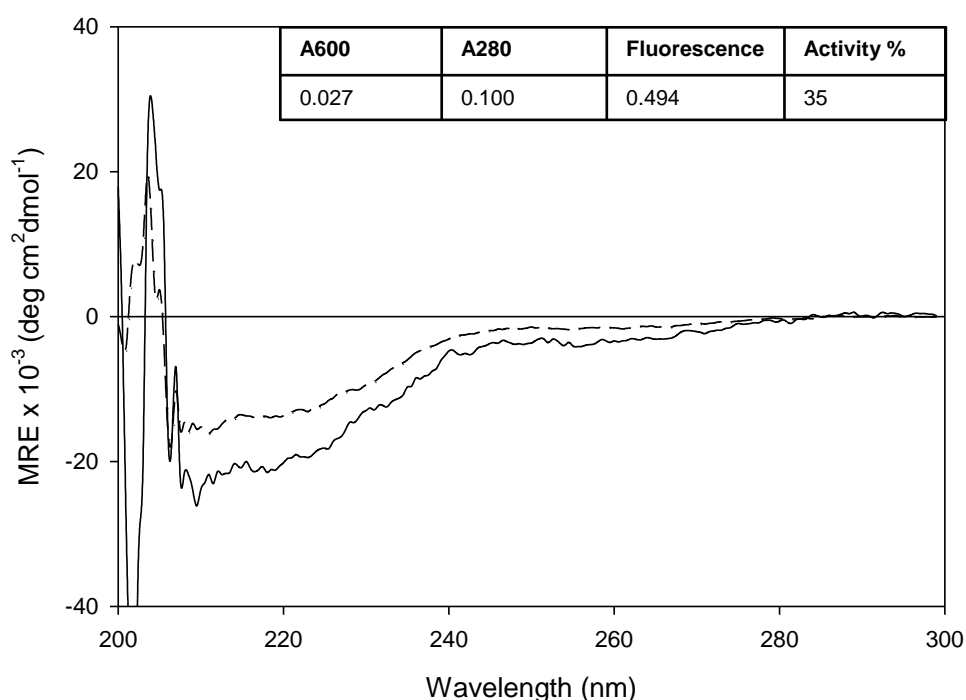


Figure 3.16 Circular dichroism spectra of a high activity refold (—) and native active lysozyme (- -)

Figure 3.17 shows the CD spectra of refolded protein with an activity of 2%. The refolded sample lacks the secondary structure detected for the standard. Whilst there is some α -helical structure present, the characteristic peak with shoulder is absent. The

CD spectra of the refolded protein does not display the features associated with a completely random coil structure (negative peak around 195 nm), and the sample may have some α -helical properties, due to the slight negative peak at 210 nm. The positive peak observed at 205 nm could be attributed to the presence of noise from the low concentration of DTT present in the sample, but could also result from the presence of anti-parallel β -sheet. Partially folded intermediates typically have significant native-like structure, whereas aggregates show a greater amount of β -structure relative to the native form (Fink, 1998). Therefore the presence of some α -helix and perhaps an increase in β -structure could indicate the presence of aggregates.

The tables in Figure 3.16 and Figure 3.17 summarise the assay results for the samples tested using CD. The low fluorescence and lack of activity support the lack of structure discovered in the corresponding CD spectrum in Figure 3.17. The sample with a higher fluorescence and activity had a CD spectrum similar to the native standard (Figure 3.16), supporting the presence of refolded protein in this sample. Therefore the CD supports the assay results for both a low and a higher activity condition.

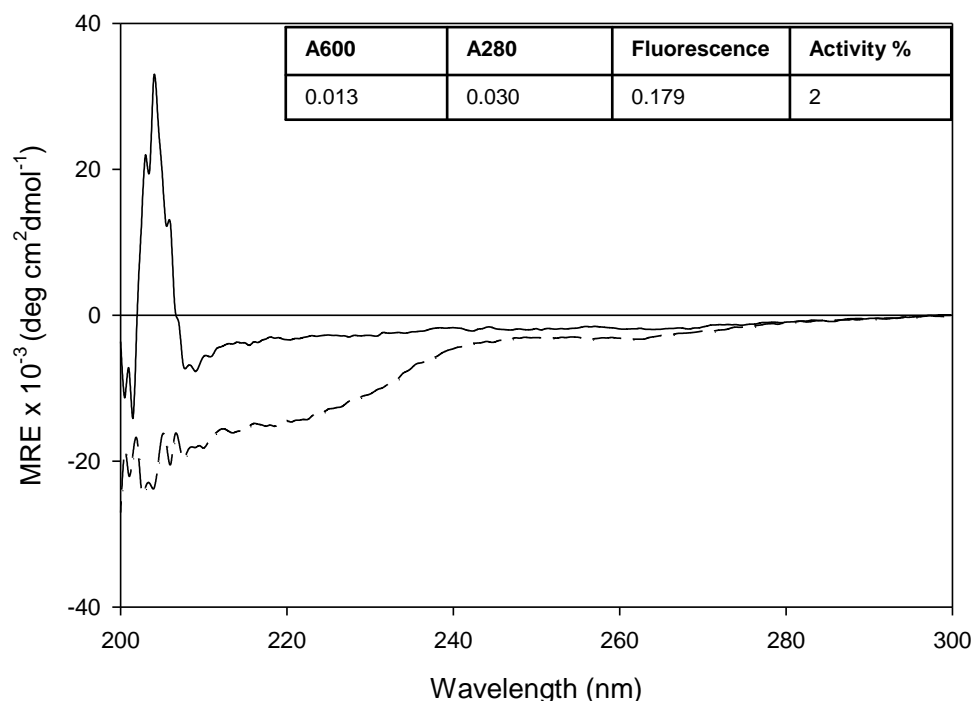


Figure 3.17 Circular dichroism spectra of a low activity refold (—) and native active lysozyme (---)

In summary, the physical effects of mixing (bubbles and vortexes introducing surfaces for denaturation) appear to be significant during refolding. By contrast, the entrained

oxygen concentration does not appear to be changing the redox potential sufficiently to alter the refolding yield over a 24 hour period, and therefore it is likely that it remains constant in a static period over this time. These results demonstrate the importance of mixing mode and have allowed us to identify an optimum mixing condition for microscale refolds, in this case the static balanced redox ratio, for subsequent folding studies. These results suggest that the best use of the intrinsic fluorescence assay would be for eliminating low yielding conditions in screens of multiple conditions, rather than for specifically identifying the highest yielding conditions, as it can be misleading in its predictions. In order to gain a greater understanding of how this might work, we aimed to explore a hierarchical assay concept with a larger data set.

3.3.4 Hierarchical assays using lysozyme

3.3.4.1 Absorbance

Figure 3.18 shows the relationship between absorbance measurements at 600 nm and lysozyme activity after refolding in 12 different buffers and two different dilution factors. The cut-off point of 0.25 A.U was selected based on visual observations of aggregates at absorbance values higher than this value, due to the scattering of light by large aggregates. Consequently, high absorbance is correlated to low activity. Low absorbance values were observed for soluble refolds with a range of activities, and the cut-off point included almost all samples that had activity greater than 40%. This assay identified aggregation in 32% of conditions tested, thus reducing the number of samples for the next stage in the hierarchy to 68%. In the remaining soluble samples, 54% had activities >50%, indicating that absorbance scattering is a suitable first filter to eliminate aggregating refold conditions from further study. Nevertheless, it does not identify the degree of folding in the soluble phase, as highlighted by 48% of samples with an absorbance less than 0.25 A.U. also having an activity of less than 50%. One refold condition is present which has a high activity and high absorbance which contradicts the relationship between low absorbance and high activity. While this could be a systematically erroneous data point, the triplicate data had a standard deviation of 7%. This condition could indicate a kinetic partition between refolding to soluble active protein and misfolding to aggregates, with the sample containing a mixture of inactive aggregates and native active protein. Kiefhaber (1995) found 20% of lysozyme folds via a direct pathway rather than an intermediate even at high protein concentrations and that this pathway may out-compete aggregation. The aggregation of lysozyme has also

been found to level off regardless of protein concentration Goldberg et al. (1991). Therefore it is possible to find active protein even in the presence of aggregates. However it is more likely that it is a consequence of the dilution step prior to activity measurements, which may have re-solubilised some of the aggregates in this case, leading to a greater reported activity.

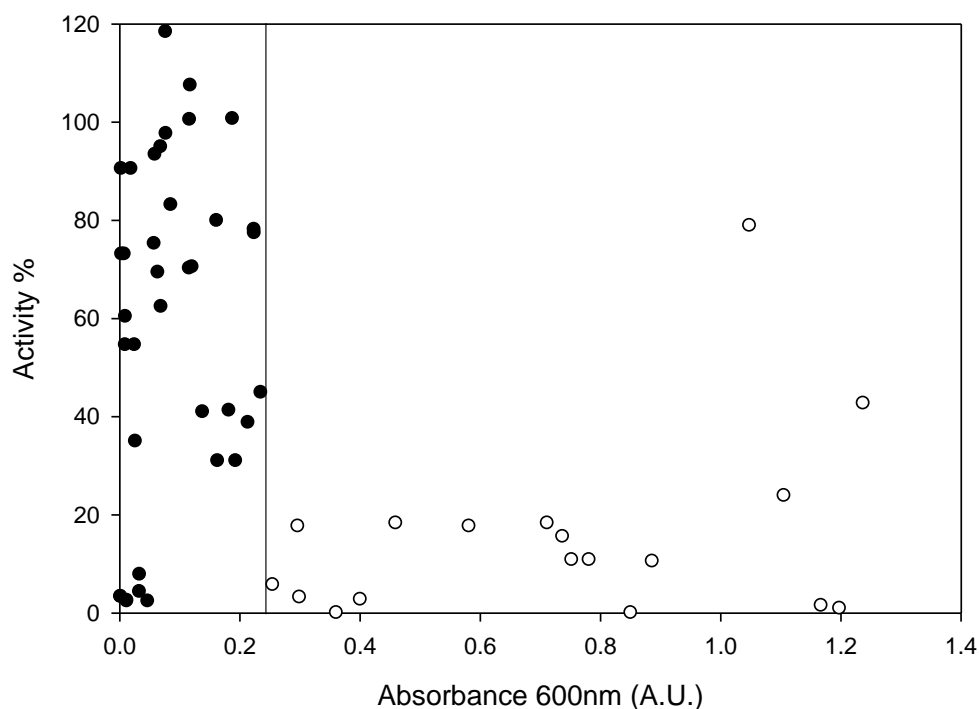


Figure 3.18 Absorbance (600 nm) as a function of activity for lysozyme refolds. Aggregating samples (○), soluble samples (●) and cut-off line at 0.25 A.U. (- -).

3.3.4.2 Fluorescence

The relationship between relative fluorescence and activity for both aggregating and soluble refolded lysozyme is presented in Figure 3.19. Adjusting the intrinsic fluorescence to relative fluorescence allows rapid identification of high yielding conditions as values close to 1 represent native structure formation with correspondingly high levels of activity (denatured protein has a relative fluorescence close to zero). The relative fluorescence for aggregated samples ranged from 0.4-2.2. Aggregates often result in misleading high intrinsic fluorescence values due to light scattering, whereas all soluble samples had fluorescence values below 1.1. The overlap between these two populations highlights the importance of first filtering out aggregates using the absorbance assay.

Soluble refolds conditions with a relative fluorescence close to 1.0 were generally associated with a high lysozyme activity, indicating a high level of native protein environment. The majority of high activity samples had fluorescence values above 0.6 A.U. In general, as the relative fluorescence increases from 0.2 to 1.0, the activity also increases (Figure 3.19), indicating progressively higher refolding yields as more native structure is obtained. Interestingly, relative fluorescence values greater than 1 are associated with low activity, suggesting the presence of soluble misfolded protein with near-native structure and fluorescence intensity greater than that of the native protein. This is supported by our previous findings for oxidising refolds, which had a high relative fluorescence but low activity (Section 3.3.3.1.2). The greater than native fluorescence indicates increased burial of tryptophan and tyrosine fluorophores into hydrophobic regions that are related to those found in the native protein structure. Other authors have reported that intermediate folding states for lysozyme have a fluorescence intensity that is higher than native and refolded protein at the emission wavelength used (340 nm) Raman et al. (1996), and therefore the results observed could be explained by misfolded intermediates.

The highest activity levels correspond to relative fluorescence values in the range of 0.83-1.02 fluorescence units as shown by the cut-off lines in Figure 3.19. Therefore, it is possible to select the highest yielding conditions for more detailed analysis by slower and more resource intensive assays to confirm yield. In cases where direct assays for biological function are not available or suitable for high-throughput automation, refolding conditions could be selected based on fluorescence values in a pre-defined range as they are likely to have refolded to a high activity.

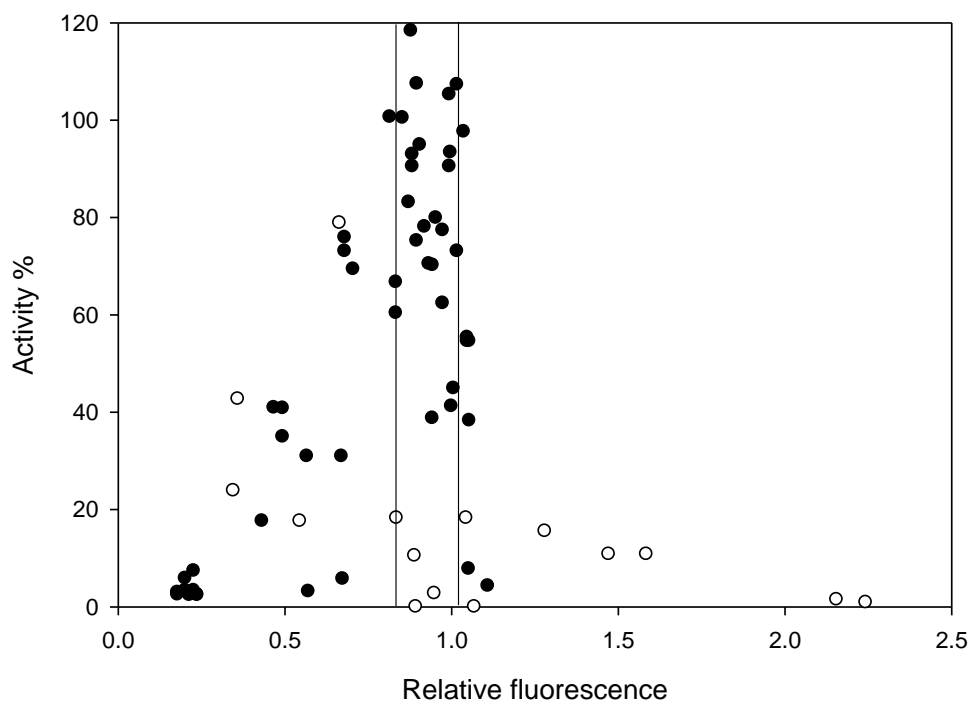


Figure 3.19 An activity measurement as a function of relative fluorescence for lysozyme refolds. Each point represents a triplicate or average of 9 data points. Aggregating samples (○), soluble samples (●) and cut-off lines at 0.83 and 1.02 A.U. (-).

3.3.4.3 Activity assay

The highest activities were reported under conditions of 1.2M final guanidine concentration and a DTT:cystamine redox pair with varying redox potentials. This agrees with previous findings that this is an optimal condition for refolding (Mannall et al., 2007). A guanidine concentration of 1-2 M has been reported to help maintain chain flexibility and prevent interactions that lead to aggregation. De Bernardez Clark et al. (1998) showed that increasing guanidine affected the competition between folding and aggregation, and found an optimum final concentration of 1.3M in the refold which skewed the refold in favour of folding. Mannall et al. (2007) compared concentrations 0.53 M and 2.38 M GdnHCl using the same redox pair and buffer and found a concentration of 1.2 M to be optimal for yield. On the other hand, a low activity and the presence of aggregates were associated with a cysteine: cystine or DTT: cystamine redox pair with a low final guanidine concentration of 0.53 M. The lower concentration of guanidine may prove insufficient to prevent intermolecular interactions, leading to the formation of aggregates. The cluster of soluble refolds with low activity (4 data points) represent conditions with balanced or reducing cysteine/cystine redox buffer, with one under a reducing redox potential, DTT:cystamine and 1.2M guanidine. The

reducing condition could prevent disulphide bonds from forming and a stable native fold from being reached as previously described (Section 3.3.3.1.2).

3.3.5 Hierarchical assays using DHFR IBs

3.3.5.1 Absorbance

The hierarchical assays were then tested using inclusion body derived material of a different protein, DHFR to see if they could be translated to less pure and more industrially relevant material. Figure 3.20 shows the relationship between absorbance (600 nm) and activity obtained with DHFR from purified, washed and unwashed inclusion bodies refolded at different concentrations using three different buffers, 3 final protein conditions and two different dilution factor (1:15 and 1:20). Conditions with high absorbance showed no enzyme activity (with the exception of one data point), whereas conditions with low absorbance gave high activities due to more successful soluble refolds. The aggregates found for DHFR have a much lower absorbance than for lysozyme (0.55 A.U. for DHFR compared with up to 1.25 A.U. for lysozyme), indicating larger aggregates were formed in the lysozyme refold conditions. For the soluble DHFR refolds, activities ranged from 0-12 $\Delta\text{OD}\cdot\text{min}^{-1}\cdot\text{mg}^{-1}$ and had an absorbance of less than 0.07 A.U. The 0.25 A.U. cut-off for lysozyme could be used to differentiate soluble and aggregated condition, or a much lower cut-off point of 0.1 A.U. could be suitable for DHFR. In contrast to the data for lysozyme, almost all conditions with aggregate formation had no active activity. The data falls into two distinct populations, the refold either resulted in aggregation with no active protein, or the protein remained soluble and refolded with varying levels of activity. The data for lysozyme was more complex with mixed populations of aggregate, misfolded and active protein, resulting in conditions with a high absorbance and activities ranging from 0-20%. However it is possible that testing a wider range of conditions for DHFR could lead to the presence of both aggregate and active protein.

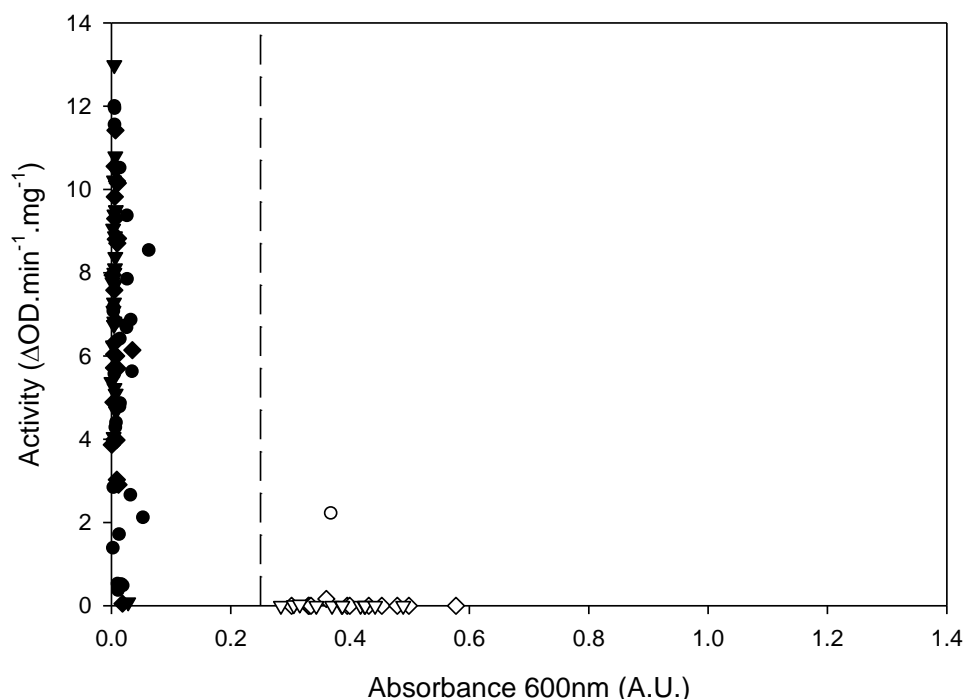


Figure 3.20 Absorbance (600 nm) as a function of activity for DHFR refolds. Each point represents a triplicate. Soluble refold samples, purified (●), unwashed (◆), washed (▲), and aggregated refold samples, purified (○), unwashed (◇), washed (Δ), and cut-off at 0.25 A.U. (- -).

3.3.5.2 Fluorescence

Figure 3.21 shows that an increasing fluorescence rapidly results in a more active refold, peaking at 6,000-10,000 A.U. The initial relationship between fluorescence and activity agrees with previous work, which shows that unfolded DHFR has a lower fluorescence than folded DHFR at the emission wavelength used for this study (Uversky et al., 1996). It has also been reported that after an initial decrease during the first few seconds of refolding, fluorescence increases over longer time points at 22°C as the DHFR folds (Clark et al. 1996). Therefore the activity rise with increasing fluorescence reflects the protein taking on more native structure. However once a fluorescence of 11000 A.U. is reached a gradual decrease in activity is observed, suggesting the presence of soluble misfolded protein in the refold that is lowering yield. The exact optimal fluorescence value for DHFR was unknown as no standards were available, consequently relative fluorescence could not be calculated. Nonetheless, DHFR demonstrates an optimal fluorescence range for successful refolding as shown by the cut offs at 5110-7610 A.U, which select approximately 75% of the data points with an activity of over 10 $\Delta\text{OD}\cdot\text{min}^{-1}\cdot\text{mg}^{-1}$. Data points in this region are correlated with a high activity and therefore such information can be used as selection criteria for future

assays. In this case, 12% of the conditions tested could be selected for further analysis. Lowering this activity threshold to $5 \Delta\text{OD}\cdot\text{min}^{-1}\cdot\text{mg}^{-1}$ gives new broader boundaries of fluorescence between 2446 and 9962, selecting 54% of all conditions tested for further studies.

The distribution of fluorescence data relative to activity differs from lysozyme. DHFR displays a positive skew, with a peak with a sharp shoulder on the left and a longer shoulder on the right. This is a mirror image of the negative skew observed for lysozyme, where an increasing fluorescence caused a gradual increase in activity until fluorescence greater than 1 is reached and activity quickly decreases. This reflects the different direction fluorescence is changing in during folding. For lysozyme, fluorescence decreases as the protein folds Katoh et al. (1999), whereas for DHFR fluorescence increases during folding. This is a result of the different microenvironment of the tryptophan residues in these two proteins, which can either become buried in non-polar environments, or exposed to fluorescence quenching by solvent or polar groups within the protein. Consequently, intermediates and misfolded species will have a characteristic fluorescence which are in different parts of the plots for DHFR and lysozyme and may explain the reverse pattern observed.

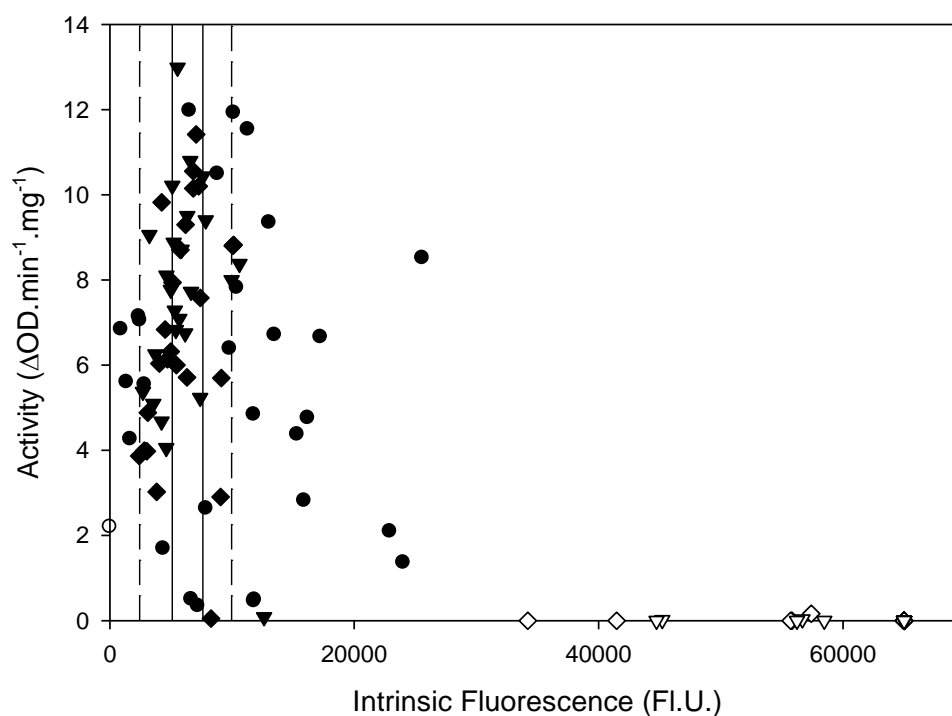


Figure 3.21 Activity measurements as a function of relative fluorescence for DHFR refolds. Each point represents a triplicate. Soluble refold samples, purified (●), unwashed (◆), washed (▲), and aggregated refold samples, purified (○), unwashed (◇), washed (Δ), and cut-off lines shown at fluorescence of 5110 and 7610 (—) and 2446 and 9962 (---) A.U.

3.3.5.3 Activity assay

The optimal condition for refolding was for washed IBs with a final protein concentration of $0.035\text{ mg}\cdot\text{ml}^{-1}$ using $50\text{mM Tris}\cdot\text{HCl}$, pH 7.2, which resulted in an activity of $13\ \Delta\text{OD}\cdot\text{min}^{-1}\cdot\text{mg}^{-1}$. The lowest yielding conditions were those corresponding to washed and unwashed inclusion bodies with a high protein concentration of $2.2\text{ mg}\cdot\text{ml}^{-1}$ in the same buffer, illustrating the importance of low protein concentration in obtaining high yields. The highest yields for refolding purified protein on the other hand were in Buffer 2 (Table 2) and by using different dilution factors and final protein concentrations yields of between 6.9 and $12\ \Delta\text{OD}\cdot\text{min}^{-1}\cdot\text{mg}^{-1}$ were achieved. However washed and unwashed IBs refolded less successfully with this buffer, reaching activities of 5.4 - 9.1 and 3.9 - $7.6\ \Delta\text{OD}\cdot\text{min}^{-1}\cdot\text{mg}^{-1}$ respectively. This demonstrates how different refold buffers prove optimal for different levels of IB purity.

3.4 Conclusions

Absorbance and fluorescence assays can be used in conjunction to rapidly evaluate a large number of refold conditions in a 96-well plate. Measurement of particulate formation by absorbance light scattering provides an initial filter to eliminate aggregating conditions. Intrinsic fluorescence spectroscopy can then be used to identify conditions that produce protein with the most native-like tertiary structure. The refold process and assays were successfully translated to a robotic platform and were demonstrated to have approximately equal errors and advantages for assay consistency.

Investigating the effect of oxidation and shaking on refolding confirmed that the automated assays could function as a hierarchy to eliminate unfavourable refolds. The automated microscale refolding process and assay hierarchy were then used to explore a wider range of lysozyme refold conditions, showing relative fluorescence was a good predictor of yield once aggregating conditions have been screened out by an absorbance assay. The assays were demonstrated to be generically applicable to more industrially relevant IB proteins sourced from fermentation material, in the form of DHFR. An optimal relative fluorescence range for both these proteins could be used as selection criteria for resource intensive and low throughput analytical methods to confirm yield. Confirming the final yield of fewer samples (corresponding to the highest yielding conditions) alleviates the analytical bottleneck and reduces time scales, allowing rapid optimisation of protein refolding at high throughput to achieve greater yields of bioactive product from inclusion bodies. This established refolding and assay sequence could become an even more powerful tool if expanded to include other bioprocess steps typically studied during process development, thus limiting the number of costly and time consuming large scale studies. The study conducted in this chapter was useful for establishing automated refolding and assays, however it is necessary to develop a sequence of operations with integrated assays in order to evaluate the whole process and be able to quantify changes made to upstream operations to final product quality and yield.

4 Development of linked automated microscale unit operations

4.1 Introduction

The development of a manufacturing process requires considerable laboratory and pilot scale work, often costly in terms of manpower, time and capital resources. Obtaining process design information early on is important to prevent process development from being a bottleneck stage and ending up on the critical path and ultimately delaying product launch (Titchener-Hooker et al. 2008). The latter would diminish the period of market exclusivity in which to recoup R&D costs. In order to achieve this, process development must be both cost-effective and use minimal quantities of material. Microscale experimentation offers a potential solution as it addresses both issues. A number of studies have investigated microwell-based fermentation (Duetz et al., 2000; Elmahdi et al., 2003; John et al., 2003; Puskeiler et al., 2005), bioconversion (Doig et al. 2002; Lye et al. 2003), microfiltration (Jackson et al., 2006; Rayat et al., 2010), protein stability (Aucamp et al., 2005) and protein refolding studies (Vincentelli et al., 2004; Willis et al., 2005; Mannall et al., 2009; Dechavanne et al., 2011). Combining multiple unit operations allows investigation of the parameters affecting each unit operation, the study of interactions between unit operations and the generation of material for downstream refolding studies.

Integrating microscale experimentation with robotic platforms allows rapid process development as a large number of process conditions can be studied in parallel, resulting in enhanced experimental throughput and deeper process knowledge. Despite the capital cost of robotic platforms, automation has considerable advantages due to improved speed, accuracy, precision and efficiency. It also enables walk-away operation improving efficiency and reducing human error. Automation has been used to develop and link a number of individual unit operations using liquid handling, robotics and integration of centrifugation (Nealon et al., 2005). This has facilitated the development of linked process sequences for fermentation and whole cell bioconversion (Ferreira-Torres et al., 2005; Baboo et al., 2012). The “whole bioprocess” approach involves a sequence of unit operations at the microscale which can be used to predict large scale performance and analyse the effect of upstream

operations on downstream yields. The availability of new techniques, such as AFA for microscale lysis, allows the application of these processes to intracellular products such as inclusion bodies. In particular when microscale lysis is combined with novel flow cytometry techniques, process monitoring of cell rupture and inclusion body release is possible (Medwid et al., 2007).

The aim of this chapter is to create a whole automated bioprocess from fermentation to inclusion body harvest developed at the microscale that can be combined with the solubilisation, refolding and assays described in the previous chapter. The sequence is based on current industrial scale inclusion body processes and has been demonstrated using DHFR as a model system. The sequence is not intended as a direct ultra scale down version due to the complexities involved in scaling each unit operation. However it will allow the study of the impact of upstream fermentation conditions on downstream refolding yields. The experimental approach required the inclusion body production process to be understood at the pilot scale first. The microscale bioprocess was then developed by establishing robust fermentation in the microwell in order to supply material for the sequential development of each downstream unit operation.

4.2 *Materials and methods*

The microscale sequence experiments were conducted as detailed in 2.2.5. The pilot scale process was conducted as described in 2.2.2. The analytical techniques used to obtain results are detailed in 2.5.1- 2.5.4.

4.3 *Results and Discussion*

4.3.1 Introduction to Automated Microscale Bioprocess Sequence

The whole bioprocess sequence is an extension of the automated refold and hierarchical assays described in the previous chapter and is illustrated in Figure 3.8. It will provide upstream steps for the generation of DHFR inclusion bodies, which can then be solubilised and refolded to study the effect of fermentation conditions on inclusion body yield and quality. The whole bioprocess sequence was formed by combining microscale unit operations for the fermentation, isolation and solubilisation of inclusion bodies (Figure 4.1). It was developed to reflect the inclusion body

processes commonly employed in industry at the pilot and large scale and illustrated in Figure 4.2. The large scale process consists of fermentation to produce intracellular inclusion bodies. The cells are then harvested using centrifugation and resuspended in buffer. The resuspended cells are then lysed using high pressure homogenisation to release the inclusion body from the cell and generate small cellular debris. This material then undergoes centrifugation or microfiltration to separate the larger dense inclusion bodies from the smaller cellular debris. The harvested inclusion bodies can then undergo multiple cycles of resuspension and centrifugation to wash contaminants associated with the surface of the inclusion bodies. The washed inclusion bodies can then be solubilised in a high concentration of denaturant (urea or guanidine hydrochloride), and renatured, with or without prior purification using dilution refolding into a larger quantity of buffer (Clark, 2001). The equivalent large scale unit operation is discussed and then compared to microscale alternatives.

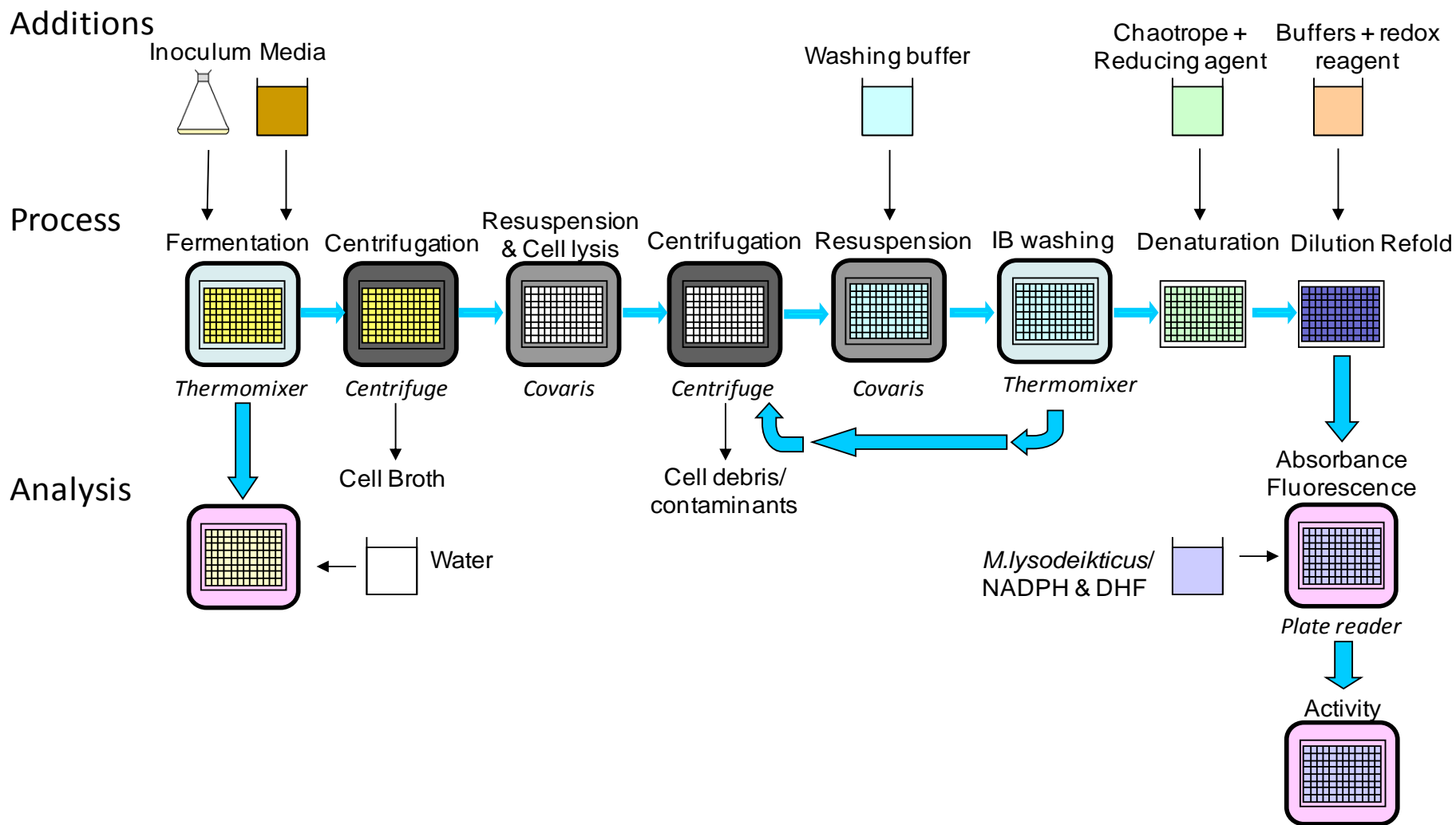


Figure 4.1 Microscale Automated Bioprocess Sequence

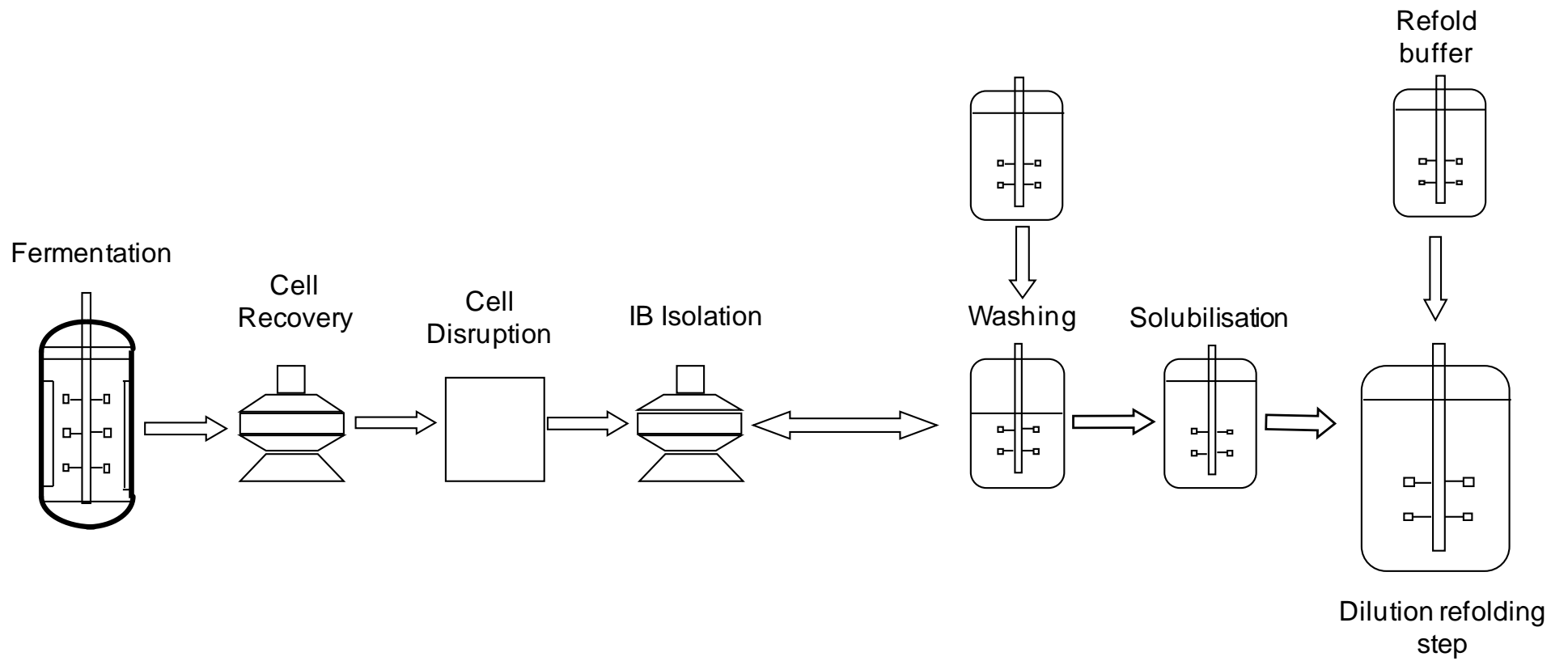


Figure 4.2 Common Inclusion Body Bioprocess Sequence

4.3.2 Fermentation

Pilot scale fermentations in a 20 L vessel were conducted to reproduce previous growth and inclusion body expression, which can then be scaled down to the microwell resulting in a fermentation step related to the larger scale operation. The material generated from the 20 L fermentations was also used for assay development experiments in the previous chapter. Pilot scale fermentations were performed using a protocol optimised for inclusion body production, with induction set at the early exponential phase (Davies, 2009). Table 4.1 shows OD, wet cell weight and dry cell weight obtained for 20 L fermentations at different temperatures. A post induction temperature drop was chosen to investigate the robustness of IB production as it can be used to slow growth and inclusion body production. The results show cells reached optical densities (OD) of up to 12.6 A.U. and dry cell weights of 5.3 g.L⁻¹. The dry cell weight (DCW) is expected to be proportional to the OD of cells, however after induction, the expression of inclusion bodies resulted in a higher absorbance than expected from the cell density. It has been previously reported that disparities exist between turbidity profiles and cell concentration, which have been attributed to the formation of inclusion bodies after induction and morphological changes in the cells (Fieschko et al., 1985; Ryan et al., 1996). At the 20L scale wet cell weights of approximately 14 g.L⁻¹ have been reported with this expression system (corresponding to DCW~ 3.5 g.L⁻¹). Higher growth was only observed at 7L scale with wet cell weights of 35 g.L⁻¹ (DCW~ 7.5 g.L⁻¹) (Davies, 2009).

Table 4.1 Cell growth at harvest (8 hours of fermentation)

Temperature after induction (°C)	OD (A.U.)	Wet cell weight (g.L ⁻¹)	Dry cell weight (g.L ⁻¹)
37	11.4	43.5	5.3
37	12.6	43.6*	5.3*
37	12.0	42.0*	5.1*
25	4.4	27.4	2.2

*Determined indirectly using calibration curves

Figure 4.3 shows the growth curves obtained for the different fermentation processes at the 20 L scale. The cells were induced at 3.5 hours as early exponential induction was shown to be optimal for inclusion body production in this strain (Davies, 2009). After induction at the early exponential phase, the cells continue to grow well at 37 °C, reaching ODs of around 12 A.U. 4.5 hours after induction. The fermentation with a post-induction temperature drop to 25 °C shows no growth for a few hours immediately after induction and has significantly slower growth overall, with a final OD of only 4.4. Jones et al. (1987) found that when the temperature is dropped to 10 °C, growth stopped for 4 hours before a new growth rate is established. In their study, the proteins expressed were in very limited amount and only 13 proteins were produced. It is thought that a sub optimal temperature below 37 °C blocks an early step in protein synthesis to restrict bacterial growth (Broeze et al., 1978).

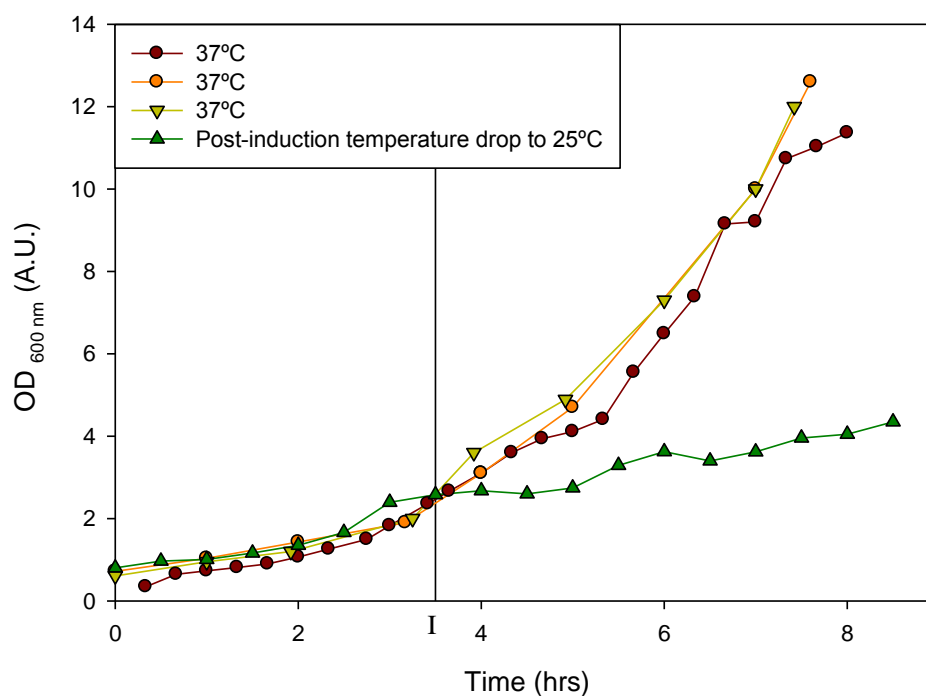
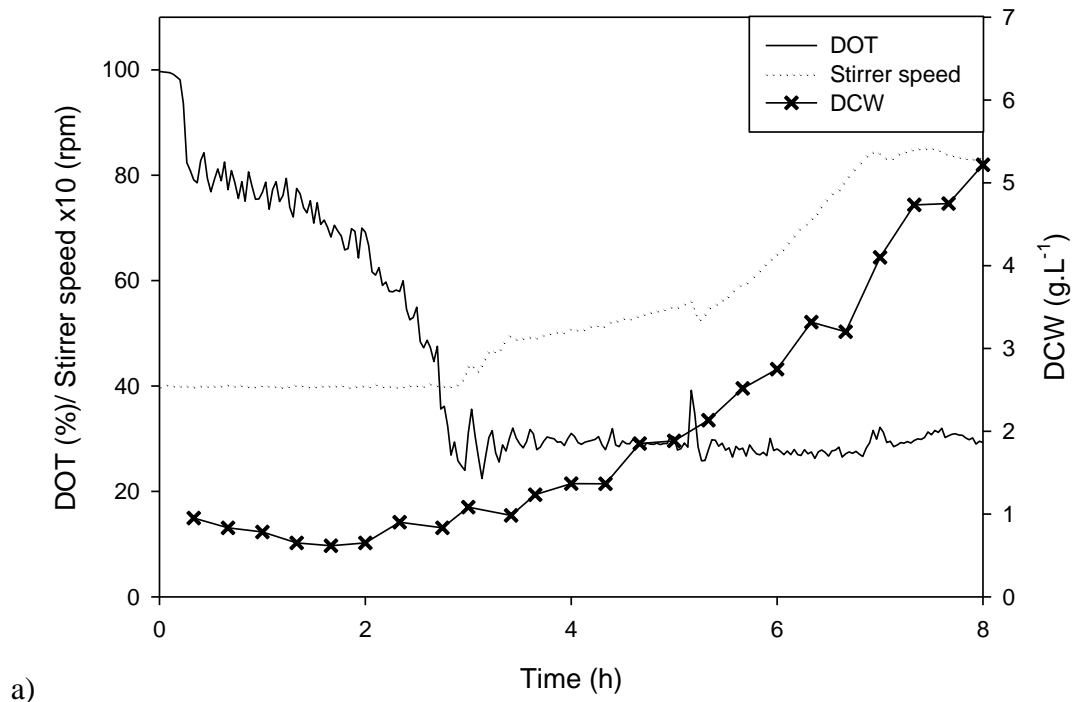


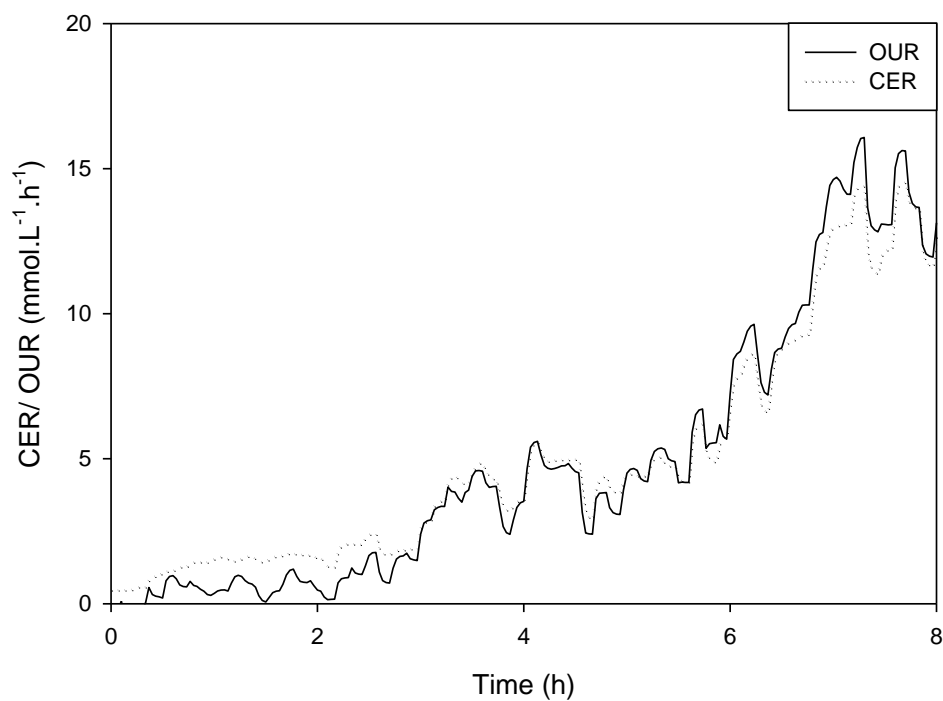
Figure 4.3 20 L DHFR fermentations at different post induction temperatures. Induction time denoted by the line labelled I.

Figure 4.4 shows the DOT, DCW and stirrer speed profiles obtained for the fermentation performed at 37 °C. As the cells reach the early exponential phase, the available oxygen is below 40%. In order to maintain a minimum dissolved oxygen concentration (DOT) of 30%, the impeller speed (set on cascade control) is increased

to maintain this concentration as the cells enter the exponential phase. The impeller speed continues to increase as the cells grow and eventually remains constant around 7 hours.



a)



b)

Figure 4.4 20L Fermentation profile with early exponential induction, grown at 37°C. Figure a) shows the dissolved oxygen tension (DOT), dry cell weight (DCW) and impeller speed. Figure b) illustrates the oxygen uptake rate (OUR) and carbon dioxide evolution rate (CER).

Figure 4.5 shows the SDS-PAGE results obtained using samples from the 20 L fermentation. During induction, an increasing amount of DHFR is present, as can be observed with the increased thickness of the band at 24.5 kDa in lanes 5, 7 and 9. This agrees with the result found from a Bradford assay presented in Figure 4.6. Figure 4.6 shows the levels of soluble and insoluble protein present throughout fermentation. Low levels of insoluble protein are present initially but, after induction at 3.5 hours, insoluble protein increases from 0.1 mg.ml^{-1} at 4 hours to 0.4 mg.ml^{-1} at 8 hours. Additionally, a large increase in the concentration of soluble protein present is detected, resulting from the increased number of cells. Before induction a very faint band is present in lane 3 with the same molecular weight as the product, resulting from the expression of DHFR from the plasmid. The low level of expression and the presence of DHFR before induction suggest the plasmid is constitutively active, which has previously been reported by Davies (2009).

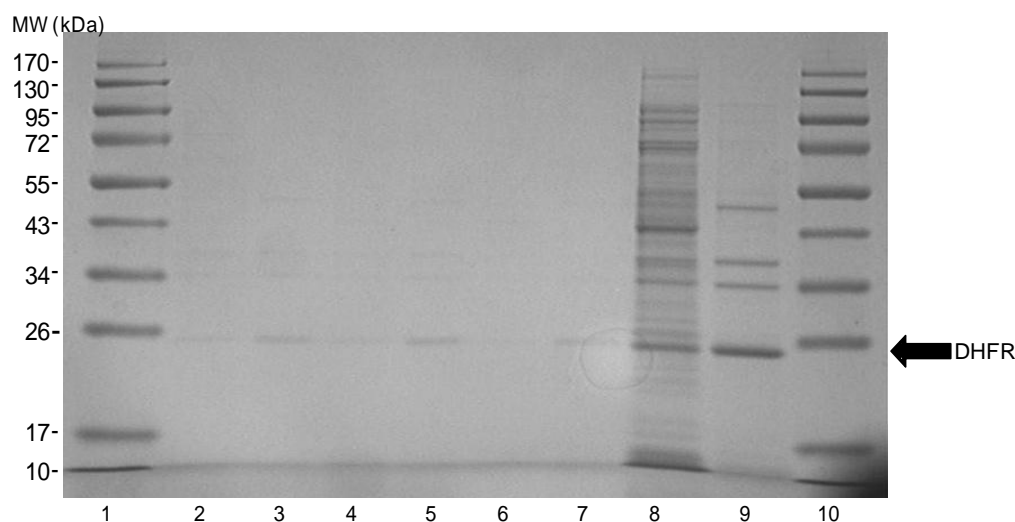


Figure 4.5 SDS PAGE of 20 L Fermentation at 37 °C at different time points. Lanes:

- 1 Molecular weight ladder
- 2 Soluble cell fractions of samples taken at 2 hours
- 3 Insoluble cell fractions of samples taken at 2 hours
- 4 Soluble cell fractions taken at 4 hours
- 5 Insoluble cell fractions taken at 4 hours
- 6 Soluble cell fractions taken at 6 hours
- 7 Insoluble cell fractions taken at 6 hours
- 8 Soluble cell fractions taken at 8 hours
- 9 Insoluble cell fractions taken at 8 hours
- 10 molecular weight ladder

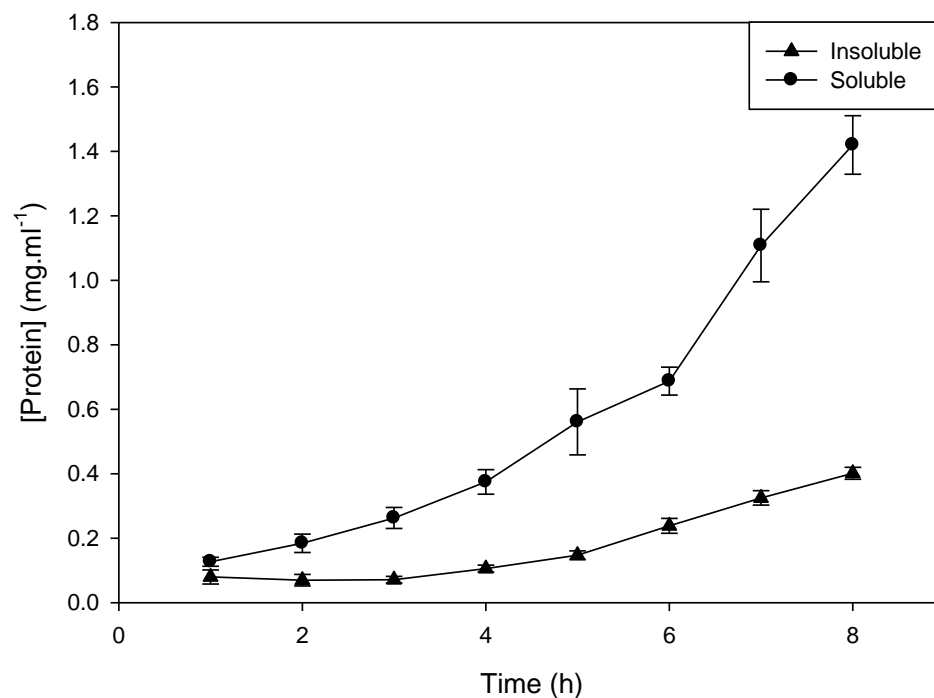


Figure 4.6 Soluble and insoluble protein fractions during 20L fermentation at 37 °C measured by Bradford Assay

Figure 4.7 shows the DOT, DCW, temperature and stirrer speed profiles obtained for the fermentation performed with a post induction temperature drop. Initially the cells show similar growth to previous runs, although the dry cell weight and OD is slightly lower due to the inoculum having a lower cell density. However once the cells start to grow exponentially, the DOT decreases. When the cells are induced at the early exponential phase, growth reaches a steady state and the DOT increases again. Post-induction, growth starts again after a period of 3.5 hours, confirmed by a sharp decrease in DOT. It is therefore believed that the fermentation would need to be conducted for a much longer time frame than 8.5 hours to achieve final dry cell weights similar to those observed previously.

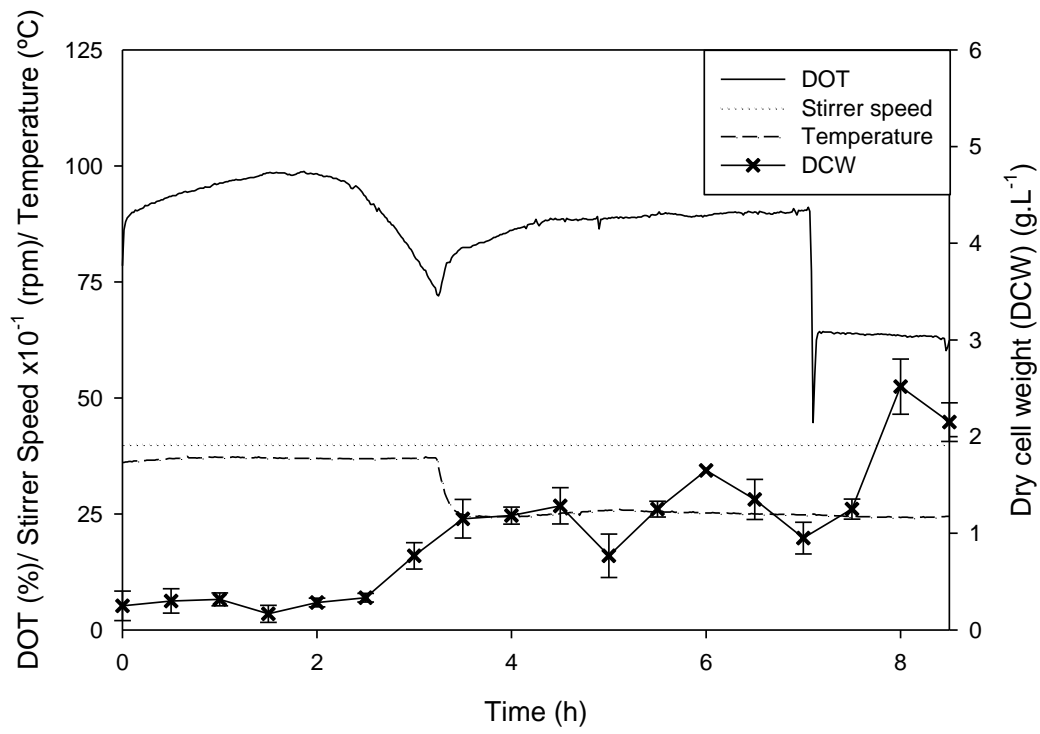


Figure 4.7 20L Fermentation profile with early exponential induction and a temperature drop to 25 $^{\circ}\text{C}$

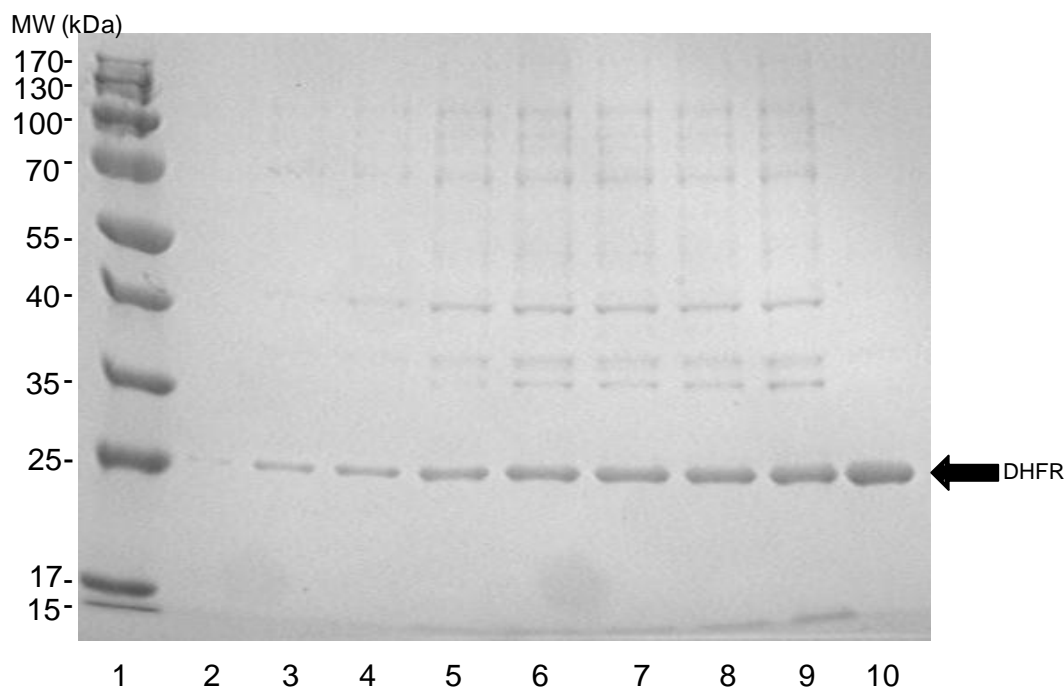


Figure 4.8 SDS PAGE of insoluble cell fraction from 20 L Fermentation with post induction temperature drop to 25 °C. Lanes contain the insoluble cell fractions for the following:

- 1 Molecular weight ladder
- 2 0.5 hours
- 3 1.5 hours
- 4 2.5 hours
- 5 3.5 hours
- 6 4.5 hours
- 7 6.5 hours
- 8 7.5 hours
- 9 harvest
- 10 Inclusion body harvested after the second centrifugation step.

Figure 4.8 presents the SDS-PAGE results for insoluble cell fractions for the post-induction temperature drop fermentation. Despite the poor growth detected during this fermentation, the cells produce considerable amounts of insoluble DHFR as inclusion bodies. Following the second centrifugation step inclusion bodies of high purity are observed. This demonstrates that inclusion bodies are produced even under a lower temperature conditions that favours soluble production, and hence inclusion body production is robust in this strain. Schein and Noteborn (1988) found decreasing the growth temperature to 23-30 °C resulted in 30-90% of the expression product becoming soluble, indicating that between 10-70% of the product still

remained in inclusion bodies. During this fermentation, energy may be conserved by the slow growth rate and instead redirected towards IB production. The cells are at a lower density at the end of the fermentation and have not been subjected to the same stress as for high cell density fermentations. This could improve the cell debris size profile resulting in improved purification. Wong et al. (1996) showed repeated homogenisation passes results in a better fractionation of inclusion bodies and cell debris improving inclusion body purity due to their differing sedimentation properties. If the cells are less resistant to shear, repeated homogenisation may help create small debris which is more easily separated from denser, larger inclusion bodies.

After the fermentation methods had been established at the large scale, it was then necessary to transfer the protocol to the small scale to try and achieve similar growth. The fermentation was scaled down without maintaining a fixed parameter, as the goal was not to have a scaled down matched process but a means of investigating how perturbations in fermentation effect inclusion body refolding. Figure 4.9 shows the growth profiles obtained using the same media (terrific broth) in shake flasks and microwell geometry. For the shake flasks a long lag phase is observed for 3 hours and after 10 hours an OD of 6.2 A.U. is reached. It appears that growth is reaching steady state after 10 hours, suggesting further incubation time would not result in higher ODs for this condition. Micheletti et al. (2006) obtained DCW of 6 g.L^{-1} using an *E. coli* culture in 1 ml microwell 96 DSW plates grown at 1000 rpm, which corresponds to an OD of approximately 12 A.U.. The cells in this experiment grew to reach an OD of 12.7 A.U., which matches that achieved at the 20 L scale.

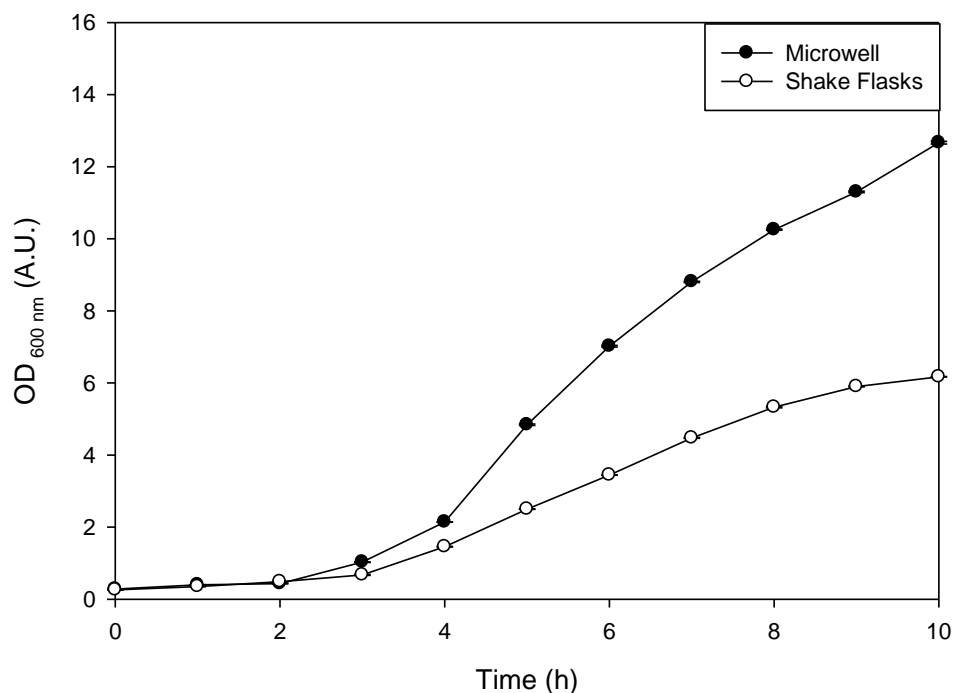


Figure 4.9 Comparison of growth at 37°C with no induction in microwell (fill volume 1 ml, shaking 1000 rpm) and 1L shake flasks (fill volume 100 ml, shaking 200 rpm)

Optimisation of the inoculate preparation step was carried out to reduce the lag phase observed for *E. coli* growth in microwells (Figure 4.9). Figure 4.10 shows the lag phase was reduced to 2 hours. The shorter lag phase allowed the cells to reach an OD of approximately 12 A.U. in the same time scale of 8 hours as the 20 L fermentations. Cells were induced after 4 hours of growth to mimic the early exponential induction step at a larger scale. Induction did not appear to slow growth significantly in the microwells, with an OD of 11.4 and 11.8 A.U. achieved in the induced and non-induced wells, respectively, at the end of the fermentation. The experiments demonstrated that growth similar to the 20 L can be achieved in microwells for this strain.

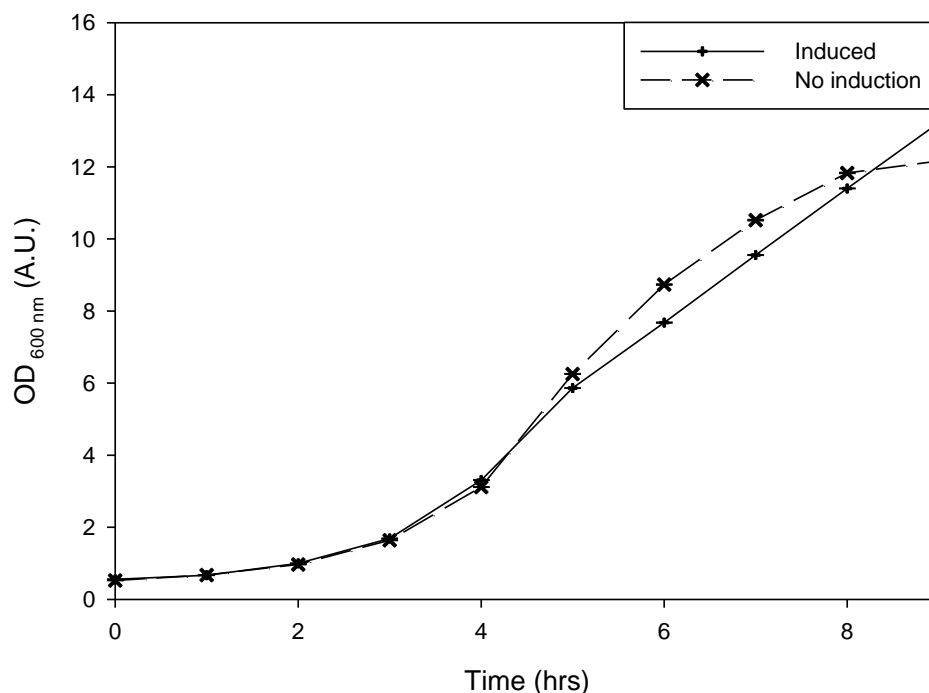


Figure 4.10 Automated microwell fermentation at 37 °C, with induction at 4 hours using 0.125 mM IPTG, fill volume of 1 ml and shaking at 1000 rpm.

4.3.3 Centrifugation for cell harvest

Centrifugation to harvest cells from the 20 L fermentations involved the use of the CARR Powerfuge or CSA-1 centrifuge. The aim of this step is to maximise both the cell separation and the dewatering levels. At the microscale, the deep well plate was covered and placed in a microplate centrifuge along with an identical plate for balancing. Table 4.2 shows that a percentage clarification of close to 100% can be achieved in only 15 minutes at 4000 rpm for the microwell fermentation broth. This clarification level is much higher than that achieved in large scale centrifugation, which usually has lower clarification levels (Lander et al., 2005). Higher centrifugal forces can be achieved in a small scale centrifuge in comparison to industrial centrifuges. Additionally, material appears to settle quicker at the small scale. It has been shown that ultra scale down (USD) centrifugation methodology over predicts clarification at process scale for high solid density feeds, possibly as a result of increased interparticulate forces at the microscale (Tustian et al., 2007).

Table 4.2 Clarification achieved for supernatant fraction after centrifuging microplate at 4000 rpm

Sample	Centrifugation (min)	time	OD	Clarification (%)
Feed	0		11.333	0
Supernatant	10		0.101	99.787
Supernatant	15		0.078	99.999
Media	-		0.077	100

Following centrifugation at the microscale, the supernatant needs to be removed from the sedimented pellet in the bottom of the V-shaped well using the liquid handling arm of the robot to pipette the liquid. Increasing volumes of supernatant were removed in order to observe the maximum volume that could be removed without the pellet being disturbed and cells becoming present in the supernatant (causing an increase in OD). Figure 4.11 shows the OD of the removed fermentation broth as the volume removed by automated pipetting increases. Initially OD is constant as the volume removed increases up to 710 μl . As a larger volume is aspirated, the tip of the pipette comes into closer contact with the pellet, disturbing the pellet and resulting in more cells being carried over into the clarified fermentation broth. The optimum volume for aspiration is 710 μl , however this will change for different fermentations depending on the wet cell weight and hence the final size of the pellet. Other settings were adopted to try and minimise the breakthrough of cells, such as decreasing the pipetting velocity and minimising the liquid tracking distance (the depth by which the tip is below the liquid surface). A lower volume of 400 μl was used in the automated sequence to avoid loss of cells. Furthermore a wetter pellet reflects the larger scale where equivalent dewatering cannot be achieved, and consequently fermentation broth is carried over into the next step.

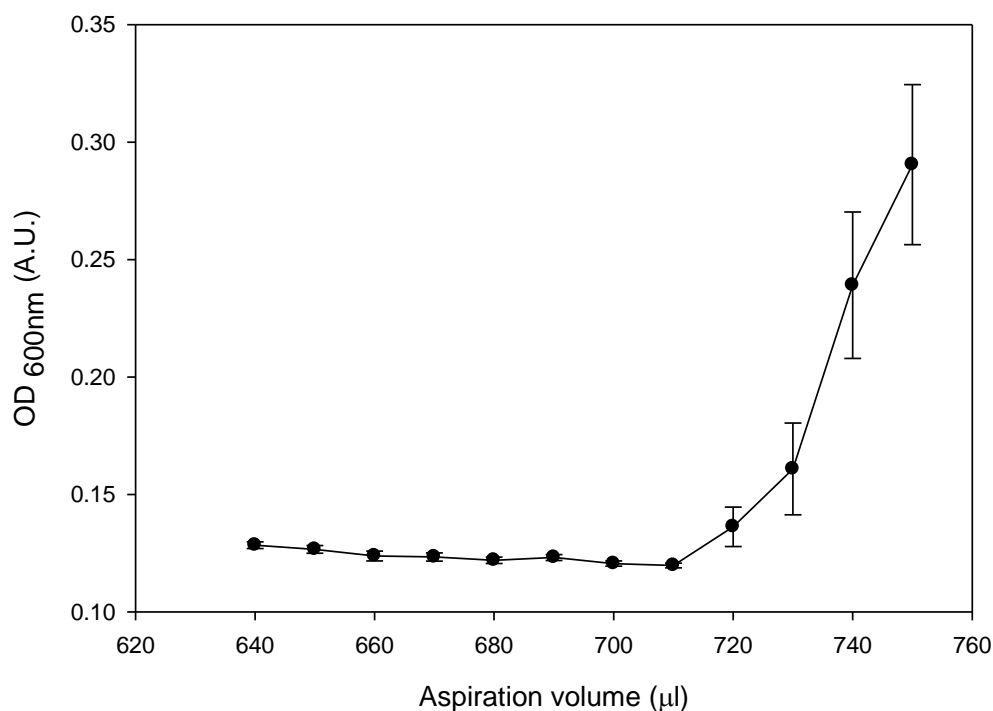


Figure 4.11 Clarification of supernatant after removal of different volumes from the pellet.

4.3.4 Resuspension

The cells were resuspended to give the same concentration as for the large scale process. The OD was measured at each stage to monitor cell loss from the centrifugation and resuspension steps. Figure 4.12 shows the concentration of cells present at each stage and illustrates where cells are lost in the process. Despite the induced cells having a higher OD, the pellet of the non-induced cells was larger. This is a result of the inclusion bodies resulting in a greater absorbance for the induced cells, which is not necessarily reflective of greater cell growth. The non-induced cells with a larger pellet were more susceptible to disturbance by the liquid handling pipette tip and therefore more cells were lost in the broth supernatant after centrifugation. Additionally more cells failed to be resuspended because the pellet was larger in size and more difficult to fully resuspend. The induced cells, on the other hand, had minimal losses during broth removal following centrifugation and also resuspended to a greater degree. Consequently higher cell densities, as observed for the non-induced cells, can represent greater hurdles in the microscale process.

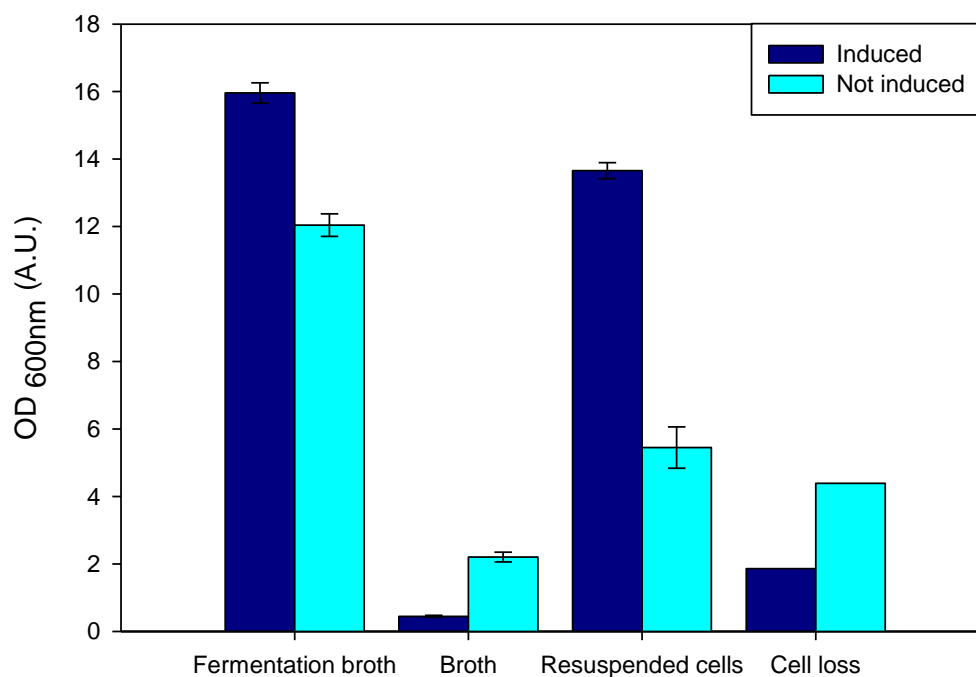


Figure 4.12 Cell losses during the microwell process for induced and non-induced cells, showing the cell concentration at fermentation harvest, in the broth removed after centrifugation, at the resuspension stage and the total cell loss from fermentation through to resuspension.

4.3.5 Cell lysis using sonication and AFA

Cell lysis can be challenging at the microscale because of the lack of high throughput technologies available in 96-well plate format. Using a technique such as sonication for the treatment of 96 samples can be time consuming and labour intensive. It also requires substantial liquid handling resulting in the loss of any cells that have failed to resuspend. One potential solution is to use a mechanical disruption technique which is compatible with 96-well plate format. The Covaris E210 uses adaptive focusing acoustics (AFA) to lyse cells and offers an automated solution which is compatible with 96-round bottom wells plates and glass vials.

A method for lysis was developed based on the lysis protocol by Wenger et al., which shows optimal lysis at 20% duty cycle (dc) and an intensity (I) of 500 mV (intensity=10). Duty cycle is the percentage of time in which the transducer is producing acoustic waves, and the intensity is proportional to the amplitude of the pressure wave. The cycles per burst and the cell density were shown not to be important factors in cell disruption (Wenger et al., 2008). A treatment time of only 2

minutes under conditions of $d_c = 20\%$, $I = 10$ was found to be sufficient for complete release of soluble antibody fragment (Perez-Pardo et al. 2011).

Samples were exposed to lysis conditions, set in the Covaris, for different times and compared to chemical lysis and standard lab sonication as shown in Figure 4.13. The presence of increasing amounts of protein in the supernatant fraction shows that cell rupture has taken place and the contents of the cell is released. In inclusion body processes the protein of interest is in the pellet, therefore a high concentration of protein in the supernatant (soluble) fraction and a relatively high purity in the pellet (insoluble) fraction is desirable. Increasing the treatment time in the Covaris from 30 seconds to 200 seconds does not result in any cell lysis in the microwell format, as demonstrated by the similar protein concentration obtained in the soluble fraction. Almost 100% of the protein remains in the pellet indicating the cells have not ruptured, as in the control condition of unlysed cells. However cell lysis occurs when using chemical lysis in microwells and by sonication for the same volume and concentration of cells. Under these conditions a greater concentration of protein 0.5 mg.ml^{-1} is observed in the soluble fraction, which is significantly greater than the 0.1 mg.ml^{-1} present in the unlysed control well. The differing concentration of insoluble protein present in AFA and unlysed samples results from liquid handling operations causing variability in the concentration of cells and consequently total protein concentration.

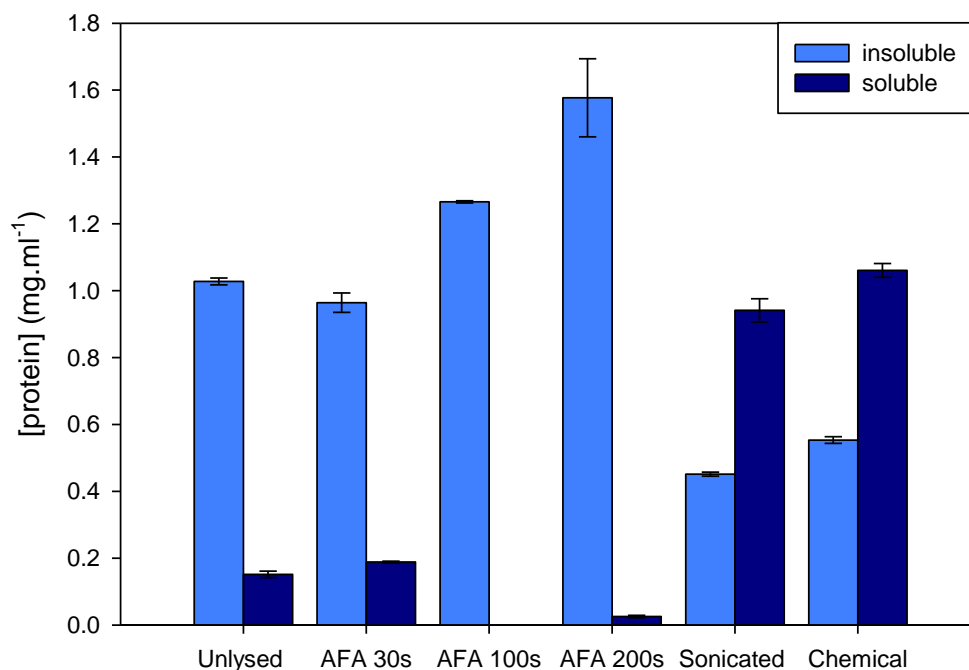


Figure 4.13 Protein release under different conditions, showing unlysed cells, cells treated with AFA in microwells for different lengths of time, sonicated cells and chemically lysed cells. The concentration of protein in soluble and insoluble cell fractions is determined by Bradford assay.

Figure 4.14 illustrates the protein concentration in the soluble and insoluble fractions of cells lysed under different conditions. No significant difference is observed between the unlysed (control) sample and samples exposed to increasing periods of times of acoustic focusing, despite achieving a power input of 115 Watts (Wenger et al., 2008). The soluble fractions show low concentrations of protein and only very faint protein bands are visible after electrophoresis (Figure 4.14). The sonicated sample, on the other hand, has a higher concentration of protein in the soluble fraction. Additionally, fewer bands are visible in the insoluble fraction as the pellet increases in purity and more contaminating soluble proteins are lost to the supernatant fraction.

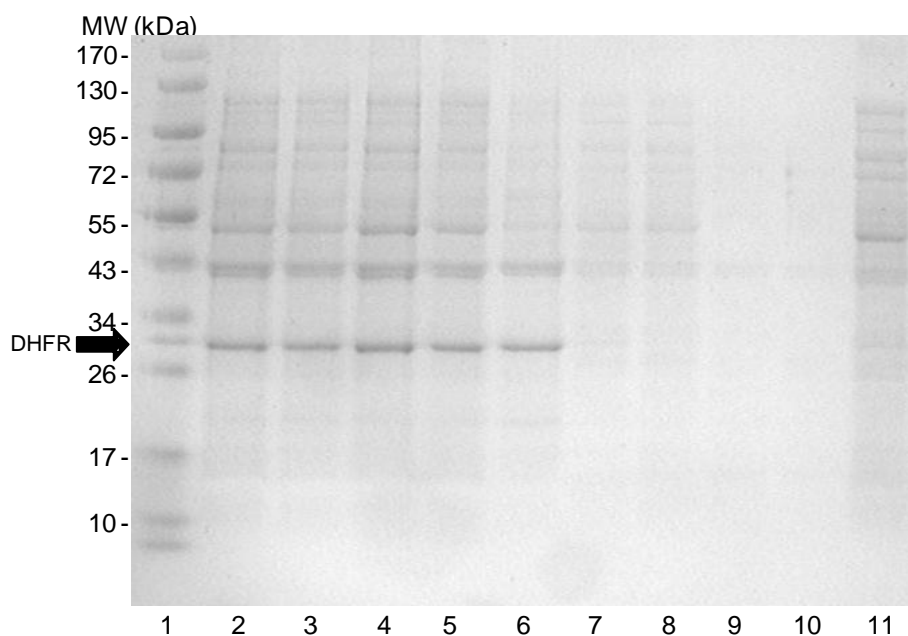


Figure 4.14 SDS PAGE analysis of soluble and insoluble cell fractions of cell suspension exposed to sonication and different AFA (Covaris) treatment times in microwells. Lanes:

- 1 Molecular weight ladder.
- 2 Insoluble fraction of control (no rupture)
- 3 Insoluble fraction of 30 s AFA exposure
- 4 Insoluble fraction of 100 s AFA exposure
- 5 Insoluble fraction of 200 s AFA exposure
- 6 Insoluble fraction of sonicated samples
- 7 Soluble fraction of control (no rupture)
- 8 Soluble fraction of 30 s AFA exposure
- 9 Soluble fraction of 100 s AFA exposure
- 10 Soluble fraction of 200 s AFA exposure
- 11 Soluble fraction of sonicated sample

Figure 4.15 shows that the inclusion body pellet also has a greater purity under chemical lysis or sonication. The soluble fraction is populated by an increased number of high molecular weight proteins and the insoluble fraction shows the presence of DHFR and only two or three major contaminants. The insoluble fraction for the Covaris induced lysis resembles that for the control with no lysis, both show DHFR in the presence of many other contaminants. This finding is in agreement with results obtained using the Bradford assay where no lysis has occurred in the Covaris under these conditions (Figure 4.13).

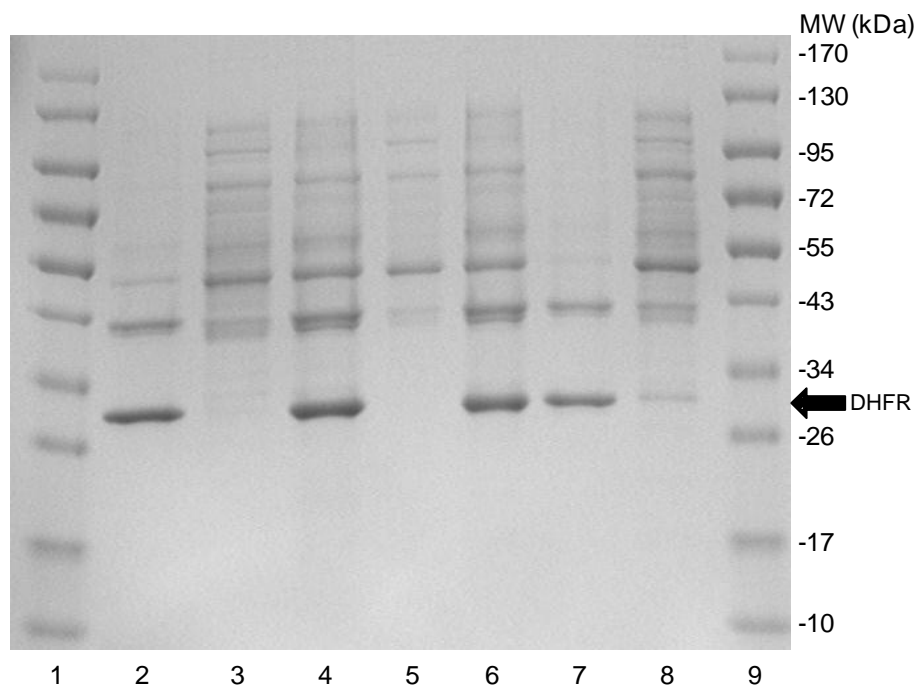


Figure 4.15 SDS PAGE analysis of soluble and insoluble fractions of cell suspension exposed to sonication, AFA (Covaris) and chemical lysis. Lanes:

- 1 Molecular weight ladder
- 2 Insoluble cell fractions for chemical lysis
- 3 Soluble cell fractions for chemical lysis
- 4 Insoluble cell fractions for control (unruptured cells)
- 5 Soluble cell fractions for control (unruptured cells)
- 6 Insoluble cell fraction for AFA treated cells
- 7 Insoluble cell fraction of sonicated cells
- 8 Soluble cell fractions of sonicated cells
- 9 Molecular weight ladder

Cell lysis had not been observed using 400 μl and treatment times of up to 200 seconds, therefore the range of conditions tested were extended to 400 seconds and different volumes were used. Additionally vials were used instead of microwell plates, to investigate whether reason for the cell behaviour observed could be attributed to the microwell format. Figure 4.16 shows that AFA treatment of cell suspension volumes of 300 μl and 500 μl in microwell plates resulted in the absence of protein in the soluble fraction as it was found for the control sample with no lysis. This indicates that no cell lysis has occurred, as confirmed by the blur of bands observed in the insoluble fractions corresponding to intracellular proteins.

Cell lysis is, however, observed when the treatment was carried out in vials, with significantly less bands of protein found in the insoluble fraction contaminating the recombinant protein. The soluble fraction also has many bands present, showing that the cells have lysed and released their contents. Lysis does not appear to be as complete as that previously observed for chemical lysis or sonication (Figure 4.15), where less contaminating protein is present in the insoluble fraction. Cell rupture using hydrodynamic cavitation methods has been reported to release periplasmic proteins over cytoplasmic proteins (Balasundaram & Pandit 2001) and the size of inclusion bodies coupled with the size of the debris produced may result in IB separation being more difficult. In this particular experiment however, AFA is shown to cause a clear improvement if compared to the sonication method, which appears to result in more contaminating protein in the insoluble fraction (Figure 4.16). The variability in the results obtained using sonication methods may result from different cell suspensions being used. The growth rate is known to influence cell lysis, with cells in the rapid growth phase rupturing more easily than those in stationary phase. Cells characterised by slower growth have had more time to produce peptidoglycans that strength cell walls (Balasundaram et al. 2009; Engler & Robinson 1981) and could therefore be more resistant to sonication. The variability observed could also result from the sonication times not being long enough for complete cell lysis. For this reason cycle time was increased from 10 cycles of 10s on and 10s off to 8 cycles of 20s on, 20s off.

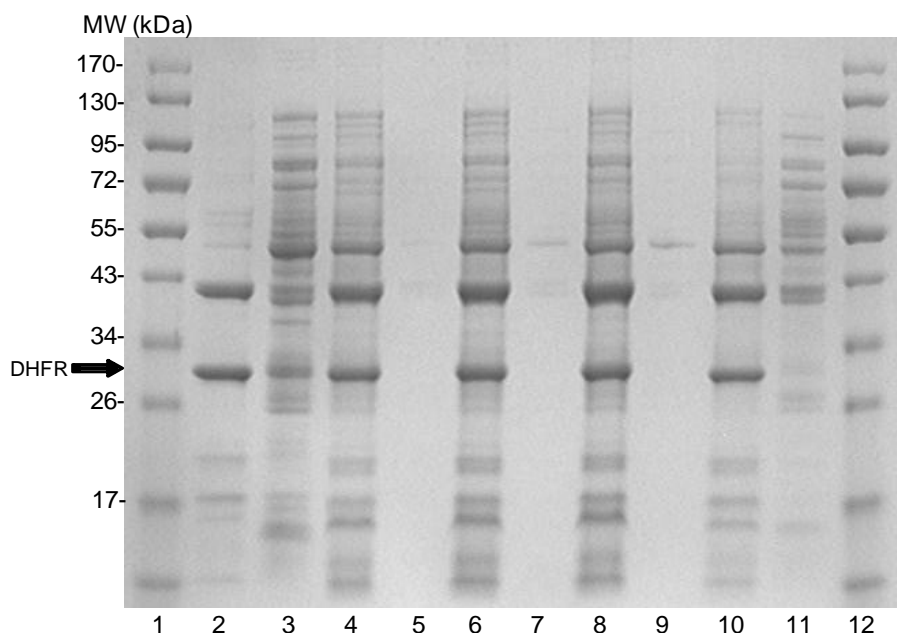


Figure 4.16 SDS PAGE analysis of cell suspension exposed to sonication, AFA (Covaris) in vials and in microwells using different volumes. Lanes:

- 1 Molecular weight ladder
- 2 Insoluble fraction for 500 µl cell suspension treated with AFA in vials
- 3 Soluble fractions for 500 µl cell suspension treated with AFA in vials
- 4 Insoluble fraction of 300 µl cell suspension treated with AFA in wells
- 5 Soluble fraction of 300 µl cell suspension treated with AFA in wells
- 6 Insoluble fraction of 500 µl cell suspension treated with AFA in wells
- 7 Soluble fraction of 500 µl cell suspension treated with AFA in wells
- 8 Insoluble fractions of a control with no lysis
- 9 Soluble fractions of a control with no lysis
- 10 Insoluble fractions of sonicated cell suspension
- 11 Soluble fractions of sonicated cell suspension
- 12 Molecular weight ladder

Figure 4.17 shows the protein released in AFA in different formats as compared to sonicated and unlysed cells. It supports the SDS PAGE analysis that the amount of protein that has been released is little when microwells plates were used with AFA as the protein concentration is approximately equal to that found in the soluble fraction. The concentration of protein in the soluble supernatant after AFA treatment in vials is very high reflecting cell rupture. The soluble fraction has a concentration of 2 mg.ml^{-1} , which is over double the 0.81 mg.ml^{-1} found in the insoluble fraction. A similar ratio can be observed in the sonicated sample, with 0.94 mg.ml^{-1} in the soluble

fraction and 0.45 mg.ml^{-1} in the insoluble fraction, which shows the fraction of protein release is approximately equal to that obtained in vials using AFA. Slightly less protein is found in the pellet (insoluble fraction) of the vials, which agrees with the findings of SDS-PAGE (Figure 4.13) that less contaminating protein is present. A similar fraction of release of soluble protein demonstrates that the efficiency of the lysis process is equivalent to, or even better than, traditional sonication methods. Lysis in vials was selected as the best cell rupture method using AFA for subsequent experiments.

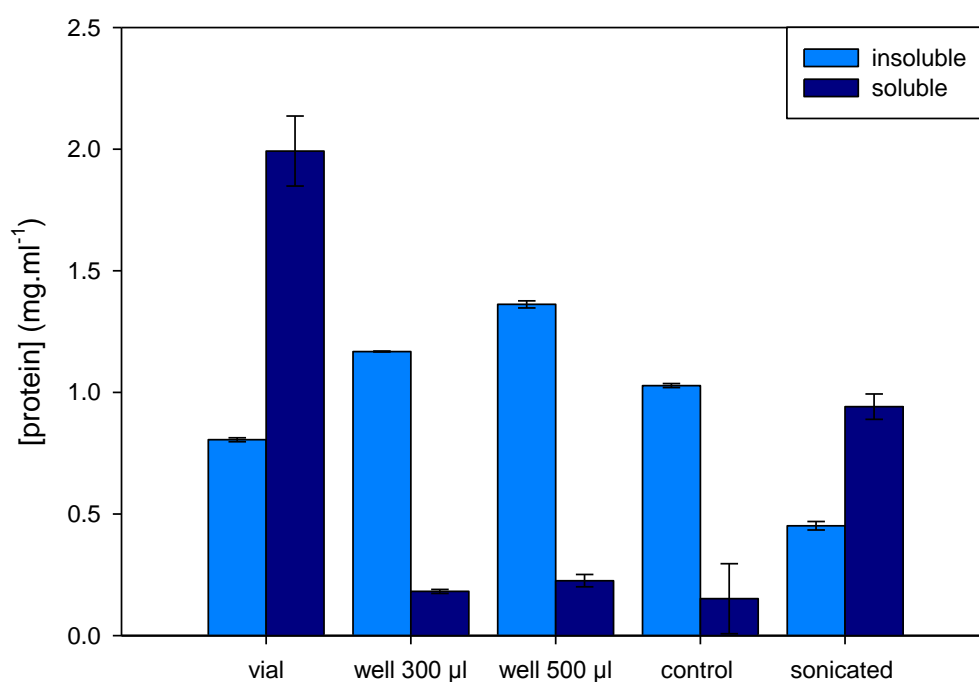


Figure 4.17 Protein release using AFA with different formats (microwell and vial) compared with sonication. The concentration of protein in soluble and insoluble cell fractions is determined by Bradford assay.

Different volumes of cell suspension were investigated using the AFA methods in vials. Volumes of 450, 600, 900 and 1350 μl were selected and all show soluble protein release into the supernatant and similar patterns of contaminating protein bands present in the insoluble fraction (Figure 4.18). The results of the Bradford assay (Figure 4.19) performed using these sample volumes, show the soluble protein concentrations for all 4 volumes tested to be between 0.18 and 0.20 mg.ml^{-1} . The concentration of insoluble protein for a volume of $450 \mu\text{l}$ is lowest at 0.21 mg.ml^{-1} ,

with higher volumes having a slightly higher concentration between 0.25 and 0.27 mg.ml⁻¹. This demonstrates that any of these volumes in vials display cell lysis under the conditions tested. The lowest volume tested was chosen as this would prevent the pooling of material from multiple fermentation wells, allowing different conditions to be kept separate and potentially more fermentation variables explored.

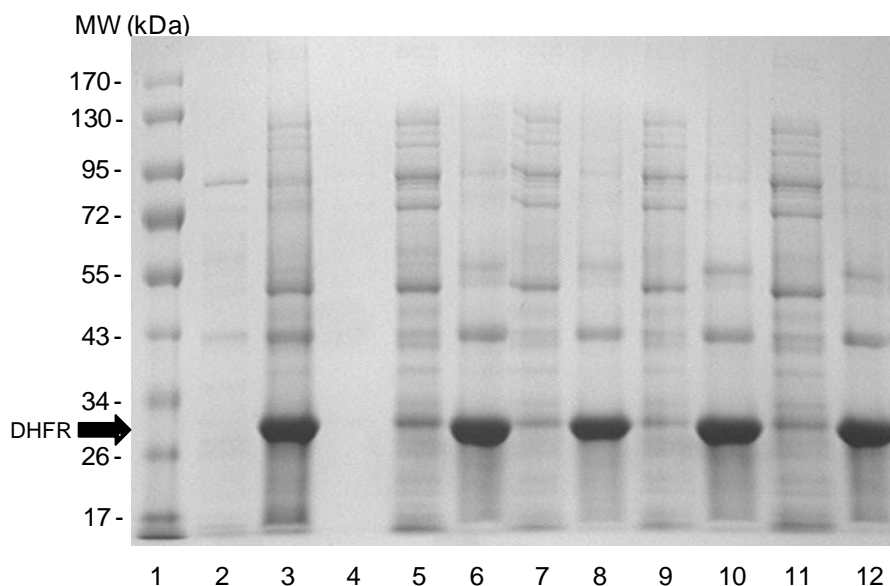


Figure 4.18 SDS PAGE analysis of cell suspension exposed to sonication and AFA in vials using different volumes. Lanes:

- 1 Molecular weight ladder
- 2 Soluble fractions of sonicated cells
- 3 Insoluble fractions of sonicated cells
- 4 soluble fraction of control (unruptured) cells
- 5 Soluble fractions of 450 µl of cell suspension treated in vials with AFA
- 6 Insoluble fraction of 450 µl of cell suspension treated in vials with AFA
- 7 Soluble fraction of 650 µl of cell suspension treated in vials with AFA
- 8 Insoluble fraction of 650 µl of cell suspension treated in vials with AFA
- 9 Soluble fraction of 900 µl of cell suspension treated in vials with AFA
- 10 Insoluble fraction of 900 µl of cell suspension treated in vials with AFA
- 11 Soluble fraction of 1350 µl of cell suspension treated in vials with AFA.
- 12 Insoluble fraction of 1350 µl of cell suspension treated in vials with AFA

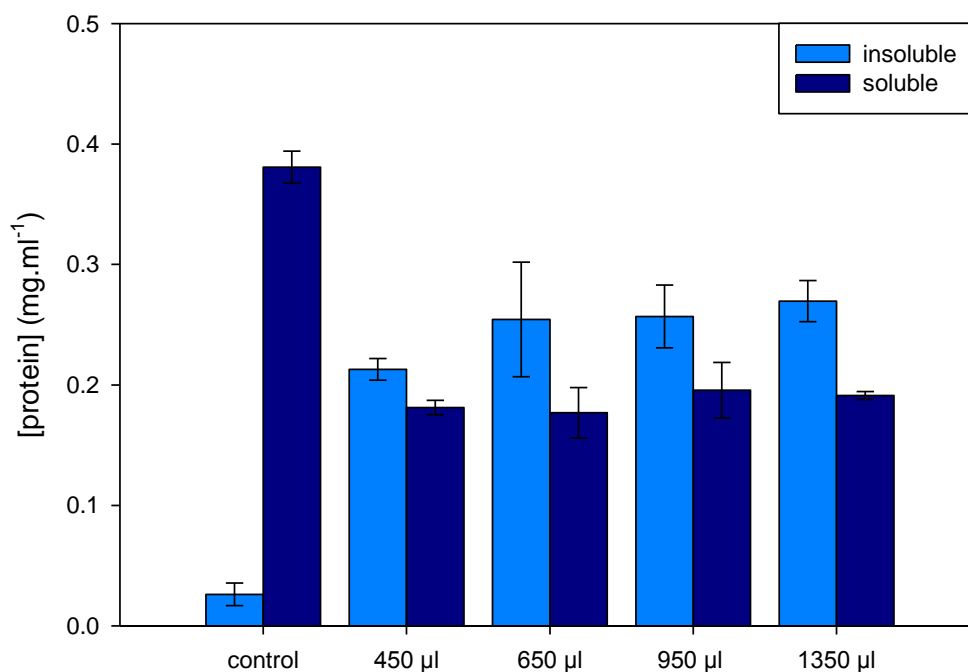


Figure 4.19 Protein release using AFA in vials with different volumes, compared with a control of no lysis. The concentration of protein in soluble and insoluble cell fractions is determined by Bradford assay.

In order to establish the best method for cell lysis (sonication or AFA), information on the presence of cell debris was required. In order to monitor changes in particle size Dynamic Light Scattering was used, as shown in Figure 4.20 for large scale fermentation data. Intact cells appear to have an average size of 1.1 µm, with peaks showing larger aggregates of 5 µm and 120 µm. After the first pass of homogenisation, the peak at 120 µm is no longer present, indicating the aggregates have been broken up by the shear experienced in the homogeniser. The peak, present at 5 µm, also decreases. The particle size of the main peak at 1.1 µm decreases to 0.8 µm. Davies (2009) found a peak at 0.7 µm after homogenisation of this strain, which had a high concentration of insoluble DHFR present. It is therefore likely that the peak at 0.8 µm corresponds to inclusion bodies. Successive passes of homogenisation result in the emergence of a new peak at 0.2 µm, resulting from cell debris. Agerkvist et al. (1990) reported the transition of a cell debris peak from 0.457 to 0.191 µm after increasing passes of *E. coli* through a high pressure homogeniser. The peak at 0.8 µm also decreases in volume slightly between the second and third pass, which could

result from a decrease in the number of inclusion body particle size due to shear effects. After the second centrifugation step in the process to harvest the inclusion bodies, the peak at 0.2 μm disappears as the cell debris is lost in the supernatant and the inclusion bodies are harvested as the pellet.

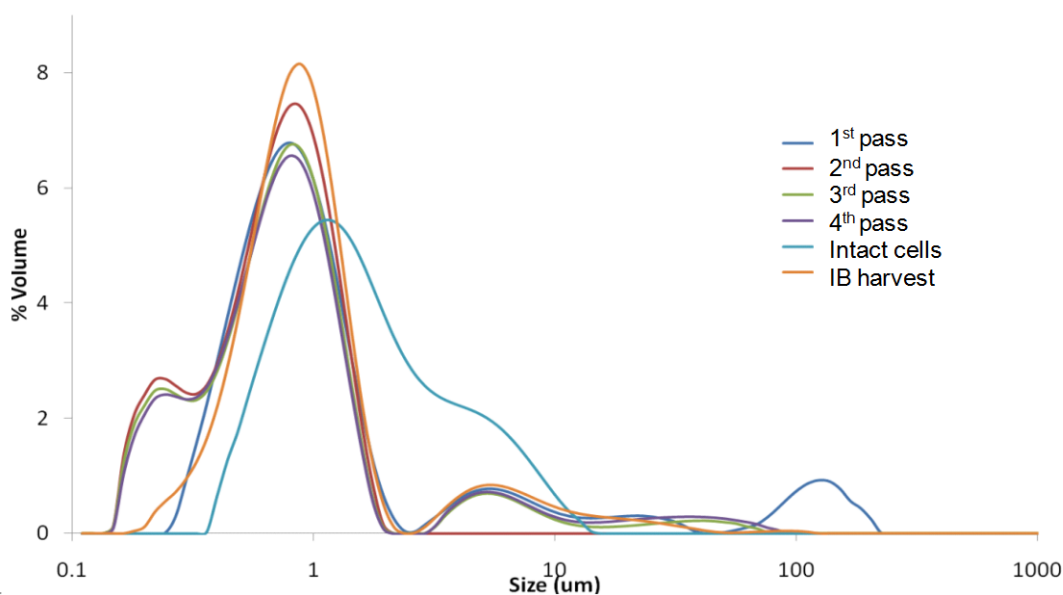


Figure 4.20 Particle size distribution for material from a 20 L fermentation, determined using laser diffraction for intact cells. Whole cells and harvested IBs were compared with cells which had undergone different numbers of homogenisation passes at 500 bar in a Manton-Gaulin Lab 60 high pressure homogeniser.

Particle size measurements carried out using DLS required 5-10 ml of material. In order to run a similar experiment with microscale-derived material, the content of at least 10 wells is required to obtain reliable results. Therefore the technique is not ideal for the analysis of microwell scale experiments and flow cytometry was explored as an alternative. Flow cytometry was used to investigate the difference between cells lysed using the Covaris and those lysed with a sonicator with regards to cell debris size and inclusion body release using SYTOX Green staining. SYTOX Green is a cyanine dye which can only penetrate cells with compromised plasma membranes. It has a high affinity for nucleic acids, and when bound gives a 500-fold increase in the fluorescence emission (Roth et al., 1997). SYTOX Green gives superior detection in comparison to other available dyes (propidium iodide) and allows the discrimination of permeabilised cells from intact cells. The staining process also increases the fluorescence of the inclusion bodies. Medwid et al. (2007)

suggested the dye molecules diffuse into submicron pores in the inclusion body structure and become trapped. This could explain why the relative amount of fluorescence is lower than that caused by nucleic acid binding. Medwid et al. (2007) also showed that SYTOX Green is capable of distinguishing inclusion bodies from unruptured cells and cell debris, potentially enabling the quantification of IB production.

Figure 4.21, Figure 4.22, Figure 4.23 and Figure 4.24 show the relative fluorescence and light scattering for unruptured cells, inclusion bodies, sonicated cells and Covaris lysed cells respectively. Unruptured (intact) cells show a fluorescence peak at 300 Fl.U (Figure 4.21). When these cells are ruptured by sonication, this shifts to a lower relative fluorescence of 40, as shown in Figure 4.23. The AFA treated sample also shows a shift to lower fluorescence, with a peak centred on a relative fluorescence of 30 (Figure 4.24). This demonstrates that lysis in the Covaris using AFA is resulting in cell rupturing and inclusion body release. Medwid et al. (2007) found that SYTOX Green bound both cells and IBs and a lower fluorescence intensity indicated cell lysis and IB release. The pure inclusion body sample has a peak fluorescence of 30 (Figure 4.22), so the peaks in the lysed samples represent the inclusion bodies. Both the sonicated and Covaris samples have a shoulder to the right of the main peak, which is a clear second peak centred around 70 Fl.U in the sonicated cells (Figure 4.23, Figure 4.24). This could result from cell debris containing nucleic acids which have bound dye. The forward scatter data does not show a significant difference between intact cells and ruptured cells. The particle size should be reduced upon lysis, but based on the dynamic light scattering data this change for 1.1 μm for an intact cell to 0.9 μm for an inclusion body might be too small. Medwid et al reported that, while inclusion bodies could be resolved from background noise (their size exists at the lower limit of flow cytometry detection), they could not be resolved from unlysed cells using light scattering methods alone due to the significant overlap of intact cells and inclusion bodies. However, the samples shown in Figure 4.24-4.25 do differ with regards to side scatter, with intact cells showing less granular content. After lysis a greater range of granularities is visualised, with substantially more granular content observed due to the release of highly refractile nature of IBs. In particular the sonicated cells have the highest granular content, this results from a greater release of inclusion bodies. The

lack of highly granular large particles present compared with the AFA treated sample implies a greater degree of lysis. Whilst the two lysis techniques differ in debris size and granularity, they both show inclusion body release.

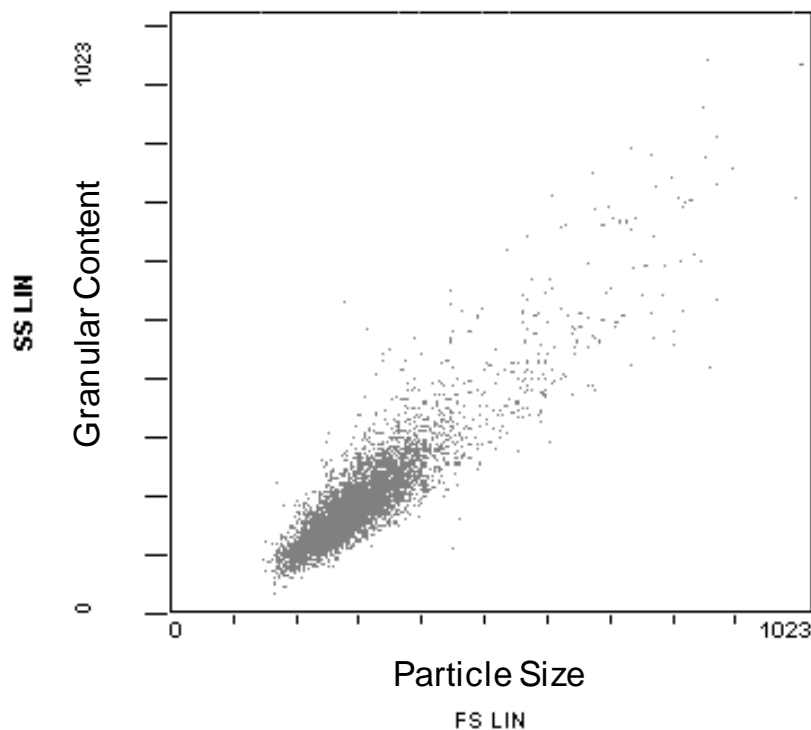
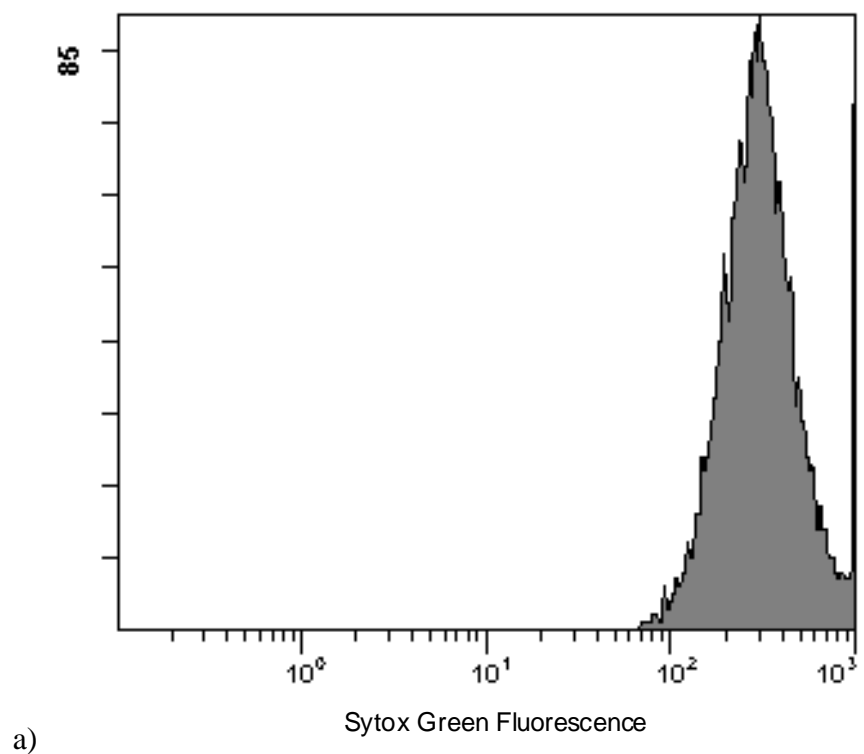
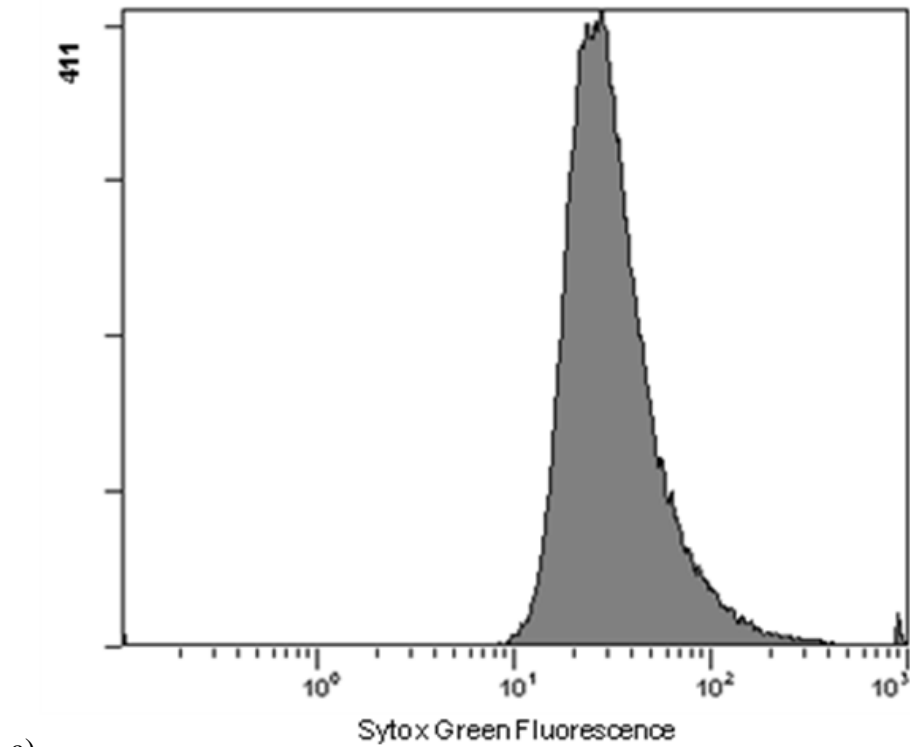
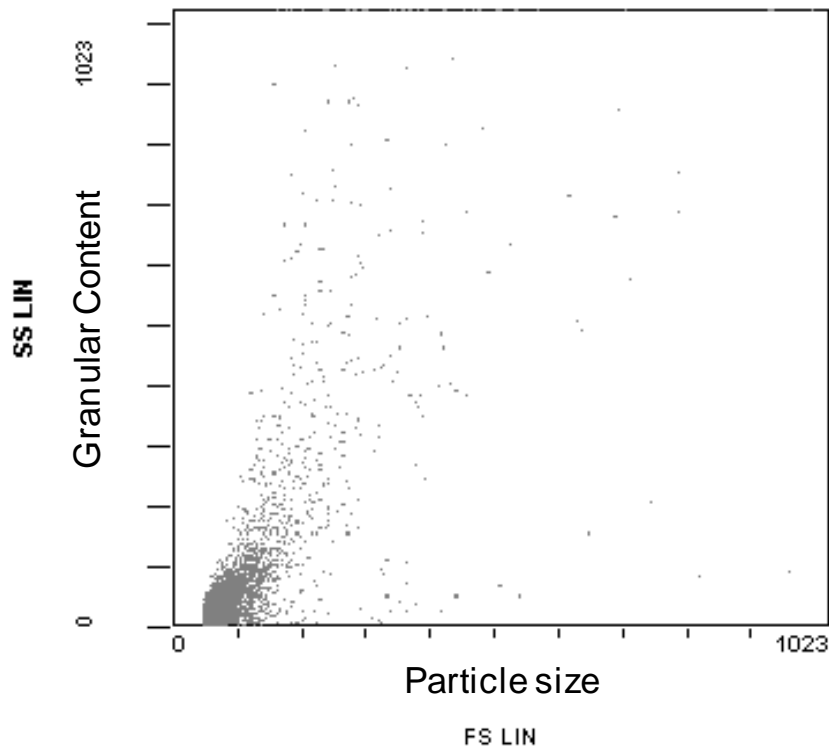


Figure 4.21 Fluorescence (525 nm emission) histograms (a) and light scatter plots (b) for intact (unruptured) cells from microwell DHFR fermentation, stained with SYTOX Green and measured for their fluorescence, particle size and granularity using a flow cytometer (see Section **Error! Reference source not found.** for method).



a)



b)

Figure 4.22 Fluorescence (525 nm emission) histograms (a) and light scatter plots (b) for isolated unwashed DHFR inclusion bodies produced by 20L fermentation, stained with SYTOX Green and measured for their fluorescence, particle size and granularity using a flow cytometer (see Section **Error! Reference source not found.** for method).

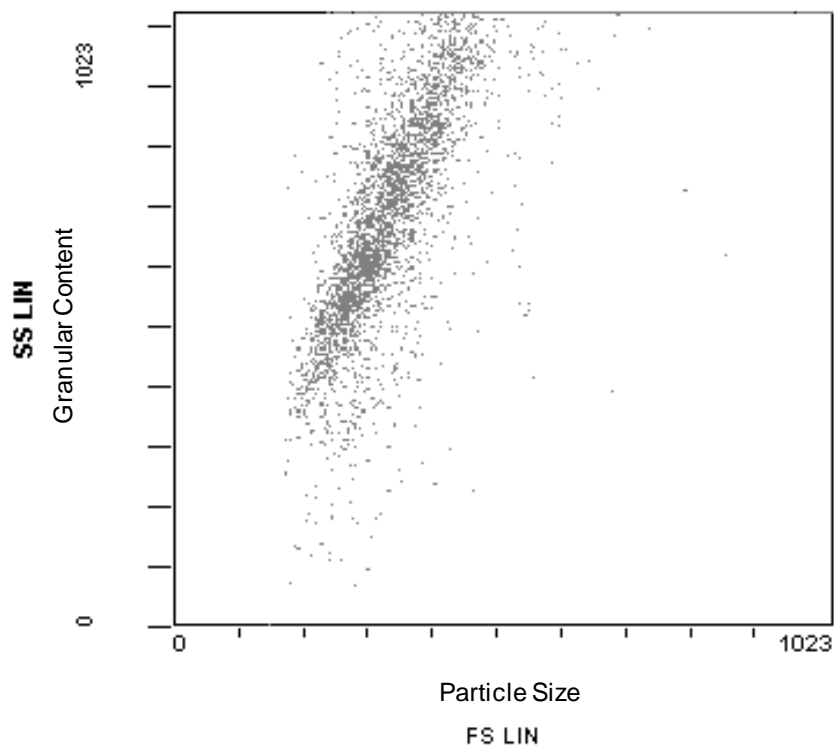
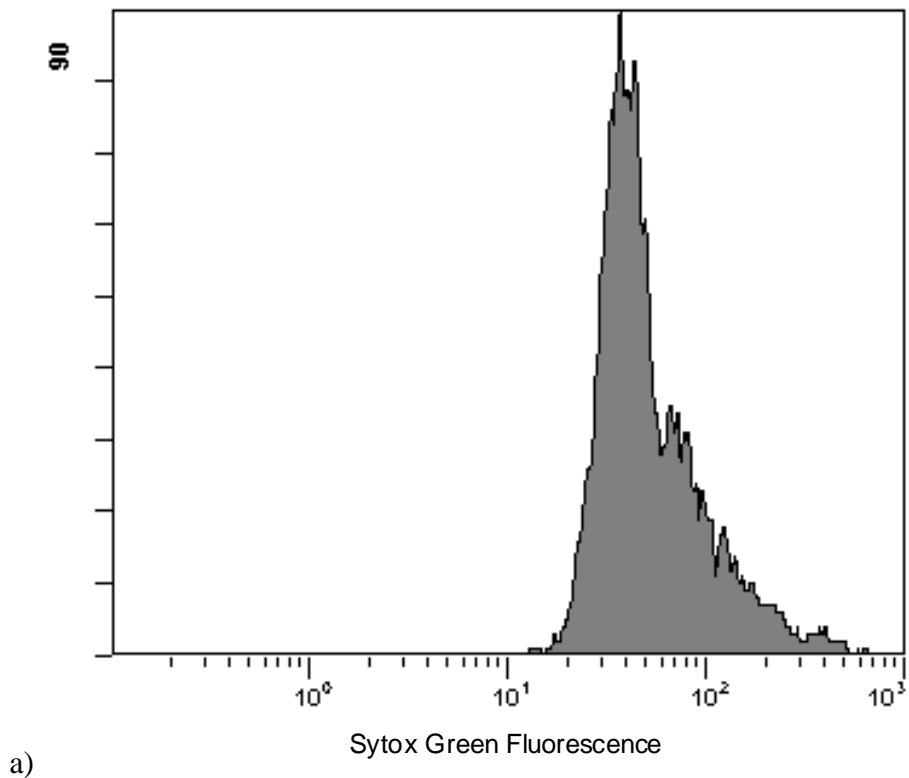
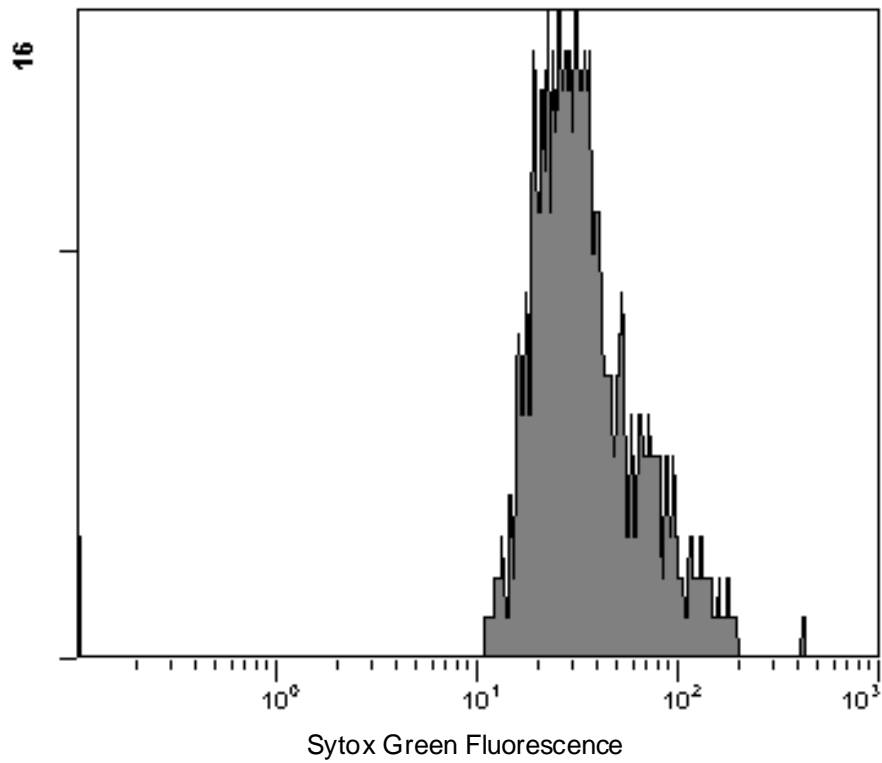
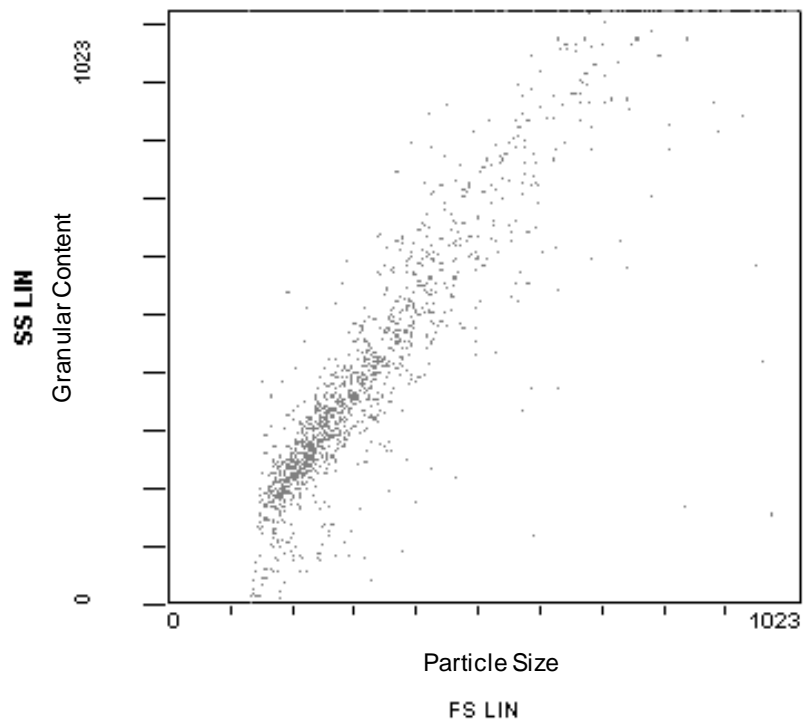


Figure 4.23 Fluorescence (525 nm emission) histograms (a) and light scatter plots (b) for sonicated cells (see Section 2.2.5.3 for conditions) from a microwell DHFR fermentation, stained with SYTOX Green and measured for their fluorescence, particle size and granularity using a flow cytometer (see Section **Error! Reference source not found.** for method).



a)



b)

Figure 4.24 Fluorescence (525 nm emission) histograms (a) and light scatter plots (b) for AFA treated (see Section 2.2.5.4) cells from microwell DHFR fermentation, stained with SYTOX Green and measured for their fluorescence, particle size and granularity using a flow cytometer (see Section 2.5.3 for method).

4.3.6 Centrifugation for IB harvest

Following cell lysis, a second centrifugation step is needed to achieve the required purity of inclusion body. The density difference between inclusion bodies and cell debris can be exploited as inclusion bodies are dense and can be pelleted, whereas the cell debris can be lost in the supernatant. Centrifugation acts as a crude purification step, resulting in the loss of some of the contaminating protein in the supernatant fraction. During large scale experiments, the total concentration of protein lost in the supernatant was 0.72 mg.ml^{-1} (Figure 4.25). This supernatant fraction has been further separated into its soluble and insoluble constituent parts, showing the loss of 0.42 mg.ml^{-1} in the insoluble fraction, some of which corresponds to the loss of the product DHFR as shown by SDS PAGE (Figure 4.26). However an insoluble protein concentration of 1.35 mg.ml^{-1} is observed in the centrifugation solids, with DHFR being the major protein present.

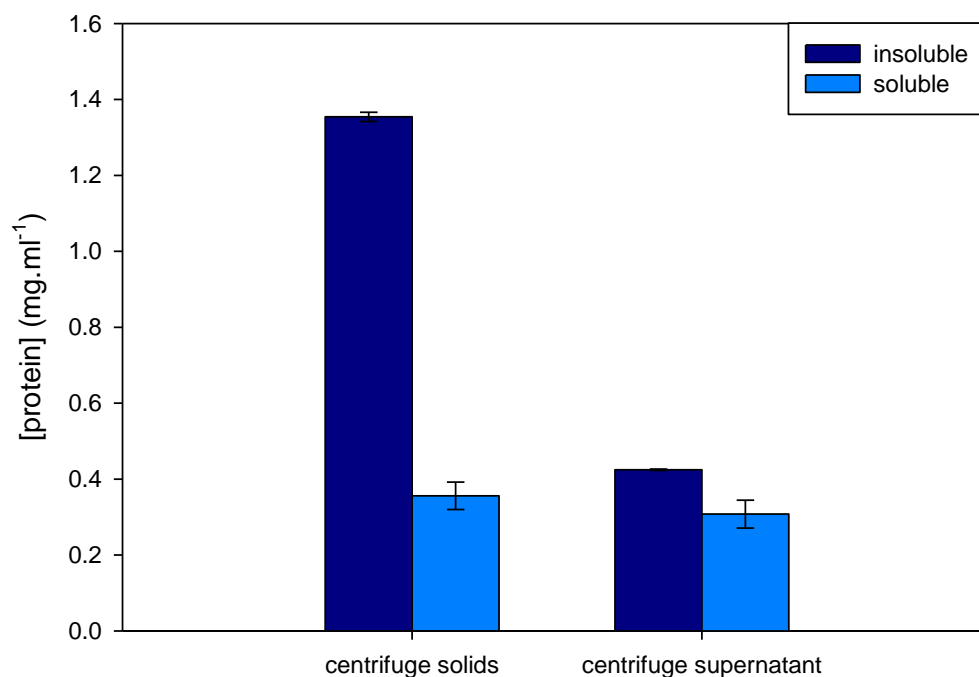


Figure 4.25 Protein concentration of insoluble and soluble fractions of centrifugation solids and supernatant, as determined by Bradford assay.

The SDS PAGE results (Figure 4.26) show the presence of a high concentration of DHFR with a significant amount of contaminants in the pelleted IBs obtained from the

centrifugation step. The bands present at 36 kDa and 40 kDa could result from outer membrane proteins. Bands present at 36, 38, 38.5 and 40 kDa have previously been attributed to outer membrane proteins of *E. coli* (Lugtenberg et al., 1975). The harvested IB pellet is typically washed using multiple cycles of resuspension and centrifugation to remove some of these contaminants before refolding.

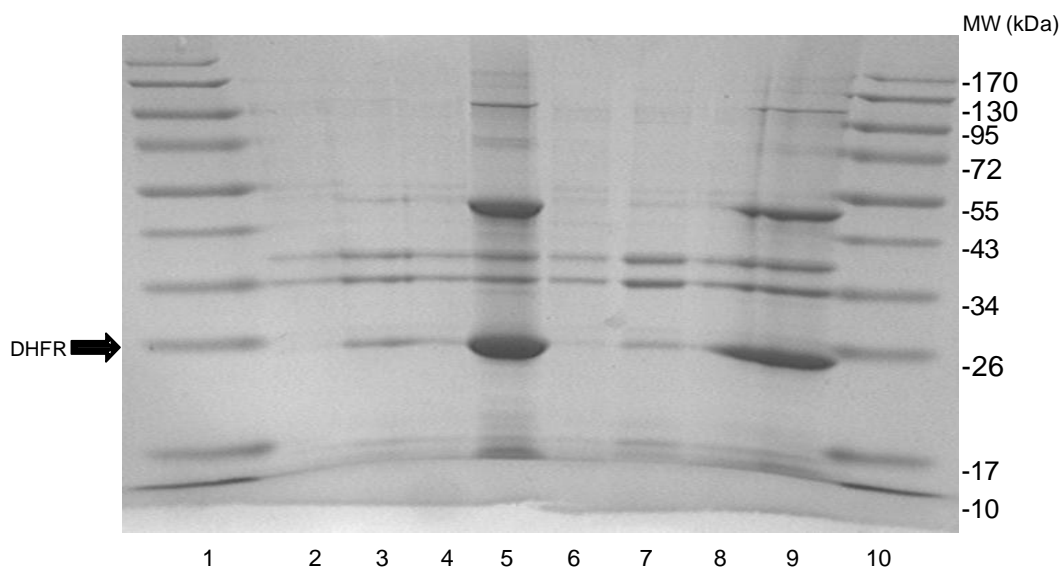


Figure 4.26 SDS PAGE showing soluble and insoluble fractions of supernatant and solids discharge of the first centrifugation step (cell harvest) and second centrifugation step after homogenisation (IB harvest).

1. Molecular weight ladder
2. Soluble fractions of the supernatant from the first centrifugation step
3. Insoluble fractions of the supernatant from the first centrifugation step
4. Soluble fractions of the pellet from the first centrifugation step
5. Insoluble fractions of the pellet from the first centrifugation step
6. Soluble fractions of the supernatant from the second centrifugation step
7. Insoluble fractions of the supernatant from the second centrifugation step
8. Soluble fractions of the pellet from the second centrifugation step
9. Insoluble fractions of the pellet from the second centrifugation step
10. Molecular weight ladder

Figure 4.27 shows the SDS-PAGE results obtained with the resulting pellet and supernatant fractions after centrifugation at the microscale. The supernatant fraction shows the presence of many contaminating protein, especially at higher molecular weights of 38 kDa and above, which will be lost during the centrifugation step. In the inclusion body pellet, a range of contaminating proteins is present. The presence of a

major contaminant at just under 40 kDa appears to match those found at the large scale that have been attributed to outer membrane proteins. The release of soluble protein and a soluble product has been shown to be the same for AFA as high pressure homogenisation for one bacterial strain (*S. cerevisiae*) (Wenger et al., 2008), and consequently this would result in the same contaminant profile. Therefore the proteins that contaminate the IB pellet at the large scale will also be present after IB harvest from AFA lysis.

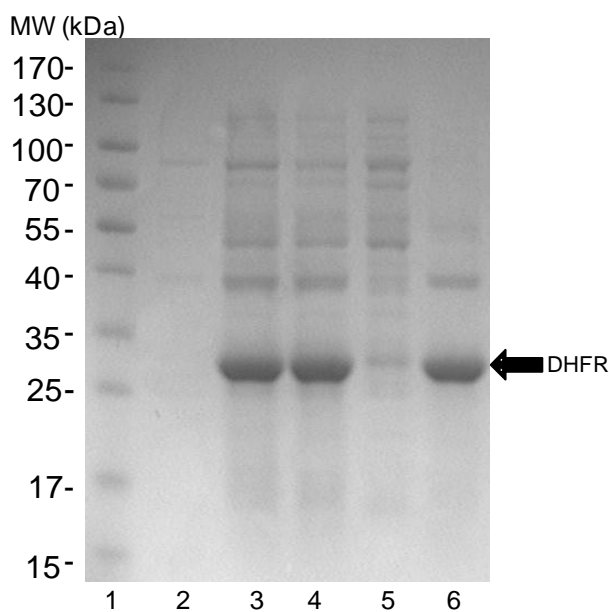


Figure 4.27 SDS-PAGE showing the purification achieved for IBs harvested after different cell lysis methods. Lanes:

- 1 Molecular weight ladder
- 2 Soluble fractions of sonicated cells (which appear not to have lysed)
- 3 Insoluble fractions of sonicated cells (which appear not to have lysed)
- 4 Insoluble fraction of control (unruptured) cells
- 5 Soluble fractions of 450 μ l of cell suspension treated with AFA
- 6 Insoluble fractions of 450 μ l of cell suspension treated with AFA

4.4 Conclusions

The aim of this chapter was to develop a microscale process sequence for producing inclusion body material for refolding. Fermentation in microwell was shown to produce comparable cell growth to that found at the 20L scale fermentations. Cells cultivated in microwell plate format reached an OD of 12 A.U., the same as the average OD obtained from large scale fermentations. 100% clarification was achieved at cell harvest using material produced at the microscale and exceeded the clarification typically observed at industrial scale. However it was difficult to remove the fermentation broth reproducibly without disturbance of the pellet. Therefore a smaller volume was removed resulting in a wetter pellet, which is more similar to the larger scale where dewatering is less. The cell resuspension step at the microscale posed some challenges as vigorous mixing is required to resuspend the pellet and consequently it was necessary to mix for a longer time than at large scale. Higher ODs and larger pellets also resulted in more cell loss during the resuspension step. The most challenging step to achieve at the microscale for high throughput studies was cell lysis. Whilst AFA provides a solution, it is not achievable in the microwell format and the efficiency of inclusion body release appears to be lower than that achieved using sonication, as shown by the flow cytometry results. The level of purification achieved in the IB harvest in the following centrifugation step shows some similarities between large scale and the microscale as the major contaminant involved is present in both samples. In conclusion a microscale process has been developed which can provide inclusion body material in sufficient quantities for refolding studies. The next chapter will explore whether it can be used to study the effect of fermentation conditions on refolding and finally if it will give results which are relevant to the large scale.

5 Application of the microscale sequence to study the effect of fermentation variables on inclusion body refolding yield

5.1 Introduction

Aggregation of over expressed recombinant protein can be partly controlled by slowing the rate of heterologous expression. Hence cultivation conditions that lead to increased cellular stress and greater protein synthesis rates also appear to promote inclusion body formation, such as high plasmid copy numbers, temperatures, cell densities, inducer concentration and strong promoters (Schein and Noteborn, 1988; Wang et al., 1999; Fahnert et al., 2004a). Strandberg and Enfors (1991) found production temperature, extracellular pH and carbon source strongly influenced inclusion body formation and in particular induction temperature was important for optimizing product yield. Aggregation has been monitored *in vivo* using FT-IR and results have shown different inclusion body formation kinetics occur in cultures at temperatures of 37 and 27°C (Ami et al., 2005). The technique also showed the protein obtained from the inclusion bodies had different conformational states depending on fermentation conditions, a finding supported by the work of others (Przybycien et al., 1994).

While previous work has focused on the effect of culture temperature, there is still a lack of understanding in how key fermentation variables alter inclusion quality and consequently the yield of bioactive protein. Maachupalli-Reddy et al. (1997) investigated the effect of typical inclusion body contaminants, such as DNA, RNA, phospholipids, lipopolysaccharides and other proteins, on lysozyme refolding. However they spiked contaminants into refolds and did not link different upstream fermentation conditions to changes observed in inclusion body quality. Valax and Georgiou (1993) analyzed β -lactamase IBs produced in *E. coli* and demonstrated that protein composition is a complex function of growth conditions (temperature and pH) and protein expression system, with protein impurities ranging from 5% to 50%, at T = 37 and 30°C respectively and a pH = 7.0.

This chapter examines the effect of fermentation conditions on the refolding yield of two proteins produced as inclusion bodies in *E. coli*, namely murine dihydrofolate reductase (mDHFR) and insulin Lispro. Murine DHFR is a small monomeric protein (M_r 21 446) (Clark et al., 1996). It has two domains and does not feature any prosthetic groups or disulphide bonds. The folding pathway of murine DHFR has been characterised (Thillet et al., 1990) and the crystal structure is known to 2 Å (Stammers et al., 1987). Davies (2009) has previously optimised DHFR refolding using diafiltration in an ultra scale down rotating disk filtration obtained from the same expression system. In chapter 4 it was shown that a microscale bioprocess sequence can be used to generate IB material for refolding and would provide an efficient tool for rapid evaluation of different process conditions. The structure of Insulin Lispro (Humalog[®]) is very similar to the native form of insulin, but the Pro-Lys amino acid residues are reversed at position B28 and B29. Insulin lispro is produced from fermentation in *E. coli* of a precursor molecule (proinsulin) with a short amino acid sequence, and leads to the formation of inclusion bodies which can take up to 20% of the cells volume (Williams et al., 1982). The *in vitro* folding mechanism of insulin has been studied (Liu et al., 2009) and a renaturation procedure that achieves yields of up to 70% has also been detailed in literature (Winter et al., 2002).

The aim of this chapter is to investigate whether the microscale process sequence established in Chapter 4 can be used to study a range of process variables and identify process changes that have an impact on subsequent operations and final product quality. In particular, an effort will be made to show that the developed process sequence can be used as a tool to study the effect of fermentation conditions on inclusion body quality and yield of active protein after refolding. In order to do this, factors upstream of refolding were altered to study the impact on downstream protein refolding. This was performed for both DHFR and insulin process sequences. The fermentation variables chosen reflected those of interest to the collaborating company, Fujifilm Diosynth Biotechnologies.

Materials and Methods

5.1.1 DHFR

The microscale sequence was performed as previously described in 2.2.5, with a fermentation time of 9 hours. The conditions used for each variable studied are described in Table 5.1. All inclusion bodies were stored at -20°C unless otherwise stated.

Table 5.1 Conditions used during microscale DHFR fermentations

Variable	Inducer concentration (mM)	Induction time (h)
Induction time	0.125	3, 3.5, 4, 4.5, 5
Inducer concentration	0.125, 0.25, 0.5	4
Inclusion body washing	0.125	3
Inclusion body storage	0.125	3

Protein assays were performed as previously described in 2.5.2. SDS-PAGE was performed as written in 2.5.1. Inclusion bodies were washed as detailed in 2.2.3. Inclusion bodies were solubilised and refolded as described in 2.2.6, in the buffers described in Table 5.2. Assays were conducted as detailed in 2.5.8.

Table 5.2 DHFR refold buffers

Buffer	Components
1 Tris	50mM Tris.HCl, pH 7.2
2 Optimised	50mM Tris.HCl, 0.25M arginine, 2mM cystine.2HCl, 2mM cysteine, pH 7.2
3 Reducing	0.25 M Potassium phosphate, 0.1 M potassium chloride, 1 mM DTT

5.1.2 Insulin

The microscale sequence was performed as previously described in 2.3.5. The conditions used for each variable studied are described in Table 5.3. All inclusion bodies were stored at -20°C unless otherwise stated.

Table 5.3 Fermentation conditions

Variable	Induction time (h)	Media	Feeding started (h)	Fermentation length (h)
Induction time	3.5, 4, 4.5, 5	Glycerol fed batch	5	18
Batch and Fed-batch	6	Glycerol batch, glycerol fed batch	5	18
Carbon source	3.5	LB, TB, Glucose batch, Glycerol batch	n/a	22

Inclusion bodies were solubilised and refolded as described in 2.3.6, in the buffers described in Table 5.4. Assays were conducted as detailed in 2.5.9.

Table 5.4 Conditions used during microscale insulin fermentations

Refold Buffer	Components
1	0.288 mM cystamine, 10% v/v hexylene glycol, 20 mM ethanolamine, pH 10.5
2	10 mM Tris, 10 mM glycine, 1 mM EDTA, 0.5 mM cysteine, 4.5 mM cystine pH 10.5
3	1M acetic acid pH 3.8

5.2 Results and Discussions

5.2.1 DHFR

5.2.1.1 Inclusion body washing

Inclusion bodies of greater purity can be obtained by washing with detergents, low concentrations of salts and urea (Taylor et al., 1986b; Khan et al., 1998; Lilie et al., 1998). Optimisation of the recovery and washing step can result in inclusion bodies with purities as high as 95% (Khan et al., 1998). Achieving a high purity inclusion body before the solubilisation step increases refolding yield and decreases the number of chromatographic steps required after folding (Singh and Panda, 2005). Figure 5.1 shows the activity obtained after the refolding step with washed and unwashed inclusion bodies when two different buffers were used. Yields of 2.83 and 1.76 $\Delta\text{OD}\cdot\text{min}^{-1}\cdot\text{mg}^{-1}$ were obtained when inclusion bodies were washed, 45% and 87% higher respectively than those achieved when no washing step was performed. An attempt was made to quantify protein and DNA content in wash fractions, however, the concentrations obtained were below the sensitivity limit of the assays available (Bradford and PicoGreen[®] assays). Valax and Georgiou (1993) determined the nucleic acid concentration of β -lactamase inclusion bodies to be very low, less than 0.5% w/w of the protein content. Results show a significant difference in yield, especially for Buffer 3 where the yield increases from 0.94 to 1.76 $\Delta\text{OD}\cdot\text{min}^{-1}\cdot\text{mg}^{-1}$. This indicates that washing is clearly beneficial and capable of increasing yields by up to 88% in buffer 3 (0.25 M Potassium phosphate, 0.1 M potassium chloride, 1 mM DTT) and 45% in buffer 1 (50mM Tris.HCl, pH 7.2). Inclusion body washing is reported to remove contaminating lipids and also membrane proteins (Lilie et al., 1998), that could otherwise co-aggregate with the target product, resulting in yield losses. Removal by IB washing can help increase the recovery of active product from denatured protein. However the presence of lipids is thought act as a folding enhancer and has shown to increase renaturation yields by 15% (Maachupalli-Reddy et al. 1997).

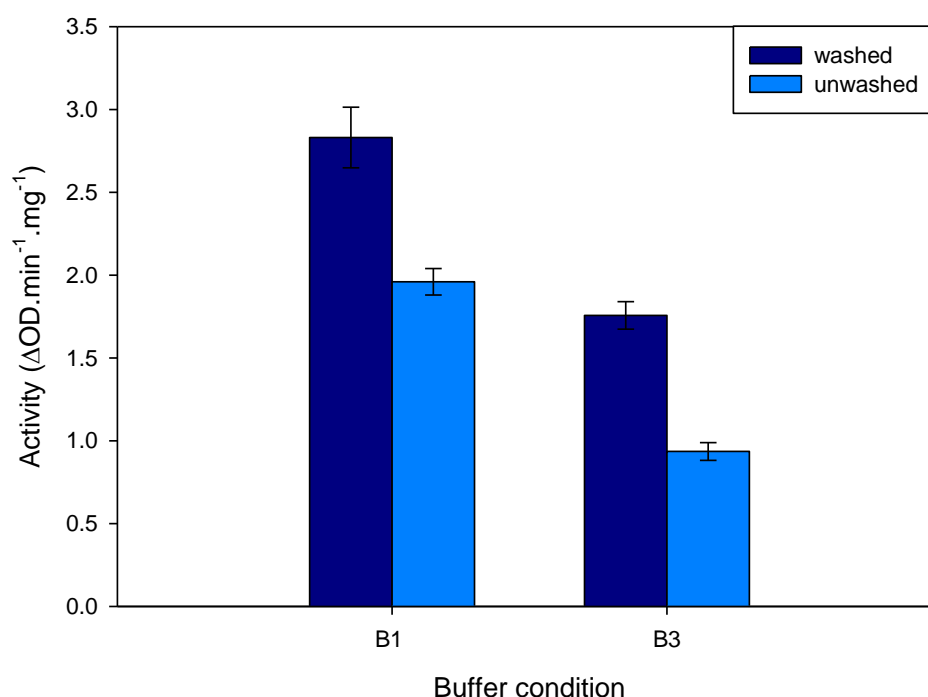


Figure 5.1 The activity of refolded DHFR under two different buffer conditions for washed and unwashed inclusion bodies, where buffer 1 (B1) is 0.288 mM cystamine, 10% v/v hexylene glycol, 20 mM ethanolamine, pH 10.5 and buffer 3 (B3) is 1M acetic acid pH 3.8.

5.2.1.2 Inducer concentration

IPTG is an expensive compound and the need for high concentrations of IPTG during large scale production can be costly. Therefore minimising the required concentration is often desirable from an economic point of view. Additionally, the concentration used can affect the expression level and cell growth. Conditions that achieve strong promotion often result in inclusion body formation. Choi et al. (2000) found that decreasing the concentration of IPTG from 1mM to 0.01 mM resulted in soluble expression instead of causing the formation of inclusion bodies. Induction using IPTG alters the metabolism and growth characteristics of *E. coli*. Kosinski et al. (1992) found concentrations of 0.05, 0.5 and 1 mM IPTG increased the specific growth rate of cells relative to non-induced cells. In the same work it was reported that an intermediate concentration of 0.1 mM IPTG, however, caused a decrease in specific growth rate for different media and *E. coli* strains. Optimisation of the inducer concentration is important not just from a titre perspective but because of its impact on the quality of inclusion bodies formed.

5.2.1.2.1 Fermentation

The growth profiles of *E. coli* obtained at different inducer concentrations are shown in Figure 5.2. The calibration curve between OD and dry cell weight is shown in Figure 9.3 in the Appendix. Cells induced with different concentrations of IPTG show remarkably similar growth profiles up until 8 hours of growth. At inducer concentrations of 0.125 and 0.25 mM the growth can be observed to slow down after 8 hours the OD decreases or plateaus, while at 0.5 mM the OD continues to increase. High IPTG concentrations have previously been found to give improved growth characteristics while low concentrations were found to damage cell growth (Kosinski et al., 1992). The non-induced cells reach stationary phase earlier than induced cells and achieve a lower final dry cell weight. Non-induced cells would be expected to achieve higher growth than induced cells as the cell is under less stress and can contribute all its energy to growth and metabolism rather than producing the recombinant product. Andersson et al. (1996) found that induction with 0.1 mM IPTG led to an increased maintenance requirement resulting in a 23% lower final biomass, a higher demand for glucose and more pronounced lysis towards the end of the culture. The increased OD observed for induced cells may result from morphological changes and the formation of refractile inclusion bodies, which increase the reported OD as previously observed by Flickinger and Rouse (1993).

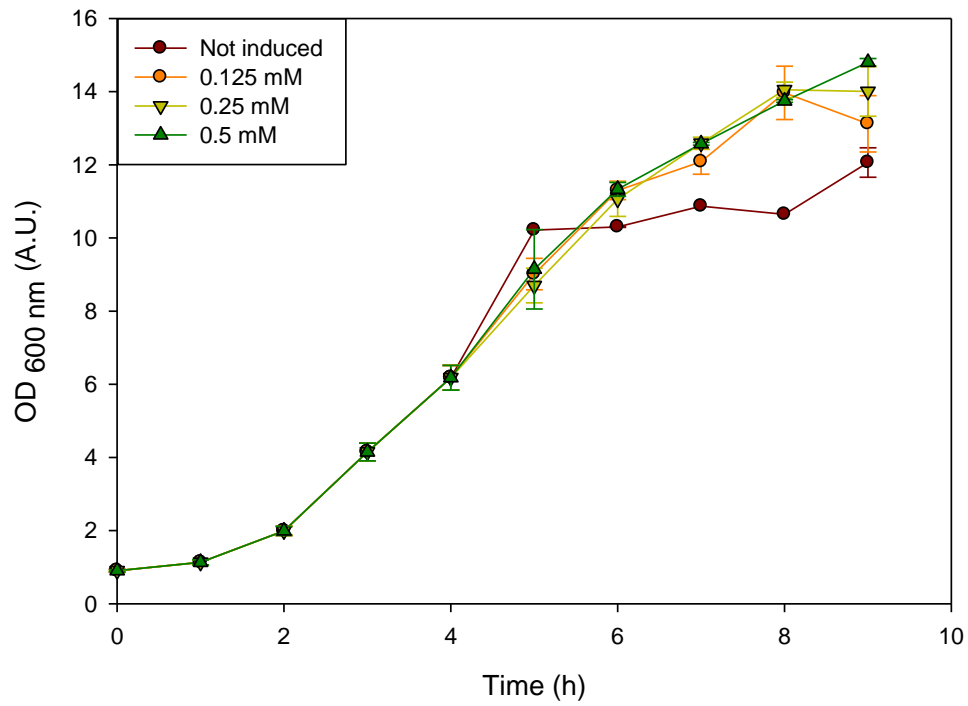


Figure 5.2 The growth profile of *E. coli* during fermentation in microwells and induction by different concentrations of IPTG.

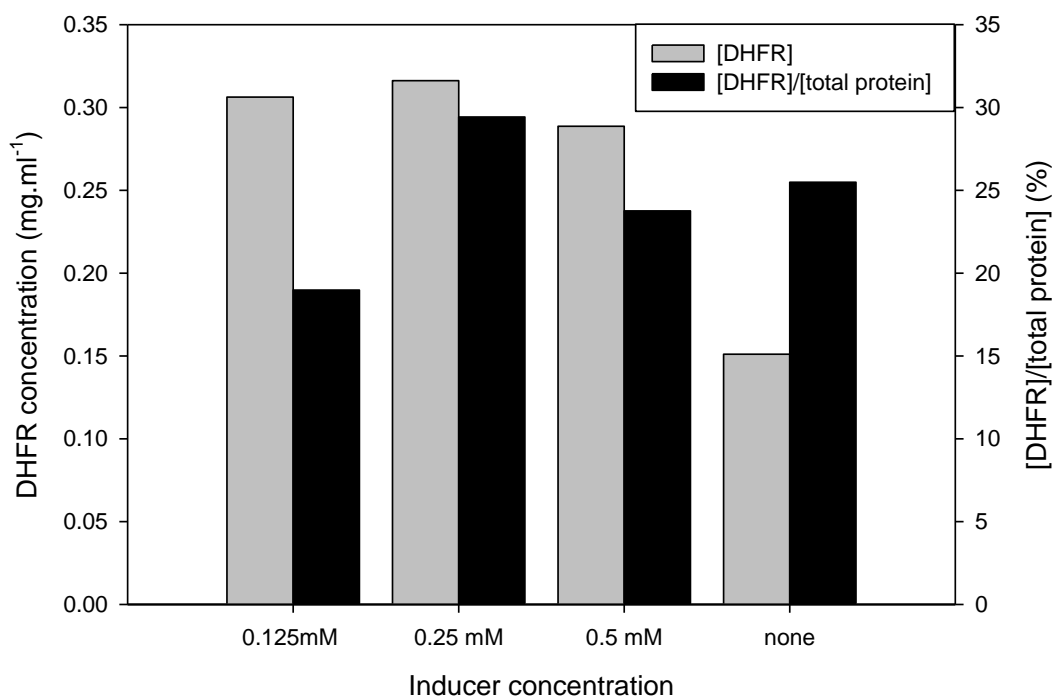


Figure 5.3 The production of DHFR under different induction regimes. DHFR concentration was determined by densitometry and purity from its relation to the total amount of protein determined by Bradford assay.

The concentration of DHFR present (determined by densitometry) relative to total protein concentration (determined by Bradford assay) under different induction conditions is shown in Figure 5.3. The non-induced cells are still producing DHFR despite no induction, as shown by a DHFR concentration of 0.15 mg.ml⁻¹. Intracellular product has been found to be present in non-induced cells previously (Andersson et al., 1996). The inducer concentration resulting in the highest protein level is 0.25 mM. This is also the condition where DHFR comprises the largest fraction of protein in the cell, which is an indication of higher purity. Whilst a concentration of 0.125 mM also gives a high protein concentration of 0.31 mg.ml⁻¹, it is a relatively small fraction of the total protein concentration present. This could result from induction not taking place in all cells because of the low concentration. An inducer concentration of 0.5 mM results in a similar concentration of DHFR as for 0.125 mM, and a slightly higher proportion of the protein present in the cell. However, due to the errors involved in densitometry and Bradford the differences between these two conditions may not be significant.

5.2.1.2.2 Refolding

Figure 5.4 shows the yields of refolds obtained from material induced at increasing IPTG concentrations. The unwashed inclusion bodies refold with higher yields for Tris buffer (50mM Tris.HCl, pH 7.2) than reducing buffer (0.25 M potassium phosphate, 0.1 M potassium chloride, 1 mM DTT), resulting in activities of 1.25 and 0.55 $\Delta\text{OD}\cdot\text{min}^{-1}\cdot\text{mg}^{-1}$ respectively. The buffer appears to have a higher impact on yield than the dilution factor for unwashed inclusion bodies. Yield is higher for a low dilution factor, perhaps because unwashed inclusion bodies have more lipids associated with them that aid folding at these dilution factors.

The concentration of inducer used during fermentation affects the end yield of bioactive product when refolding unwashed inclusion body material at low dilution factors. The optimum inducer concentration for unwashed IB folding is 0.25 mM. Since the denatured inclusion bodies have been adjusted to give refolds of the same final protein concentration, it is not the increased production of inclusion bodies which is resulting in a higher yield but a change in the quality of the inclusion body produced. An IPTG concentration of 0.25 mM achieves a maximum yield of 1.25 $\Delta\text{OD}\cdot\text{min}^{-1}\cdot\text{mg}^{-1}$ compared with 1.00 $\Delta\text{OD}\cdot\text{min}^{-1}\cdot\text{mg}^{-1}$ for 0.125 mM IPTG induction. This condition may result in IBs which accumulate with less contaminants, or have improved properties in terms structure that might aid denaturation and renaturation. Growth conditions (temperature and culture pH) have been found to have a significant impact on inclusion body composition. Valax and Georgiou (1993) proposed that the growth conditions affect the “stickiness” of the surface of inclusion bodies, resulting in greater amounts of contaminating material being absorbed on-specifically following cell lysis.

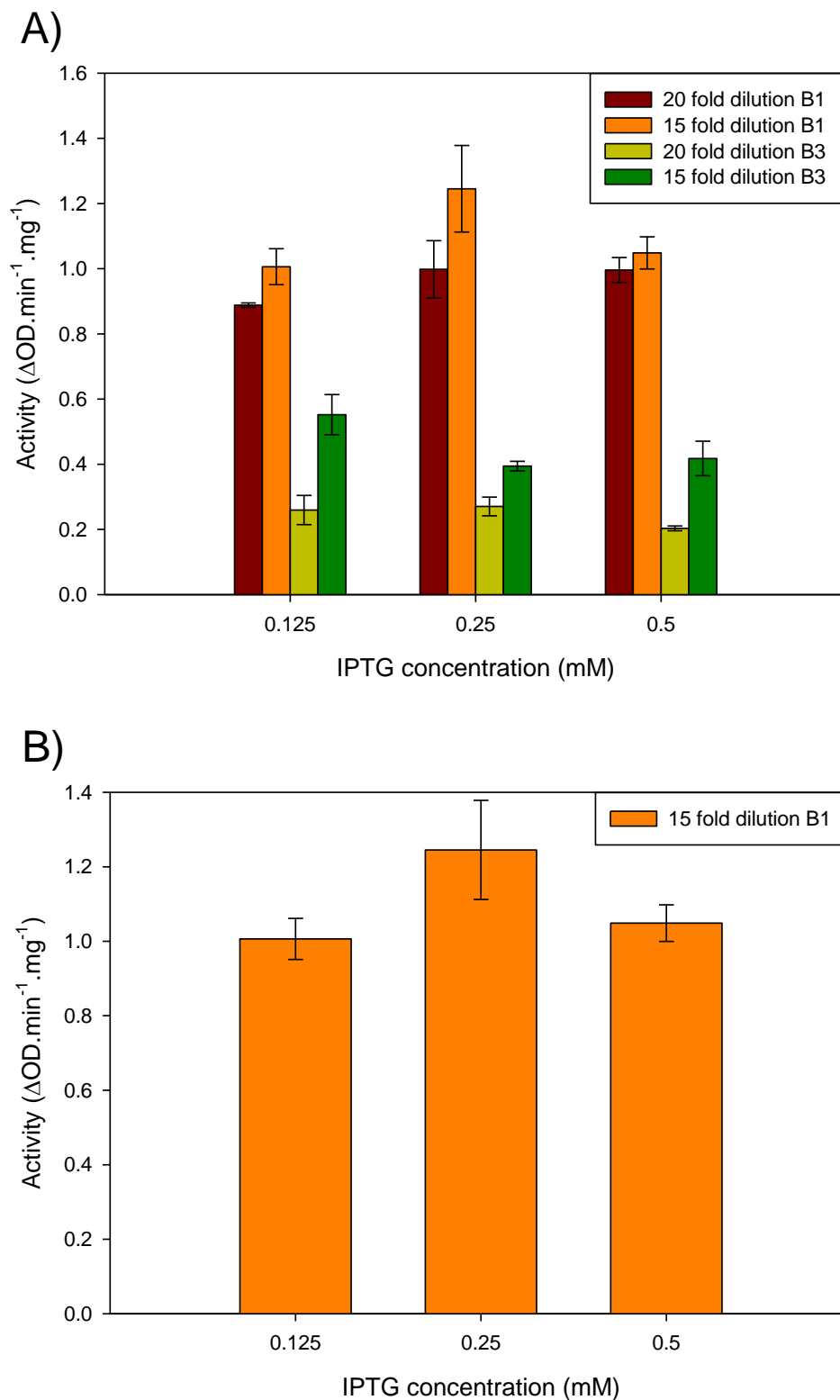


Figure 5.4 Refolding yield of unwashed IBs produced as a result of induction using 0.125, 0.25 and 0.5 mM IPTG. A) Refolded using buffer 1 or 3 and a diluting either 15 or 20 fold. B) Refolded using buffer 1 and 15 fold dilution. Measurements are an average of 3.

Figure 5.5 shows the yield of active protein for washed inclusion bodies from fermentations induced with different concentrations of IPTG and refolded using different dilution factors and buffers. The yields increase at the higher dilution factor tested, 20-fold. The highest yield of $2.0 \Delta\text{OD}\cdot\text{min}^{-1}\cdot\text{mg}^{-1}$ was achieved for a 20 fold dilution in Tris and an IPTG concentration of 0.25 mM. At a dilution factor of 15 fold yields were lower, and decreased from $1.4 \Delta\text{OD}\cdot\text{min}^{-1}\cdot\text{mg}^{-1}$ to $1.2 \Delta\text{OD}\cdot\text{min}^{-1}\cdot\text{mg}^{-1}$ at increasing IPTG concentration from 0.125 mM to 0.5 mM. Unlike the unwashed inclusion bodies, lipids and proteins will have been removed by the washing step. Without lipids to aid refolding, yields are higher when the protein concentration is lower and intra-molecular interactions, likely to lead to misfolding and aggregation, are minimised. Refolding in buffer 3 showed much higher yields of up to $1.57 \Delta\text{OD}\cdot\text{min}^{-1}\cdot\text{mg}^{-1}$ than for unwashed inclusion bodies (which had maximum yields of $0.55 \Delta\text{OD}\cdot\text{min}^{-1}\cdot\text{mg}^{-1}$ in buffer 3). This indicates the buffers influence refolding differently to give different yields with the same starting IB material. Washing inclusion bodies is important for maximising yields as shown by the increase in maximum yield from 1.25 to $2.00 \Delta\text{OD}\cdot\text{min}^{-1}\cdot\text{mg}^{-1}$.

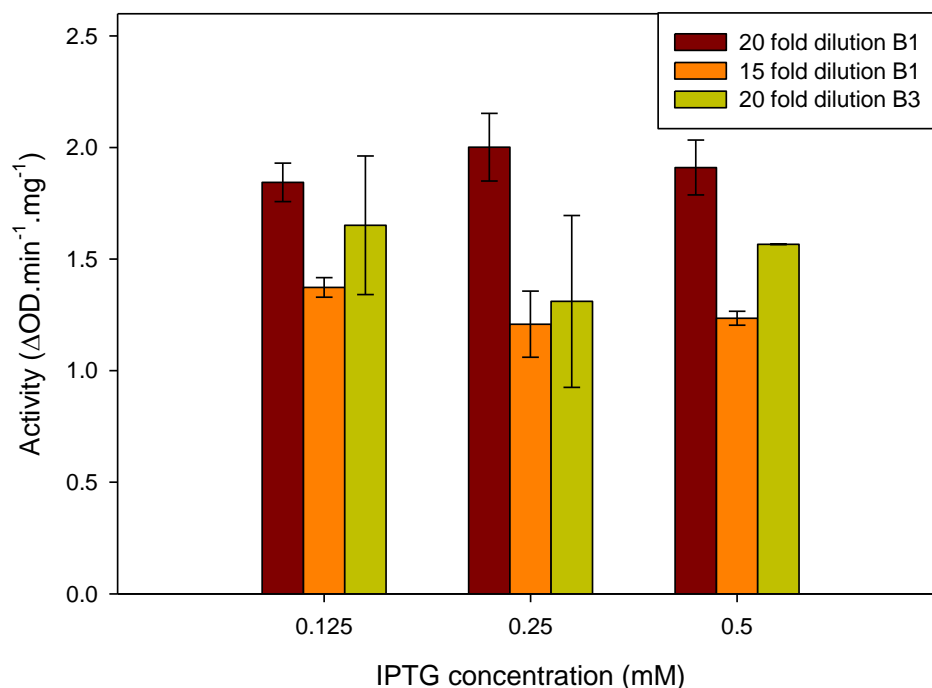


Figure 5.5 Refolding yield of washed IBs produced as a result of induction using 0.125, 0.25 and 0.5 mM IPTG and renatured using buffer 1 or 3. Measurements are an average of 3, with error bars too small to be discernible for the condition of 0.5 mM IPTG, buffer 3 and 20 fold dilution.

In conclusion, the inducer concentration used appears to have a small impact on inclusion body quality. The concentration of IPTG used to induce cells can alter activity by up to $0.26 \Delta\text{OD}\cdot\text{min}^{-1}\cdot\text{mg}^{-1}$, as observed for washed inclusion bodies refolded in buffer 3. The results also show that despite the fermentation condition, the yield can be increased by using buffer 1 and choosing an optimal dilution factor. The dilution factor appears to be the most important factor for washed IBs, with a larger dilution factor of 20 increasing yield by $0.8 \Delta\text{OD}\cdot\text{min}^{-1}\cdot\text{mg}^{-1}$ for 0.25 mM induced material refolded in buffer 1. Buffer 1 and induction by 0.25 M appears to be the optimal conditions for yield, with the choice of dilution factor depending on whether the inclusion bodies are washed or unwashed. The effect of the refold buffer used is diminished by inclusion body washing, with the previously low yielding buffer 3 showing improved yields for refolding washed inclusion bodies. This suggests the contaminant profile plays a role in the interactions of refolding.

5.2.1.3 Induction time

5.2.1.3.1 Fermentation

The automated sequence was then used to investigate the effect of induction time on cell growth. Figure 5.6 shows the growth profiles for cells induced at mid to late exponential phase. Figure 5.7 illustrates the corresponding DHFR concentration present under each induction condition and the purity in terms of the percentage DHFR present to total host cell proteins. Figure 5.6 shows similar growth curves between induction time points for the first 6 hours of fermentation. Earlier induction times result in growth profiles that achieve higher ODs than non-induced cells in the final three hours of fermentation. For induction at 3.5, 4 and 4.5 hours the higher OD achieved could be in part due to the presence of large amounts of DHFR IBs as shown by the concentration of DHFR reaching 0.3 mg.ml^{-1} in Figure 5.7. Kim and Lee (1996) found that induction at early exponential phase was important for a high level of expression. However the increased OD for induction at 3 hours cannot be attributed to IBs light scattering as the concentration of DHFR expressed is lower than that observed for non-induced cells (Figure 5.7). Despite showing good growth this condition shows very poor expression. Cells induced at 5 hours show an equivalent growth profile to non-induced cells. The densitometry results shown in Figure 5.7 show only a slight increase in DHFR concentration for cells induced at 5 hours from 0.14 to 0.16 mg.ml^{-1} . However this DHFR is at a much lower purity of 20% than non-induced cells (31%), indicating that induction is likely to influence cell metabolism. Later induction gives a lower proportion of IPTG per cell and switches on expression of the plasmid at a time when cells have entered mid-exponential growth. In conclusion, the optimal condition is induction at 3.5 hours as it shows the highest ODs, the greatest DHFR concentration and the highest purity of DHFR.

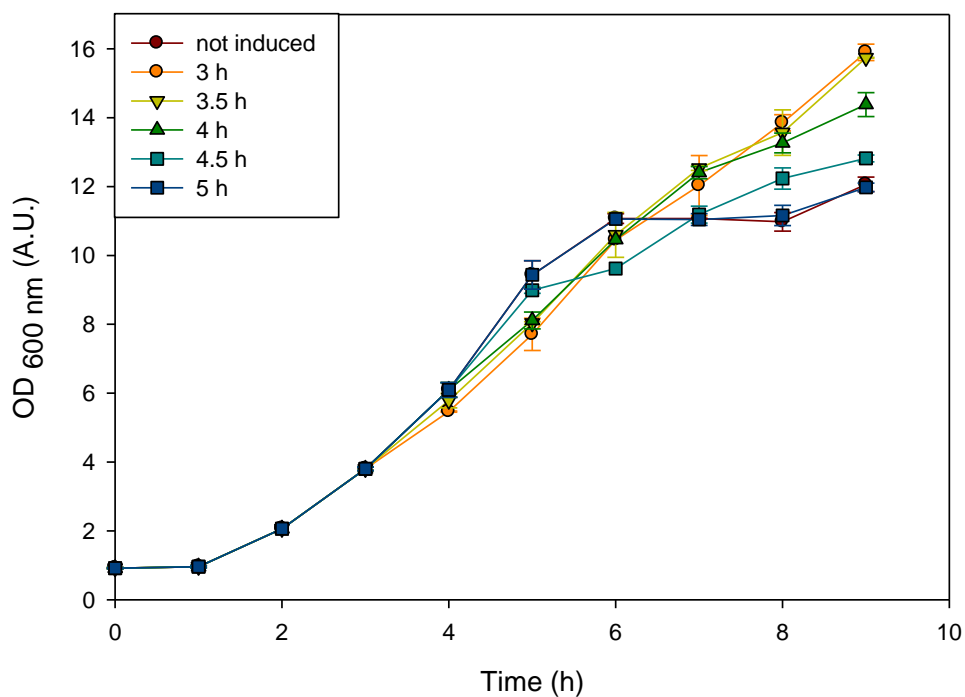


Figure 5.6 Growth curves for *E. coli* induced at different times

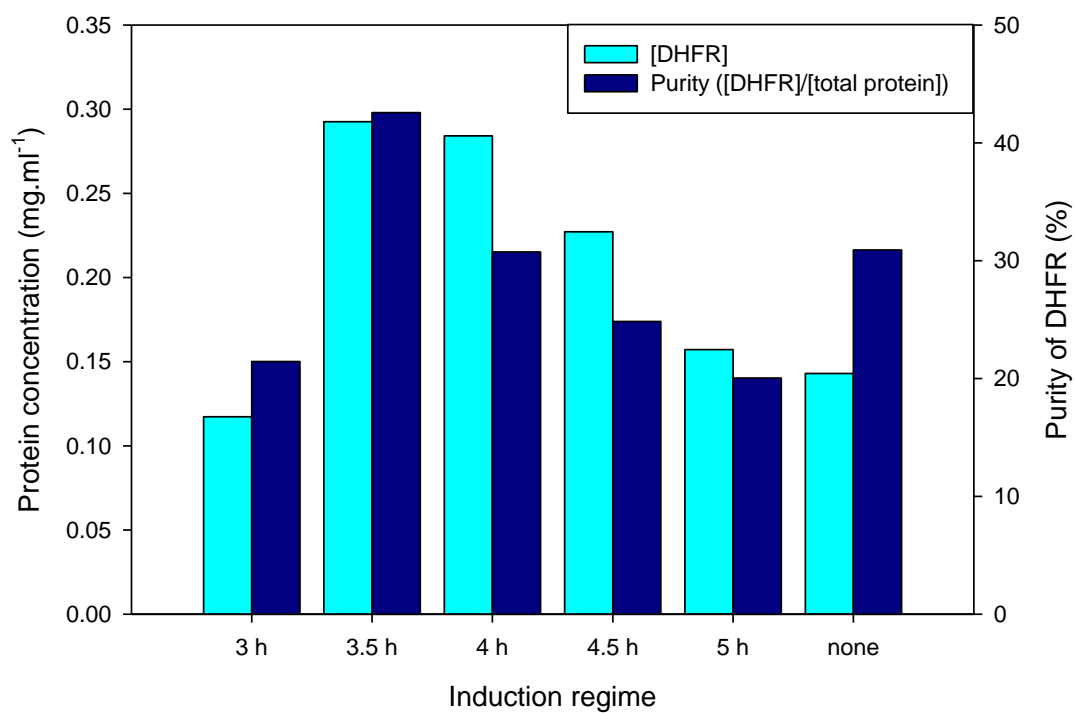


Figure 5.7 DHFR concentration and purity under different induction regimes

5.2.1.3.2 Refolding

Refolding the material from these fermentations shows that early induction produces inclusion bodies that refold to yield higher activities. Figure 5.8 shows the activity of inclusion bodies refolded from fermentation material with different induction times using buffer 1. The yield gain from using an early induction of 3 hours, as opposed to a later induction (4 hours onwards), results in an increase in activity of $0.38 \Delta\text{OD}\cdot\text{min}^{-1}\cdot\text{mg}^{-1}$, or a 16% increase. However since this condition produces significantly less DHFR IBs as shown in Figure 5.7, an induction time of 3.5 hours remains the optimum as it will give an overall more favourable yield and a slight increase refold activity from 2.45 to $2.57 \Delta\text{OD}\cdot\text{min}^{-1}\cdot\text{mg}^{-1}$ for 4 and 3.5 hours respectively.

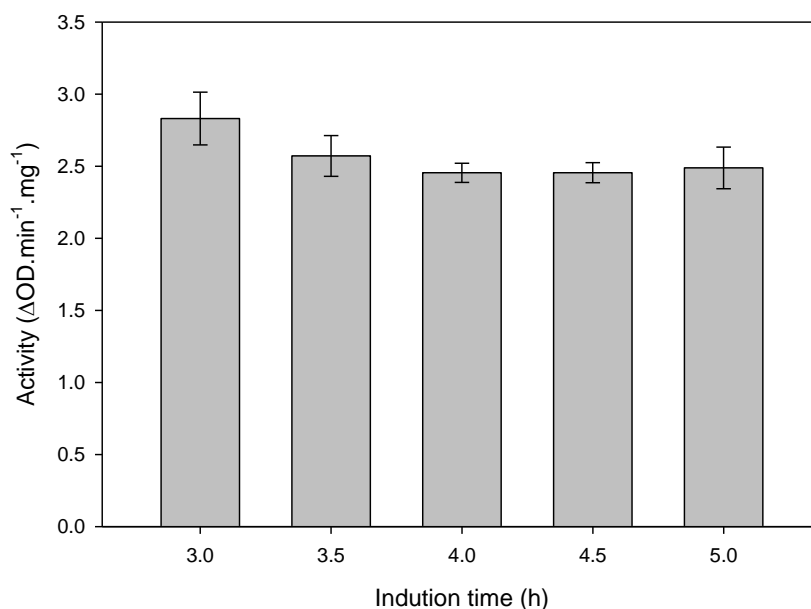


Figure 5.8 Refolding yield of washed IBs produced as a result of induction at 3, 3.5, 4, 4.5 and 5 hours during fermentation and renatured using buffer 1 to achieve a 20 fold dilution. The averages of triplicate refolds are shown.

Lower refold yields are obtained refolding in buffer 3, as previously observed for inducer concentration. Figure 5.9 shows the activities of inclusion body material from fermentations induced at different times refolded in buffer 3. The maximum yield obtained after refolding in buffer 3 is $1.53 \Delta\text{OD}\cdot\text{min}^{-1}\cdot\text{mg}^{-1}$ for an induction time of 5 hours, which in comparison is much lower than the $2.57 \Delta\text{OD}\cdot\text{min}^{-1}\cdot\text{mg}^{-1}$ maximum achieved for buffer 1. A different relationship is shown between activity and induction

time, with both early and late induction showing yield increases compared with induction at 3.5 or 4 hours. This shows that the yield gains between different induction regimes are buffer dependent and that buffer choice is more important than induction regime when achieving high yields.

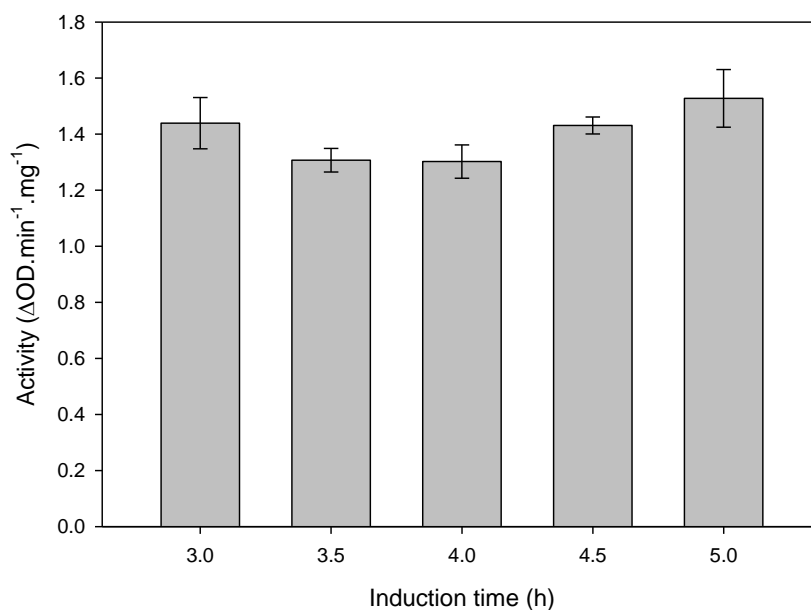


Figure 5.9 Refolding yield of washed IBs produced as a result of induction at 3, 3.5, 4, 4.5 and 5 hours during fermentation and renatured using buffer 3 to achieve a 20 fold dilution. The averages of triplicate refolds are shown.

5.2.1.4 IB storage at -20°C versus -80°C

Inclusion body harvest provides a window of opportunity to decouple upstream and downstream processing by freezing the pelleted inclusion body. The effect of the freezing storage temperature on the final yield of inclusion body refolding is poorly understood. Freezing exposes protein to stresses including low temperatures, high solute concentrations, pH changes and exposure to ice-water interface, which can lead to denaturation (Chang et al., 1996; Bhatnagar et al., 2007). Highly concentrated protein solutions show the smallest loss in activity after freezing, with transferring directly into a -40°C freezer being preferable to immersion in liquid nitrogen freezing (Jiang and Nail, 1998). A faster rate of cooling leads to a greater area of ice-water interface and Chang et al. (1996) proposed that denaturing during freezing can primarily be prescribed to denaturation at the ice-water interface. Figure 5.10 shows the yield of active protein after refolding at microscale in three different buffers using inclusion

bodies from large scale fermentations stored at -20 °C and at -80 °C for a long period of time. Inclusion bodies stored at -20 °C show consistently higher yields across all three buffers. The increase in yield is significantly higher, with -20 °C inclusion bodies refolded in Tris buffer having a yield 81% higher than -80 °C stored inclusion bodies. From these results a temperature of -20 °C might be preferred for long term storage of IBs. It was originally thought that -80 °C would prove optimal as this temperature would result in smaller ice crystals that would disrupt the protein structure less. As the protein is stabilised and in a relatively protected state, the denaturing and damaging effects of the larger crystals formed at -20 °C would not have as much affect as in a soluble protein solution. A temperature of -20 °C provides a higher yield than -80 °C, may be because by damaging the structure of contaminating protein, the contaminating protein is less able to cause yield reductions during refolding. It is also possible that denaturation at the surface of the IB at -20 °C could aid the following denaturing and solubilisation step, ultimately leading to greater yields.

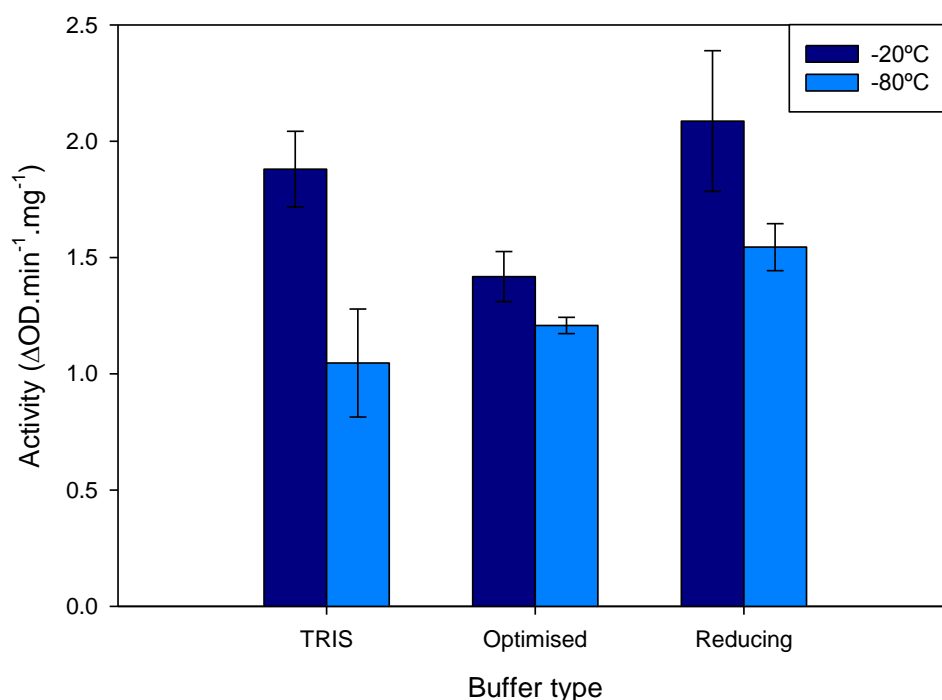


Figure 5.10 Refolding yield of washed IBs produced by large scale fermentation, stored at -20 or -80 °C and renatured using 3 different buffers. The averages of triplicate refolds are shown.

The effect of temperature on inclusion body material obtained from the microscale process sequence and stored for a shorter length of time shows a less marked affect. Figure 5.11 shows the activity for inclusion body material stored again at -20°C and -80°C, refolded in two different buffers. A storage temperature of -20°C does not result in the significantly higher yield previously observed. Refolding in Tris, a typically high yielding buffer, results in a slightly higher yield after storage at -80°C. This could be attributed to the different buffers used in this experiment. It has been previously observed that the choice of buffer has a large impact on the refolding success and can hinder yield losses due to poor expression conditions. Additionally differences in the dewatering of the inclusion body pellets between large scale and small scale centrifugation could affect the rate of freezing and the size of ice crystals, resulting in the differences observed.

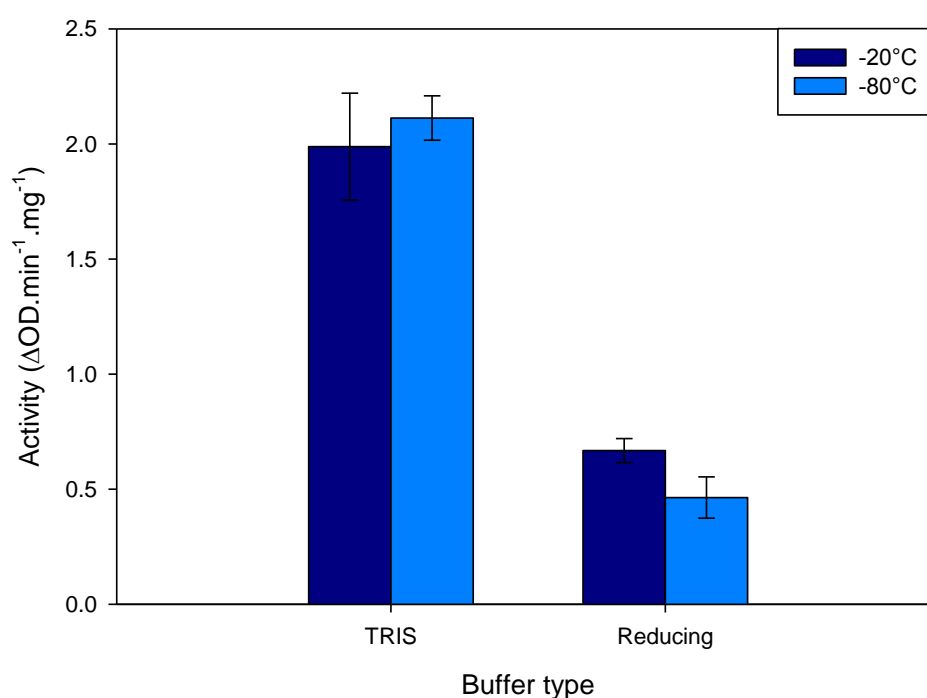


Figure 5.11 Refolding yield of washed IBs produced by microscale fermentation, stored at -20 or -80 °C and renatured using 2 different buffers to give a final protein concentration of 0.02 mg.ml⁻¹. The averages of triplicate refolds are shown.

Table 5.5 highlights the conditions found to yield more active DHFR, which could potentially be used to improve yields at the large scale. Based on the findings from the microscale process sequence, an optimal condition can be determined. However the interaction of these different optimal conditions is unknown as they have only been studied one factor at a time.

Table 5.5 Summarised optimal conditions for a high yield of active DHFR

Factor to control	Optimum identified
IPTG Concentration	0.25 mM
Induction time	3.5 h
Storage temperature	-20 °C
Refold buffer	1
Dilution factor	15 fold

5.2.2 Insulin

5.2.2.1 Establishing insulin growth on platform

E. coli was first grown in shake flasks to establish growth methods from frozen cell stocks and optimise inoculum preparation. Figure 5.12 shows growth in shake flasks for LB and complex media. In LB media growth appears to plateau early at around 12 hours with a final OD of 3.25 A.U. Cells grown in defined media reach a much higher final OD of 7, with growth slowing after 12 hours but continuing to grow gradually up until 24 hours. This shows that inoculum prepared in LB should be used before 12 hours of growth.

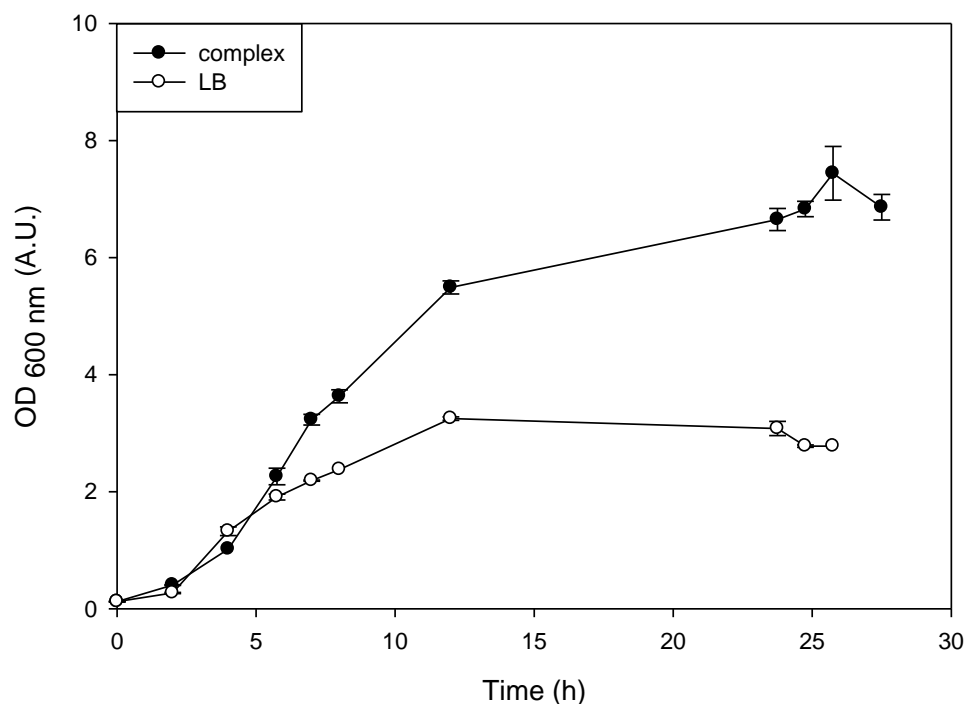


Figure 5.12 Growth profile for *E. coli* containing the insulin plasmid grown in shake flasks with no induction using two different media.

This inoculum preparation procedure was then used to inoculate the microwell fermentation. Growth profiles obtained at 1 ml scale fermentations are shown in Figure 5.13. After a lag phase of 4 hours, the cells enter the exponential phase, reaching the stationary phase around 9 hours. The cells were induced at 10 hours, but this was already too late as the cells are approaching stationary phase as shown by the non-induced cells. The concentration of IPTG added may not be sufficient to result in induction in the large majority of the cell population as the OD is high (17 A.U.). A small decrease is observed in the OD of induced cells 1 hour after induction, after which growth stops.

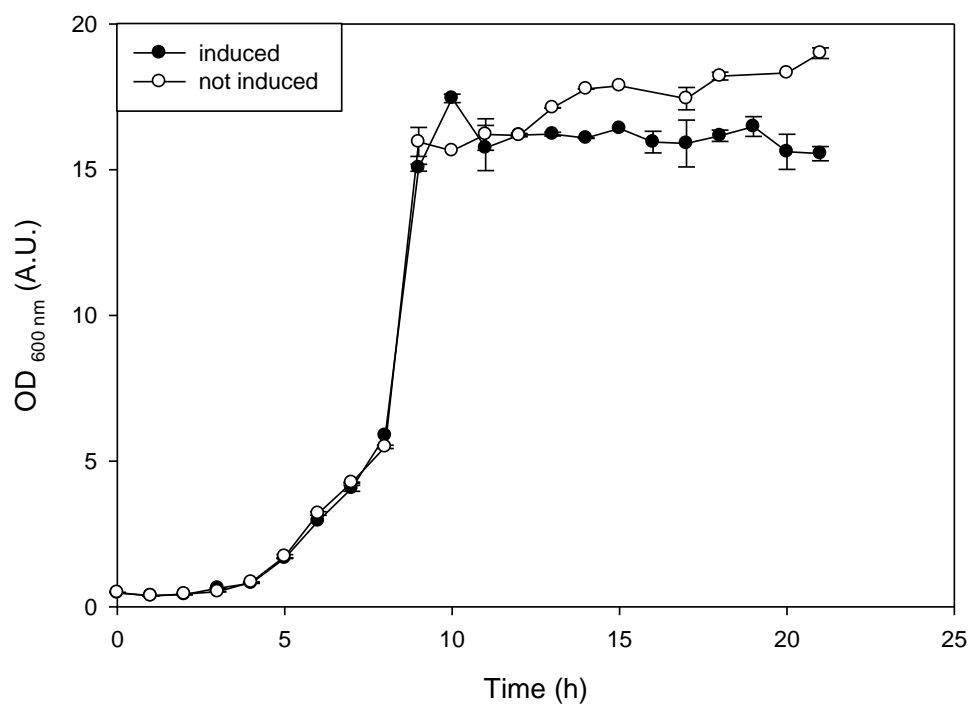


Figure 5.13 Growth profile for *E. coli* expressing insulin grown in microwells and induced at 10 h.

Insulin is present in the induced cells in the insoluble fraction, indicating that insulin IB have been formed (Figure 5.14). However it also appears to be present in the non induced cells as well. The insulin molecule being expressed by the plasmid is a pro-insulin with a short amino acid sequence attached, and consequently will have a much larger molecular weight than the Humalog insulin shown as a standard. Humalog insulin has a molecular weight of 5.8 kDa and has been through enzymatic cleavage and hydrolysis to be converted from proinsulin (9.39) kDa to insulin.

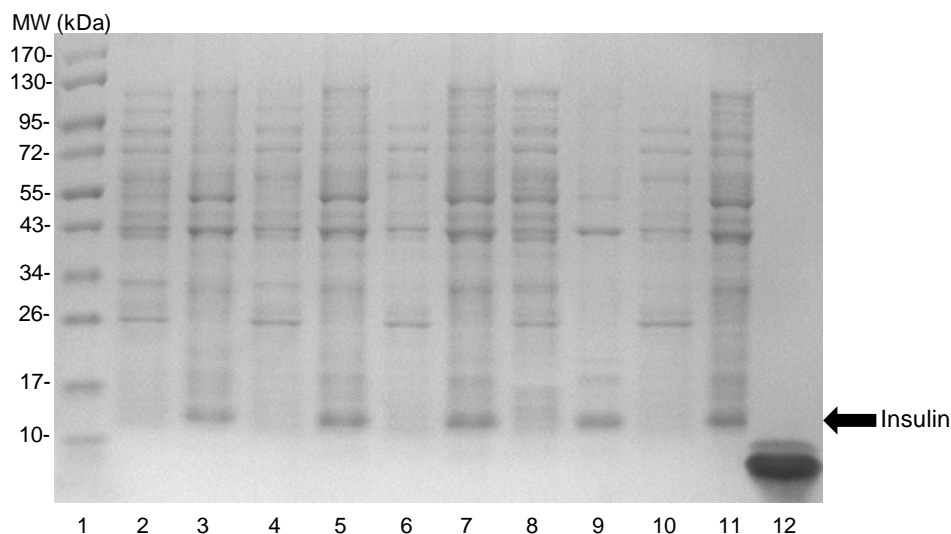


Figure 5.14 SDS PAGE of induced cells during fermentation. Lane 1 contains molecular weight ladder. Lane 2 and 3 are the soluble and insoluble fraction respectively of pre-induction cells. Lane 4 and 5 are the soluble and insoluble fraction respectively of cells 3 hours after induction. Lane 6 and 7 are the soluble and insoluble fraction respectively of cells 7.5 hours after induction. Lane 8 and 9 are the soluble and insoluble fraction respectively of cells harvested after 11 hours. Lane 10 and 11 are the soluble and insoluble fraction respectively of non-induced cells harvested after 11 hours. Lane 12 contains a Humalog insulin standard.

5.2.2.2 Induction time

5.2.2.2.1 Fermentation

Once the automated sequence had been established using insulin, the sequence was used to investigate the effect of fermentation conditions on the final yield of active insulin in this expression system. Figure 5.15 shows the growth profile for cells induced at different times. Induction between 4 and 5 hours results in a lower final OD as cells grow less after 8 hours compared with those induced at 3.5 hours. However, final ODs for induction times between 4 to 5 hours match that observed previously for non-induced cells, showing that induction at 3.5 hours is increasing the growth rate as previously observed for some induction conditions for DHFR expression. Figure 5.16 shows that acetate is present at a much higher concentration at the end of fermentation for cells induced at 3.5 hours. This could be because the cells have reached a higher OD and consequently more acetate has been produced. In comparison, no acetate was detected under the other induction conditions (within the sensitivity levels of the assay

which is 0.254 mg.l^{-1}). It is unlikely that no acetate would be present at the end of the fermentation when there is a high cell density. These cells could have switched their metabolism from glycerol to acetate, and used the acetate present as their carbon source (Dharmadi et al., 2006; Murarka et al., 2008).

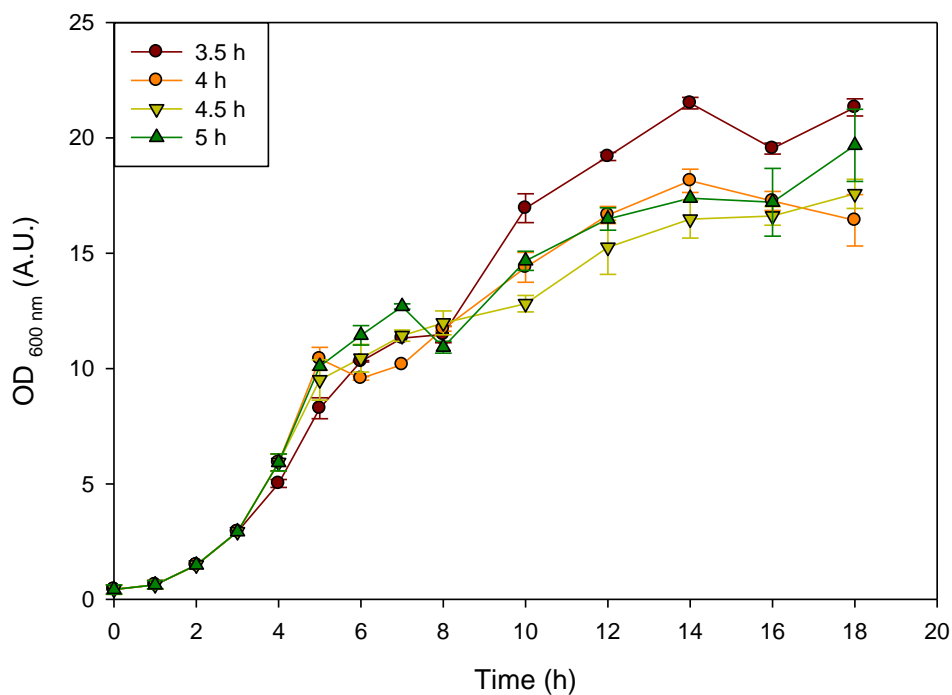


Figure 5.15 Growth profile for insulin expressing *E. coli* grown in microwells and induced at 3.5, 4, 4.5 and 5 hours. Feeding commences at 5 h hours.

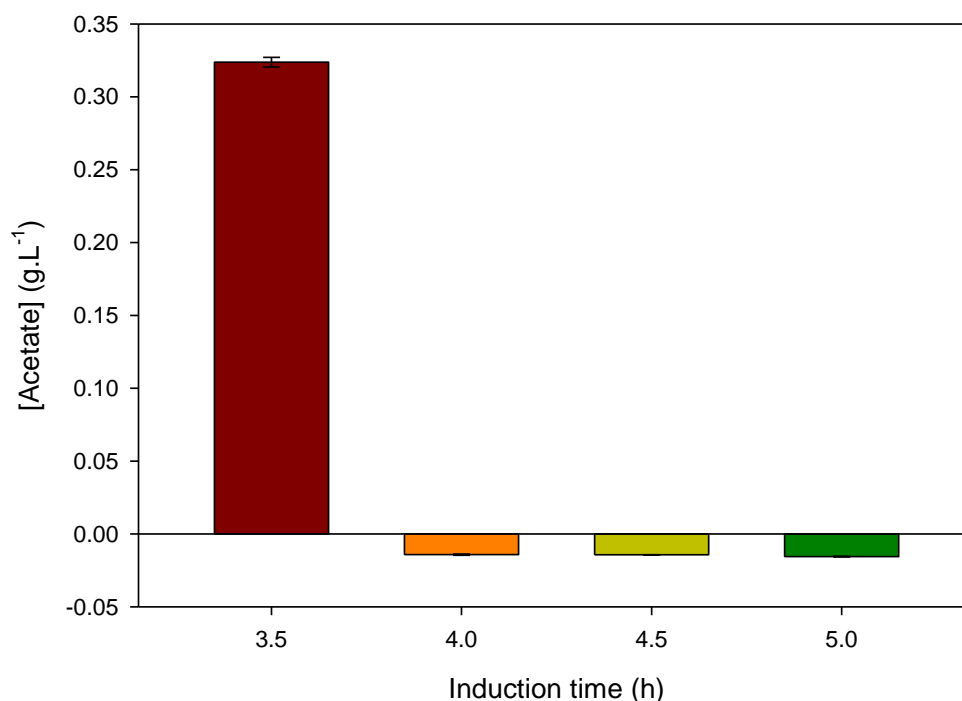


Figure 5.16 Acetate concentration at harvest under different induction conditions (induction at 3.5, 4, 4.5 and 5 hours)

5.2.2.2.2 Refolding

The inclusion bodies harvested from fermentation material induced at different times were refolded at a concentration of 0.015 mg.ml^{-1} in buffer 1 (0.288 mM cystamine, 10% v/v hexylene glycol, 20 mM ethanolamine, pH 10.5), a buffer reported to be used in industry. Figure 5.17 shows the absorbance at three wavelengths for the refolds from IB material induced at different times. No aggregation was observed visually and the high absorbance for a wavelength of 280 nm may reflect the protein concentration used in this condition. The refolds are adjusted to the same starting concentration prior to refolding based on insulin concentration determination by HPLC. However the errors involved with crude fermentation samples is quite high due to the presence of multiple contaminating proteins. The high protein concentration could also result from contributions from contaminating proteins as well as insulin. Previous experiments have shown that aggregates from insulin refolds result in a typical absorbance of 1-2 A.U. (data not shown), which are much higher than those observed. The yields from the refolds are relatively low achieving yields of between 5-10.5 %, as shown in Figure

5.17. The highest yield is 10.5% for cells induced at 4.5 hours. The lowest yield of 4.2% is observed for cells induced only half an hour earlier. There is no clear trend between induction time and refold yield, indicating that multiple factors are involved. Fluorescence does not appear to be a good predictor for yield in this case. For a high fluorescence of 19000, a yield of 10.5% is obtained yet the refold with the next highest fluorescence has a yield of only 5.9%. The refold with a low fluorescence of 9900 has a higher yield of 6.8%, suggesting a broad range of optimal fluorescence for insulin possibly resulting from mixed populations of intermediates folded and misfolded protein.

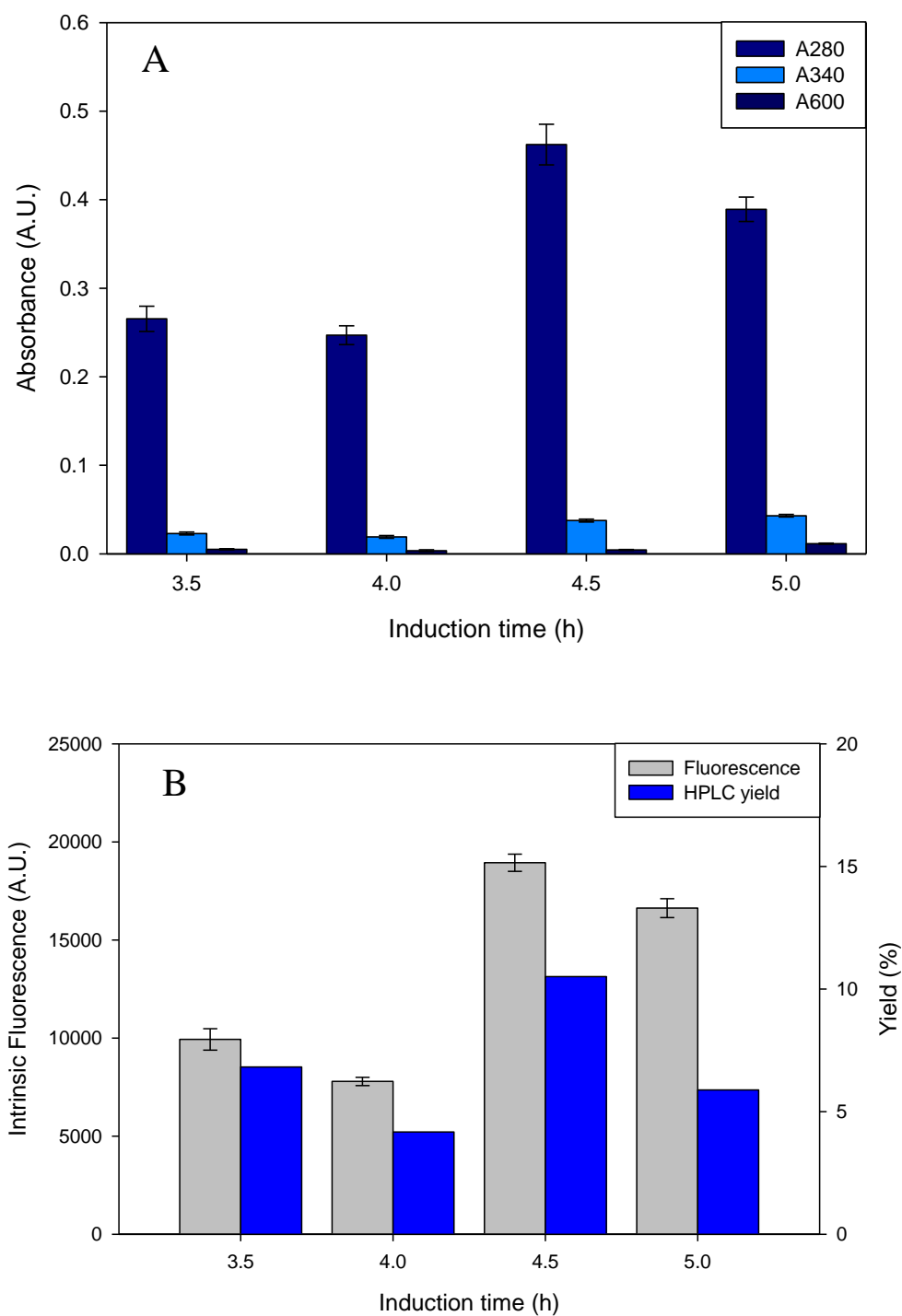


Figure 5.17 Inclusion bodies from fermentations induced at different time points and refolded in buffer 1. A) Absorbance at different wavelengths. B) Intrinsic fluorescence and yield.

Refolding was also performed using another buffer successfully. Figure 5.18 A) shows the absorbance profile for refolding IB material in buffer 2 and is very similar to that observed previously in Figure 5.17 A). Buffer 2 (10 mM Tris, 10 mM glycine, 1 mM EDTA, 0.5 mM cysteine, 4.5 mM cystine pH 10.5) was reported to be optimal for refolding proinsulin (Winter et al., 2002). The absorbance at 280 nm for IB material induced at 4.5 and 5 hours was again almost double that obtained for 3.5 and 4 hour induced material. This could be due to contaminating proteins or errors in the correct determination of insulin concentration as previously described. The yields obtained are higher than that obtained with buffer 1, achieving between 16 to 43% as illustrated in Figure 5.18 B). The highest yield is obtained for an induction time of 4.5 hours. The ranking is the same as observed for the other refold buffer, with an induction time of 3.5 hours resulting in the next highest yield closely followed by 5 hours and then 4 hours with a yield of 15.8%. The fluorescence measured is lower for buffer 2 despite the same protein concentration, resulting in fluorescence results of between 4900-11000 Fl.U. It is noteworthy that these conditions also resulted in higher yields than those refolded in buffer 1.

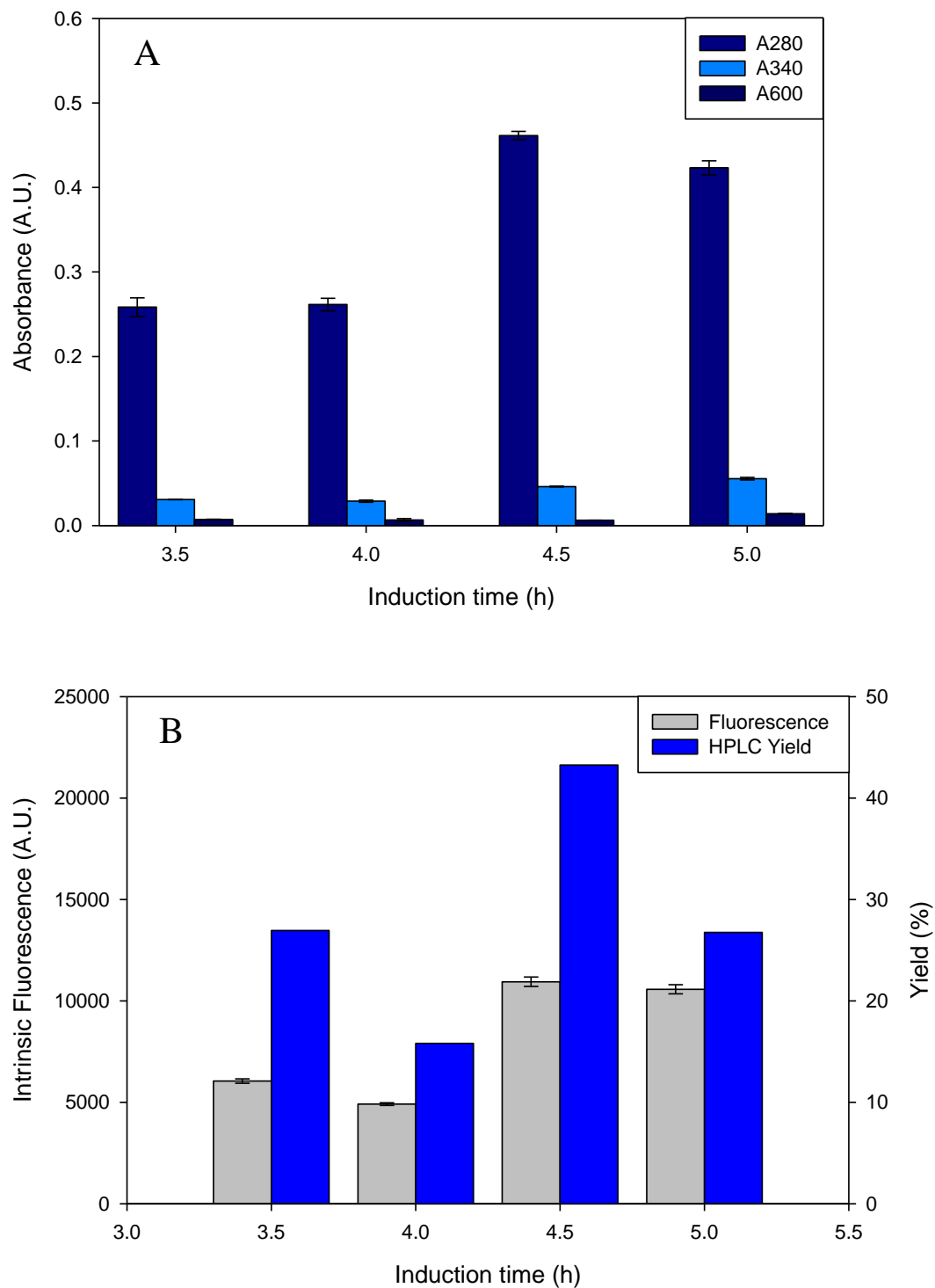


Figure 5.18 Inclusion bodies from fermentations induced at different time points refolded in buffer 2. A) Absorbance at different wavelengths. B) Intrinsic fluorescence and yield.

5.2.2.3 Fed batch versus batch feeding strategies

Fed-batch strategies are often used during high cell density fermentations to control the growth rate of cells. Figure 5.19 illustrates the different growth profiles observed for fed batch and batch feeding strategies. Cells initially grew faster in the fed-batch media, before reaching stationary phase after 5 hours. The cells then remain in stationary phase even after feeding at 9 hours, although growth appears to commence again in the last hour of the fermentation. This could result from the feed rate being too slow initially and limiting growth. The second phase of growth may result from a metabolic shift, for instance to metabolising acetate. Fed-batch fermentation typically produces a higher biomass (Lewis et al., 2004), which could explain the high initial growth rate. In contrast, the cells growing in the batch media grow slower initially and after 6 hours switched to a reduced growth rate, rather than the plateau observed for the fed-batch cells. At 11 hours the cells then started to grow at a slightly faster rate, increasing in OD dramatically in the last hour of fermentation as described previously for the fed-batch cells (Figure 5.19). The batch fermentation contains a much higher initial carbon concentration and this could cause substrate inhibition and account for the slower growth in the batch culture during the first 12 hours of the fermentation (Lee 1996). The batch fermentation has a higher level of acetate at harvest as shown in Figure 5.20 with an end concentration of 0.32 g.L^{-1} , whilst fed batch has a concentration of 0.25 g.L^{-1} . An excess of carbon under aerobic conditions leads to the formation of acidic by-products, of which acetate is the most predominant. During high cell density cultures, growth can be severely limited by the presence of acidic by-products (Landwall and Holme, 1977; Anderson et al., 1984; Lischke et al., 1993). However the concentrations are below the minimum concentration to cause growth inhibition of 5 g.L^{-1} (Lee 1996).

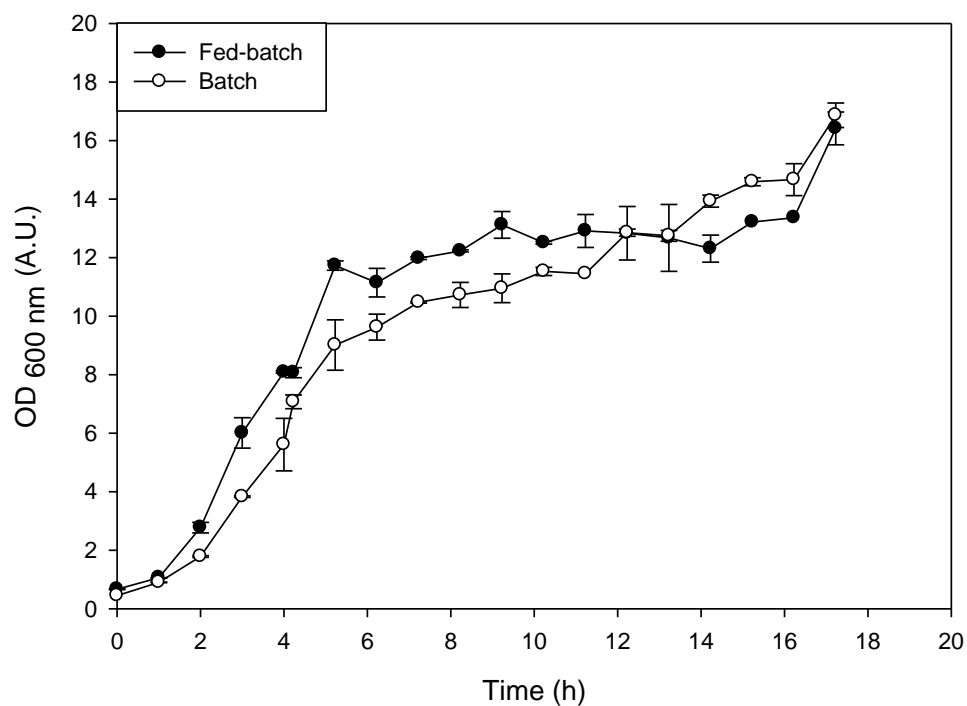


Figure 5.19 Growth profile for *E. coli* expressing insulin grown in microwells and induced at 6 h. Feeding commences at 5 h for fed-batch fermentation.

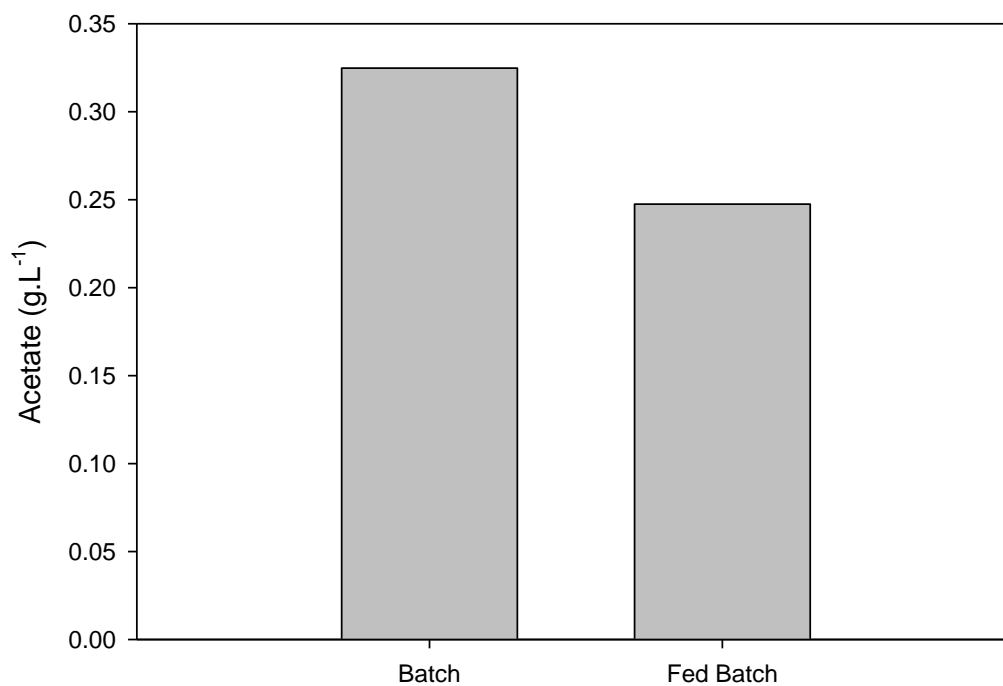


Figure 5.20 Acetate concentration at harvest for batch and fed-batch fermentations

The inclusion body harvest material from the batch and fed-batch fermentation was refolded in buffers 2 and 3. Buffer 2 had previously out performed buffer 1 (see Section 5.2.2.2.2) and buffer 3 (1M acetic acid pH 3.8) was included as it was reported to be used in industry for refolding insulin. Figure 5.21 illustrates the results from the hierarchical assays for refolding in acetic acid. The absorbance at 280 nm is much higher at 0.88 and 1.3 A.U. than what was previously obtained for buffer 1 (0.46 A.U. for refold of 4.5 h induction IB material), despite the refolds being conducted at the same concentration. The absorbance is particularly high for the fed batches refold with an A340 of 0.44 A.U, which could indicate the formation of fine aggregates. However the A600 is still only 0.1 A.U. so large aggregates do not appear to be present. The difference between batch and fed batch absorbance is also shown by the fluorescence measurements. Fluorescence results obtained using the fed-batch material resulted in 33% higher yield than batch IBs. The yield for the batch refold is 19%, 4% higher than the yield obtained for the fed batch fermentation, therefore there may be some yield losses due to aggregation.

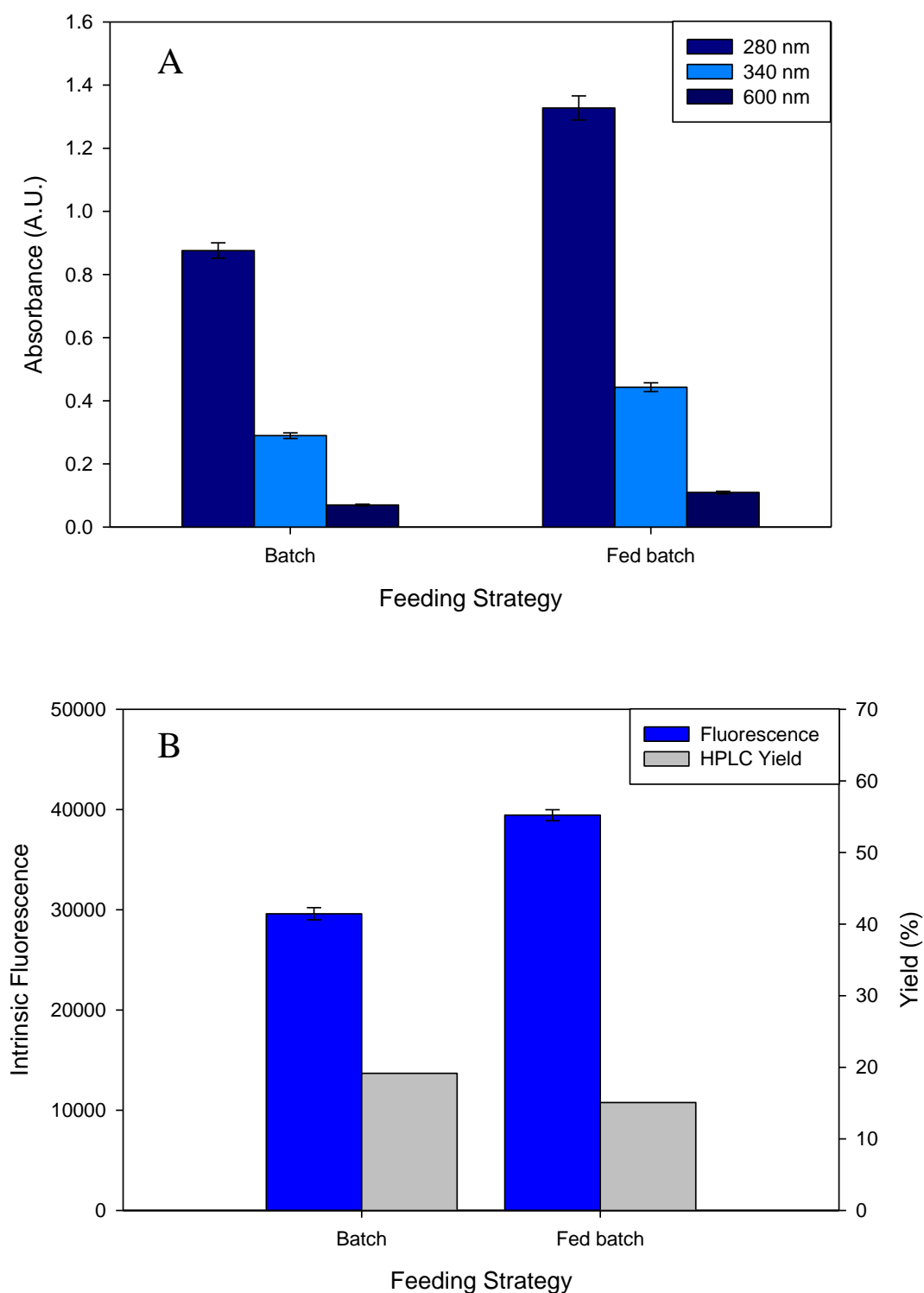


Figure 5.21 Inclusion bodies from batch and fed-batch fermentations refolded in acetic acid buffer 3. A) Absorbance at different wavelengths. B) Intrinsic fluorescence and yield.

Refolding in the buffer 2, which has been described as optimal for insulin by Winter et al. (2002), resulted in higher yields than in buffer 3 (acetic acid). Figure 5.22 illustrates the results for buffer 2 and shows the absorbance is lower when refolding in this buffer than when refolding the same starting material in buffer 3. This confirms that the high absorbance previously observed for acetic acid was buffer or refold state dependent (as opposed to being purely concentration dependent). However the absorbance difference of 0.23 A.U. between fed batch and batch refolds remains, and could result from increased protein contaminants in the IB material from the fed batch fermentation. Table 5.6 shows the fermentation titre and illustrates a higher insulin titre for batch fermentation with a lower cell concentration. Consequently the insulin is expected to have a higher purity than for the fed batch material, as there is a lower ratio of cellular material. The insulin titre datum is supported by SDS-PAGE gels showing the concentration of insulin is higher for the batch fermentation, while the concentration in the fed batch sample is too low to be determined by densitometry at the dilution factor used (data not shown). In order to achieve the same denatured protein concentration for batch and fed-batch fermentation in the solubilisation step, the batch sample was diluted by a greater factor. Hence the level of contaminating protein is lowered further for batch refold and could explain the lower protein concentration (A280) observed in Figure 5.21.

Table 5.6 Fermentation titre as determined by HPLC and dry cell weight.

Fermentation condition	Insulin concentration (mg.ml ⁻¹)	Dry cell weight (g.L ⁻¹)
Batch	1.4	12.7
Fed-batch	0.9	20

The yields obtained in Figure 5.22 B) are much higher than previously observed for all the other refold and fermentation conditions, with the highest yielding condition present in batch IB material which has a yield of 64%. This is also significantly higher than the 52% obtained from fed batch material. Previous research studies indicate that fed batch is a better condition for protein expression in terms of increasing biomass yield (Lewis

et al., 2004), having a slower growth rate control to achieve better expression (Jensen and Carlsen, 1990; Riesenberg et al., 1991) and avoiding catabolite repression (Cutayar and Poillon 1989). The dry cell weights indicate that the fed-batch fermentation yields a greater biomass (Table 5.6). However the expression levels are lower and consequently the burden of contaminating proteins appears to be higher as illustrated by the high A280 shown in Figure 5.21A), resulting in aggregation and lower yields. Therefore in this case it can be speculated that batch fermentation is optimal for both fermentation titre and final yield of active product from refolding.

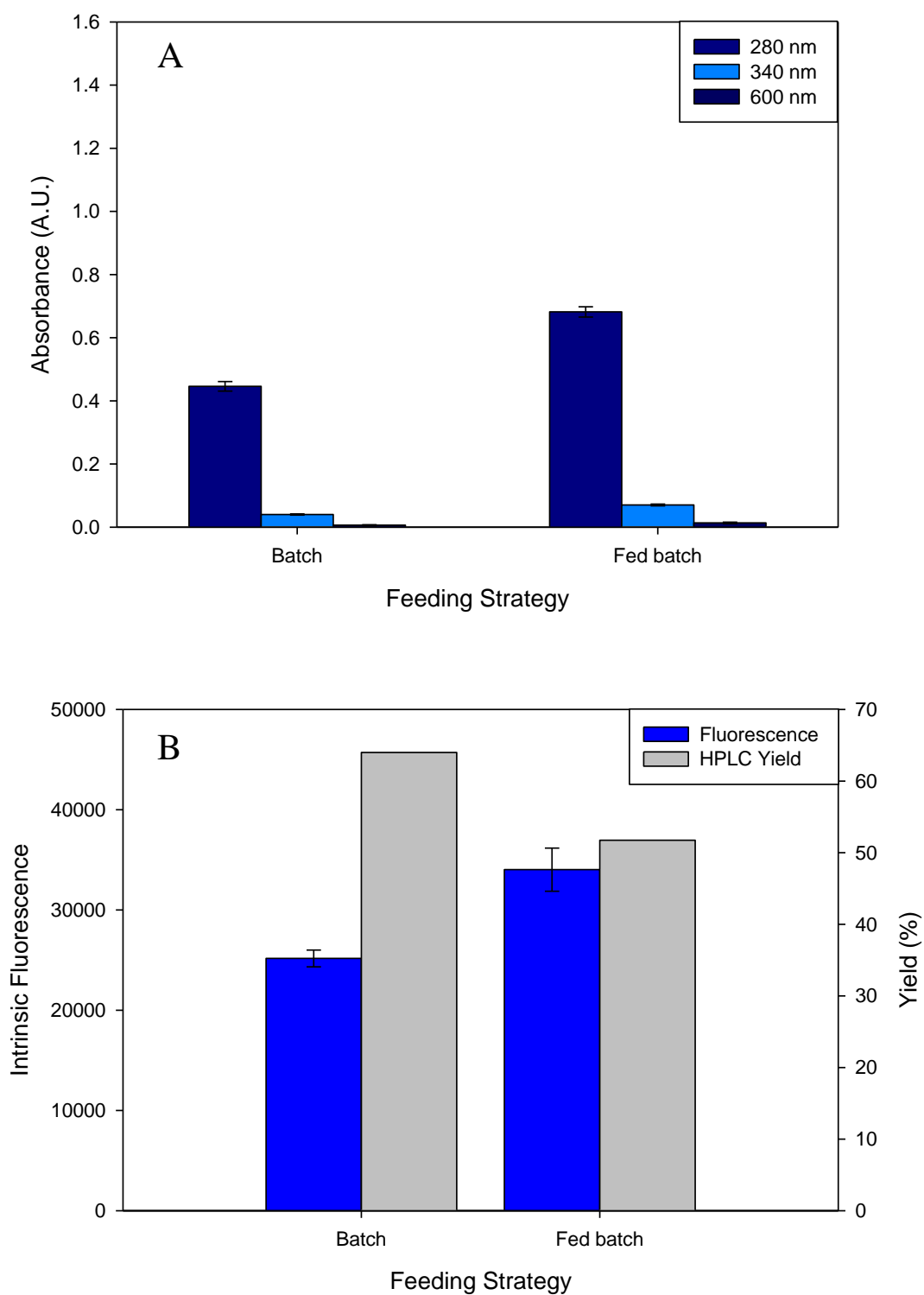


Figure 5.22 Inclusion bodies from batch and fed-batch fermentations refolded in buffer 2. A) Absorbance at different wavelengths. B) Intrinsic fluorescence and yield.

5.2.2.4 Media composition

Figure 5.23 illustrates the fermentation growth curves obtained using different media compositions. The optimal media for cell growth was shown to be a glycerol based complex media. Cells grown in glycerol media reach a final OD of 22.3 and show exponential growth until 14 hours of fermentation. On the other hand, cells grown in a glucose based media reach a lower OD of 21.2 and display a different growth profile, ending exponential growth at the earlier time of 12 hours. The cells then start to grow significantly again after 18 hours, which implies a nutrient limitation and possibly a switch of metabolism.

The cells grown in terrific broth (TB) have the poorest initial growth rate but after 15 hours they begin to grow exponentially before reaching stationary phase at 18 hours. The cells grown in LB enter exponential phase earlier because the inoculum was grown in the same media. However after 4 hours they reach the stationary phase earlier than those grown in TB, possibly as the cells grown in LB reach carbon limitation. TB contains a defined carbon source (glycerol) as well as yeast extract and tryptone, whereas LB contains approximately five times less yeast extract.

The cells grown in TB and LB have almost no acetate present, as shown in Figure 5.24. This could result from the lower cell densities achieved which result in less acetate production or could indicate the cells have utilised the acetate as a carbon source. During the majority of *E. coli* cultures once the glucose or glycerol has been consumed the cells reuse the acetate present through activation of the tricarboxylic acid cycle (Luli and Strohl, 1990). Acetate is more of a problem at a pH of below 7, where a greater fraction is present as undissociated acid (Landwall and Holme, 1977). TB has a good buffering capacity as it contains KH_2PO_4 and K_2HPO_4 , which buffer the media and limit pH decreases. Glycerol fermentation has been reported to produce acetate although its formation is strain dependent as the pathway that produces acetate is not essential for the metabolism of glycerol (Eiteman and Altman, 2006a; Murarka et al., 2008). Hence the lack of acetate observed could result from a combination of these two factors. The fermentations in glucose and glycerol based media are more likely to encounter problems with acetate toxicity due to their high cell densities and the low final pH

observed (Figure 5.24). The level of acetate is high in both these fermentations reaching up to 0.35 g.L^{-1} (Figure 5.24), indicating that the carbon resources have not been completely depleted as acetate has not been utilised. A concentration of 0.35 g.L^{-1} has been reported as not being toxic to cells (Lee 1996). The low final pH of 5.5 and 6 for glucose and glycerol respectively could affect the intracellular environment. Strandberg and Enfors (1991) found that a lower fermentation pH results in an increase in total inclusion body protein (at induction temperatures of 39 and 42°C), but once the pH had dropped below 5.5 the activity of the protein decreased. However a pH of 6.3 has been found to optimal for growth on glycerol (Murarka et al., 2008).

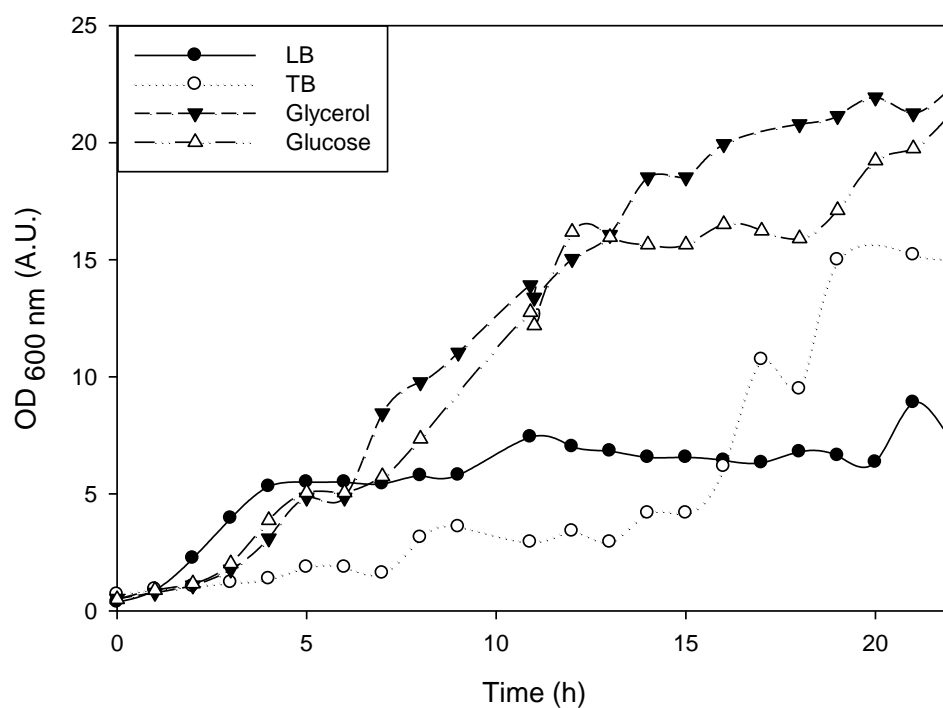


Figure 5.23 Growth profile for *E. coli* expressing insulin grown in microwells and induced at 3.5 h. Cells are grown in 4 different medias: Luria Bertani (LB), Terrific Broth (TB), glycerol based complex media and glucose based complex media.

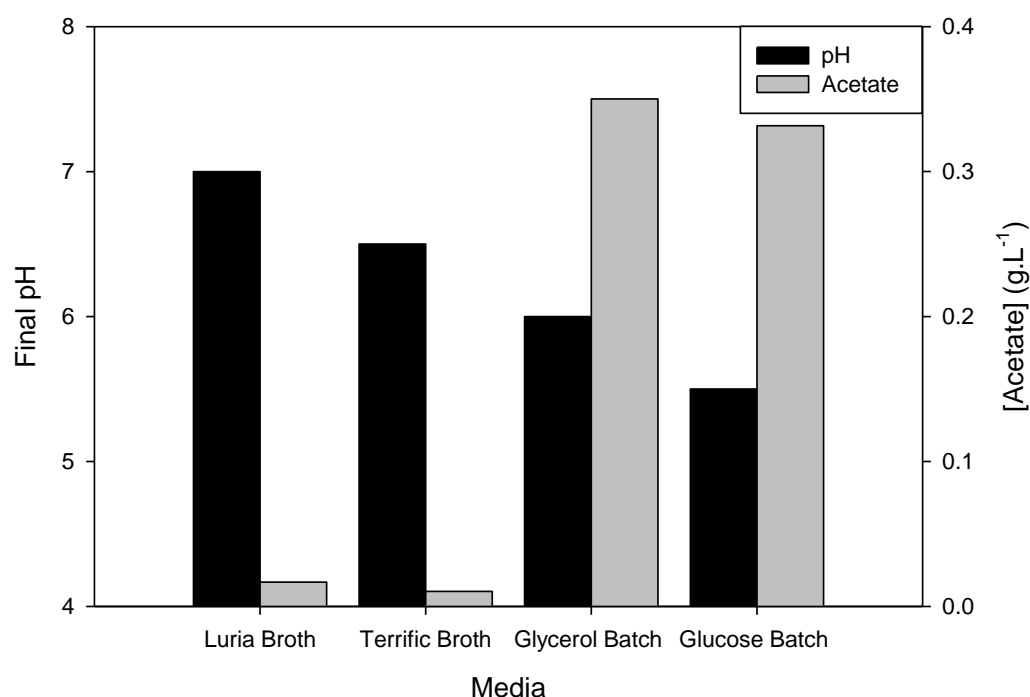


Figure 5.24 Acetate concentration and final pH at harvest for cells fermented in different medias, grown in microwells.

Inclusion bodies harvested from these fermentations were then refolded using the microscale process sequence in buffer 2. The inclusion bodies all showed a low absorbance at the three wavelengths, as illustrated in Figure 5.25 A). The absorbance at 280 nm showed only small differences between the four separate fermentation conditions. Intrinsic fluorescence showed more sensitivity to variation between the fermentation conditions, with TB and glucose derived inclusion bodies having a higher fluorescence of 13300 and 12000 FL.U respectively. TB and glucose derived inclusion bodies also had the lowest refold yields of 17% and 18% respectively (Figure 5.25 B). Inclusion bodies from the LB fermentation had a lower fluorescence of 10400 FL.U., but the refold yield remained a relatively low 19%. Inclusion bodies formed during growth on the glycerol based media had the lowest fluorescence of 9370 and the highest yield of 33%. Therefore a glycerol based complex media is optimum for both cell growth and IB quality, although it results in the production of a higher concentration of acetate.

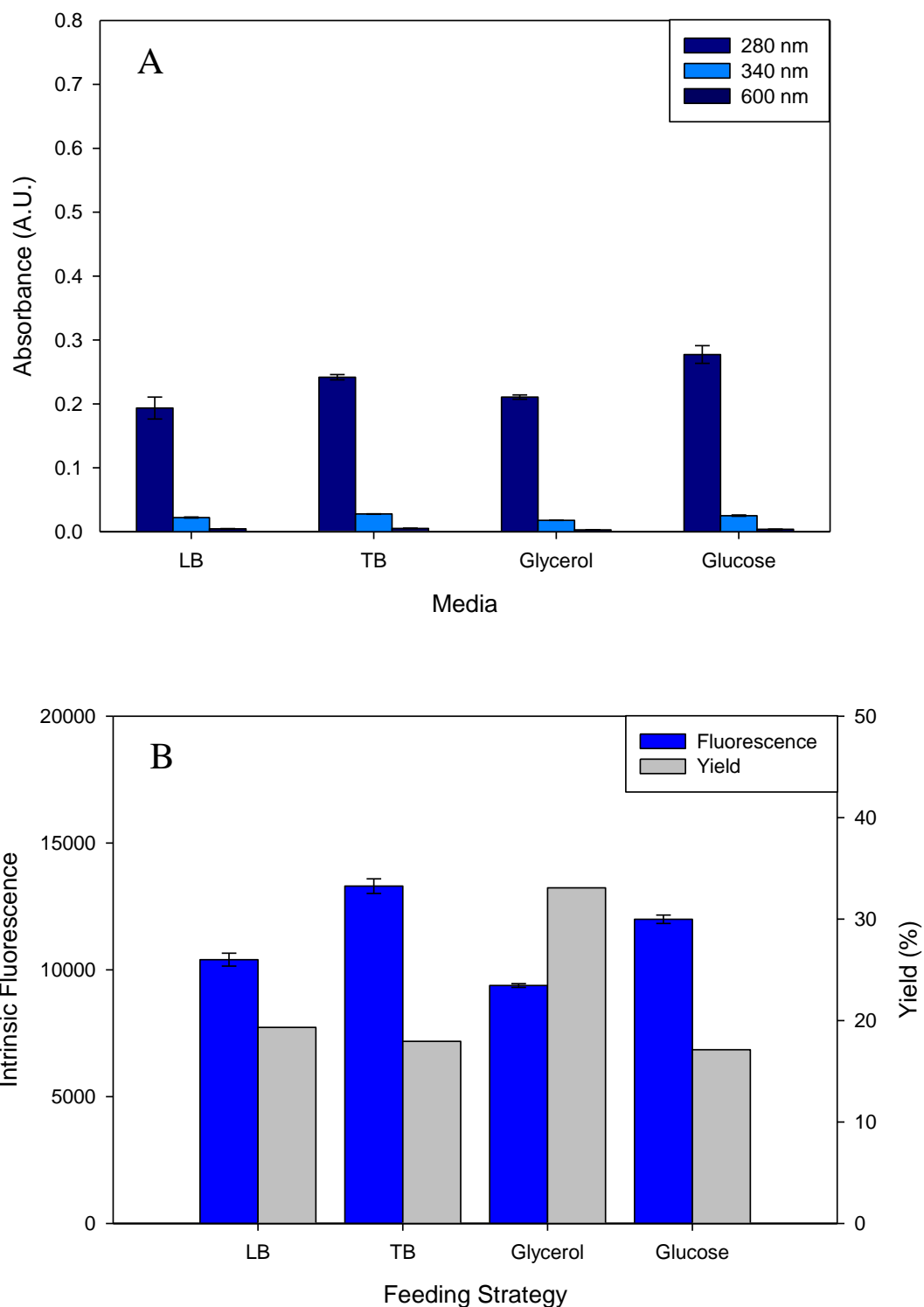


Figure 5.25 Inclusion bodies from fermentations in 4 different medias refolded in buffer 2. A) Absorbance at different wavelengths. B) Intrinsic fluorescence and yield.

The use of intrinsic fluorescence as selection criteria for choosing high yielding conditions appears to be problematic for insulin. Large variations in fluorescence appear to have only subtle effects in yield, as illustrated by the contrast in yields for proteins with close fluorescence values. Figure 5.26 shows a fluorescence value of between 10,500 and 35,000 appears to be desirable and could be used in future assays for selecting high yielding conditions for slower HPLC assays.

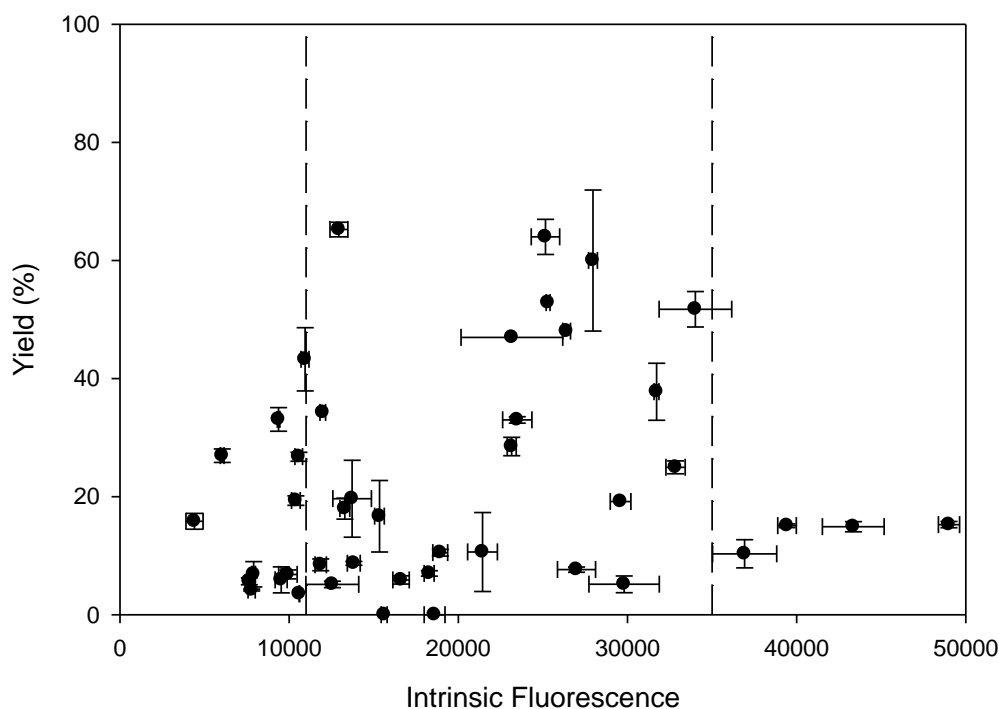


Figure 5.26 Yield as a function of relative fluorescence for insulin refolds. Each point represents a duplicate (yield measurements) or triplicate (fluorescence measurements). Cut-off lines at 10500 and 35000 FIU. (—).

Table 5.7 summarises the optimal condition for each of the fermentation parameters investigated independently. These variables resulted in inclusion bodies that refolded to give the highest yields of active refolded protein.

Table 5.7 Summarised optimal conditions for a high yield of active insulin

Factor to control	Optimum identified
Induction time	4.5 h
Feeding strategy	Batch
Media	Glycerol complex media
Refold buffer	Rudolph

5.3 Conclusions

The automated microscale process sequence allows the study of multiple process variables in parallel. Studies investigating the effect of induction time showed that the process sequence could be successfully used to investigate up to 5 different fermentation conditions in parallel on a single microwell plate, even while allowing for triplicates and a sacrificial well approach to sampling. The number of variables investigated could be expanded further if differing downstream parameters were also developed and suitably integrated.

Fermentation conditions have been demonstrated to effect inclusion body refolding yield. The fermentation conditions investigated were previously linked to solubilising inclusion body expression and caused perturbations in yield. For DHFR the inducer concentration was the most important fermentation variable for optimising the inclusion bodies formed during fermentation, increasing the refolding yield by a maximum of 25%. However, the maximum yield change caused by DHFR fermentation differences was small in comparison to IB washing and storage temperature, which had greater effects on the refolding yield of DHFR, increasing yields by 88% and 81% respectively. Refolding buffer also played an important role in increasing yield losses for DHFR, with buffer 1 and a 15 fold dilution factor resulted in the highest refold yields and could increase yields even for less desirable fermentation conditions.

The sequence showed broader applicability as it was adapted for insulin fermentation and processing with minor adjustments. Insulin displayed a greater sensitivity to changes in fermentation conditions as it showed clearer trends of the effect of fermentation conditions on refolding yield. In particular, the choice of fermentation

media caused a doubling of refolding yield from 17 to 33%. The optimal fermentation condition was shown to be batch fermentation in glycerol based complex media with induction at 4.5 hours is suggested for future experiments to maximise downstream refolding yield. The choice of refolding buffer also showed an important role in maximising yield with buffer 2 giving the highest yields and acetic the lowest. The intrinsic fluorescence assay was less sensitive to insulin refolding than observed for the previous proteins studied, showing its utility is protein specific. However knowledge of target fluorescence could improve this if the intrinsic fluorescence of the correctly folded form of pro-insulin was known.

This approach has clear advantages in terms of resources due to its scale, the use of automation and because of the speed due to the use of parallel experimentation. However uncontrolled microscale fermentation is vastly different to the industrial scale where cells experience a far greater process control (pH and dissolved oxygen tension) and substantial differences in terms of mixing and hydrodynamics. Whether the findings of this chapter can be translated from microscale and used as a predictive tool for large scale manufacture is the subject of the next chapter.

6 Translation of fermentation and refolding processes

6.1 Introduction

High cell density cultures of *E. coli* have a number of advantages in terms of high volumetric productivity, reduced production and investment costs and improved cell separation and product recovery downstream (Riesenberg et al., 1991). However they also can have a number of drawbacks, as an example, the oxygen demand of an increased number of cells can lead to low soluble oxygen saturation (Riesenberg et al., 1991). Under anaerobic conditions, in the presence of few alternative electron acceptors, inhibitory metabolic by-products such as acetate, lactate, formate and ethanol are produced (Clark, 1989). It has been shown that expression of a recombinant product in *E. coli* is higher at reduced growth rate for interferon α -1 (Riesenberg et al., 1990). Fed-batch cultivations are often used to allow control of the growth rate leading to lower acetate levels (Shiloach and Fass, 2005) and maintain dissolved oxygen concentration within a certain range, thus improving final product formation.

Maintaining a sufficient oxygen supply is usually a challenge when cultivating cells at a high cell density (Riesenberg et al., 1991). The oxygen transfer rate depends on the oxygen concentration difference, which provides the driving force, and on both the overall oxygen mass transfer coefficient (k_L) and the specific gas-liquid surface area (a).

$$\text{OTR} = k_L a (C_L^* - C_L)$$

Equation 6.1

Where C_L^* is the equilibrium oxygen concentration (mol.L^{-1}) and C_L is the actual saturated oxygen concentration (mol.L^{-1}). In aerobic fermentations with plentiful nutrients, oxygen is the limiting factor for growth and consequently the volumetric oxygen mass transfer coefficient ($k_L a$) can be used as scaling parameter (Ferreira-Torres et al., 2005; Micheletti et al., 2006). The $k_L a$ is dependent on the fluid properties, system geometry, gas-liquid interfacial area and operating variables (Doig et al., 2005a).

It has been demonstrated that the microwell process sequence can be used to investigate the effect of fermentation conditions on inclusion body refolding yield, but the degree to

which this relates to the large scale has not yet been investigated. Conventionally micro titre plates have been used for cell line selection and secondary metabolite screening (Duetz, 2007) instead of trying to mimic large scale fermentation conditions at the microscale. Reproducing the environment and process control of a large scale fermenter remains challenging at the microscale and, as a result, differences in growth and product formation are often observed. Several studies have addressed these concerns by developing modifications to microwell designs to provide pH control, mechanical agitation and air sparging systems that give higher k_{La} s (Micheletti and Lye, 2006). Additionally, new technologies are becoming commercially available, such as the BioLector (Funke et al., 2010) and ambr™ for mammalian cell lines (Wen et al., 2012), which allow parallel process control in high throughput systems.

The aim of this chapter is to investigate how the microscale fermentation results compare with those obtained at the pilot scale using an industrially relevant protein. It will also investigate whether k_{La} is an appropriate scaling parameter for this fermentation process and whether the large scale fermentation can be reproduced at the microwell in terms of yield and inclusion body quality. Finally it will address relevance of the microscale sequence to the large scale and its use as a predictive tool to allow ranking of process variables. The experimental approach was to first follow an existing fermentation protocol optimal for *E. coli* growth (provided by the collaborating company Fujifilm Diosynth Biotechnologies). This was used to establish optimal fermentation performance at the 100 L scale. The k_{La} was then determined in the 100 L fermenter and using correlations determined in the literature for microwells, 100 L fermentation conditions were arrived at that could then be scaled down to microwell based on k_{La} to the microwell. The different fermentation scales were compared based on titre and refolding yield. The reported scale invariance of the downstream refolding unit operation was also studied by comparing refold yields at different refolding scales.

6.2 Materials and methods

The large scale fermentations and processing were conducted as described in 2.3.2, using the media described in Table 2.8. Growth was monitored using OD, wet and dry cell weight measurements as described in 2.5.2. The microscale fermentation and processing was carried out as detailed in 2.3.5 and OD measured using the sacrificial well technique. The conditions for the fermentations are summarised in Table 6.1 for scale comparison. The fermentation titre was determined using RP-HPLC as described in 2.5.9.1.1 and 2.5.9.1.2.

Table 6.1 Fermentation conditions

	1	2	3	microwell
Fill volume (L)	100	70	70	0.001
Inoculum OD	6.46	6.73	8.65	
Impeller / shaking speed (rpm)	250 (initial)	275	450	1000
Feeding started (h)	9.65	13.23	N/A	N/A
Feed rate (g.L ⁻¹ .h ⁻¹)	11	1.15*	N/A	N/A
Induction OD	50	24.6	9.5	
Induction time (h)	10.65	16.85	6	6
Fermentation length (h)	22	29	18.3	18

*Average overall feed rate, initially started with 2 g.L⁻¹.h⁻¹ but decreased continually until after 20h when it remained at 0.89 g.L⁻¹.h⁻¹

The refold conditions used for the 200 ml scale refolds are shown in Table 6.2.

Table 6.2 Refold conditions for 200 ml dilution refolding. Fermentation material 1: 100 L fed batch fermentation with cascade control with enriched oxygen, 3: 70 L batch fermentation at 475 rpm. Refold buffer 1: 0.288 mM cystamine, 10% v/v hexylene glycol and 20 mM ethanolamine, 2: 10 mM Tris, 10 mM glycine, 1 mM EDTA, 0.5 mM cysteine, 4.5 mM cystine.

	Fermentation material	Washing procedure	Solubilisation concentration (g.L ⁻¹)	Dilution factor	Refold buffer	Final protein concentration (g.L ⁻¹)
1	1	Washed	1.5	18	1	0.08
2	1	Washed	1.5	18	2	0.08
3	1	Unwashed	1.5	18	1	0.08
4	1	Unwashed	1.5	18	2	0.08
5	3	Washed	1.5	18	1	0.08
6	3	Washed	1.5	18	2	0.08
7	3	Unwashed	1.5	18	1	0.08
8	3	Unwashed	1.5	18	2	0.08
9	1	Unwashed	10	10	1	1.00
10	1	Unwashed	10	19	2	0.53
11	1	Washed	10	17.2	1	0.58
12	1	Washed	10	17.2	2	0.58
13	1	Washed	10	18	1	0.56
14	1	Washed	10	18	1	0.56
15	1	Washed	10	18	2	0.56
16	1	Unwashed	10	18	1	0.56
17	1	Unwashed	10	18	2	0.56

6.3 Results and Discussion

6.3.1 Volumetric mass transfer ($k_{L}a$) determination

The $k_{L}a$ was initially estimated for the microwell plate format using the correlation determined by Doig et al. (2005) for microwell plates, which has been shown to fit data sets besides their own to within $\pm 30\%$ (Hermann et al., 2003).

$$k_{L}a = c_1 \frac{D_{O_2}}{d_w} a_i Re^{0.68} Sc^{0.36} Fr^x Bo^y$$

Equation 6.2

This correlation was determined for deep round wells (DRW) while for deep square wells the $k_{L}a$ has been estimated to be 30% higher than the corresponding values measured in the round geometry (Micheletti et al., 2006). The square shape of the wells are thought to introduce a baffling effect which impacts on fluid mixing improving mass transfer processes (Duetz et al., 2000). A maximum shaking speed of 1000 rpm resulted in fairly high $k_{L}a$ of between 210 to 370 h^{-1} for water and media respectively, as shown in Table 6.3. This results largely from differences in the Bond number resulting from different wetting tensions determined by Doig et al. (2005). One of the physical effects introduced by miniaturisation is the increased importance of the surface tension which opposes the liquid movement caused by the g-forces associated with orbital shaking, thus modifying the air-liquid surface area (Duetz, 2007).

Table 6.3 $k_{L}a$ values determined with a fill volume of 1 ml and shaking speed of 1000 rpm using Equation 1.

Microwell	$k_{L}a$ (h^{-1})
Water	210
Media	370

The determined values show similarity to previously predicted $k_{L}a$ values, Micheletti et al. (2006) calculated a value of 259.2 h^{-1} with media using the same correlation. Experimentally derived values for 96-well plates also show approximate agreement with the values calculated in this work using Eq 1. Ferreira-Torres et al., (2005) obtained a $k_{L}a$ value of 198 h^{-1} for a fill volume of 0.5 ml, $N = 1000$ rpm and an identical shaking diameter of 3 mm. The range of $k_{L}a$ values required for microbes growth is between 36

to 540 h^{-1} (Tribe et al., 1995), indicating that the microwell may be able to fulfil the oxygen requirement.

The $k_L a$ was predicted for the 100 L fermenter using the correlation derived by (Linek et al., 2004) (Equation 6.2). The equation was found to fit the experimentally obtained data by Linek et al., (2004) with a mean deviation of 4.7%. It also fits the data of Alves et al., (2004) after minor modification with a mean deviation of 24.4%.

$$k_L = 0.523 \left(\frac{ev}{\rho} \right)^{1/4} \left(\frac{D}{v} \right)^{1/2} \quad (3)$$

This correlation predicted oxygen mass transfer values of between 96 to 169 h^{-1} depending on impeller speed and working volume. They suggest a good overlap with the range of values obtained at the microwell and that a mid-range impeller speed could potentially be used to mimic the microwell conditions.

Table 6.4 $K_L a$ values determined with different fill volumes of a 146.5 L fermenter at different impeller speeds using Equation 2.

Pilot scale fermenter	rpm	$k_L a \text{ (h}^{-1}\text{)}$
70 L	450	127
	275	96
100 L	700	169

When the $k_L a$ was determined experimentally for the 146.5L fermenter using the static gassing out technique, the values were much higher than predicted by the correlation, as shown in Figure 6.1. The overall trend of increasing $k_L a$ with faster impeller speeds agrees with current findings of $k_L a$ increasing with increasing power dissipated into the liquid. Puthli et al., (2005) found that the $k_L a$ increased with increasing impeller speed for a triple impeller configuration. This was attributed to the rapid breakage of air bubbles into smaller sized bubbles caused by the use of an higher power input per unit volume, enhancing the air-liquid interfacial area for oxygen mass transfer.

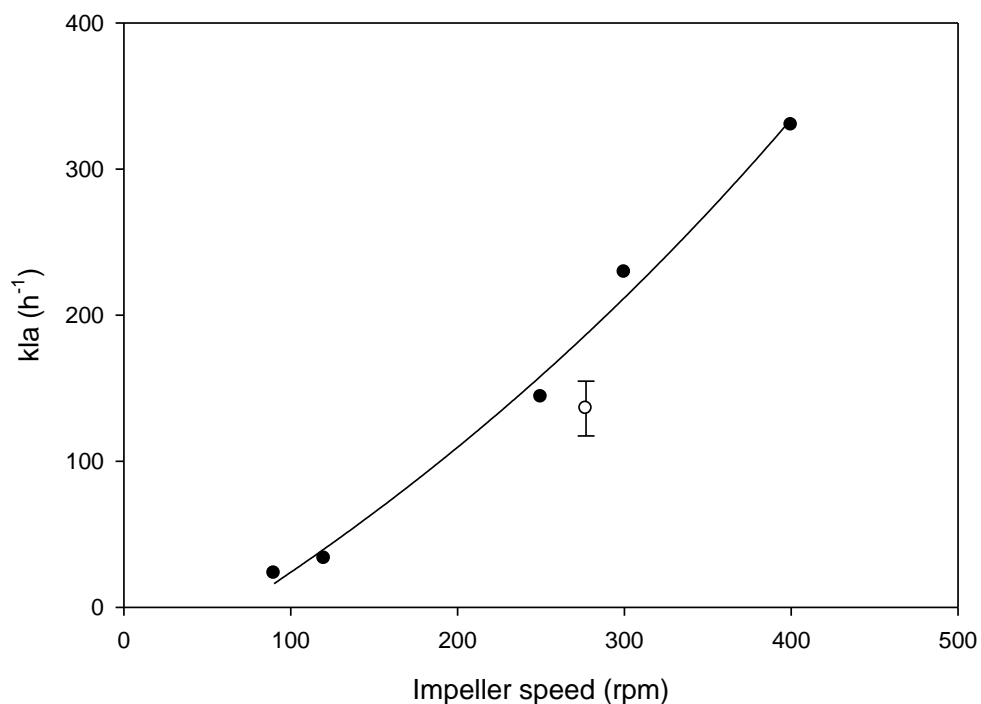


Figure 6.1 k_{La} determined in large scale fermenter with 70L of media and at varying impeller speeds. Points were fitted to an exponential growth curve with the equation $y = (0.6542(e^{(0.0018x)} - 1)/0.0018) - 47.6714$

Table 6.5 Experimentally predicted k_{La} based on regression shown in Figure 6.1

Impeller speed (rpm)	k_{La} (h^{-1})
100	24
200	110
300	213
400	336
450	406
500	483

However the k_{La} values obtained are much higher than those predicted by the equation. The k_{La} for an impeller speed of 450 rpm was determined experimentally as $372 h^{-1}$ in contrast to the $127 h^{-1}$ predicted from Equation 2, which could result for a number of reasons. The correlation used was developed for a dual impeller system, whereas the

fermenter used in this work has a triple impeller system. It has been reported that the number of impellers is immaterial and only the power dissipated in the fluid is important (Oldshue, 1966; Van't Riet, 1979). However Van't Riet, (1979) asserted that confidence in this statement is problematic when fluctuations with differences of up to 40% have been observed for mass transfer, which could be related to the low experimental accuracy. Conversely (Puthli et al., 2005) found that a triple impeller system resulted in a higher k_{La} relative to a two impeller system, especially at higher gas flow rates of above $0.00002 \text{ m}^3\text{s}^{-1}$ (as used in this work). They also found that k_{La} was highest for the triple impeller system even at similar levels of total power dissipation. Therefore the third impeller could significantly contribute the increase of the k_{La} values, introducing large errors in the predicted k_{La} values. Additionally the same value for bubble surface area was used in the correlation for the different impeller speeds due to the lack of available data or models predicting bubble surface area. The bubble surface area would be expected to increase at faster impeller speeds. Gas hold up also increases at higher impeller speeds (Gogate et al., 2000), allowing more time for oxygen transfer. The bubble size also changes for different power dissipations, and consequently could be subject to change due to the extra third impeller, thereby introducing further error into the correlation.

The microscale fermentation in traditional well plate format presents unavoidable limitations in terms of oxygen mass transfer, as aeration can solely be achieved by gas exchange at the surface of the liquid. At the large scale, oxygen mass transfer is aided by the use of direct sparging of air or enriched oxygen and mixing via an impeller. Therefore an appropriate impeller speed for the large scale fermentation should be chosen based on the highest k_{La} achievable at the microscale to avoid oxygen limitation and realistically compare the two systems. Based on the large scale experimentally derived k_{La} values, impeller speeds of 275 rpm and 450 rpm were selected. An impeller speed of 275 rpm was shown to correspond to a k_{La} of approximately 200 h^{-1} and it was chosen to match the k_{La} of 210 h^{-1} estimated for the microwell plate format with water. An impeller speed of 450 rpm corresponds to a k_{La} of 372 h^{-1} which matches the k_{La} estimated for microwell plate format with media. Ideally k_{La} should be maintained at a level where further increases in oxygen transfer do not result in higher yields as this would then provide a robust scaling factor. For this reason fermentation were

conducted at both a high and low k_{La} values to establish the limitations of this scale-up approach.

6.3.2 Fed batch 100L fermentation

The initial fermentation condition chosen reflects the industry standard fermentation protocol for *E. coli* production with fed batch operation and enriched oxygen combined with cascade control to achieve a DOT of above 30%. The growth curve obtained using these operating conditions is shown in Figure 6.2 and shows exponential growth between 4 and 15 hours. The DOT also decreases significantly after 4 hours (Figure 6.3) as the cells have grown substantially and therefore the oxygen demand is much greater. Feeding was started at 10 hours after a DOT spike was observed indicating depletion of carbon resources (Figure 6.3). The respiratory quotient (RQ) remains fairly constant throughout the fermentation, with the exception of the spikes observed around 9 hours when it increases in value from 1 to 92. This occurred at the same time around the time that gas blending started with enriched oxygen and results from the fermenter equipment failing to maintain a constant airflow rate. The cells continue to grow for 15 hours as shown by the dry cell weight and carbon dioxide evolution rate (CER), and after this point the cells enter the stationary phase. The dry cell weight is approximately 25% of the observed wet cell weight, as typically observed for *E. coli* (Bratbak and Dundas, 1984).

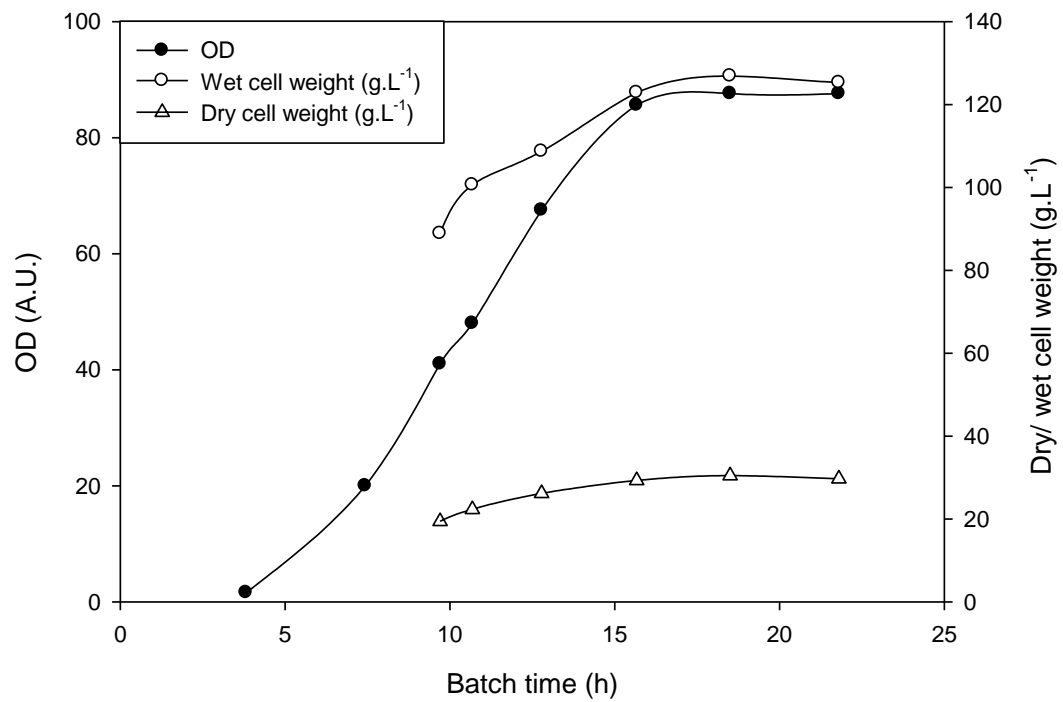


Figure 6.2 Growth profiles showing the optical density, wet and dry cell weight for 100 L fermentation with cascade control and enriched oxygen

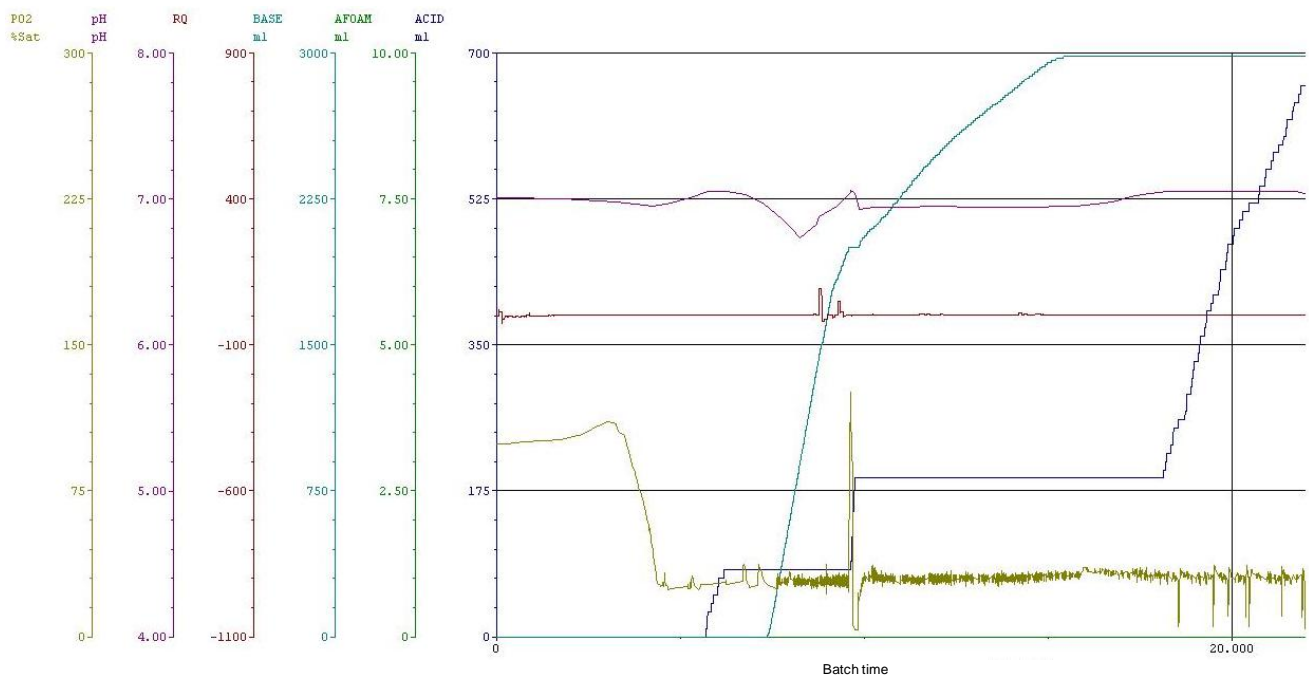


Figure 6.3 Fermentation trace of the dissolved oxygen (pO_2), pH, respiratory quotient (RQ), and volume of acid, base and antifoam added.

6.3.3 Fed batch 70 L low k_La fermentation

One of the aims of this chapter was to compare the large scale fermentation to the results obtained in the microwell plate format using a matched k_La approach. Therefore, the fermentation had to operate within the constraints of the microwell system, with a constant low k_La , no oxygen enrichment and cascade control and consequently low oxygen availability at high ODs. The fermentation protocol was adapted to allow a lower maximum oxygen uptake rate in fed batch mode, to limit growth initially because of the low availability of oxygen due to the reduced impeller speed. In order to do this, the starting media contained less glycerol to ensure the cells grow to a lower cell density and then feeding was started to control growth at a lower rate so the cells can survive at low impeller speed with limited oxygen. The knowledge gained from the previous fermentation was used to determine the point of the maximum OUR, which was around 8 hours and corresponded to an OD of 20. Therefore a media was used with only 15 g.L⁻¹ glycerol and 20 g.L⁻¹ yeast, which would enable it to achieve an OD of 20.

The OD, wet and dry cell weight profiles obtained in the 70 L fermenter are illustrated in Figure 6.4 and show the cells reached exponential growth after a lag phase 2 hours shorter than observed previously. The cells reached an OD 4.8 A.U., higher than the 3.1 A.U. for previous fermentation in the equivalent time frame. A faster growth rate was not expected due to the lower initial carbon concentration, and can be attributed to the higher inoculum OD and the dynamic conditions of the fermenter. The 70 L fermentation had more turbulent mixing ($Re=132,000$ for 70 L fermentation and $Re=120,000$ for 100 L fermentation) during the initial fermentation period before cascade control started, which may have resulted in faster growth. Figure 6.5 shows the dissolved oxygen concentration, pH profile, stirrer speed, airflow rate and inlet oxygen concentration for the 70 L fermentation. The DOT decreased to below 2% after 4 hours and no DOT spike occurs as previously observed at 9 hours is observed and therefore there is no exhaustion of the carbon source after establishment of exponential growth. Under a DOT of close to zero, cells are extremely oxygen limited and will grow anaerobically producing high concentrations of acetic acid. The amount of base required to maintain a constant pH increases after 4 hours to neutralise the acidity generated by the production of acetic acid. This accumulated acetic acid could then be used as a carbon source between 8 and 12 hours, thus explaining the lack of carbon

deprivation, and the decrease in acetate levels from 0.35 to 0.04 g.L⁻¹ from 8 to 16.6 hours. Feeding was started at 13.2 hours at a reduced rate of 2 g.L⁻¹.h⁻¹ to limit growth. Initially no increase was observed in growth rate after 1 hour of continuous feeding and the feed was terminated after 45 minutes. A DOT spike was then observed at 14.7 hours, showing the cells were carbon source limited and feeding was then started again at a rate of 4 g.L⁻¹ (lower than what was used in the previous experiment in order to maintain a lower growth rate). The feeding rate was continually decreased throughout the fermentation in an attempt to maintain a higher DOT value. Induction occurred at 16.9 hours and cells continued to grow steadily reaching a final OD of 34.4 A.U. and a dry cell weight of 12.4 g.L⁻¹.

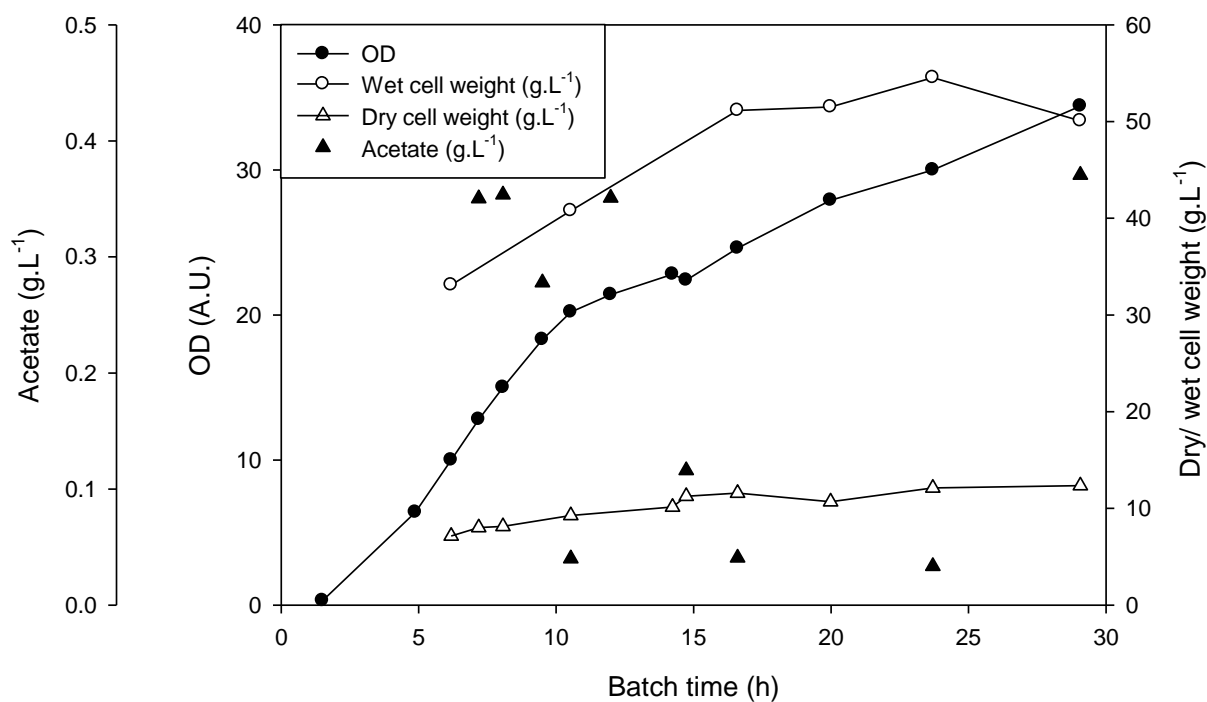
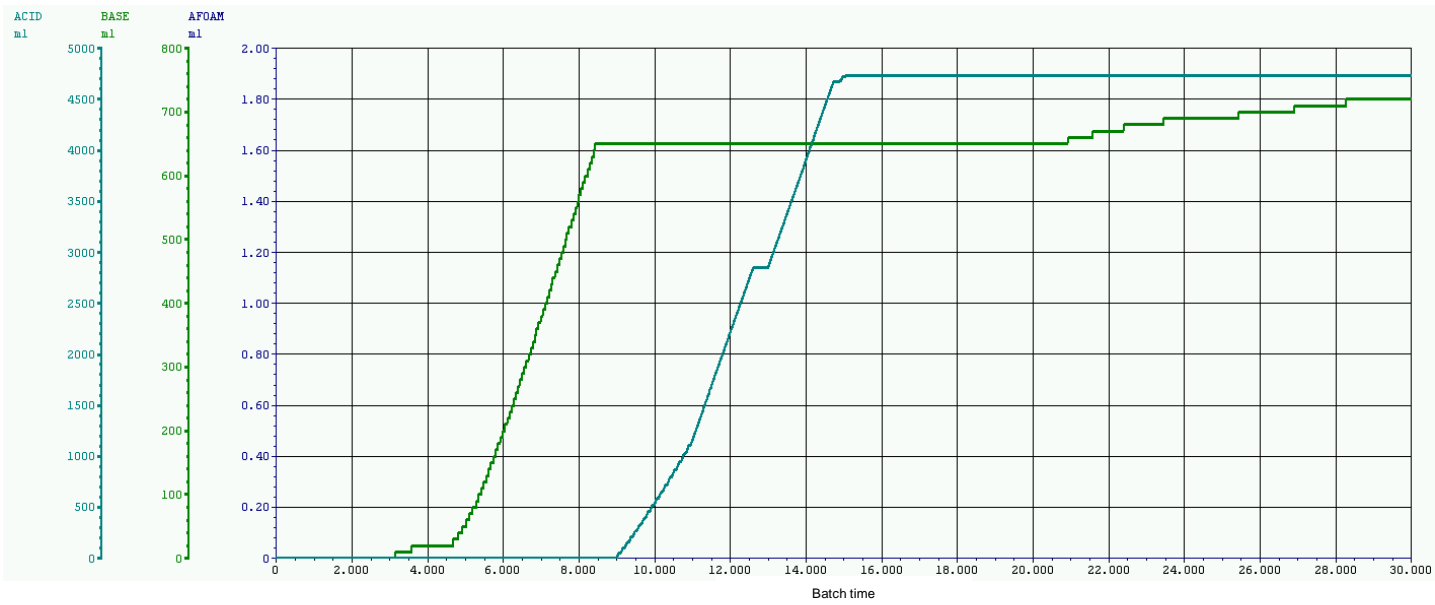
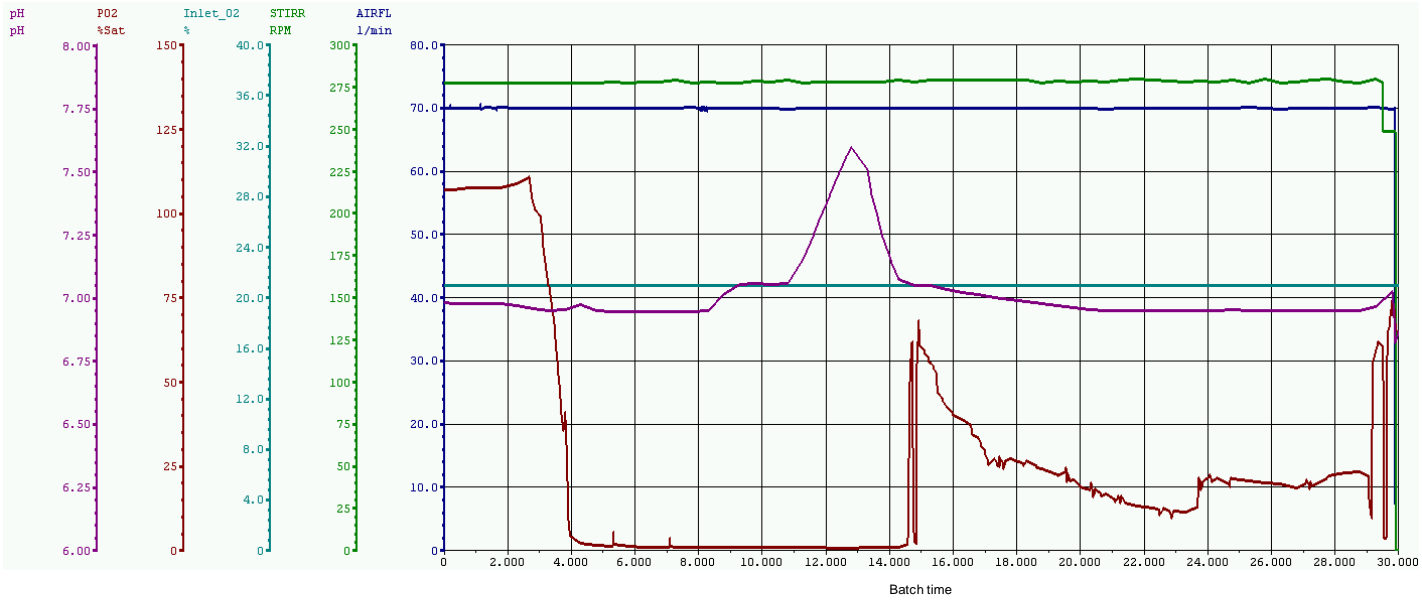


Figure 6.4 Growth profiles showing the optical density, wet and dry cell weight for 70 L fermentation with a Reynolds number of 132,000.



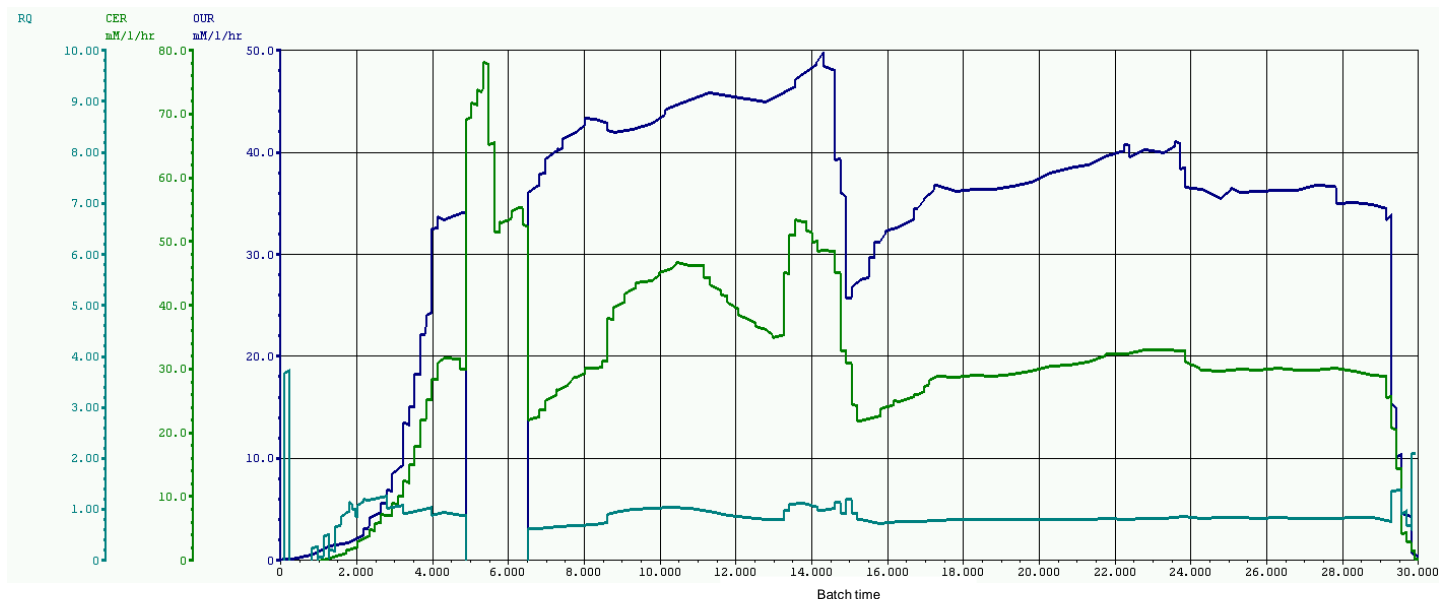


Figure 6.5 Fermentation traces of 1) dissolved oxygen (pO_2), pH, inlet oxygen concentration, stirrer speed and airflow rate. 2) Volume of acid, base and antifoam added. 3) respiratory quotient (RQ), carbon dioxide evolution rate (CER) and oxygen uptake rate (OUR).

The aim of this chapter was to conduct the large scale process in a manner that reproduced the oxygen limitations present in microwell plate format. The fermentation results obtained demonstrate that cells growing in the microwell geometry at this k_La would be severely oxygen limited after just 4 hours of fermentation. Anaerobic growth generates increasing amounts of acetate which is then utilised by the cells as a carbon source. Acetate also inhibits growth and has been reported to reduce recombinant protein production (Jensen and Carlsen, 1990; Luli and Strohl, 1990). The production of acetic acid also has the knock-on effect of altering the pH of media, and in the microwell with no pH control this could have detrimental effects. The media used also has been known to precipitate which could affect the supply of nutrients to cells, downstream recovery and purification (Shiloach and Fass, 2005).

6.3.4 Batch 70 L high k_La fermentation

Due to the oxygen limitations observed when running the 70L fermentation at $N = 275$ rpm, a large scale fermentation was conducted at a higher impeller speed $N = 450$ rpm. An impeller speed of 450 rpm corresponds to the highest k_La predicted for the microwell geometry. The growth profiles for OD, wet and dry cell weight are shown in Figure 6.6. The cells initially grew slower than previously observed, reaching an OD of 2 A.U. after 4 hours. Cells start to grow exponentially at approximately 5 hours, but 3

hours later OD and wet cell weight measurements show growth slows again (Figure 6.6). This change in growth rate is also demonstrated by the OUR and CER data, which are shown in Figure 6.7 B). A drop of OUR and CER at approximately 8 hours is observed indicating cell death and a corresponding rise in available dissolved oxygen is observed after 9 hours as shown in Figure 6.7 A). After 10 hours, the OUR and CER start increasing again reaching the same levels as previously observed after 11 hours, as cells start to grow. The oscillations between growth and stationary phase appear dependent on the concentration of dissolved oxygen available; showing that even at this higher k_{La} value growth is oxygen limited. The maximum oxygen uptake rate was found to be $123 \text{ mM.L}^{-1}.\text{h}^{-1}$, which is significantly lower than $200 \text{ mM.L}^{-1}.\text{h}^{-1}$ obtained for the 100 L fermentation with cascade control and enriched oxygen levels.

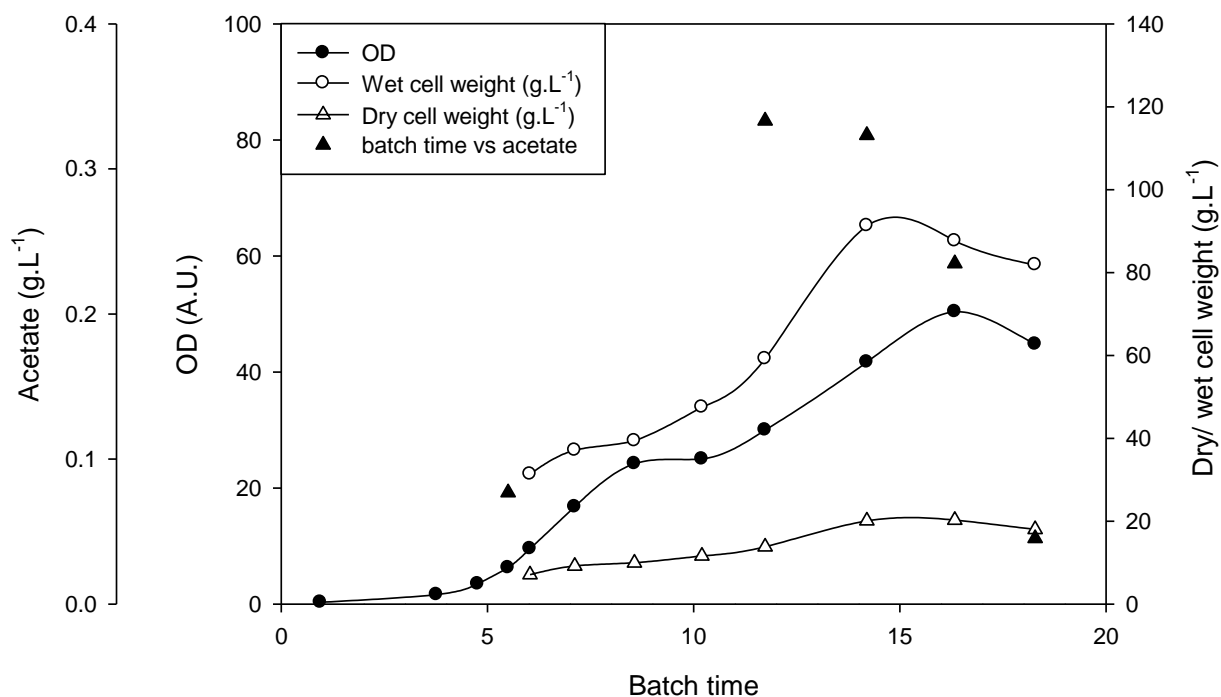
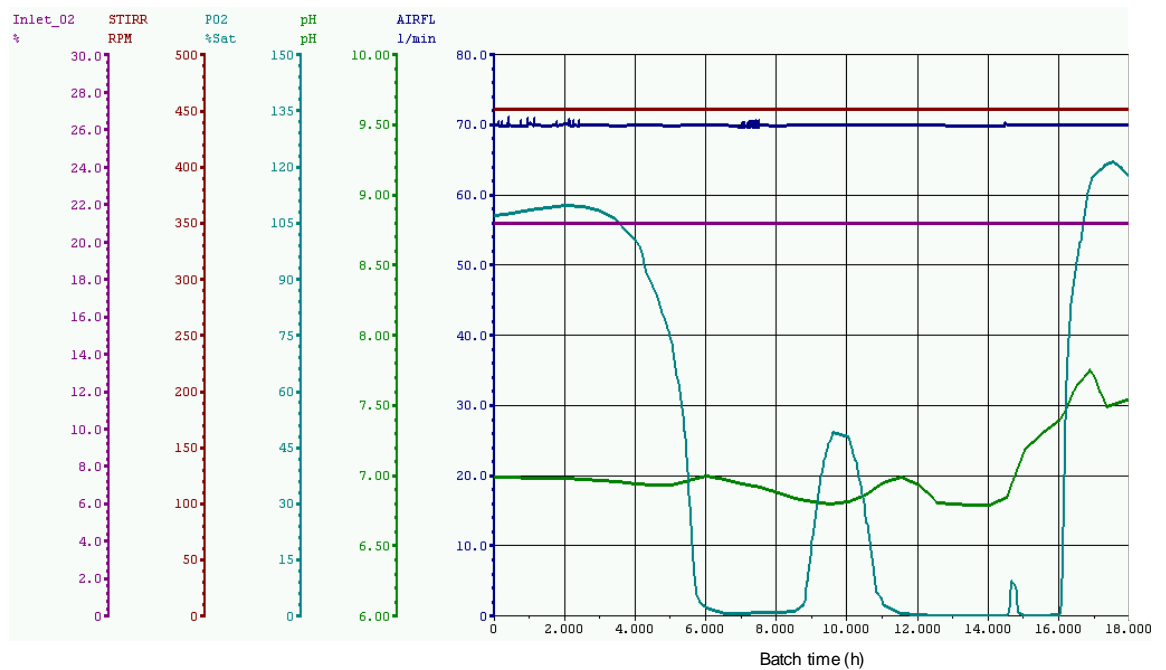


Figure 6.6 Growth profiles showing the optical density, wet and dry cell weight for 70 L fermentation with a Reynolds number of 215,000.

A)



B)



Figure 6.7 Fermentation traces of A) inlet oxygen concentration, stirrer speed, dissolved oxygen (pO_2), pH and airflow rate. B) respiratory quotient (RQ), carbon dioxide evolution rate (CER) and oxygen uptake rate (OUR).

6.3.5 Experimental k_{La} determination at the microscale

After the large scale fermentations were conducted at 275 and 450 rpm, k_{La} was measured directly in the microwell. The experimentally derived values were found to be significantly lower than those predicted by the correlation (Eq 1) and lower than either of the k_{La} at which the large scale fermentations were performed. Figure 6.8 shows that k_{La} increases with increasing shaking speeds from 16 to 46 h^{-1} . The trend observed in microplate geometry is similar to that obtained at the large scale. Results obtained in this work are also in agreement with the findings of (Doig et al., 2005a), where an increase in shaking speed resulted in a non-linear increase in k_{La} for 96 DRW plates and 3mm shaking diameter. Hermann et al. (2003) also found that k_{La} increases when shaking speeds are increased in a similar system.

Experiments were conducted to elucidate the relationship between k_{La} and fill volume. Higher k_{La} were obtained at decreasing fill volumes as illustrated in Figure 6.9, which shows k_{La} values between 70 and 107 h^{-1} for different fill volumes. The values obtained fall within the ranges of previously determined k_{La} values in microwell plates of 60 to 200 h^{-1} (Duetz et al., 2000; Duetz W.A. and Witholt B., 2001; Hermann et al., 2003; Duetz and Witholt, 2004; Doig et al., 2005a). Decreasing the fill volume from 1.0 ml to 0.6 ml increases k_{La} from approximately 70 h^{-1} to 105 h^{-1} . Ferreira-Torres (2008) reported the k_{La} changing from 51 h^{-1} to 102 h^{-1} under the same operating conditions but different fermentation media. The maximum oxygen transfer rate is reported to increase with decreasing fill volume as it is related to the mass transfer area, which is a function of shaking volume and diameter (Hermann et al., 2003).

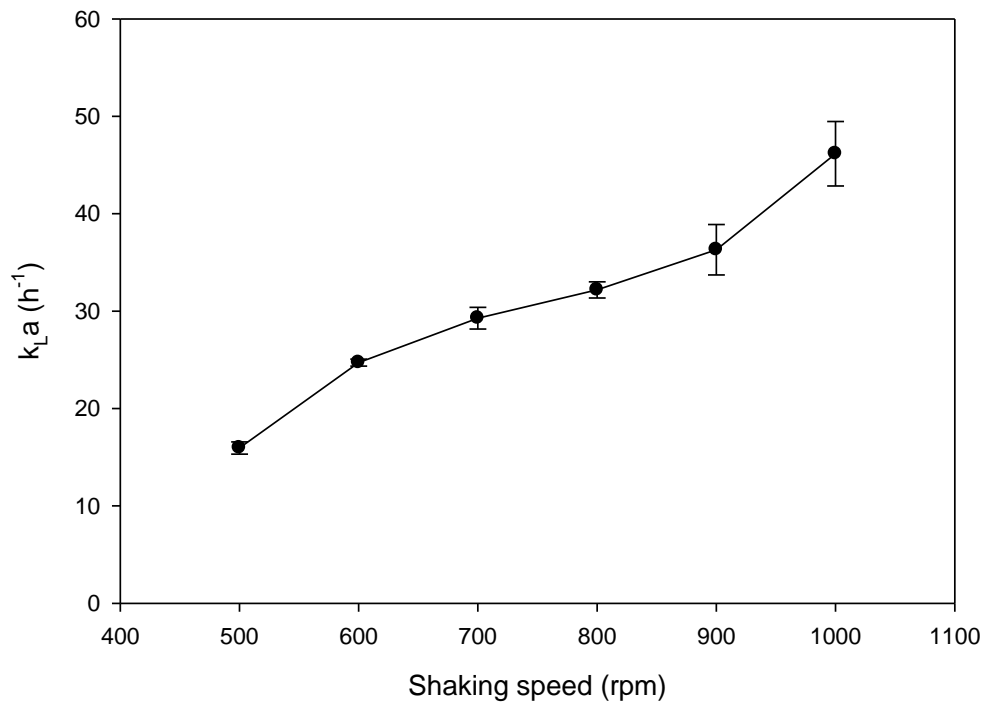


Figure 6.8 Measured $k_{L,a}$ values in a 96 DSW plate as a function of shaking speed with a shaking diameter of 3 mm and fermentation media, plus additions and no antifoam. Error bars are shown for an average of 3 measurements per data point

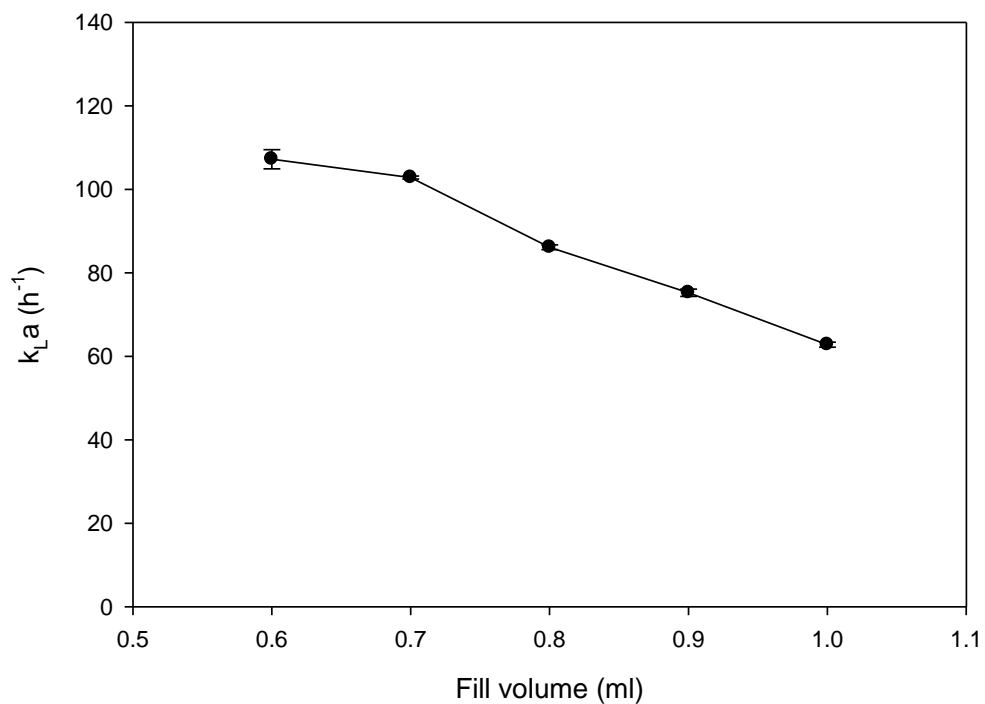


Figure 6.9 Measured $k_{L,a}$ values in a 96 DSW plate as a function of fill volume for fermentation batch media and 0.02% antifoam (PPG). Error bars are shown for an average of 3 measurements per data point.

The k_{La} experiments in microwell plate format highlighted the oxygen limitations present in this geometry and posed some difficulties in finding similar k_{La} values for the microwell and the 70L bioreactor scale. It can be speculated that there is an upper limit to the applicability of the matched k_{La} approach. The scaling factor in this work is 70,000 and to the best of our knowledge no successful scale-up approaches have been demonstrated between shaken and stirred system at similar scale ratios. The results obtained at the highest k_{La} tested in this work in stirred bioreactor geometry showed that cells were oxygen limited and therefore it is likely that cells experience similar oxygen limitations in the microwell plate format where k_{La} is lower than either values tested at large scale. A smaller fill volume could be used to achieve a slightly higher k_{La} in the microwell system. Ferreira-Torres (2008) obtained a k_{La} of 158 h^{-1} , obtained at a fill volume of 0.2 ml and shaking speed $N = 1000 \text{ rpm}$ in the same system. However a higher k_{La} value of 195 h^{-1} was obtained in the 70 L bioreactor at an impeller speed of 275 rpm and oxygen availability was limited with cells reaching a low final DCW of 12 g.L^{-1} . Therefore even near the maximum oxygen transfer conditions of the microwell system, cells are still oxygen limited and therefore this is not an ideal condition for scale-up. A fill volume of 0.2 ml introduces additional problems as evaporation is an issue over the course of an 18 hour long fermentation. The microwell plate fermentations were conducted with no lid to aid oxygen transfer via surface aeration. Volume losses from evaporation may result in inaccuracies in OD measurements making comparison between scales rather challenging. In addition minimum volume requirements are set by the subsequent process step and the use of sacrificial well approach. Consequently a compromise is needed between volume requirements and achievement of the minimum oxygen transfer levels in the well. Therefore large scale datum was compared to the yields achieved from a reproducible and accurate microwell fermentation procedure with identical media and inoculums preparation.

6.3.6 Batch microwell fermentation

The growth profile of the batch microwell fermentation is shown in Figure 6.10. The microwell fermentation displays different growth characteristics to the larger scale, reaching a much lower final OD. After a short lag phase the cells enter exponential phase. After 6 hours of fermentation the cells enter stationary phase and continue to grow at a much slower rate. This is probably a consequence of the induction carried out at 6 hours, which results in a change in metabolism and stresses to the cells.

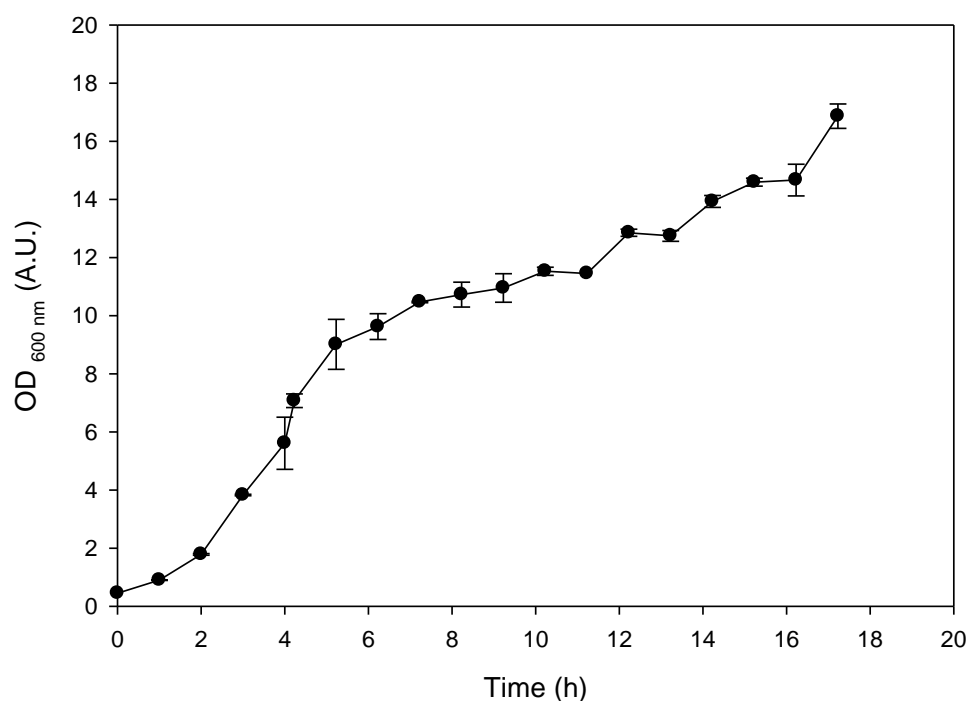


Figure 6.10 Growth profile showing the optical density of the microscale batch fermentation with a fill volume of 1 ml and a shaking speed of 1000 rpm.

The final OD achieved in the microwell geometry is 17 A.U., less than 50% of the lowest OD reached at large scale in this work (Table 6.6), confirming that at this $k_L a$ the cells experience oxygen limitations that reduce the growth rate. There could also be other growth limiting factors at the microscale, a lack of pH control could result in unfavourable conditions. The fermentation pH is an important factor for cell growth and product formation as it effects membrane permeability, cell morphology and enzyme activity (Elmahdi et al., 2003). Whilst the microwell growth data shows a lower number of cells was achieved, cells reached a similar level of productivity as the product titre shows it yields the same amount of product (1.4 g.L^{-1}) as the 100L

fermentation process where oxygen limitations did not occur (Table 6.6). Although the oxygen transfer rate may be limited at the microwell, it could provide the oxygen required for product expression and metabolism but insufficient for rapid growth and hence result in similar cell productivities. The results shown in Table 6.6 also demonstrate the importance of an early induction time as the fermentation conducted at a k_{La} of 195 h^{-1} (higher than the microwell) produces no product probably as a result of the different feeding and induction strategy employed.

Table 6.6 Comparison of growth characteristics and titre for the fermentation conditions studied.

Fermentation Condition	Final OD (A.U.)	Dry Cell Weight (g.L ⁻¹)	Product titre (g.L ⁻¹)
100 L cascade control, enriched O ₂	87.6	29.7	1.40
70 L 275 rpm	34.4	12.4	0
70 L 450 rpm	44.8	18.0	0.74
Microwell	16.9		1.42*

*measured on a different HPLC column and system

6.3.7 Scalability of refolding

Refolds were conducted at different scales (4.5 L, 200 ml and 300 μl) in order to compare pilot scale and microscale yields. The refolding yields obtained at different scales are shown in Figure 6.11 for buffer 1 (0.288 mM cystamine, 10% v/v hexylene glycol and 20 mM ethanolamine) and buffer 2 (10 mM Tris, 10 mM glycine, 1 mM EDTA, 0.5 mM cysteine, 4.5 mM cystine). Washed inclusion bodies refold gave similar yields in buffer 1 for 300 μl , 200 ml and 4.5 L scales resulting in yields of 15, 12 and 14 % respectively, demonstrating scale invariance. Results for refolding in a different buffer (buffer 2) agree with this finding, as the yield difference is only 4% for the microlitre and millilitre scale. This shows that microscale refolding is capable of predicting large scale refolding yield and can be a good substitute for time consuming and resource intensive pilot scale refolds.

Unwashed inclusion bodies from the same large scale fermentations show a slightly larger yield difference of 5%, with a yield of 5% for millilitre scale and 10% for microlitre scale. Therefore the yield at the microlitre scale is almost double that found

at the millilitre scale and this could be due to the different solubilisation procedures used. The time allowed for solubilisation at the microscale is 4 times longer, which could result in a larger concentration of reduced insulin for refolding at the microscale and consequently a higher yield. Previous attempts to use a shorter solubilisation procedure identical to the lab scale at the microscale resulted in aggregation during refolding due to the presence of insoluble IB particles in the denatured protein. This appears to be a significant problem, in particular, for the unwashed inclusion bodies where the largest yield difference exists. This suggests unwashed inclusion bodies are potentially more difficult to solubilise at the microscale. The mixing mechanism used for solubilisation at the microscale is shaking as opposed to direct stirring with a magnetic bead at the lab scale. Shaking is less efficient than magnetic stirrer bars which are capable of achieving greater speeds and shear rates. The solubilisation procedure has a significant impact on the refolding yield, and at large scale the solubilisation procedure lasts 1 hour instead of four hours at the microwell. However if the refold yield is assessed as a function of the concentration of solubilised IBs present in the denatured material, yields appear much higher as shown in Figure 6.12, with the refold at 4.5 L clearly outperforming the yield at other scales. The solubilisation procedure was less efficient at the largest scale and hence the fully denatured insulin available for refolding was lower. When this difference was taken into account the yield achieved is higher than previously thought. The refolding yield is also higher at lower concentrations of protein (Clark, 2001). Therefore in order to aid future comparisons between scales, the solubilisation step needs to be optimised first or material taken directly from large scale solubilisation for use at the microscale.

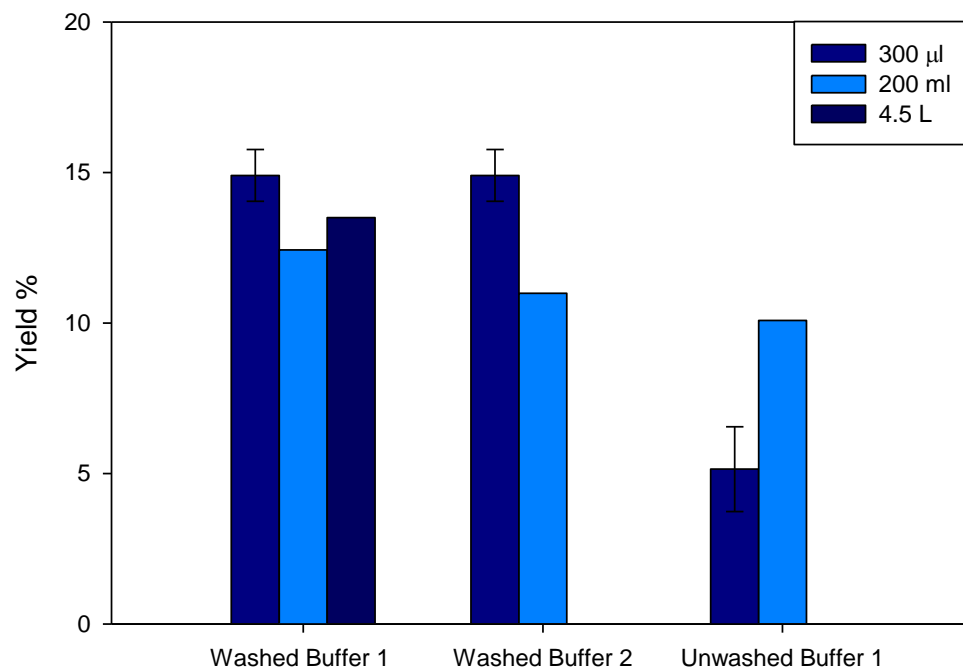


Figure 6.11 Refolding washed and unwashed inclusion bodies from the first fermentation in buffer 1 and 2 at different scales.

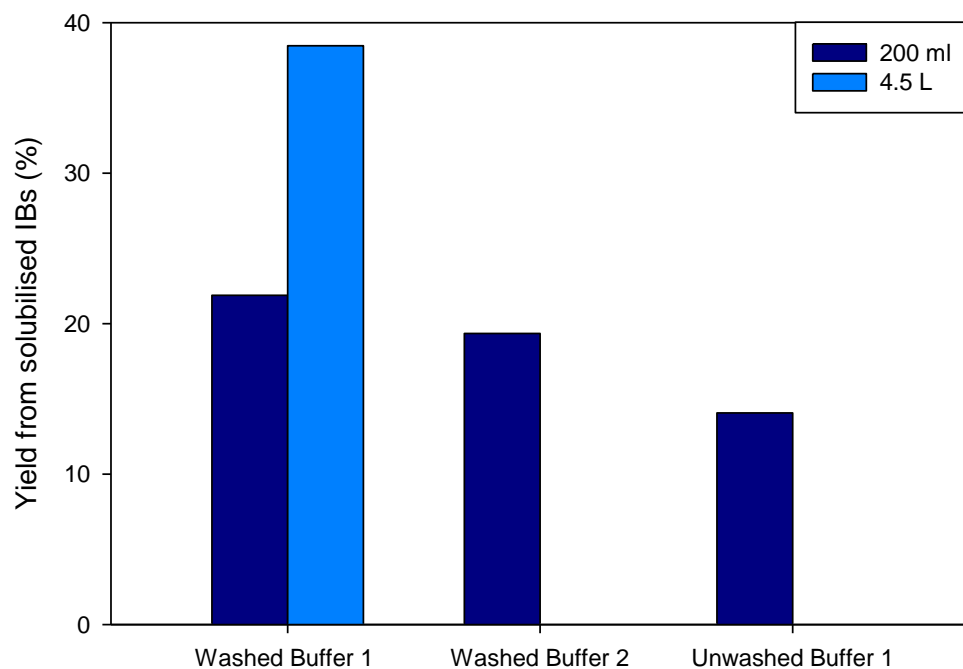


Figure 6.12 Refolding washed and unwashed inclusion bodies from the first fermentation in buffer 1 and 2 at different scales, with yield determined from concentration of fully solubilised protein as tested by HPLC method

6.3.8 Effect of oxygen limitation on IB refolding yield

The effect of the fermentation process conditions on refolding yield was assessed using material from fermentations at 100 L and 70 L at the higher k_{La} values tested, refolded at the microscale. Higher refolding yields were obtained with IB material from the 100 L fermentation than for the 70 L (with a constant impeller speed and no oxygen enrichment), thus indicating that fermentation conditions impact refolding yield for insulin, as previously found for DHFR. Figure 6.13 shows the refold yield of washed IBs from the 100 L fermentation (where DOT was maintained at 30%) and the 70 L fermentation (where DOT was close to zero for a large majority of the time). IB material from the 70 L fermentation with lower oxygen levels achieves a refold yield of 7% compared with 33% for the 100 L fermentation, when refolded in buffer 2. Refolding in buffer 1 results in higher yields of 20 and 38% for 70 L and 100 L fermentations respectively, showing this to be superior buffer for refolding insulin and capable of majorly improving refolding yield for suboptimal fermentation conditions. Therefore the fermentations show a significant refolding yield difference under the same refold conditions, therefore showing that the low oxygen and more stressful fermentation conditions impacts the refold yield and consequently must result in a change in the quality of the inclusion bodies. During the 70 L fermentation at the higher k_{La} oxygen is severely limited after 5.5 hours and increases above 30% for only 4 hours of the remaining 8.5 hours when cell growth is stationary (Figure 6.7). Whilst this fermentation is a more extreme example of oxygen limitation than would be observed during a production process, it shows that even after IB washing the IBs retain properties intrinsic to them that affect the refolding success. There is ample evidence to show oxygen availability has numerous negative effects on *E. coli*. Under anaerobic conditions and high concentrations of acetate, cells are probably under increased stress, altering metabolism and expression. *E. coli* is capable of switching metabolic mode to the most energetically favourable system for the current environment, depending on the availability of oxygen and electron acceptors (Spiro and Guest, 1991). It has been estimated that the availability of oxygen influences the expression of 200 genes in *E. coli* (Unden et al., 1995). Oxygen limitation during the growth phase has been shown to decrease growth rate and biomass yield (Li et al., 1992), however its effect on the expression of heterologous protein is not well understood. There have been contradicting reports on this effect that suggest oxygen limitation can modulate the expression of recombinant proteins positively or negatively depending on the host-vector and expression system (Bhattacharya and Dubey, 1997; Qoronfleh, 1999). For

example, Li et al. (1992) discovered anaerobic growth results in a decrease in plasmid content in all strains and an increase in β -galactosidase specific activity in two of the strains tested (although volumetrically the activity was lower because of the decreased biomass compared with aerobic fermentation). In addition to the direct effects of low oxygen on metabolism and expression, acetate is produced due to either a fast growth rate (oxygen consumption rate limitations) or a low dissolved oxygen concentration (Eiteman and Altman, 2006b). Acetate is a weak acid and can diffuse across the plasma membrane and release a proton in the cytoplasm (Lasko et al., 2000). This lowers the transmembrane proton gradient and cytoplasmic pH, thus reducing cellular energy supply and simultaneously resulting in toxic intracellular conditions (Axe and Bailey, 2004).

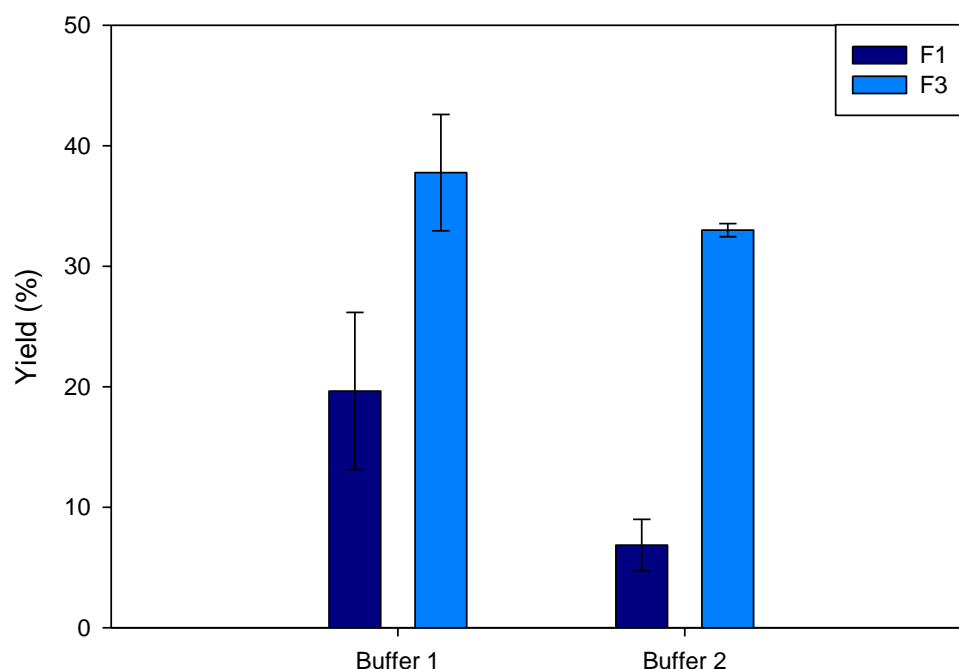


Figure 6.13 The effect of fermentation conditions on yield after refolding at the microscale washed inclusion bodies in two different buffers. F1: Fermentation with cascade control and enriched oxygen and a maximum impeller speed of 700 rpm. F3: Fermentation at the high kLa matched condition, with a constant impeller speed of 450 rpm. Buffer 1 0.288 mM cystamine, 10% v/v hexylene glycol, 20 mM ethanolamine, pH 10.5. Buffer 2 10 mM Tris, 10 mM glycine, 1 mM EDTA, 0.5 mM cysteine, 4.5 mM cystine, pH 10.5.

6.3.9 Microscale fermentation and refold system for large scale yield predictions

The yields obtained at different refold scales have been shown to be similar for the same fermentation material, with small differences caused by the differing solubilisation procedure between scales. Therefore microscale refolding can be used as a tool for screening many refold conditions using large scale fermentation material, which will allow the rapid analysis of multiple refold conditions in parallel early on in process development. However given that the fermentation conditions effect inclusion body quality and consequently refold yield, it is important to investigate whether the microscale fermentation and process as whole can be used for the prediction of the effect of process variables on yield given the differences between microscale fermentation and large scale fermentation.

Figure 6.14 illustrates the maximum yields obtained when refolding at the microscale IB material from the microscale fermentation and large scale fermentations (100 L and 70 L). The results are contrary to expectations as, based on the k_{La} , the conditions experienced in the microwell are more similar to the 70 L fermentation. The microscale process has a yield of 64 % whereas the 70 L fermentation shows a much lower maximum yield of 38 %. The maximum microscale refold yield obtained for material from the microscale fermentation and process of 64 % are similar to the 65 % yield of the 100 L fermentation. Therefore the microscale process sequence can attain similar yields to standard large scale fermentation conditions and processing when the same solubilisation procedure is used. The microscale process has definite promise for use early on in process development to estimate large scale yield from either large scale material (as shown in Section 6.3.7) or material from the microscale fermentation and process, and identify scaling issues. The fermentation conditions experienced in the microwell may have been more favourable than those in the 70 L fermentation with a slightly higher k_{La} value because final OD at the microscale is 62 % lower (Table 6.6) and consequently the demand for oxygen is lower.

The maximum yields achievable for different fermentation and process scales illustrated in Figure 6.14 are not under the same refold condition, but show different optimal refold buffers. Microscale IB material refolds optimally in buffer 2, which has shown to be

optimal for proinsulin by Winter et al., (2002) at lab scale. IB material from the large scale fermentations shows optimal yields when refolding in buffer 1. Buffer 1 contains hexylene glycol, which has been shown to improve refolding of activin-A from inclusion bodies when 5% hexylene glycol is present (Ejima et al., 2006). Hexylene glycol can stabilise the native form of proteins by preferential exclusion (Seefeldt et al., 2008). It also contains cystamine, a reducing agent which with break interchain disulphide bonds promoting the disulphide shuffling to form the correct pairings of the 3 disulphide bonds in insulin (Rudolph and Lilie, 1996). The pH of both the buffers is alkaline, a mild alkaline pH has been shown to be optimal for disulphide bond disruption as it proceeds through nucleophilic attack by the thiolate anion (Vallejo and Rinas, 2004). Figure 6.14 shows that it is possible to achieve high yields from microscale fermentation material and it could be used to predict potential yields at the large scale. IB material that has experienced different fermentation conditions appears to interact with refold buffers differently depending on the components and properties of the buffer. Consequently the optimal buffer is different, reflecting a difference in the inclusion body material and the optimal buffer required to guide it through its folding pathway to achieve an optimal yield.

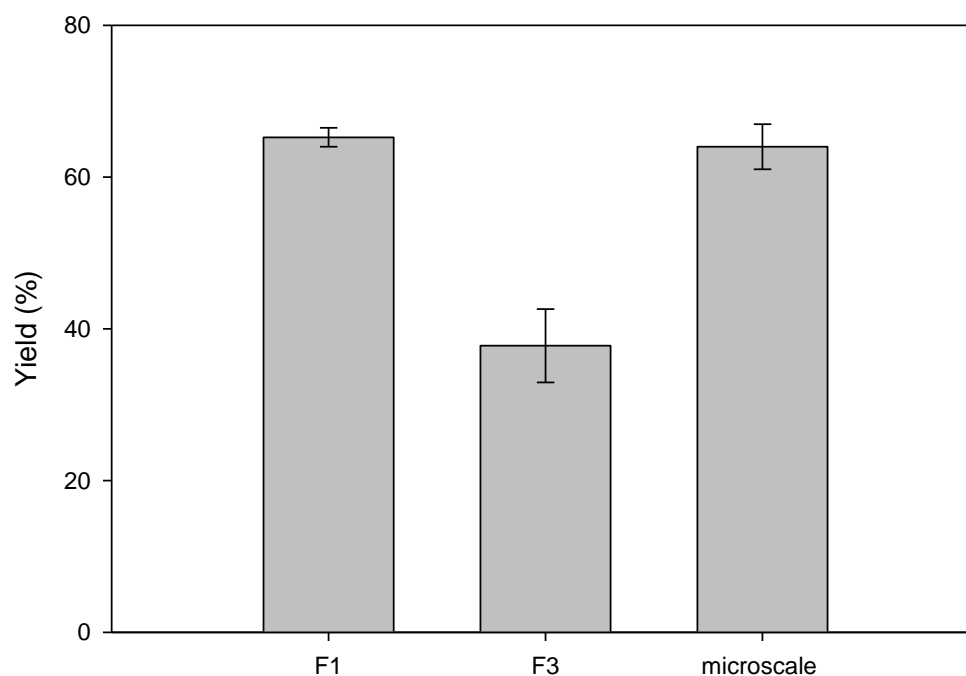


Figure 6.14 Maximum yields obtained from refolding at the microscale IB material from the fermentations. Maximum conditions for each of the fermentation conditions are as follows, F1: washed IB, buffer 1, 0.1 g.L⁻¹. F3: washed IB, buffer 1, 0.15 g.L⁻¹. Microscale fermentation: unwashed IB in buffer 2.

6.3.10 The effect of refold buffer on purity of refold

In order to investigate how the refold buffer influences yield further, the purity of the active refolded protein formed in relation to the total contaminants content was studied. The purity of the refold is a function of both fermentation contaminants and the different refold species present (such as intermediates and misfolded protein species), which may be eluted at different times from the column. A higher purity refold offers a distinct advantage for further downstream processing steps as it would reduce the impurities load on following chromatography steps. Figure 6.15 shows the purity of washed and unwashed IB material from 100 L (F1) and 70 L (F3) fermentations and refolded in buffer 1 or 2. The washing of the inclusion bodies appears to dictate the refold purity depending on the source of fermentation material. The purity is highest for the 100 L fermentation (F1) washed IBs refolded in buffer 2, which has a purity of 62%. The refold purity for the 100 L fermentation is higher in both buffers when the IBs are washed, whereas the refold purity for the 70 L fermentation (F3) is higher in both buffers when the IBs are unwashed. This is unexpected as washing to remove contaminants from the surface of the inclusion body should improve the purity of the refold. However this suggest contaminants are beneficial for the refolding of 70 L fermentation material, perhaps resulting in less off path partially folded protein intermediates. The contaminants appear detrimental to the refolding of 100 L fermentation material. This could be because the contaminant profile is different between these two different fermentation conditions.

The buffer chosen drastically impacts the purity of the refold. Unwashed material refolds with a lower purity in buffer 2 in comparison with buffer 1, decreasing the purity from 60 to 45% and 46 to 23% for 70 L (F3) and 100 L fermentation (F1) respectively. Therefore for suboptimal fermentation conditions, such as the low oxygen experienced for the 70 L fermentation (F3), the purity is optimised by using unwashed the inclusion bodies refolded in buffer 2. However for the washed material the relationship with buffer is more complex as the optimal buffer is different for the different fermentations. The washing procedure causes a change in the IB material from the 100 L fermentation (F1), resulting in buffer 2 becoming more favourable for purity of the refold. This indicates that contaminants play a role in the interactions between folding protein and buffer choice. In order to choose the right refold buffer to maximise

purity, the fermentation condition and washing of the inclusion body must be considered as these two factors interact to determine refold purity.

Figure 6.16 illustrates the relationship between yield and purity, showing that yields of above 90% have purities greater than 40%. There is one noticeable exception, where the yield is 85% but the purity is 23%, but this might not reflect a truly high yielding condition as the same starting material achieved a yield of up to 150% (under a different refold condition). Achieving an accurate assessment of the protein titre in a inclusion body slurry by RP-HPLC is challenging because of the granular and viscous nature of the inclusion body slurry, which can result in inaccurate estimates. In general, the highest yielding refold conditions are the highest in terms of purity, as there is a large concentration of active product present that consists of the largest proportion of protein present.

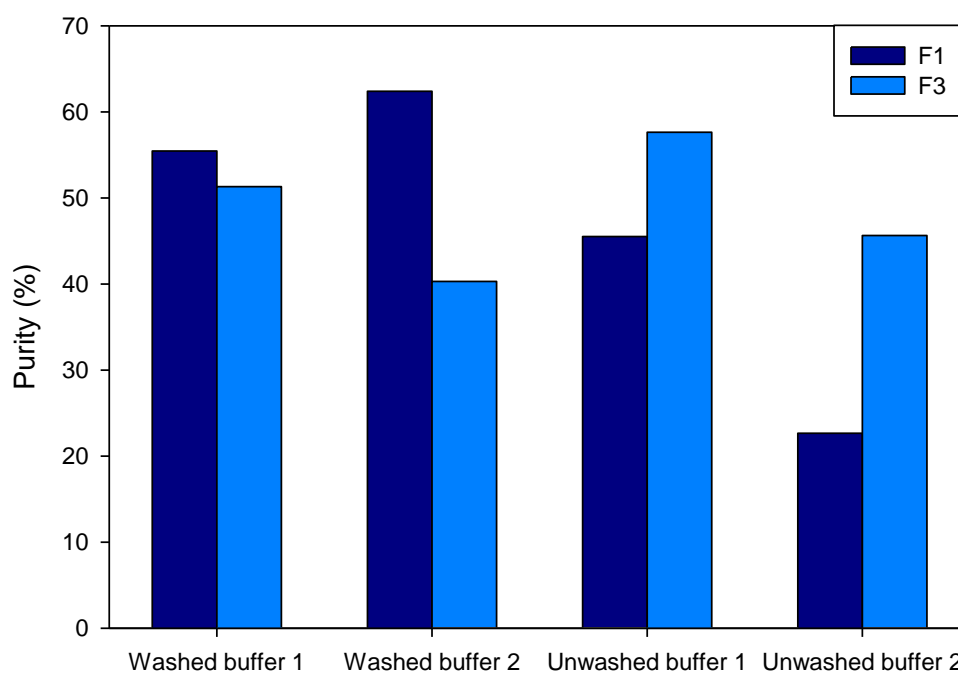


Figure 6.15 Purity of active protein in 200 ml refolds for the different large scale fermentations, with different IB washing regimes and refold buffers. Refolds used material solubilised at a concentration of 1.5 g.L^{-1} and an 18 fold dilution factor. F1: Fermentation with cascade control and enriched oxygen and a maximum impeller speed of 700 rpm. F3: Fermentation at the high $k_L a$ matched condition, with a constant impeller speed of 450 rpm.

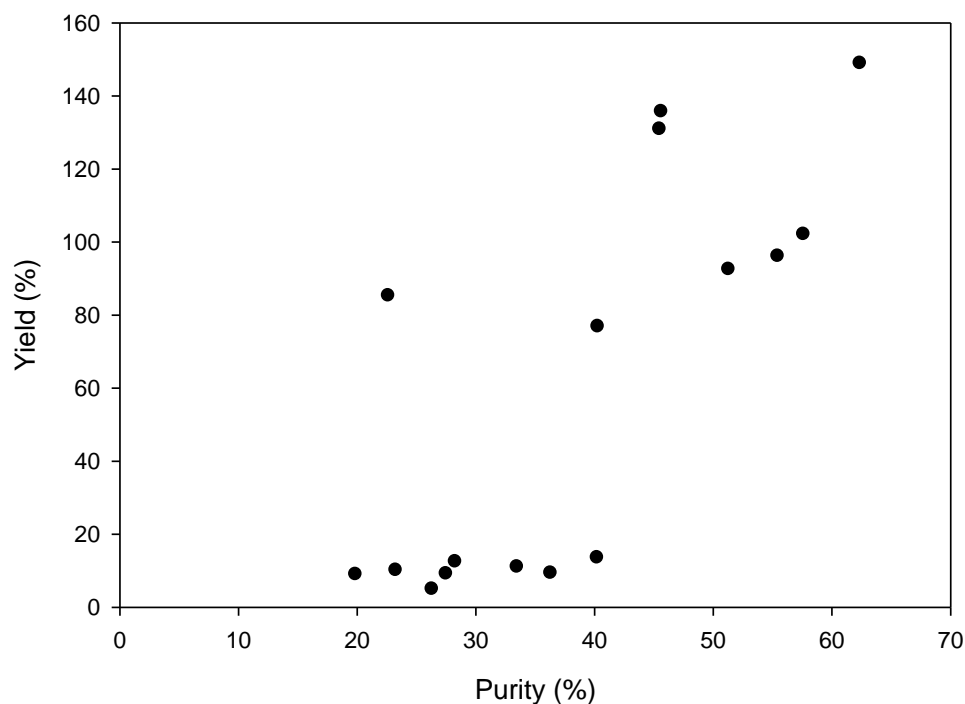


Figure 6.16 Yield as a function of purity for refolds at the 200 ml scale with varying refold conditions (IB washing, buffer, dilution factor, final protein concentration).

6.3.11 Effect of different refold conditions on insulin

The large scale fermentation material was refolded at the lab scale to investigate the effect of different refold conditions on insulin. The IB material from the 70 L fermentation at the higher k_{La} which was refolded at the 200 ml scale is collectively shown in Figure 6.17. It shows the highest yielding condition is from washed IB material from the first fermentation, diluted 18 fold in buffer 2 to give a low final protein concentration of 0.08 g.L^{-1} . This shows that fermentation with cascade control and enriched oxygen ultimately produces the highest yielding product. The second highest yielding condition was unwashed IB material from the 70 L fermentation refolded in buffer 2 and the same dilution factor and protein concentration. This indicates that poor yielding fermentations that experience oxygen deprivation can still be productive and high yields obtained if a different strategy is adopted downstream. As previously observed unwashed inclusion bodies can result in high yields under some conditions (Section 5.2.1.1) as lipid contaminants may aid folding. Ultimately however a fermentation condition with no oxygen or carbon limitations and pH control results in

the highest yielding condition as the quality of inclusion bodies is improved and hence the refold yield and purity is higher.

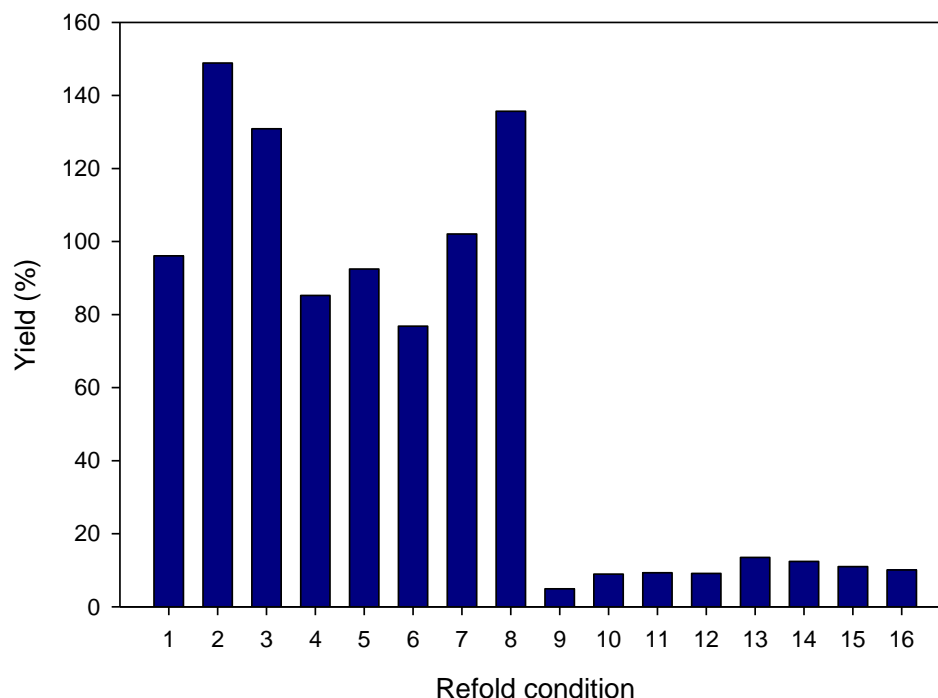


Figure 6.17 The refolding yield of IB material from the first fermentation (cascade control and enriched oxygen) and the high k_{La} fermentation. For details of each refolding condition see Table 6.2.

6.4 Conclusions

This chapter has demonstrated that the microscale fermentation is capable of producing a similar product titre to pilot scale fermentation (100 L). However, it was not possible to use a matched k_{La} approach due to the oxygen limitations observed during the microwell fermentation and the oxygen requirements of the strain used. A fixed k_{La} does not work as a scaling parameter for high cell density cell culture unless the oxygen transfer capacity present is in excess of that required for the final OD. Currently oxygen limitations in the microwell hamper the ability to reach the ODs observed at the 100 L scale. This demonstrates that the oxygen conditions experienced in the microwell geometry are significantly different from normal operational limits at the 70 or 100 L scale. The 70 L fermentation at higher k_{La} values than the microwell resulted in oxygen limitation and for the lower k_{La} tested no product expression, showing a minimum requirement of oxygen transfer for product expression. The microwell fermentation must experience longer periods of oxygen limitation as the k_{La} is lower than both of the

70 L fermentations. This could be overcome by the use of miniature bioreactors at the microscale, which would allow increased oxygen transfer through sparging and/or impeller driven mixing.

The microscale refold is able to produce similar yields of refolded protein as larger scale refolds (200 ml and 4.5 L). Dilution refolding is reported to be scale invariant (Middelberg, 2002), and as such microscale refolding could provide a high throughput method for analysing refold conditions during process development. However, differences were observed between refold yields at the pilot and lab scale when efficiency of solubilisation step was taken into account. Achieving high degrees of IB solubilisation is challenging at all scales, particularly for unwashed inclusion bodies, and may give varying results depending on the degree of solubilisation of the inclusion bodies. In order to aid future scale comparisons, the solubilisation step must first be optimised to provide equivalent protein concentrations at the different scales.

The previous chapter has demonstrated that inclusion body quality is affected by the fermentation conditions. This is supported by evidence in this chapter, which has shown the differences in growth profiles and oxygen availability between microwell and large scale fermentations alter IB quality and concurrently refolding yields. Refolding experiments at the microscale demonstrate material from the microscale process sequence achieves comparable yields to pilot scale IB material refolded at the same scale (when using the same solubilisation procedure). The optimal refolding condition was different for the microscale and pilot scale material due to the varying inclusion body quality resulting from their different fermentation source. However it demonstrates high yields can be achieved with the microscale process sequence and that with further development it may be possible to use the microscale process sequence as a predictive tool. Optimisation of the solubilisation step in future would allow better scale-up of the refold step. Additionally, the use of a miniature bioreactor for microscale fermentation would allow control of the key process parameters, pH and dissolved oxygen, and provide better mixing and oxygen transfer capabilities. This in turn would provide processing conditions similar to large scale fermentation and consequently IBs which have product quality properties that are equivalent to the large scale. This is necessary if the results at the microscale are to have relevance for large

scale process development and enable the process sequence to be used in studies for QbD purposes.

7 Conclusive remarks and future recommendations

7.1 Automated, high throughput assays for IB yield determination

A novel microscale methodology with a hierarchy of assays to evaluate protein refolding was clearly established in this chapter. The translation of the refold process and related assays to a robotic platform demonstrated approximately equal errors to manual operation, with automation having additional advantages in terms of consistency and speed. The hierarchy of assays developed in this work was used to explore a wider range of lysozyme refold conditions, showing relative fluorescence was a good predictor of yield once aggregating conditions have been screened out by an absorbance assay. In conclusion, the automated microscale refolding process described would allow the rapid evaluation of a large number of conditions to optimise protein refolding to achieve higher product yields from inclusion bodies. Measurement of particulate formation by absorbance scattering provides an initial filter to eliminate aggregating conditions, and intrinsic fluorescence spectroscopy identifies conditions that produce protein with the most native-like tertiary structure. Assays to directly measure native protein yields, which are typically available at lower throughput or at higher costs, could then be used to validate fewer samples and alleviate the analytical bottleneck. The hierarchical orthogonal assays enables the analysis of refold conditions on a much shorter time scale by selecting only the most promising conditions for characterisation by resource intensive analytical methods such as RP-HPLC. An optimal relative fluorescence range could be used to select 29% of the samples from the conditions tested, which also gave the highest activities values (83-113%). The assays were demonstrated to be generically applicable to IB proteins sourced from fermentation material in the form of DHFR. In this case an intrinsic fluorescence boundary of between 5110-7610 captured 75% of the data points with a high activity of over $10 \Delta\text{OD}\cdot\text{min}^{-1}\cdot\text{mg}^{-1}$.

7.2 Developing an automated, whole bioprocess for IB production at the microscale

The development of an automated linked bioprocess sequence showed it was possible to develop a whole bioprocess at the microscale that required very little manual intervention with the exception of offline cell lysis. This has numerous advantages over manual operations as reproducibility is improved between experiments due to the reduction in error and improvement in precision and accuracy of the liquid handling. Improvements in productivity were also obtained from the increased speed of automated manipulations and walk away operation. Growth of DHFR expressing *E. coli* in microwells reached comparable optical densities as the 20 L scale. Higher levels of clarification were achieved at the microscale during the cell harvest step due to the higher centrifugal forces achievable in a microcentrifuge. However this also posed challenges as the more compacted pellet was harder to resuspend, resulting in cell losses. Adaptive focused acoustics was demonstrated to be the best method for high throughput lysis, although the method efficiency is lower than what is achievable by conventional sonication. This was shown by the application of a recently developed flow cytometry technique for measuring inclusion bodies during processing, which was used to study cell lysis. However the resulting inclusion body pellet from AFA lysis showed a similar contaminant profile to large scale inclusion body harvest.

7.3 The effect of fermentation conditions on refolding

The results shown in Chapter 5 show that fermentation conditions have a significant impact on IB refolding quality and yields. For DHFR IBs, inducer concentration and time were important variables for maximising yields. Doubling the IPTG concentration from 0.125 mM to 0.25 mM resulted in a 24 % increase in yield of active protein from unwashed inclusion bodies. However yield differences between conditions were much smaller for washed inclusion bodies, highlighting the importance of certain contaminants that aid refolding or effect IB quality. An earlier induction time of 3 hours resulted in a 10% increase in yield over later induction, but resulted in the accumulation of lower concentrations of protein and therefore a later induction time was considered more economical. Inclusion bodies are often frozen after harvest as it provides an ideal point at which to decouple the process. The storage temperature

showed little effect for microscale fermentation material stored over a few months, but material from larger scale fermentations stored at -20°C over a period of several years refolded to give higher yield of active protein. The sequence demonstrated its broad applicability by its adaption to insulin IB production and refolding. The bioprocess sequence was used to study the effect of induction time, feeding strategy and media. A glycerol carbon source results in a higher yield of 33% instead of 18% obtained for the worst fermentation media condition (terrific broth) at equal protein concentration. This demonstrates a significant difference in IB quality, which is additional to the almost three times higher fermentation titre for glycerol based media. The optimal conditions were shown to be induction at 4.5 hours (mid exponential phase) and batch operation, possibly as the feeding rate was too high for fed-batch. In conclusion the sequence showed it could be used as a tool to investigate the effects of fermentation conditions on yield in order to select optimal fermentation conditions for both insulin and DHFR inclusion body production. It also showed that variations in fermentation condition caused changes in inclusion body quality as shown by the varying refold yields at equivalent conditions, as well as titre differences.

7.4 Scale up of fermentation and refolding processes

The microscale fermentation is capable of producing a high titre of product equivalent to the large scale. However it was not possible to match the k_{LA} and hence the oxygen transfer capabilities of the large scale. Consequently the fermentation in the microwell format was shown to be oxygen limited, which had corresponding implications for the inclusion body quality produced. The refolding step did not show scale invariance, although this could result from the difficulties of achieving reproducible solubilisation of inclusion body material between scales rather than differences in the engineering environment. The microscale bioprocess sequence was able to attain equally high final yield of active protein as large scale material refolded at the same scale. However this was under a different refold condition from the large scale optimal condition because of difference in inclusion body quality and its interactions with refolding buffer. It can be therefore concluded that the automated microscale bioprocess has the potential for predicting yield, identifying scaling issues and for investigating the interactions between different unit operations.

7.5 Future recommendations

7.5.1 Assay development

The next stage for the development of the automated hierarchical refold assays would be to automate the analysis of the results through further programming. The existing data analysis was a bottleneck in the high throughput process. Additionally, using a randomised plate layout results in time consuming data analysis to match the high yielding wells to the conditions used, so automated analysis will allow faster recognition of critical refolding parameters. When there is no fast activity assay available analysing the yield using HPLC assays also contributes significantly to the length of the sequence. The RP-HPLC assay used for insulin in this work was 57 minutes. Ultimately, combining the automated refold and hierarchical assays with new UPLC methods could enable an even faster analytical method for identifying active protein, shorter lag times and increase robotic platform productivity further.

7.5.2 Sequence development

The automated linked bioprocess sequence could be developed further to incorporate unit operations after inclusion body refolding. The next unit operation to add would be purification, which could be performed using existing technologies such as Atolls MediaScout[®] Robocolumns that are compatible with the robotic platform used. The other challenge surrounding the current bioprocess is that it does not act as a direct large-scale mimic. Further development is required of each unit operation to match the conditions observed at the large scale, for example the cell debris profile after lysis, which will impact upon yields in the following unit operation.

7.5.3 Applications of the whole bioprocess approach

The whole bioprocess approach could be used to investigate a number of further fermentation variables that have been demonstrated to have an effect on inclusion body formation. For example, the whole bioprocess approach could be used as a host screening tool to explore the role of stronger promoters and high plasmid copy numbers in inclusion body formation. Alternatively, it could also be used to screen a wider scope of refolding conditions such as other additives, redox reagents, pHs and buffering systems.

7.5.4 Scaling-up

The most significant improvement to the process would be the addition of fermentation control through the use of micro-bioreactors. This would allow online pH and DOT monitoring and control, along with direct sparging and/or impeller driven mixing to achieve higher oxygen transfer rates. This would provide an engineering environment more akin to the large scale in terms oxygen transfer and mixing. Consequently higher k_{La} values will be achievable, which will allow k_{La} to be used as a scaling parameter for high cell density *E. coli* fermentation. The online measurement of pH and DOT and the introduction of control loops will allow improved control of fermentation variables within the same operating parameters as the large scale. This would lead to more meaningful results and this methodology could be used alongside DOE to map critical process parameters in fermentation. The results could then be translated to the larger scale, allowing improved process development. Additionally, the resulting inclusion bodies from controlled microscale fermentation will have quality attributes that are more similar to larger scale fermentation products, enabling better predictions of refolding yields during early refold screening studies. The final results chapter also showed that the solubilisation step needs to be optimised further to give similar efficiencies to large scale solubilisation to allow direct comparisons between refolding scales.

Regulatory bodies increasingly require Quality by Design (QbD) principles to be followed for the approval of a new biological drug product (Rathore and Winkle, 2009). This requires a detailed understanding of both the product and the process, in order to evaluate the impact of the process on the product's key quality attributes and consequently its clinical properties. This involves a large investment of resources at the research and development stage as intensive research is required to map the design space of a chain of unit operations in a process. This is an area where high throughput microscale technologies will become increasingly important as it facilitates parallel experimentation of multiple process variables at the small scale and hence allows the cost effective implementation of QbD. The sequence developed could be used to investigate critical process parameters that effect the critical quality attributes of the product during fermentation and refolding. However for the microscale results to be

meaningful, they need to be scaleable or predictive of the large scale, which may require increased process control during fermentation.

7.6 Overall conclusions

The main findings are summarised below in relation to each of the thesis objectives described in Chapter 1.

1. An automated microwell-based dilution refolding system was demonstrated with automated hierarchical generic assays to allow the analysis and selection of high yielding conditions. The hierarchical generic assay methodology is a novel approach for optimising refolding conditions at high throughput, using two non-invasive functionally independent assays to select optimal refold conditions, which can be applied to different protein products.
2. An automated bioprocess was developed for the production, processing and refolding of inclusion bodies. This was the first time (to the author's knowledge) an automated sequence of unit operations has been applied to inclusion body refolding.
3. A whole bioprocess approach was used to study the effect of fermentation conditions on IB refolding yields. It demonstrated the importance of inclusion body washing, fermentation media and inclusion body storage to maximising refold yields. This allowed the optimisation of processing variables at the microscale whilst minimising resource requirements. The addition of fermentation control at the microscale and further development of the sequence could allow in the future the identification of critical processing parameters and the mapping of the design space required for Quality by Design.
4. Validation of the fermentation and refolding step identified scaling issues. Oxygen was limited during microwell fermentation and consequently k_{La} did not provide a valid scaling parameter, illustrating the challenges associated with scaling up to manufacturing scale. High fermentation titres and refold yields could be achieved at the microscale. However the optimal conditions for refolding at large scale did not directly translate to the microscale due to

differences in solubilisation efficiency, showing the complexities involved in scaling up.

8 References

- Adams, C.P., and Brantner, V.V. (2006). Estimating The Cost Of New Drug Development: Is It Really \$802 Million? *Health Aff* 25, 420–428.
- Agerkvist, I., and Enfors, S. (1990). Characterization of *E. coli* cell disintegrates from a bead mill and high pressure homogenizers. *Biotechnology and Bioengineering* 36, 1083–1089.
- Allen, S.P., Polazzi, J.O., Gierse, J.K., and Easton, A.M. (1992). Two novel heat shock genes encoding proteins produced in response to heterologous protein expression in *Escherichia coli*. *J Bacteriol* 174, 6938–6947.
- Alves, S.S., Maia, C.I., and Vasconcelos, J.M.T. (2004). Gas-liquid mass transfer coefficient in stirred tanks interpreted through bubble contamination kinetics. *Chemical Engineering and Processing: Process Intensification* 43, 823–830.
- Ami, D., Natalello, A., Gatti-Lafranconi, P., Lotti, M., and Doglia, S.M. (2005). Kinetics of inclusion body formation studied in intact cells by FT-IR spectroscopy. *FEBS Lett.* 579, 3433–3436.
- Anderson, K.W., Grulke, E., and Gerhardt, P. (1984). Microfiltration Culture Process for Enhanced Production of rDNA Receptor Cells of *Escherichia Coli*. *Nature Biotechnology* 2, 891.
- Andersson, L., Yang, S., Neubauer, P., and Enfors, S. (1996). Impact of plasmid presence and induction on cellular responses in fed batch cultures of *Escherichia coli*. *Journal of Biotechnology* 46, 255–263.
- Anfinsen, C.B. (1973). Principles that Govern the Folding of Protein Chains. *Science* 181, 223–230.
- Aucamp, J.P., Cosme, A.M., Lye, G.J., and Dalby, P.A. (2005). High-throughput measurement of protein stability in microtiter plates. *Biotechnology and Bioengineering* 89, 599–607.
- Aucamp, J.P., Martinez-Torres, R.J., Hibbert, E.G., and Dalby, P.A. (2008). A microplate-based evaluation of complex denaturation pathways: Structural stability of *Escherichia coli* transketolase. *Biotechnology and Bioengineering* 99, 1303–1310.
- Axe, D.D., and Bailey, J.E. (2004). Transport of lactate and acetate through the energized cytoplasmic membrane of *Escherichia coli*. *Biotechnology and Bioengineering* 47, 8–19.
- Baboo, J.Z., Galman, J.L., Lye, G.J., Ward, J.M., Hailes, H.C., and Micheletti, M. (2012). An automated microscale platform for evaluation and optimization of oxidative bioconversion processes. *Biotechnology Progress* 28, 392–405.

- Balasundaram, B., Harrison, S., and Bracewell, D.G. (2009). Advances in product release strategies and impact on bioprocess design. *Trends in Biotechnology* 27, 477–485.
- Balasundaram, B., and Pandit, A.B. (2001). Significance of location of enzymes on their release during microbial cell disruption. *Biotechnology and Bioengineering* 75, 607–614.
- Baneyx, F. (1999). Recombinant protein expression in *Escherichia coli*. *Current Opinion in Biotechnology* 10, 411–421.
- Baneyx, F. (2004). Keeping up with protein folding. *Microb Cell Fact* 3, 6.
- Baneyx, F., and Mujacic, M. (2004). Recombinant protein folding and misfolding in *Escherichia coli*. *Nature Biotechnology* 22, 1399.
- Berg, J.M., Tymoczko, J.L., and Stryer, L. (2002). *Biochemistry* (New York: W H Freeman).
- De Bernardez Clark, E., Hevehan, D., Szela, S., and Maachupalli-Reddy, J. (1998). Oxidative Renaturation of Hen Egg-White Lysozyme. Folding vs Aggregation. *Biotechnology Progress* 14, 47–54.
- Beuselinck, L., Govers, G., Poesen, J., Degraer, G., and Froyen, L. (1998). Grain-size analysis by laser diffractometry: comparison with the sieve-pipette method. *CATENA* 32, 193–208.
- Bhatnagar, B.S., Bogner, R.H., and Pikal, M.J. (2007). Protein Stability During Freezing: Separation of Stresses and Mechanisms of Protein Stabilization. *Pharmaceutical Development and Technology* 12, 505–523.
- Bhattacharya, S.K., and Dubey, A.K. (1997). Effects of dissolved oxygen and oxygen mass transfer on overexpression of target gene in recombinant *E. coli*. *Enzyme and Microbial Technology* 20, 355–360.
- Bolin, J.T., Filman, D.J., Matthews, D.A., Hamlin, R.C., and Kraut, J. (1982). Crystal Structures of *Escherichia Coli* and *Lactobacillus Casei* Dihydrofolate Reductase Refined at 1.7 Å Resolution. I. General Features and Binding of Methotrexate. *J. Biol. Chem.* 257, 13650–13662.
- Bowden, G.A., and Georgiou, G. (1990). Folding and aggregation of beta-lactamase in the periplasmic space of *Escherichia coli*. *The Journal of Biological Chemistry* 265, 16760.
- Bratbak, G., and Dundas, I. (1984). Bacterial dry matter content and biomass estimations. *Appl Environ Microbiol* 48, 755–757.
- Broeze, R.J., Solomon, C.J., and Pope, D.H. (1978). Effects of low temperature on in vivo and in vitro protein synthesis in *Escherichia coli* and *Pseudomonas fluorescens*. *Journal of Bacteriology* 134, 861–874.

- Buchwalder, A., Szadkowski, H., and Kirschner, K. (1992). A fully active variant of dihydrofolate reductase with a circularly permuted sequence. *Biochemistry* 31, 1621–1630.
- Buckle, A.M., Devlin, G.L., Jodun, R.A., Fulton, K.F., Faux, N., Whisstock, J.C., and Bottomley, S.P. (2005). The matrix refolded. *Nature Methods* 2, 3–3.
- Buswell, A.M., and Middelberg, A.P.J. (2002). Critical Analysis of Lysozyme Refolding Kinetics. *Biotechnology Progress* 18, 470–475.
- Buswell, A.M., and Middelberg, A.P.J. (2003). A new kinetic scheme for lysozyme refolding and aggregation. *Biotechnology and Bioengineering* 83, 567–577.
- Buswell, M.A., Ebtinger, M., Vertés, A.A., and Middelberg, A.P.J. (2002). Effect of operating variables on the yield of recombinant trypsinogen for a pulse-fed dilution-refolding reactor. *Biotechnology and Bioengineering* 77, 435–444.
- Carrió, M., González-Montalbán, N., Vera, A., Villaverde, A., and Ventura, S. (2005). Amyloid-like Properties of Bacterial Inclusion Bodies. *Journal of Molecular Biology* 347, 1025–1037.
- Carrió, M., and Villaverde, A. (2002). Construction and deconstruction of bacterial inclusion bodies. *Journal of Biotechnology* 96, 3–12.
- Carrió, M.M., Corchero, J.L., and Villaverde, A. (2006). Dynamics of in vivo protein aggregation: building inclusion bodies in recombinant bacteria. *FEMS Microbiology Letters* 169, 9–15.
- Carrió, M.M., Cubarsi, R., and Villaverde, A. (2000). Fine architecture of bacterial inclusion bodies. *FEBS Letters* 471, 7–11.
- Carrió, M.M., and Villaverde, A. (2001). Protein aggregation as bacterial inclusion bodies is reversible. *FEBS Letters* 489, 29–33.
- Chang, B.S., Kendrick, B.S., and Carpenter, J.F. (1996). Surface-induced denaturation of proteins during freezing and its inhibition by surfactants. *J Pharm Sci* 85, 1325–1330.
- Chiti, F., Taddei, N., White, P.M., Bucciantini, M., Magherini, F., Stefani, M., and Dobson, C.M. (1999). Mutational analysis of acylphosphatase suggests the importance of topology and contact order in protein folding. *Nature Structural & Molecular Biology* 6, 1005.
- Choi, J.H., Jeong, K.J., Kim, S.C., and Lee, S.Y. (2000). Efficient secretory production of alkaline phosphatase by high cell density culture of recombinant *Escherichia coli* using the *Bacillus* sp. endoxylanase signal sequence. *Appl. Microbiol. Biotechnol.* 53, 640–645.
- Clark, A.C., Hugo, E., and Frieden, C. (1996). Determination of Regions in the Dihydrofolate Reductase Structure That Interact with the Molecular Chaperonin GroEL†. *Biochemistry* 35, 5893–5901.

- Clark, D.P. (1989). The fermentation pathways of *Escherichia coli*. *FEMS Microbiology Letters* 63, 223–234.
- Clark, E.D.B. (2001). Protein refolding for industrial processes. *Current Opinion in Biotechnology* 12, 202–207.
- Clarke, P.R. (1970). Physical and Chemical Aspects of Ultrasonic Disruption of Cells. *The Journal of the Acoustical Society of America* 47, 649.
- Crommelin, D.J.A., Storm, G., Verrijck, R., De Leede, L., Jiskoot, W., and Hennink, W.E. (2003). Shifting paradigms: biopharmaceuticals versus low molecular weight drugs. *International Journal of Pharmaceutics* 266, 3–16.
- Cutayar, J.M., and Poillon, D. (1989). High cell density culture of *E. coli* in a fed-batch system with dissolved oxygen as substrate feed indicator. *Biotechnology letters* 11, 155–160.
- Davies, J.F., Delcamp, T.J., Prendergast, N.J., Ashford, V.A., Freisheim, J.H., and Kraut, J. (1990). Crystal structures of recombinant human dihydrofolate reductase complexed with folate and 5-deazafolate. *Biochemistry* 29, 9467–9479.
- Davies, R. (1959). Observations on the use of ultrasound waves for the disruption of micro-organisms. *Biochimica Et Biophysica Acta* 33, 481–493.
- Davies, R. (2009). Integrated recovery and refolding of protein inclusion bodies from *E.coli* in a vibrating membrane system.
- Dechavanne, V., Barrillat, N., Borlat, F., Hermant, A., Magneat, L., Paquet, M., Antonsson, B., and Chevalet, L. (2011). A high-throughput protein refolding screen in 96-well format combined with design of experiments to optimize the refolding conditions. *Protein Expression and Purification* 75, 192–203.
- Dharmadi, Y., Murarka, A., and Gonzalez, R. (2006). Anaerobic fermentation of glycerol by *Escherichia coli*: A new platform for metabolic engineering. *Biotechnology and Bioengineering* 94, 821–829.
- Dickson, M., and Gagnon, J.P. (2004). Key factors in the rising cost of new drug discovery and development. *Nature Reviews Drug Discovery* 3, 417.
- Dill, K.A., Ozkan, S.B., Shell, M.S., and Weikl, T.R. (2008). The Protein Folding Problem. *Annual Review of Biophysics* 37, 289–316.
- Dobson, C.M. (2004a). Experimental investigation of protein folding and misfolding. *Methods* 34, 4–14.
- Dobson, C.M. (2004b). Principles of protein folding, misfolding and aggregation. *Seminars in Cell & Developmental Biology* 15, 3–16.
- Dobson, C.M., Evans, P.A., and Radford, S.E. (1994). Understanding how proteins fold: the lysozyme story so far. *Trends in Biochemical Sciences* 19, 31–37.

- Dobson, C.M., Šali, A., and Karplus, M. (1998). Protein Folding: A Perspective from Theory and Experiment. *Angewandte Chemie International Edition* 37, 868–893.
- Doig, S.D., Pickering, S.C.R., Lye, G.J., and Baganz, F. (2005a). Modelling surface aeration rates in shaken microtitre plates using dimensionless groups. *Chemical Engineering Science* 60, 2741–2750.
- Doig, S.D., Pickering, S.C.R., Lye, G.J., and Baganz, F. (2005b). Modelling surface aeration rates in shaken microtitre plates using dimensionless groups. *Chemical Engineering Science* 60, 2741–2750.
- Doig, S.D., Pickering, S.C.R., Lye, G.J., and Woodley, J.M. (2002). The use of microscale processing technologies for quantification of biocatalytic Baeyer-Villiger oxidation kinetics. *Biotechnology and Bioengineering* 80, 42–49.
- Doulah, M.S. (1977). Mechanism of disintegration of biological cells in ultrasonic cavitation. *Biotechnology and Bioengineering* 19, 649–660.
- Duetz, W.A. (2007). Microtiter plates as mini-bioreactors: miniaturization of fermentation methods. *Trends in Microbiology* 15, 469–475.
- Duetz, W.A., Rüedi, L., Hermann, R., O’Connor, K., Büchs, J., and Witholt, B. (2000). Methods for Intense Aeration, Growth, Storage, and Replication of Bacterial Strains in Microtiter Plates. *Appl Environ Microbiol* 66, 2641–2646.
- Duetz W.A., and Witholt B. (2001). Effectiveness of orbital shaking for the aeration of suspended bacterial cultures in square-deepwell microtiter plates. *Biochemical Engineering Journal* 7, 113–115.
- Duetz, W.A., and Witholt, B. (2004). Oxygen transfer by orbital shaking of square vessels and deepwell microtiter plates of various dimensions. *Biochemical Engineering Journal* 17, 181–185.
- Eaton, W.A., Munoz, V., Thompson, P.A., Henry, E.R., and Hofrichter, J. Kinetics and dynamics of loops, alpha-helices, beta-hairpins, and fast-folding proteins. *Accounts of chemical research* 31, 745–753.
- Eiteman, M.A., and Altman, E. (2006a). Overcoming acetate in *Escherichia coli* recombinant protein fermentations. *Trends in Biotechnology* 24, 530–536.
- Eiteman, M.A., and Altman, E. (2006b). Overcoming acetate in *Escherichia coli* recombinant protein fermentations. *Trends in Biotechnology* 24, 530–536.
- Ejima, D., Ono, K., Tsumoto, K., Arakawa, T., and Eto, Y. (2006). A novel “reverse screening” to identify refolding additives for activin-A. *Protein Expression and Purification* 47, 45–51.
- Ellis, R.J., and Minton, A.P. (2003). Cell biology - Join the crowd. *Nature* 425, 27–28.

- Elmahdi, I., Baganz, F., Dixon, K., Harrop, T., Sugden, D., and Lye, G.. (2003). pH control in microwell fermentations of *S. erythraea* CA340: influence on biomass growth kinetics and erythromycin biosynthesis. *Biochemical Engineering Journal* 16, 299–310.
- Engler, C.R., and Robinson, C.W. (1981). Effects of organism type and growth conditions on cell disruption by impingement. *Biotechnology Letters* 3, 83–88.
- Eyles, S.J., Radford, S.E., Robinson, C.V., and Dobson, C.M. (1994). Kinetic Consequences of the Removal of a Disulfide Bridge on the Folding of Hen Lysozyme. *Biochemistry* 33, 13038–13048.
- Fahey, E., Chaudhuri, J., and Binding, P. (2000). Refolding of low molecular weight urokinase plasminogen activator by dilution and size exclusion chromatography - A comparative study. *Sep. Sci. Technol.* 35, 1743–1760.
- Fahnert, B., Lilie, H., and Neubauer, P. (2004a). Inclusion bodies: formation and utilisation. *Adv. Biochem. Eng. Biotechnol.* 89, 93–142.
- Fahnert, B., Lilie, H., and Neubauer, P. (2004b). Inclusion Bodies: Formation and Utilisation. In *Physiological Stress Responses in Bioprocesses*, (Springer Berlin / Heidelberg), pp. 93–142.
- Ferreira-Torres, C. (2008). Microscale process characterisation of oxidative conversions. University of London.
- Ferreira-Torres, C., Micheletti, M., and Lye, G.J. (2005). Microscale process evaluation of recombinant biocatalyst libraries: Application to Baeyer-Villiger monooxygenase catalysed lactone synthesis. *Bioprocess and Biosystems Engineering* 28, 83–93.
- Ferrer-Mirallas, N., Domingo-Espín, J., Corchero, J.L., Vázquez, E., and Villaverde, A. (2009). Microbial factories for recombinant pharmaceuticals. *Microbial Cell Factories* 8, 17.
- Fersht, A.R. (2000). Transition-State Structure as a Unifying Basis in Protein-Folding Mechanisms: Contact Order, Chain Topology, Stability, and the Extended Nucleus Mechanism. *PNAS* 97, 1525–1529.
- Fieschko, J., Ritch, T., Bengston, D., Fenton, D., and Mann, M. (1985). The Relationship Between Cell Dry Weight Concentration and Culture Turbidity For A Recombinant *E. Coli* K12 Strain Producing High Levels of Human Alpha Interferon Analogue. *Biotechnology Progress* 1, 205–208.
- Fink, A.L. (1998). Protein aggregation: folding aggregates, inclusion bodies and amyloid. *Folding and Design* 3, R9–R23.
- Fischer, B., Sumner, I., and Goodenough, P. (1993). Isolation, renaturation, and formation of disulfide bonds of eukaryotic proteins expressed in *Escherichia coli* as inclusion bodies. *Biotechnology and Bioengineering* 41, 3–13.

Flickinger, M.C., and Rouse, M.P. (1993). Sustaining protein synthesis in the absence of rapid cell division: An investigation of plasmid-encoded protein expression in *Escherichia coli* during very slow growth. *Biotechnol. Prog.* 9, 555–572.

Frantz, S. (2004). Leaving the bench for the clinic. *Nature Reviews Drug Discovery* 3, 371.

Funke, M., Buchenauer, A., Schnakenberg, U., Mokwa, W., Diederichs, S., Mertens, A., Müller, C., Kensy, F., and Büchs, J. (2010). Microfluidic biolector—microfluidic bioprocess control in microtiter plates. *Biotechnology and Bioengineering* 107, 497–505.

Georgiou, G., Telford, J.N., Shuler, M.L., and Wilson, D.B. (1986). Localization of Inclusion Bodies in *Escherichia Coli* Overproducing Beta-Lactamase or Alkaline Phosphatase. *Appl. Environ. Microbiol.* 52, 1157–1161.

Gerami, S.M., Farajnia, S., Mahboudi, F., and Babaei, H. (2011). Optimizing refolding condition for recombinant tissue plasminogen activator. *IRANIAN JOURNAL of BIOTECHNOLOGY* 9,.

Gogate, P.R., Beenackers, A.A.C., and Pandit, A.B. (2000). Multiple-impeller systems with a special emphasis on bioreactors: a critical review. *Biochemical Engineering Journal* 6, 109–144.

Goldberg, M.E., and Guillou, Y. (1994). Native disulfide bonds greatly accelerate secondary structure formation in the folding of lysozyme. *Protein Science* 3, 883–887.

Goldberg, M.E., Rudolph, R., and Jaenicke, R. (1991). A kinetic study of the competition between renaturation and aggregation during the refolding of denatured-reduced egg white lysozyme. *Biochemistry* 30, 2790–2797.

Grant, Y., Matejtschuk, P., and Dalby, P.A. (2009). Rapid optimization of protein freeze-drying formulations using ultra scale-down and factorial design of experiment in microplates. *Biotechnology and Bioengineering* 104, 957–964.

Gu, Z., Zhu, X., Ni, S., Su, Z., and Zhou, H.-M. (2004). Conformational changes of lysozyme refolding intermediates and implications for aggregation and renaturation. *The International Journal of Biochemistry & Cell Biology* 36, 795–805.

Guise, A.D., and Chaudhuri, J.B. (2001). Initial protein concentration and residual denaturant concentration strongly affect the batch refolding of hen egg white lysozyme. *Biotechnology and Bioprocess Engineering* 6, 410–418.

Heath, W.F., Belagaje, R.M., Brooke, G.S., Chance, R.E., Hoffmann, J.A., Long, H.B., Reams, S.G., Roundtree, C., Shaw, W.N., and Sliker, L.J. (1992). (A-C-B) Human Proinsulin, a Novel Insulin Agonist and Intermediate in the Synthesis of Biosynthetic Human Insulin. *J. Biol. Chem.* 267, 419–425.

Hermann, R., Lehmann, M., and Büchs, J. (2003). Characterization of gas–liquid mass transfer phenomena in microtiter plates. *Biotechnology and Bioengineering* 81, 178–186.

Hevehan, D.L., and De Bernardez Clark, E. (1997). Oxidative renaturation of lysozyme at high concentrations. *Biotechnology and Bioengineering* 54, 221–230.

Hua, Q.-X., Nakagawa, S.H., Jia, W., Hu, S.-Q., Chu, Y.-C., Katsoyannis, P.G., and Weiss, M.A. (2001). Hierarchical Protein Folding: Asymmetric Unfolding of an Insulin Analogue Lacking the A7–B7 Interchain Disulfide Bridge†. *Biochemistry* 40, 12299–12311.

Islam, R.S. (2007). Novel engineering tools to aid drug discovery processes. University of London.

Islam, R.S., Tisi, D., Levy, M.S., and Lye, G.J. (2008). Scale-up of *Escherichia coli* growth and recombinant protein expression conditions from microwell to laboratory and pilot scale based on matched kLa. *Biotechnology and Bioengineering* 99, 1128–1139.

Jackson, N.B., Liddell, J.M., and Lye, G.J. (2006). An automated microscale technique for the quantitative and parallel analysis of microfiltration operations. *Journal of Membrane Science* 276, 31–41.

Jensen, E.B., and Carlsen, S. (1990). Production of recombinant human growth hormone in *Escherichia coli*: Expression of different precursors and physiological effects of glucose, acetate, and salts. *Biotechnology and Bioengineering* 36, 1–11.

Jiang, S., and Nail, S.L. (1998). Effect of process conditions on recovery of protein activity after freezing and freeze-drying. *European Journal of Pharmaceutics and Biopharmaceutics* 45, 249–257.

John, G.T., Klimant, I., Wittmann, C., and Heinzle, E. (2003). Integrated optical sensing of dissolved oxygen in microtiter plates: A novel tool for microbial cultivation. *Biotechnology and Bioengineering* 81, 829–836.

Johnson, C.W.J. (1990). Protein secondary structure and circular dichroism: A practical guide. *Proteins: Structure, Function, and Bioinformatics* 7, 205–214.

Jones, P.G., VanBogelen, R.A., and Neidhardt, F.C. (1987). Induction of proteins in response to low temperature in *Escherichia coli*. *Journal of Bacteriology* 169, 2092 – 2095.

Jungbauer, A., Kaar, W., and Schlegl, R. (2004). Folding and refolding of proteins in chromatographic beds. *Current Opinion in Biotechnology* 15, 487–494.

Kane, J.F., and Hartley, D.L. (1988). Formation of recombinant protein inclusion bodies in *Escherichia coli*. *Trends in Biotechnology* 6, 95–101.

Kapur, R., Giuliano, K.A., Campana, M., Adams, T., Olson, K., Jung, D., Mrksich, M., Vasudevan, C., and Taylor, D.L. (1999). Streamlining the Drug Discovery Process by Integrating Miniaturization, High Throughput Screening, High Content Screening, and Automation on the CellChip™ System. *Biomedical Microdevices* 2, 99–109.

Katoh, S., and Katoh, Y. (2000). Continuous refolding of lysozyme with fed-batch addition of denatured protein solution. *Process Biochemistry* 35, 1119–1124.

- Katoh, S., Sezai, Y., Yamaguchi, T., Katoh, Y., Yagi, H., and Nohara, D. (1999). Refolding of enzymes in a fed-batch operation. *Process Biochemistry* 35, 297–300.
- Khan, F., Chuang, J.I., Gianni, S., and Fersht, A.R. (2003). The kinetic pathway of folding of barnase. *J. Mol. Biol.* 333, 169–186.
- Khan, R.H., Rao, K.B.C.A., Eshwari, A.N.S., Totey, S.M., and Panda, A.K. (1998). Solubilization of Recombinant Ovine Growth Hormone with Retention of Native-like Secondary Structure and Its Refolding from the Inclusion Bodies of *Escherichia coli*. *Biotechnology Progress* 14, 722–728.
- Kiefhaber, T. (1995). Kinetic traps in lysozyme folding. *PNAS* 92, 9029–9033.
- Kiefhaber, T., Rudolph, R., Kohler, H.-H., and Buchner, J. (1991). Protein Aggregation in vitro and in vivo: A Quantitative Model of the Kinetic Competition between Folding and Aggregation. *Nature Biotechnology* 9, 825.
- Kim, S., and Lee, Y.I. (1996). High-level expression and simple purification of recombinant human insulin-like growth factor I. *Journal of Biotechnology* 48, 97–105.
- Kolaj, O., Spada, S., Robin, S., and Wall, J.G. (2009). Use of folding modulators to improve heterologous protein production in *Escherichia coli*. *Microbial Cell Factories* 8, 9.
- Kopito, R.R. (2000). Aggresomes, inclusion bodies and protein aggregation. *Trends in Cell Biology* 10, 524–530.
- Kosinski, M.J., Rinas, U., and Bailey, J.E. (1992). Isopropyl- β -D-thiogalactopyranoside influences the metabolism of *Escherichia coli*. *Applied microbiology and biotechnology* 36, 782–784.
- Lander, R., Daniels, C., and Meacle, F. (2005). Efficient, Scalable Clarification of Diverse Bioprocess Streams. *BioProcess International* 32–40.
- Landwall, P., and Holme, T. (1977). Influence of Glucose and Dissolved Oxygen Concentrations on Yields of *Escherichia coli* B in Dialysis Culture. *J Gen Microbiol* 103, 353–358.
- Lasko, D.R., Zamboni, N., and Sauer, U. (2000). Bacterial response to acetate challenge: a comparison of tolerance among species. *Applied Microbiology and Biotechnology* 54, 243–247.
- Lebaron, P., Catala, P., and Parthuisot, N. (1998). Effectiveness of SYTOX Green Stain for Bacterial Viability Assessment. *Applied and Environmental Microbiology* 64, 2697–2700.
- Lee, C.T., Buswell, A.M., and Middelberg, A.P.J. (2002). The influence of mixing on lysozyme renaturation during refolding in an oscillatory flow and a stirred-tank reactor. *Chemical Engineering Science* 57, 1679–1684.

- Lee, S.Y. (1996). High cell-density culture of *Escherichia coli*. *Trends in Biotechnology* 14, 98–105.
- Lewis, G., Taylor, I., Nienow, A., and Hewitt, C. (2004). The application of multi-parameter flow cytometry to the study of recombinant *Escherichia coli* batch fermentation processes. *Journal of Industrial Microbiology & Biotechnology* 31,.
- Li, M., Su, Z.-G., and Janson, J.-C. (2004). In vitro protein refolding by chromatographic procedures. *Protein Expression and Purification* 33, 1–10.
- Li, X., Robbins, J.W., and Taylor, K.B. (1992). Effect of the levels of dissolved oxygen on the expression of recombinant proteins in four recombinant *Escherichia coli* strains. *Journal of Industrial Microbiology & Biotechnology* 9, 1–9.
- Lilie, Schwarz E., and Rudolph R. (1998). Advances in refolding of proteins produced in *E. coli*. *Current Opinion in Biotechnology* 9, 497–501.
- Linek, V., Kordac, M., Fujasova, M., and Moucha, T. (2004). Gas-liquid mass transfer coefficient in stirred tanks interpreted through models of idealized eddy structure of turbulence in the bubble vicinity. *Chemical engineering and processing* 43, 1511–1517.
- Lischke, H.H., BRANDES, L., WU, X., and SCHÜGERL, K. (1993). Influence of acetate on the growth of recombinant *Escherichia coli* JM103 and product formation. *Bioprocess engineering* 9, 155–157.
- Liu, M., Wan, Z., Chu, Y.-C., Aladdin, H., Klaproth, B., Choquette, M., Hua, Q., Mackin, R.B., Rao, J.S., De Meyts, P., et al. (2009). Crystal Structure of a “Nonfoldable” Insulin. *J Biol Chem* 284, 35259–35272.
- Lorimer, G.H. (1996). A Quantitative Assessment of the Role of the Chaperonin Proteins in Protein Folding in Vivo. *FASEB J* 10, 5–9.
- Lugtenberg, B., Meijers, J., Peters, R., Hoek, P. van der, and Alphen, L. van (1975). Electrophoretic resolution of the “major outer membrane protein” of *Escherichia coli* K12 into four bands. *FEBS Letters* 58, 254–258.
- Luli, G.W., and Strohl, W.R. (1990). Comparison of growth, acetate production, and acetate inhibition of *Escherichia coli* strains in batch and fed-batch fermentations. *Appl. Environ. Microbiol.* 56, 1004–1011.
- Lye, G.J., Ayazi-Shamlou, P., Baganz, F., Dalby, P.A., and Woodley, J.M. (2003). Accelerated design of bioconversion processes using automated microscale processing techniques. *Trends in Biotechnology* 21, 29–37.
- Ma, Z., Merkus, H.G., De Smet, J.G.A., Heffels, C., and Scarlett, B. (2000). New developments in particle characterization by laser diffraction: size and shape. *Powder Technology* 111, 66–78.
- Maachupalli-Reddy, J., Kelley, B.D., and Clark, E.D.B. (1997). Effect of Inclusion Body Contaminants on the Oxidative Renaturation of Hen Egg White Lysozyme. *Biotechnology Progress* 13, 144–150.

- Major, J. (1998). Challenges and Opportunities in High Throughput Screening: Implications for New Technologies. *J Biomol Screen* 3, 13–17.
- Makrides, S.C. (1996). Strategies for achieving high-level expression of genes in *Escherichia coli*. *Microbiological Reviews* 60, 512–538.
- Mannall, G.J., Myers, J.P., Liddell, J., Titchener-Hooker, N.J., and Dalby, P.A. (2009). Ultra scale-down of protein refold screening in microwells: Challenges, solutions and application. *Biotechnology and Bioengineering* 103, 329–340.
- Mannall, G.J., Titchener-Hooker, N.J., Chase, H.A., and Dalby, P.A. (2006). A critical assessment of the impact of mixing on dilution refolding. *Biotechnology and Bioengineering* 93, 955–963.
- Mannall, G.J., Titchener-Hooker, N.J., and Dalby, P.A. (2007). Factors affecting protein refolding yields in a fed-batch and batch-refolding system. *Biotechnology and Bioengineering* 97, 1523–1534.
- Marco, A. de (2007). Protocol for preparing proteins with improved solubility by co-expressing with molecular chaperones in *Escherichia coli*. *Nature Protocols* 2, 2632.
- Martínez-Alonso, M., González-Montalbán, N., García-Fruitós, E., and Villaverde, A. (2009). Learning about protein solubility from bacterial inclusion bodies. *Microb Cell Fact* 8, 4.
- Matagne, A., and Dobson, C.M. (1998). The folding process of hen lysozyme: a perspective from the “new view”. *Cellular and Molecular Life Sciences* 54, 363–371.
- Matagne, A., Radford, S.E., and Dobson, C.M. (1997). Fast and slow tracks in lysozyme folding: insight into the role of domains in the folding process. *Journal of Molecular Biology* 267, 1068–1074.
- Mayor, U., Guydosh, N.R., Johnson, C.M., Grossmann, J.G., Sato, S., Jas, G.S., Freund, S.M.V., Alonso, D.O.V., Daggett, V., and Fersht, A.R. (2003). The complete folding pathway of a protein from nanoseconds to microseconds. *Nature* 421, 863.
- Medwid, R.D., Krebs, L., and Welch, S. (2007). Evaluation of *Escherichia coli* cell disruption and inclusion body release using nucleic acid binding fluorochromes and flow cytometry. *BioTechniques* 43, 777–782.
- Micheletti, M., Barrett, T., Doig, S.D., Baganz, F., Levy, M.S., Woodley, J.M., and Lye, G.J. (2006). Fluid mixing in shaken bioreactors: Implications for scale-up predictions from microlitre-scale microbial and mammalian cell cultures. *Chemical Engineering Science* 61, 2939–2949.
- Micheletti, M., and Lye, G.J. (2006). Microscale bioprocess optimisation. *Current Opinion in Biotechnology* 17, 611–618.
- Middelberg, A.P.. (2002). Preparative protein refolding. *Trends in Biotechnology* 20, 437–443.

- Millard, P., Roth, B., Yue, S., Poot, M., and Jones, L. (1995). Determination of bacterial viability with SYTOX, a bright green 488 nm-excitable nucleic acid stain. In *Abstr. Gen. Meet. Am. Soc. Microbiol.*, p. 477.
- Miot, M., and Betton, J.-M. (2004). Protein quality control in the bacterial periplasm. *Microbial Cell Factories* 3, 4.
- Miranker, A., Radford, S.E., Karplus, M., and Dobson, C.M. (1991). Demonstration by NMR of folding domains in lysozyme. *349*, 633.
- Murarka, A., Dharmadi, Y., Yazdani, S.S., and Gonzalez, R. (2008). Fermentative Utilization of Glycerol by *Escherichia Coli* and Its Implications for the Production of Fuels and Chemicals. *Appl. Environ. Microbiol.* 74, 1124–1135.
- Nealon, A.J., O’Kennedy, R.D., Titchener-Hooker, N.J., and Lye, G.J. (2006). Quantification and prediction of jet macro-mixing times in static microwell plates. *Chemical Engineering Science* 61, 4860–4870.
- Nealon, A.J., Willson, K.E., Pickering, S.C.R., Clayton, T.M., O’Kennedy, R.D., Titchener-Hooker, N.J., and Lye, G.J. (2005). Use of Operating Windows in the Assessment of Integrated Robotic Systems for the Measurement of Bioprocess Kinetics. *Biotechnology Progress* 21, 283–291.
- Oberg, K., Chrnyk, B.A., Wetzel, R., and Fink, A.L. (1994). Native-like Secondary Structure in Interleukin-1.β Inclusion Bodies by Attenuated Total Reflectance FTIR. *Biochemistry* 33, 2628–2634.
- Oldshue, J.Y. (1966). Fermentation mixing scale-up techniques, Fermentation mixing scale-up techniques. *Biotechnology and Bioengineering, Biotechnology and Bioengineering* 8, 8, 3, 3–24, 24.
- Pace, C.N., and Laurents, D.V. (1989). A new method for determining the heat capacity change for protein folding. *Biochemistry* 28, 2520–2525.
- Pace, C.N., Vajdos, F., Fee, L., Grimsley, G., and Gray, T. (1995). How to measure and predict the molar absorption coefficient of a protein. *Protein Science* 4, 2411–2423.
- Panchenko, A.R., Luthey-Schulten, Z., and Wolynes, P.G. (1996). Foldons, Protein Structural Modules, and Exons. *PNAS* 93, 2008–2013.
- Panda, A.K. (2003). Bioprocessing of Therapeutic Proteins from the Inclusion Bodies of *Escherichia coli*. In *Biotechnology in India II*, T.K. Ghose, P. Ghosh, S. Chand, S.K. Gupta, B.B. Lohray, K. Mazumdar-Shaw, P. Mishra, S. Nath, A.K. Panda, and S. Suryanarayan, eds. (Berlin, Heidelberg: Springer Berlin Heidelberg), pp. 43–93.
- Perez-Pardo, M.A., Ali, S., Balasundaram, B., Mannall, G.J., Baganz, F., and Bracewell, D.G. (2011). Assessment of the manufacturability of *Escherichia coli* high cell density fermentations. *Biotechnology Progress* 27, 1488–1496.
- Przybycien, T.M., Dunn, J.P., Valax, P., and Georgiou, G. (1994). Secondary Structure Characterization of β-Lactamase Inclusion Bodies. *Protein Eng.* 7, 131–136.

- Puskeiler, R., Kaufmann, K., and Weuster-Botz, D. (2005). Development, parallelization, and automation of a gas-inducing milliliter-scale bioreactor for high-throughput bioprocess design (HTBD). *Biotechnology and Bioengineering* 89, 512–523.
- Puthli, M.S., Rathod, V.K., and Pandit, A.B. (2005). Gas–liquid mass transfer studies with triple impeller system on a laboratory scale bioreactor. *Biochemical Engineering Journal* 23, 25–30.
- Qiao, Z.-S., Guo, Z.-Y., and Feng, Y.-M. (2001). Putative Disulfide-Forming Pathway of Porcine Insulin Precursor during Its Refolding in Vitro†. *Biochemistry* 40, 2662–2668.
- Qoronfleh, M. (1999). Dissolved oxygen concentration affects the accumulation of HIV-1 recombinant proteins in *Escherichia coli*. *Applied Biochemistry and Biotechnology* 80, 107–120.
- Radford, S.E., Buck, M., Topping, K.D., Dobson, C.M., and Evans, P.A. (1992a). Hydrogen exchange in native and denatured states of hen egg-white lysozyme. *Proteins: Structure, Function, and Bioinformatics* 14, 237–248.
- Radford, S.E., and Dobson, C.M. (1995). Insights into Protein Folding Using Physical Techniques: Studies of Lysozyme and α -lactalbumin. *Philosophical Transactions: Biological Sciences* 348, 17–25.
- Radford, S.E., Dobson, C.M., and Evans, P.A. (1992b). The folding of hen lysozyme involves partially structured intermediates and multiple pathways. 358, 302.
- Raman, B., Ramakrishna, T., and Rao, C.M. (1996). Refolding of Denatured and Denatured/Reduced Lysozyme at High Concentrations. *J. Biol. Chem.* 271, 17067–17072.
- Rathore, A.S., Branning, R., and Cecchini, D. (2007). Design space for biotech products. *Biopharm international* 20,.
- Rathore, A.S., and Winkle, H. (2009). Quality by design for biopharmaceuticals. *Nature Biotechnology* 27, 26–34.
- Rayat, A.C.M.. (2011). Microscale bioprocessing platform for the evaluation of membrane filtration processes for primary recovery.
- Rayat, A.C.M.E., Micheletti, M., and Lye, G.J. (2010). Evaluation of cell disruption effects on primary recovery of antibody fragments using microscale bioprocessing techniques. *Biotechnology Progress* 26, 1312–1321.
- Renard, D., Lefebvre, J., Griffin, M.C., and Griffin, W.. (1998). Effects of pH and salt environment on the association of β -lactoglobulin revealed by intrinsic fluorescence studies. *International Journal of Biological Macromolecules* 22, 41–49.

- Riesenberg, D., Menzel, K., Schulz, V., Schumann, K., Veith, G., Zuber, G., and Knorre, W. (1990). High cell density fermentation of recombinant *Escherichia coli* expressing human interferon alpha 1. *Applied Microbiology and Biotechnology* 34.
- Riesenberg, D., Schulz, V., Knorre, W.A., Pohl, H.-D., Korz, D., Sanders, E.A., Roß, A., and Deckwer, W.-D. (1991). High cell density cultivation of *Escherichia coli* at controlled specific growth rate. *Journal of Biotechnology* 20, 17–27.
- Rinas, U., Tsai, L.B., Lyons, D., Fox, G.M., Stearns, G., Fieschko, J., Fenton, D., and Bailey, J.E. (1992). Cysteine to serine substitutions in basic fibroblast growth factor: effect on inclusion body formation and proteolytic susceptibility during in vitro refolding. *Biotechnology (N.Y.)* 10, 435–440.
- Roth, B.L., Poot, M., Yue, S.T., and Millard, P.J. (1997). Bacterial viability and antibiotic susceptibility testing with SYTOX green nucleic acid stain. *Applied and Environmental Microbiology* 63, 2421–2431.
- Roux, P., Delepierre, M., Goldberg, M.E., and Chaffotte, A.-F. (1997). Kinetics of Secondary Structure Recovery during the Refolding of Reduced Hen Egg White Lysozyme. *J. Biol. Chem.* 272, 24843–24849.
- Rudolph, R., and Lilie, H. (1996). In vitro folding of inclusion body proteins. *FASEB J* 10, 49–56.
- Ryan, W., Collier, P., Lored, L., Pope, J., and Sachdev, R. (1996). Growth Kinetics of *Escherichia coli* and Expression of a Recombinant Protein and Its Isoforms under Heat Shock Conditions. *Biotechnology Progress* 12, 596–601.
- Schein, C.H., and Noteborn, M.H.M. (1988). Formation of Soluble Recombinant Proteins in *Escherichia coli* is Favored by Lower Growth Temperature. *Nature Biotechnology* 6, 291.
- Schellekens, H. (2002). Immunogenicity of therapeutic proteins: Clinical implications and future prospects. *Clinical Therapeutics* 24, 1720–1740.
- Seefeldt, M.B., Hesterberg, L.K., Randolph, T.W., and Carpenter, J.F. (2008). High-Pressure Refolding of Proteins in the Presence of Binding Partners.
- Shiloach, J., and Fass, R. (2005). Growing *E. coli* to high cell density—A historical perspective on method development. *Biotechnology Advances* 23, 345–357.
- Singh, S.M., and Panda, A.K. (2005). Solubilization and refolding of bacterial inclusion body proteins. *Journal of Bioscience and Bioengineering* 99, 303–310.
- Snow, C.D., Nguyen, H., Pande, V.S., and Gruebele, M. (2002). Absolute comparison of simulated and experimental protein-folding dynamics. *Nature* 420, 102–106.
- Speed, M.A., Wang, D.I.C., and King, J. (1996). Specific aggregation of partially folded polypeptide chains: The molecular basis of inclusion body composition. *Nature Biotechnology* 14, 1283.

Spiro, S., and Guest, J.R. (1991). Adaptive responses to oxygen limitation in *Escherichia coli*. *Trends in Biochemical Sciences* 16, 310–314.

Stammers, D.K., Champness, J.N., Beddell, C.R., Dann, J.G., Eliopoulos, E., Geddes, A.J., Ogg, D., and North, A.C.T. (1987). The structure of mouse L1210 dihydrofolate reductase-drug complexes and the construction of a model of human enzyme. *FEBS Letters* 218, 178–184.

Storti, F., and Balsamo, F. (2010). Particle size distributions by laser diffraction: sensitivity of granular matter strength to analytical operating procedures. *Solid Earth* 1, 25–48.

Strandberg, L., and Enfors, S.O. (1991). Factors influencing inclusion body formation in the production of a fused protein in *Escherichia coli*. *Appl Environ Microbiol* 57, 1669–1674.

Suhaili, N., Mohamed, M.S., Mohamad, R., and Ariff, A.B. (2010). Gas-liquid Mass Transfer Performance of Dual Impeller System Employing Rushtons , Concave-bladed Disc (CD-6) Turbines and Their Combination in Stirred Tank Bioreactor. *Journal of Applied Sciences Research* 6, 234–244.

Sundberg, S.A. (2000). High-throughput and ultra-high-throughput screening: solution- and cell-based approaches. *Current Opinion in Biotechnology* 11, 47–53.

Taylor, G., Hoare, M., Gray, D.R., and Marston, F. a. O. (1986a). Size and Density of Protein Inclusion Bodies. *Nature Biotechnology* 4, 553.

Taylor, G., Hoare, M., Gray, D.R., and Marston, F. a. O. (1986b). Size and Density of Protein Inclusion Bodies. *Nature Biotechnology* 4, 553–557.

Terashima, M., Suzuki, K., and Katoh, S. (1996). Effective refolding of fully reduced lysozyme with a flow-type reactor. *Process Biochemistry* 31, 341–345.

Thillet, J., Adams, J.A., and Benkovic, S.J. (1990). The kinetic mechanism of wild-type and mutant mouse dihydrofolate reductases. *Biochemistry* 29, 5195–5202.

Tissot, S., Farhat, M., Hacker, D.L., Anderlei, T., Kühner, M., Comninellis, C., and Wurm, F. (2010). Determination of a scale-up factor from mixing time studies in orbitally shaken bioreactors. *Biochemical Engineering Journal* 52, 181–186.

Titchener-Hooker, N.J., Dunnill, P., and Hoare, M. (2008). Micro biochemical engineering to accelerate the design of industrial-scale downstream processes for biopharmaceutical proteins. *Biotechnology and Bioengineering* 100, 473–487.

Treuheit, M.J., Kosky, A.A., and Brems, D.N. (2002). Inverse relationship of protein concentration and aggregation. *Pharm. Res.* 19, 511–516.

Tribe, L.A., Briens, C.L., Margaritis, A., Tribe, L.A., Briens, C.L., and Margaritis, A. (1995). Determination of the volumetric mass transfer coefficient (kLa) using the dynamic “gas out–gas in” method: Analysis of errors caused by dissolved oxygen probes, Determination of the volumetric mass transfer coefficient (kLa) using the

dynamic “gas out–gas in” method: Analysis of errors caused by dissolved oxygen probes. *Biotechnology and Bioengineering, Biotechnology and Bioengineering* 46, 46, 388, 388–392, 392.

Tustian, A.D., Salte, H., Willoughby, N.A., Hassan, I., Rose, M.H., Baganz, F., Hoare, M., and Titchener-Hooker, N.J. (2007). Adapted Ultra Scale-Down Approach for Predicting the Centrifugal Separation Behavior of High Cell Density Cultures. *Biotechnology Progress* 23, 1404–1410.

Uden, G., Becker, S., Bongaerts, J., Holighaus, G., Schirawski, J., and Six, S. (1995). O₂-Sensing and O₂-dependent gene regulation in facultatively anaerobic bacteria. *Archives of Microbiology* 164, 81–90.

Uversky, V.N., Protasova, N.Y., Rogov, V.V., Vassilenko, K.S., Gudkov, A.T., and Kutysenko, V.P. (1996). Circularly permuted dihydrofolate reductase possesses all the properties of the molten globule state, but can resume functional tertiary structure by interaction with its ligands. *Protein Science* 5, 1844–1851.

Valax, P., and Georgiou, G. (1993). Molecular Characterization of β -Lactamase Inclusion Bodies Produced in *Escherichia coli*. 1. Composition. *Biotechnology Progress* 9, 539–547.

Vallejo, L.F., and Rinas, U. (2004). Strategies for the recovery of active proteins through refolding of bacterial inclusion body proteins. *Microb Cell Fact* 3, 11.

Van’t Riet, K. (1979). Review of Measuring Methods and Results in Nonviscous Gas-Liquid Mass Transfer in Stirred Vessels. *Ind. Eng. Chem. Proc. Des. Dev.* 18, 357–364.

Vendruscolo, M., and Dobson, C.M. (2005). Towards Complete Descriptions of the Free-Energy Landscapes of Proteins. *Philosophical Transactions: Mathematical, Physical and Engineering Sciences* 363, 433–452.

Ventura, S. (2005). Sequence determinants of protein aggregation: tools to increase protein solubility. *Microbial Cell Factories* 4, 1–8.

Ventura, S., and Villaverde, A. (2006). Protein quality in bacterial inclusion bodies. *Trends in Biotechnology* 24, 179–185.

Vidugiris, G.J.A., Markley, J.L., and Royer, C.A. (1995). Evidence for a molten globule-like transition state in protein folding from determination of activation volumes. *Biochemistry* 34, 4909–4912.

Villaverde, A., and Carrió, M.M. (2003). Protein aggregation in recombinant bacteria: biological role of inclusion bodies. *Biotechnology Letters* 25, 1385–1395.

Vincentelli, R., Canaan, S., Campanacci, V., Valencia, C., Maurin, D., Frassinetti, F., Scappucini-Calvo, L., Bourne, Y., Cambillau, C., and Bignon, C. (2004). High-throughput automated refolding screening of inclusion bodies. *Protein Science* 13, 2782–2792.

Wacker, M., Linton, D., Hitchen, P.G., Nita-Lazar, M., Haslam, S.M., North, S.J., Panico, M., Morris, H.R., Dell, A., Wren, B.W., et al. (2002). N-Linked Glycosylation in *Campylobacter* Jejuni and Its Functional Transfer into *E. Coli*. *Science* 298, 1790–1793.

Wällberg, F., Sundström, H., Ledung, E., Hewitt, C.J., and Enfors, S.-O. (2005). Monitoring and quantification of inclusion body formation in *Escherichia coli* by multi-parameter flow cytometry. *Biotechnology Letters* 27, 919–926.

Walsh, G. (2004). Therapeutic insulins and their large-scale manufacture. *Applied Microbiology and Biotechnology* 67, 151–159.

Walsh, G. (2005). Biopharmaceuticals: recent approvals and likely directions. *Trends in Biotechnology* 23, 553–558.

Walsh, G., and Murphy, B. (1999). *Biopharmaceuticals, an industrial perspective* (Springer).

Wang, C., Castro, A.F., Wilkes, D.M., and Altenberg, G.A. (1999). Expression and purification of the first nucleotide-binding domain and linker region of human multidrug resistance gene product: comparison of fusions to glutathione S-transferase, thioredoxin and maltose-binding protein. *Biochem J* 338, 77–81.

Wen, Y., Zang, R., Zhang, X., and Yang, S.-T. (2012). A 24-microwell plate with improved mixing and scalable performance for high throughput cell cultures. *Process Biochemistry* 47, 612–618.

Wenger, M.D., DePhillips, P., and Bracewell, D.G. (2008). A Microscale Yeast Cell Disruption Technique for Integrated Process Development Strategies. *Biotechnology Progress* 24, 606–614.

Wenger, M.D., DePhillips, P., Price, C.E., and Bracewell, D.G. (2007). An automated microscale chromatographic purification of virus-like particles as a strategy for process development. *Biotechnology and Applied Biochemistry* 47, 131–139.

Werner, M.H., Clore, G.M., Gronenborn, A.M., Kondoh, A., and Fisher, R.J. (1994). Refolding proteins by gel filtration chromatography. *FEBS Letters* 345, 125–130.

Wierenga, P.A., Egmond, M.R., Voragen, A.G.J., and De Jongh, H.H.J. (2006). The adsorption and unfolding kinetics determines the folding state of proteins at the air-water interface and thereby the equation of state. *Journal of Colloid and Interface Science* 299, 850–857.

Wildegger, G., and Kiefhaber, T. (1997). Three-state model for lysozyme folding: triangular folding mechanism with an energetically trapped intermediate. *Journal of Molecular Biology* 270, 294–304.

Williams, D.C., Van Frank, R.M., Muth, W.L., and Burnett, J.P. (1982). Cytoplasmic inclusion bodies in *Escherichia coli* producing biosynthetic human insulin proteins. *Science* 215, 687–689.

Willis, M.S., Hogan, J.K., Prabhakar, P., Liu, X., Tsai, K., Wei, Y., and Fox, T. (2005). Investigation of protein refolding using a fractional factorial screen: A study of reagent effects and interactions. *Protein Science* *14*, 1818–1826.

Winter, J., Lilie, H., and Rudolph, R. (2002). Renaturation of human proinsulin—a study on refolding and conversion to insulin. *Analytical Biochemistry* *310*, 148–155.

Wong, H.H., O’neill, B.K., and Middelberg, A.P.J. (1996). Centrifugal processing of cell debris and inclusion bodies from recombinant *Escherichia coli*. *Bioseparation* *6*, 361–372.

Yan, H., Guo, Z.-Y., Gong, X.-W., Xi, D., and Feng, Y.-M. (2009). A peptide model of insulin folding intermediate with one disulfide. *Protein Science* *12*, 768–775.

Yang, W.Y., and Gruebele, M. (2003). Folding at the speed limit. *Nature* *423*, 193.

Zhang, H., Lamping, S.R., Pickering, S.C.R., Lye, G.J., and Shamlou, P.A. (2008). Engineering characterisation of a single well from 24-well and 96-well microtitre plates. *Biochemical Engineering Journal* *40*, 138–149.

9 Appendix

9.1 Appendix for Chapter 3

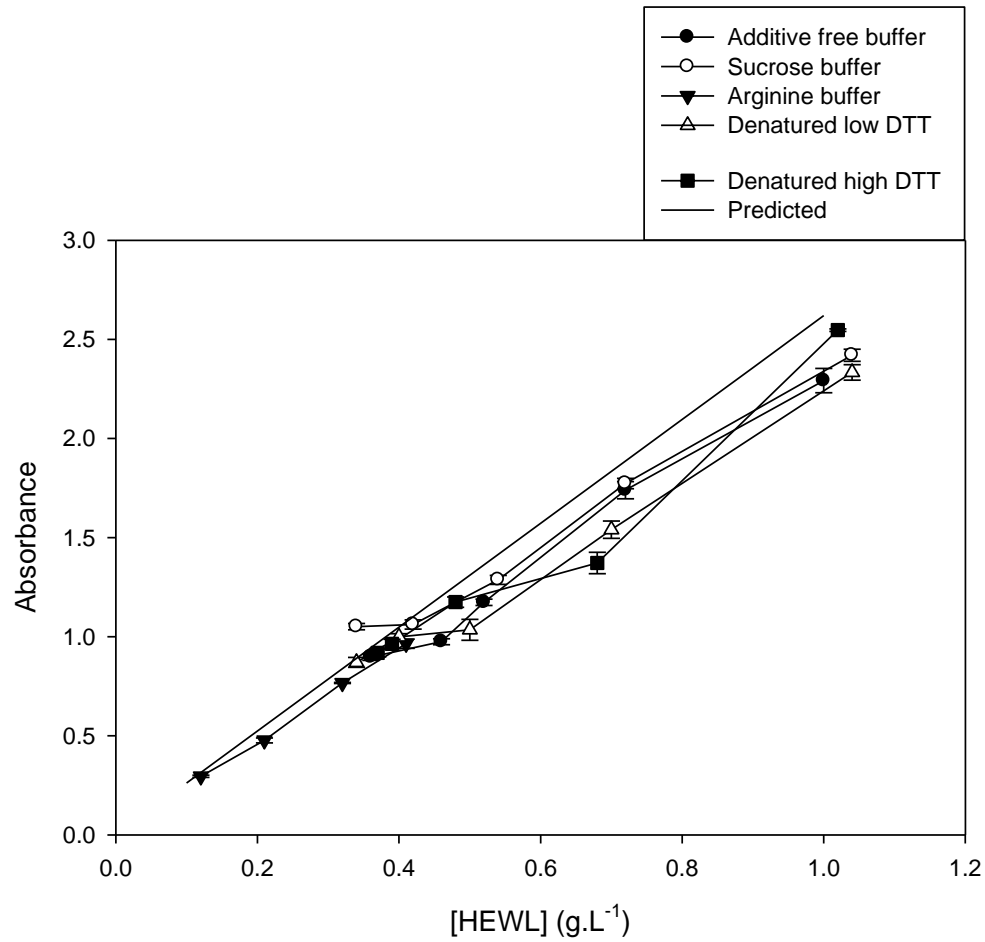


Figure 9.1 Absorbance of denatured and native protein in different buffers and at different concentrations

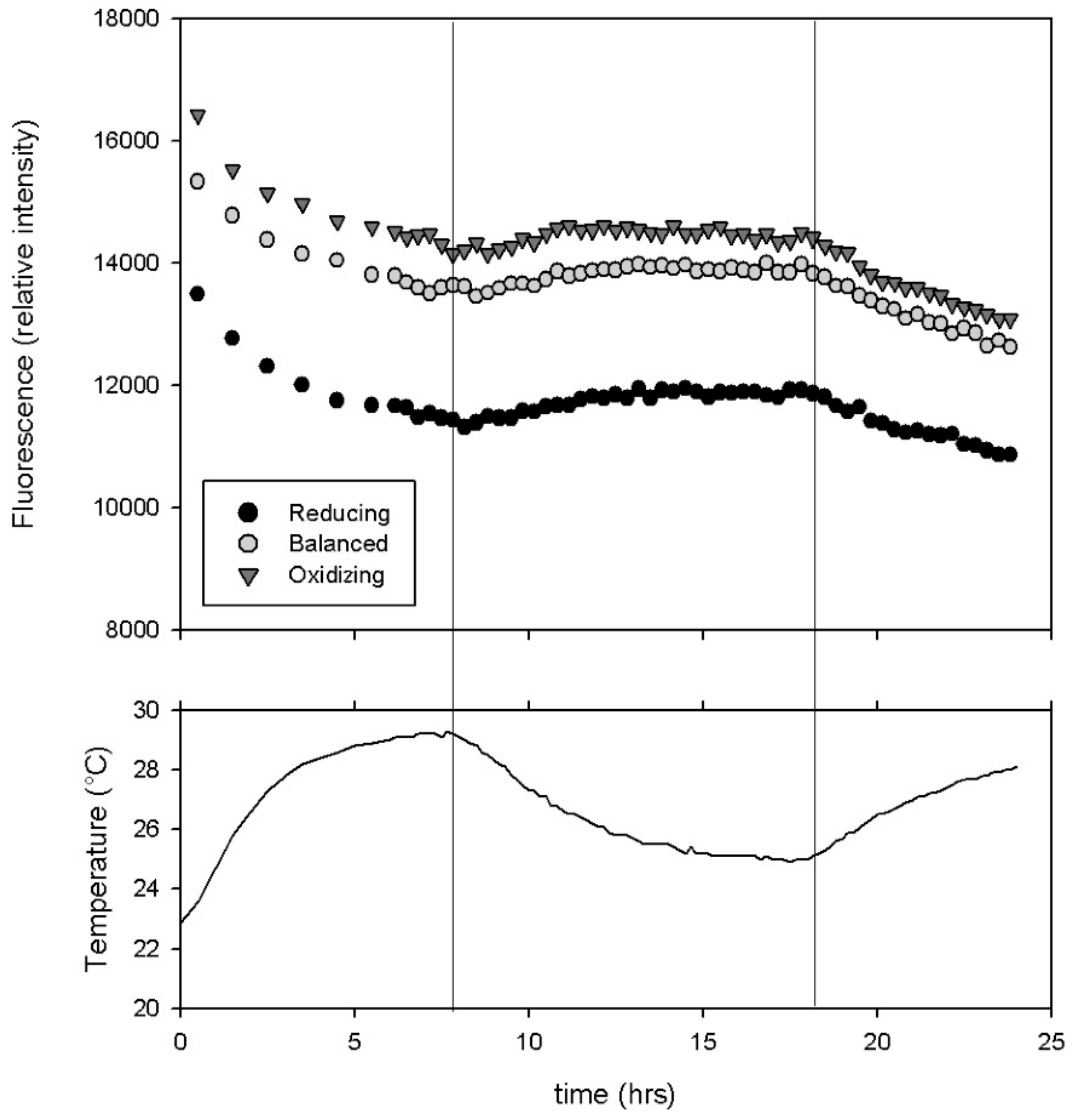


Figure .9.2 Fluorescence intensity fluctuations with temperature

9.2 Appendix for Chapter 4

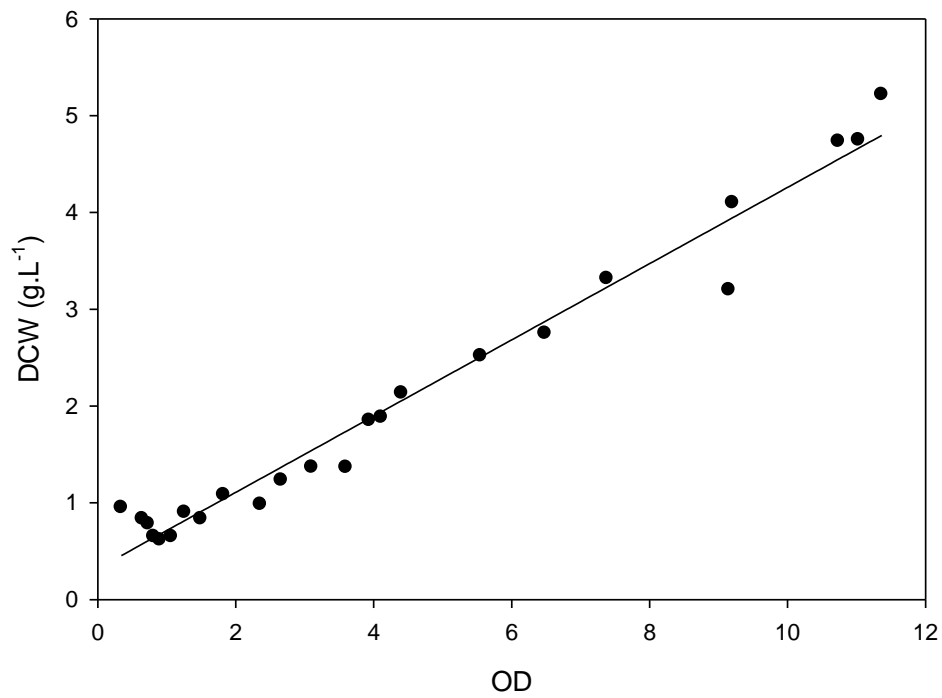


Figure 9.3 Calibration Curve for conversion between dry cell weight and OD. Best fit line: $y=0.394x+0.32$

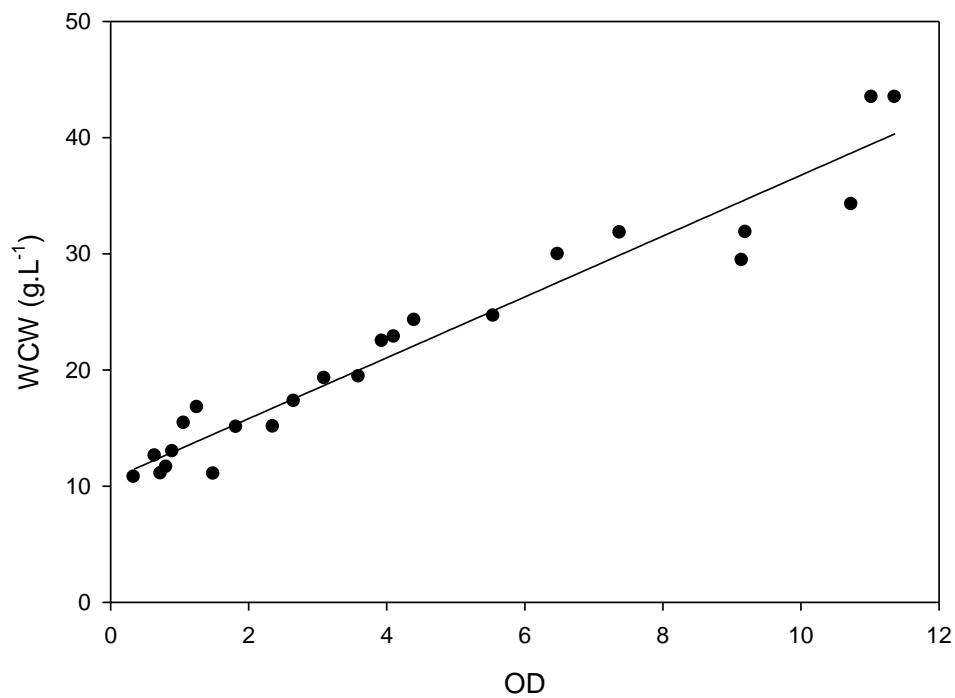


Figure 9.4 Calibration curve for conversion between wet cell weight and OD. Best fit line: $y=2.620x+10.566$

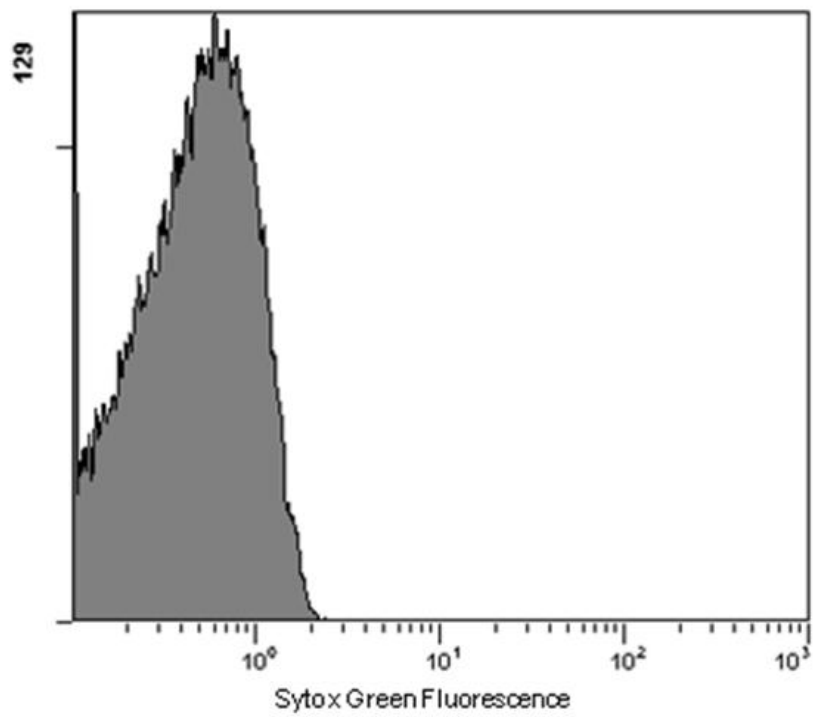


Figure 9.5 Relative fluorescence of unstained inclusion bodies determined using flow cytometry.

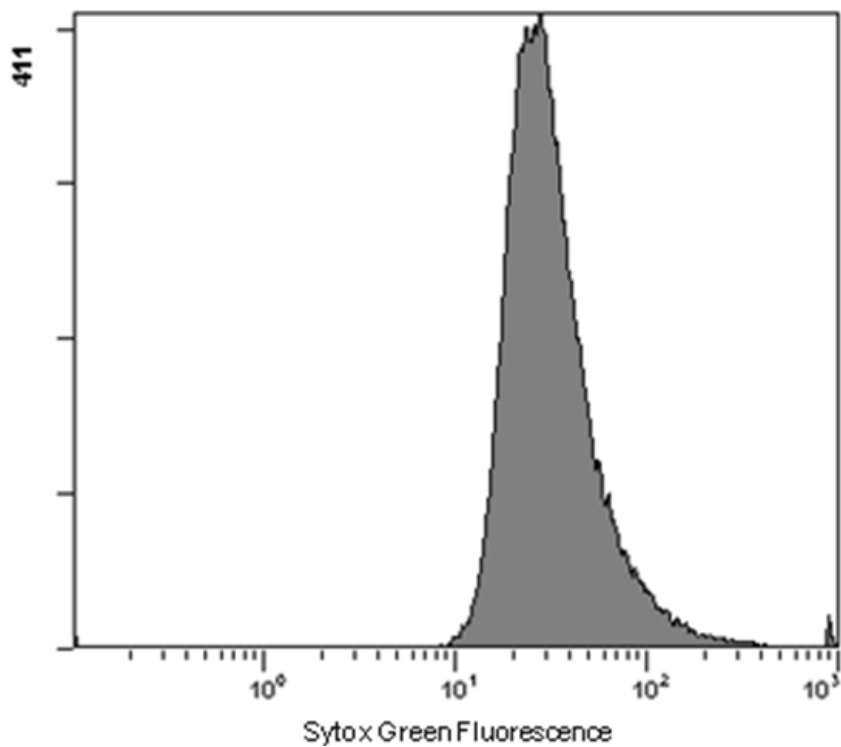


Figure 9.6 Relative fluorescence of stained inclusion bodies determined using flow cytometry.

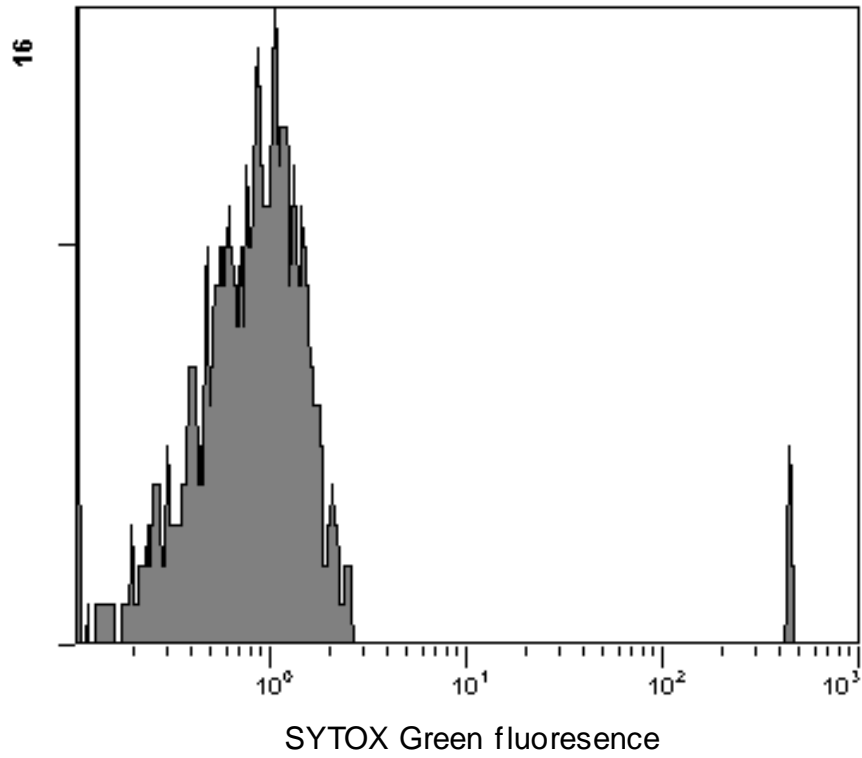


Figure 9.7 Relative fluorescence of unstained whole cells determined using flow cytometry.

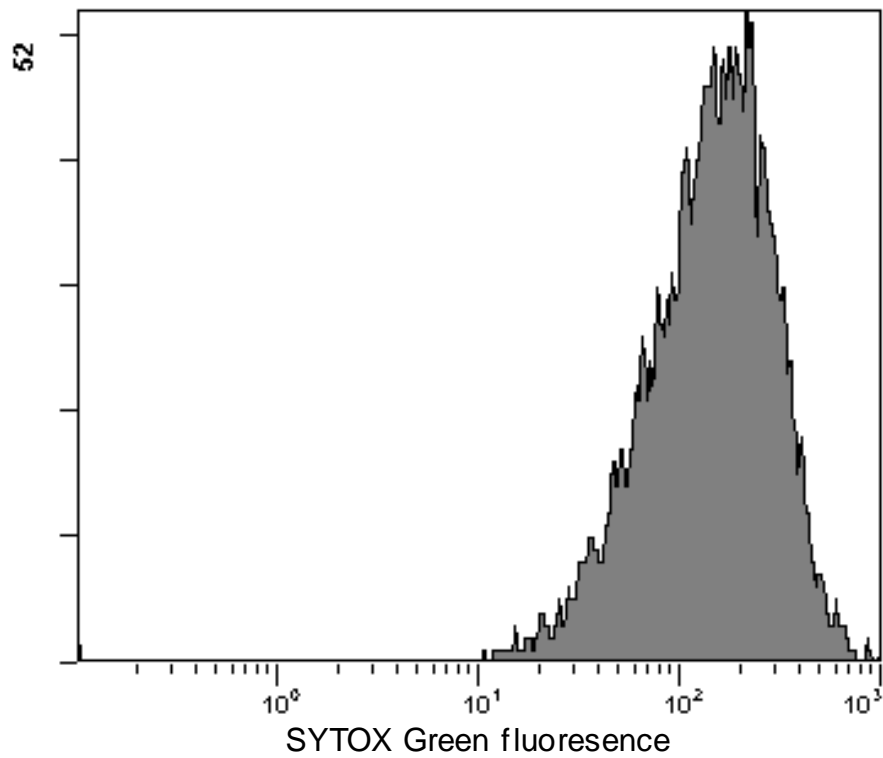
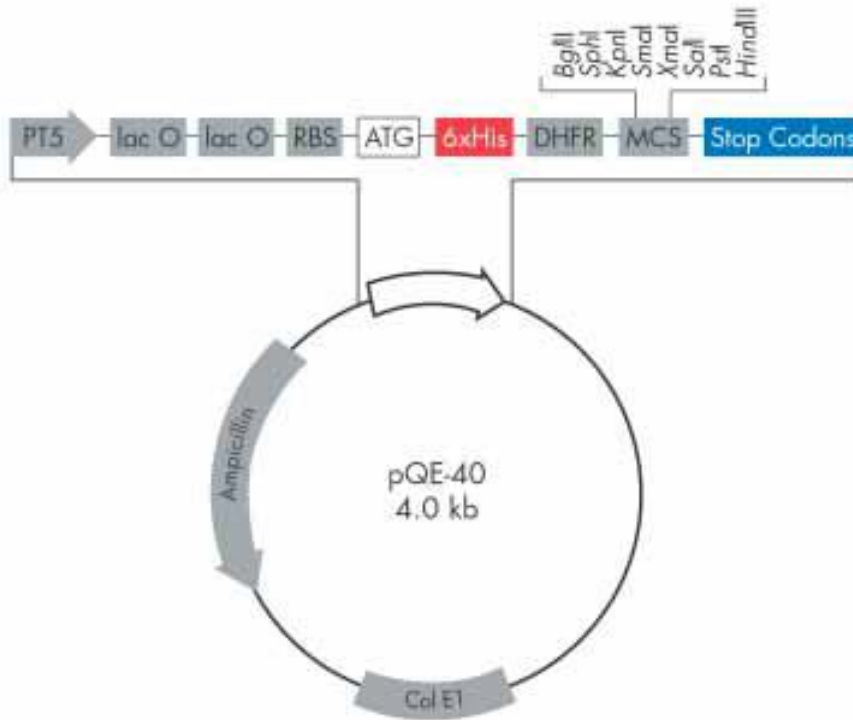


Figure 9.8 Relative fluorescence of stained whole cells determined using flow cytometry.

9.2.1 Plasmid Information

murine DHFR pQE-40

Molecular Weight	24.5 kDa
Isoelectric Point	9.2
Charge at pH 7.0	7.2



9.3 Appendix for Chapter 5

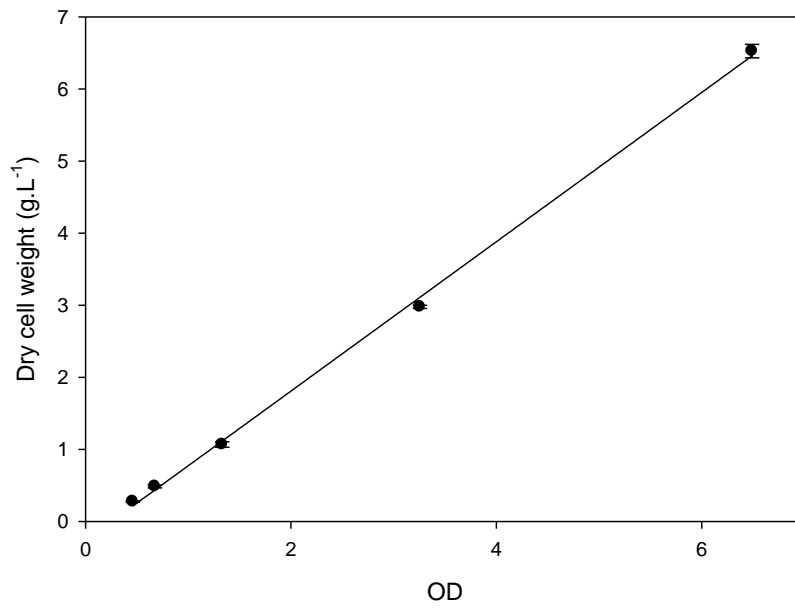
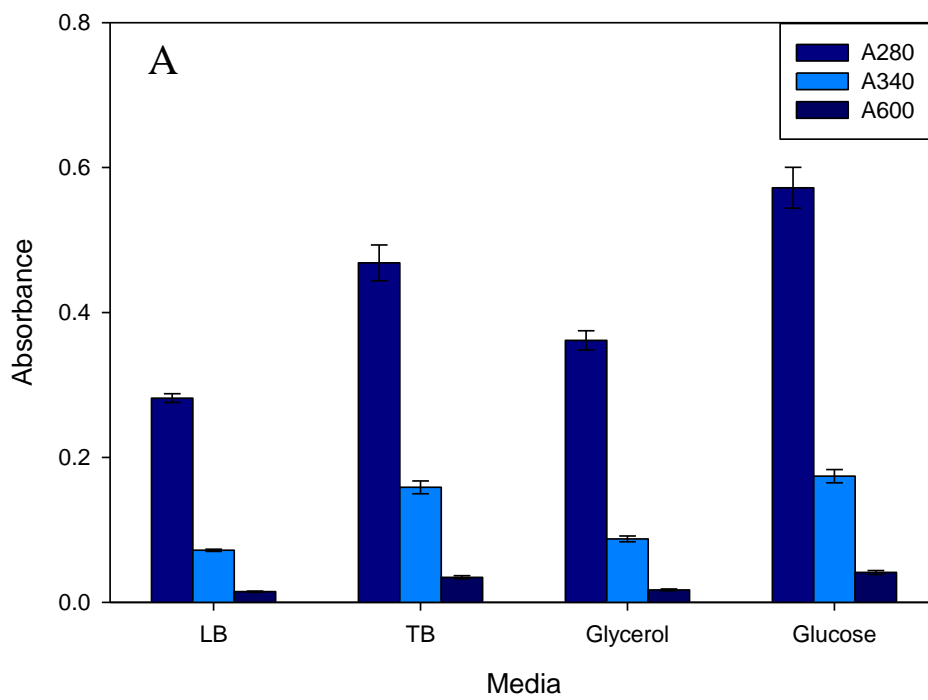


Figure 9.9 Dry cell weight calibration curve



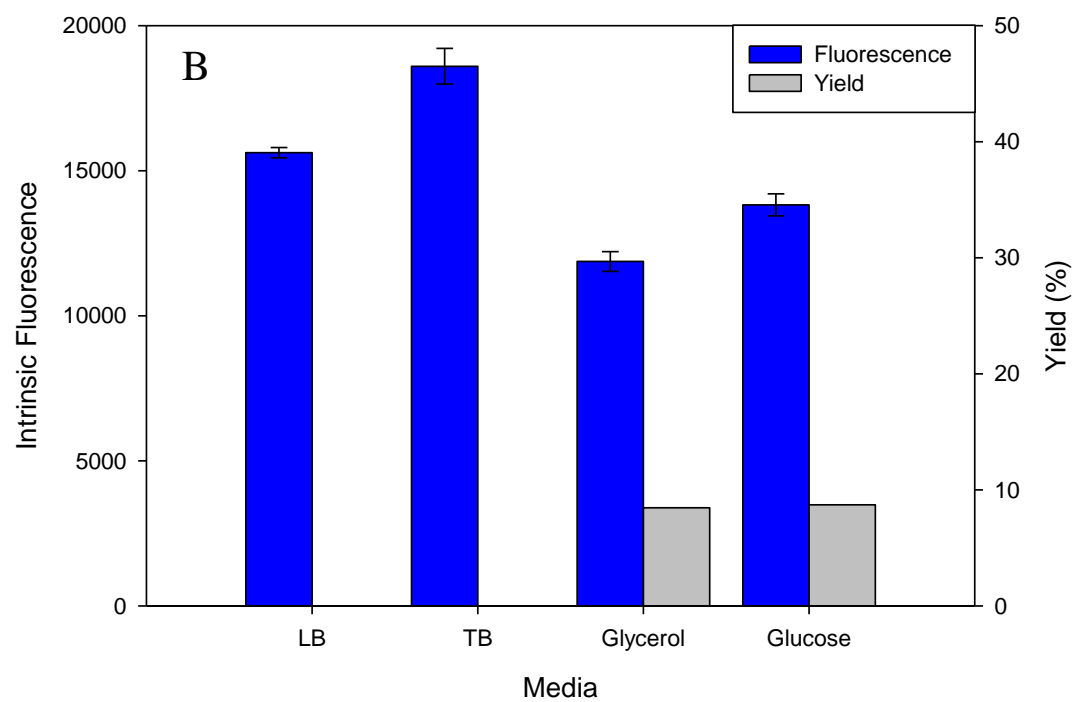


Figure 9.10 Inclusion bodies from fermentations in 4 different medias refolded in buffer 3. A) Absorbance at different wavelengths. B) Intrinsic fluorescence and yield.

9.4 Appendix for Chapter 6

9.4.1 Estimating $k_L a$

When:

$$\tau_p \ll \frac{1}{k_L a}$$

Probe response time is negligible. Therefore the rate of change in dissolved oxygen concentration is equal to the rate of oxygen transfer from gas to liquid

$$\frac{dC_L}{dt} = k_L a (C^* - C_L)$$

Where C_L = actual oxygen concentration

C^* = maximum oxygen concentration

$k_L a$ = oxygen mass transfer coefficient

t = time

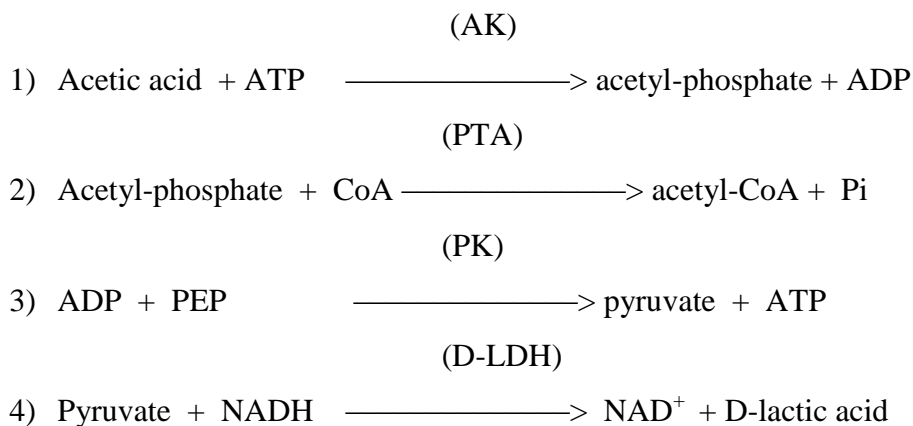
Integration gives:

$$\ln(C^* - C_L) = -k_L a \cdot t$$

Therefore a plot of $\ln(C^* - C_L)$ versus time has a gradient equal to $k_L a$. The gradient of the linear slope (in this case between 20 to 70% DOT) was taken.

9.4.2 Acetic acid determination

9.4.2.1 Reaction Sequence



9.4.2.2 Calculation

$$c = \frac{V \times MW}{\Delta A_{\text{acetic acid}}} \quad [\text{g/L}]$$

$$\epsilon \times d \times v$$

V = final volume [ml]

MW = molecular weight of acetic acid [g/mol]

ϵ = extinction coefficient of NADH at 340 nm [$l \times mol^{-1} \times cm^{-1}$]

d = light path [cm]

v = sample volume [ml]

$$c = \frac{2.66 \times 60.05}{6300 \times 1 \times 0.10} \times \Delta A_{\text{acetic acid}} \quad [\text{g/L}]$$

$$c = 0.2535 \times \Delta A_{\text{acetic acid}} \quad [\text{g/L}]$$

9.4.3 Fermentation data

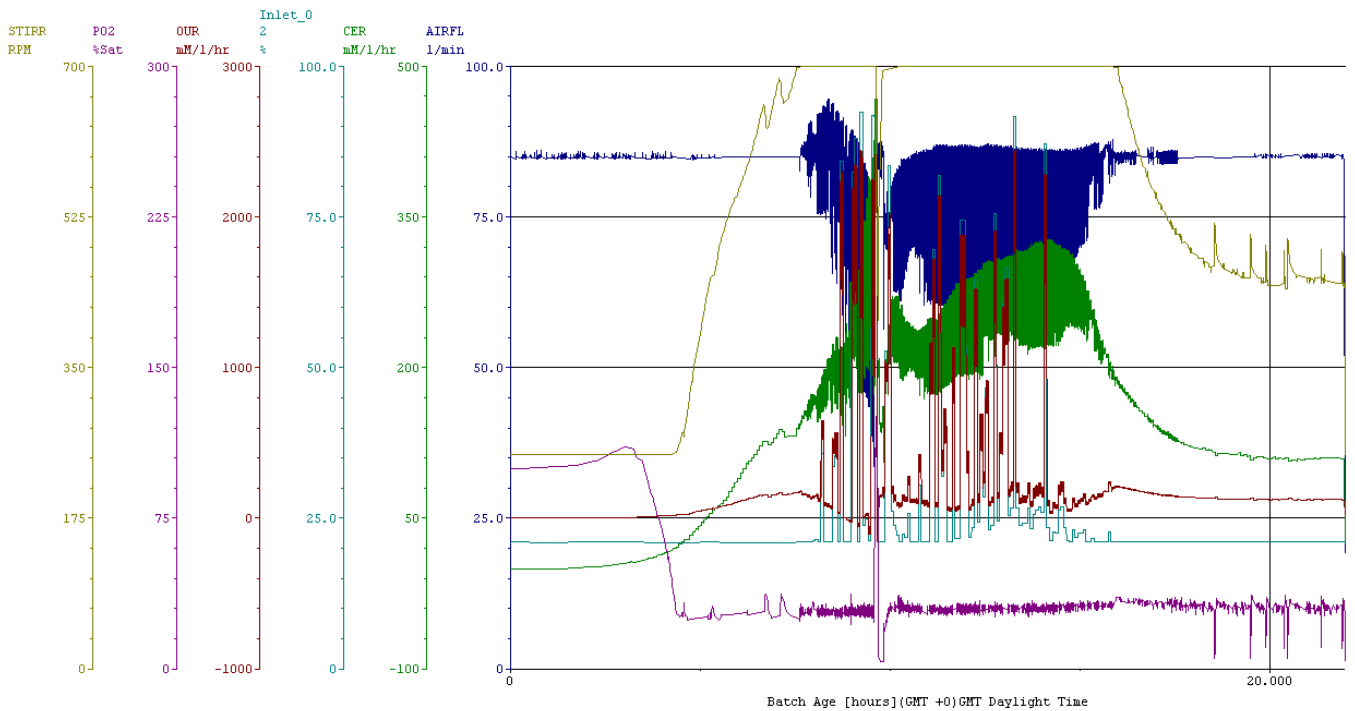


Figure 6.9.11 Fermentation trace of the stirrer speed, dissolved oxygen (pO_2), oxygen uptake rate (OUR), carbon evolution rate (CER), oxygen saturation in air inlet (Inlet_ O_2) and airflow rate (AIRFL)

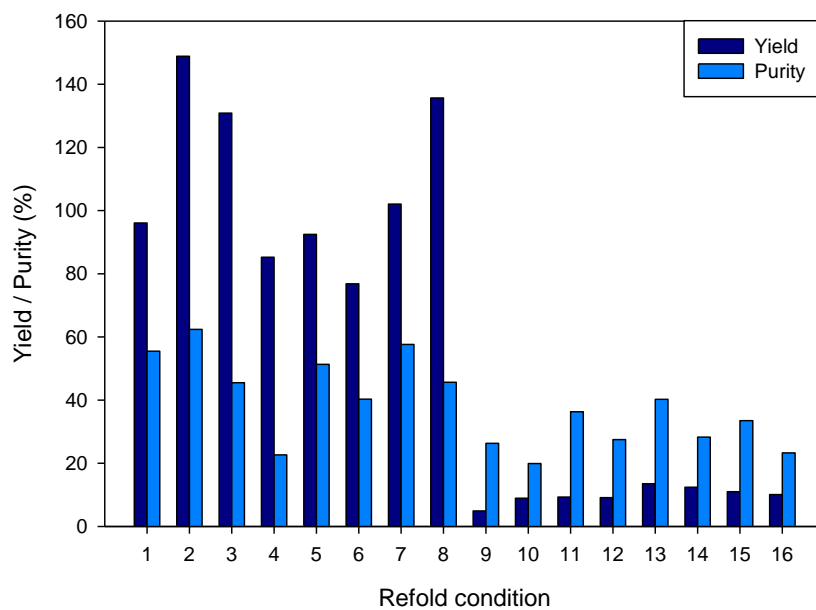


Figure 6.9.12 A summary of the yield and purity results of the 200 ml refold conditions detailed in Table X.

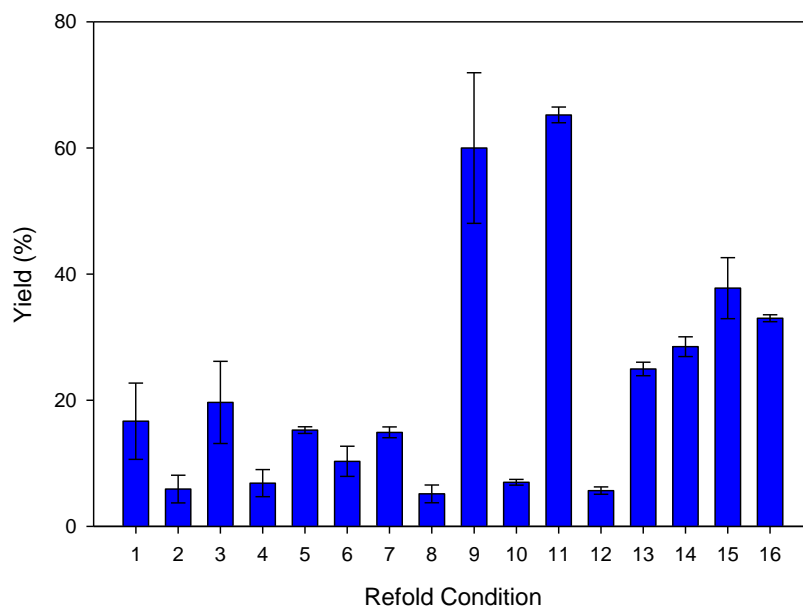


Figure 6.9.13 A summary of the yield of the microscale refolds of the large scale fermentation material

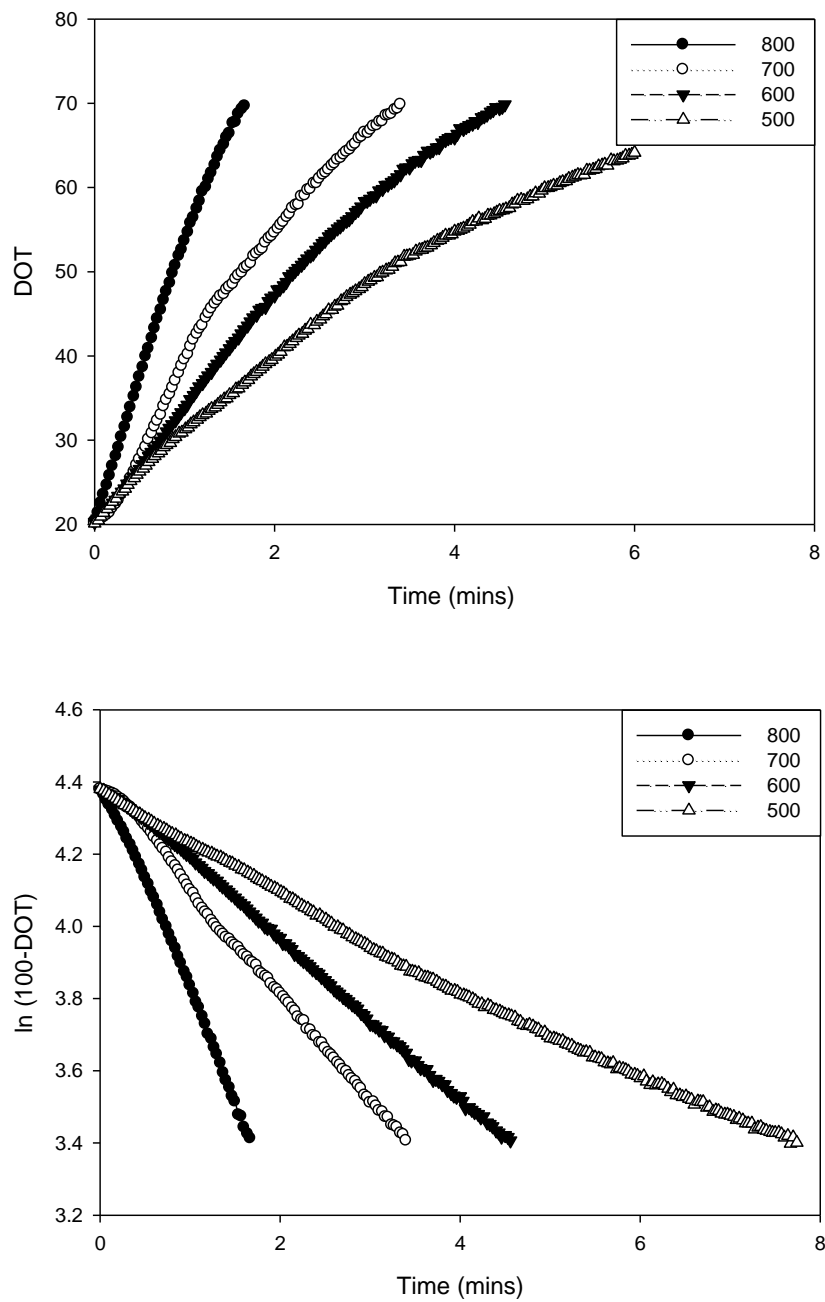


Figure 6.9.14 DOT profiles for different shaking speeds of 800, 700, 600 and 500 rpm

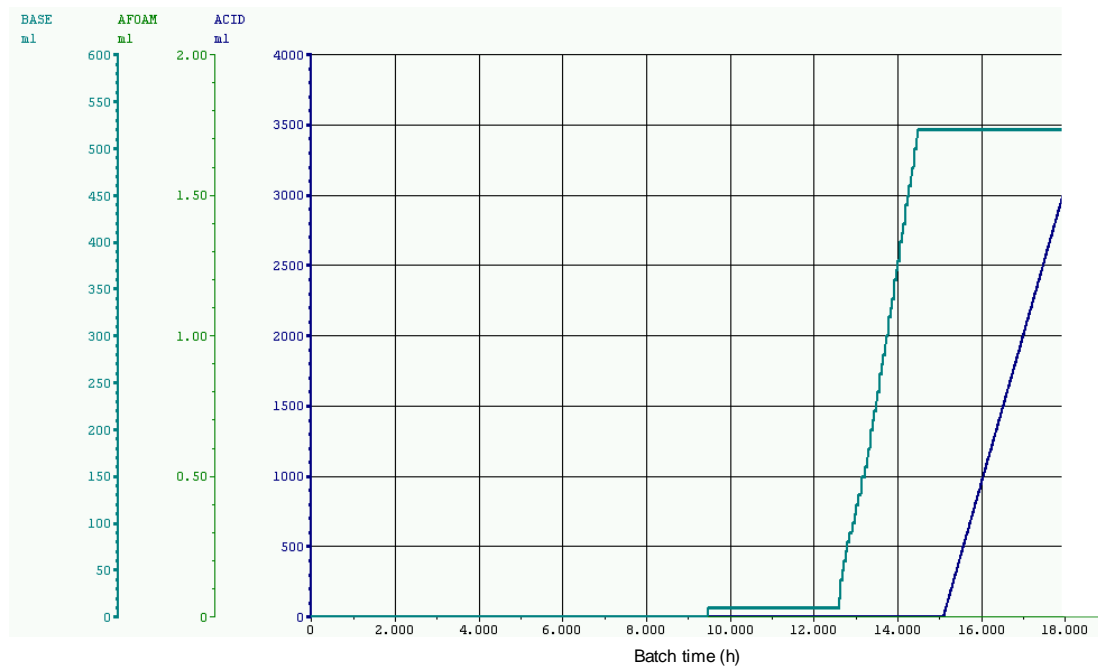


Figure 6.9.15 The acid, base and antifoam additions of the higher $k_L a$ fermentation